TREATMENT OF HIGH-STRENGTH NITROGEN WASTEWATER WITH A HOLLOW-FIBER MEMBRANE-AERATED BIOFILM REACTOR: A COMPREHENSIVE EVALUATION

Kevin R. Gilmore

Dissertation submitted to the Faculty of the
Virginia Polytechnic Institute and State University
in partial fulfillment of the requirements for the degree of

DOCTOR OF PHILOSOPHY
In
Civil Engineering

Nancy G. Love, Ph. D., Chair
Jay L. Garland, Ph.D.
John C. Little, Ph.D.
Barth F. Smets, Ph.D.
Ann M. Stevens, Ph.D.

August 4, 2008
Blacksburg, Virginia

Keywords: Wastewater treatment, hollow fiber membrane aerated biofilm reactor, ammonia oxidizing bacteria, nitrite oxidizing bacteria, nitrification, anaerobic ammonia oxidation, anammox, oxygen, mass transfer, modeling, nitric oxide, nitrous oxide

TREATMENT OF HIGH-STRENGTH NITROGEN WASTEWATER WITH A HOLLOW-FIBER MEMBRANE-AERATED BIOFILM REACTOR: A COMPREHENSIVE EVALUATION

Kevin R. Gilmore

ABSTRACT

Protecting the quality and quantity of our water resources requires advanced treatment technologies capable of removing nutrients from wastewater. This research work investigated the capability of one such technology, a hollow-fiber membrane-aerated biofilm reactor (HFMBR), to achieve completely autotrophic nitrogen removal from a wastewater with high nitrogen content.

Because the extent of oxygenation is a key parameter for controlling the metabolic processes that occur in a wastewater treatment system, the first part of the research investigated oxygen transfer characteristics of the HFMBR in clean water conditions and with actively growing biofilm. A mechanistic model for oxygen concentration and flux as a function of length along the non-porous membrane fibers that comprise the HFMBR was developed based on material properties and physical dimensions. This model reflects the diffusion mechanism of non-porous membranes; namely that oxygen follows a sorption-dissolution-diffusion mechanism. This is in contrast to microporous membranes in which oxygen is in the gas phase in the fiber pores up to the membrane surface, resulting in higher biofilm pore liquid dissolved oxygen concentrations. Compared to off-gas oxygen analysis from the HFMBR while in operation with biofilm growing, the model overpredicted mass transfer by a factor of approximately 1.3. This was in contrast to empirical mass transfer coefficient-based methods, which were determined using either bulk aqueous phase dissolved oxygen (DO) concentration or the DO concentration at the membrane-liquid interface, measured with oxygen microsensors. The mass transfer coefficient determined with the DO measured at the interface was the best predictor of actual oxygen transfer under biofilm conditions, while the bulk liquid coefficient underpredicted by a factor of 3. The mechanistic model exhibited sensitivity to parameters such as the initial lumen oxygen concentration (at the entry to the fiber) and the diffusion coefficient and partitioning coefficients of oxygen in the silicone membrane material. The mechanistic model has several advantages over empirical-based methods. Namely, it does not require experimental determination of K_L, it is relatively simple to solve without the use of advanced mathematical software, and it is based upon selection of the membrane-biofilm interfacial DO concentration. The last of these is of particular importance when designing and operating HFMBR systems with redox (aerobic/anoxic/anaerobic) stratification, because the DO concentration will determine the nature of the microenvironments, the microorganisms present, and the metabolisms that occur.

During the second phase of the research, the coupling of two autotrophic metabolisms, partial nitrification to nitrite (nitritation) and anaerobic ammonium oxidation, was demonstrated in a single HFMBR. The system successfully treated a high-strength nitrogen wastewater intended to mimic a urine stream from such sources as extended space missions. For the last 250 days of operation, operating with an average oxygen to ammonia flux (J_{O2}/J_{NH4+}) of 3.0 resulted in an average nitrogen removal of 74%, with no external organic carbon added. Control of nitrite-oxidizing bacteria (NOB) presented a challenge that was addressed by maintaining the J_{O2}/J_{NH4+} below the stoichiometric threshold for complete nitrification to nitrate (4.57 g O_2 / g NH_4^+). The DO-limiting condition resulted in formation of harmful gaseous emissions of nitrogen oxides (NO, N_2O), which could not be prevented by short-term control strategies. Controlling J_{O2}/J_{NH4+} prevented NOB proliferation long enough to allow an anaerobic ammonia-oxidizing bacteria (AnaerAOB) population to develop and be retained for >250 days. Addition of a supplemental nutrient solution may have contributed to the growth of AnaerAOB by overcoming a possible micronutrient deficiency. Disappearance of the gaseous nitrogen oxide emissions coincided with the onset of anaerobic ammonium oxidation, demonstrating a benefit of coupling these two autotrophic metabolisms in one reactor. Obvious differences in biofilm density were evident across the biofilm depth, with a region of low density in the middle of the biofilm, suggesting that low cell density or exocellular polymeric substances were primarily present in this region, Microbial community analysis using fluorescence *in situ* hybridization (FISH) did not reveal consistent trends with respect to length along the fibers, but radial stratification of aerobic ammonia-oxidizing bacteria (AerAOB), NOB, and AnaerAOB were visible in biofilm section samples. AerAOB were largely found in the first 25% of the biofilm near the membrane, AnaerAOB were found in the outer 30%, and NOB were found most often in the mid-depth region of the biofilm. This community structure demonstrates the importance of oxygen availability as a determinant of how microbial groups spatially distribute within an HFMBR biofilm.

The combination of these two aspects of the research, predictive oxygen transfer capability and the effect of oxygen control on performance and populations, provides a foundation for future application of HFMBR technology to a broad range of wastewaters and treatment scenarios.

ACKNOWLEDGMENTS

People

Tremendous thanks go to many people who contributed to my arriving at the end of this journey and the beginning of the next. Thank you to Nancy, for our years of collaboration and accomplishments, for treating me like a colleague, and for being an exceptional mentor and friend. Dr. Barth Smets, for continually challenging me to look further and in more detail. Dr. John Little, for his encouragement and expertise in mathematical modeling. Dr. Ann Stevens, for being an inspiring instructor in the classroom, assisting with molecular methods, and keeping an engineer on track in the microbiological realm. Dr. Jay Garland, for welcoming me to the labs at KSC and for long phone calls discussing results and concepts. Dr. Akihiko Terada, for providing clones and assistance with methods, guidance and useful advice concerning anaerobic ammonia oxidizers, and for his collegial discussions and collaborations, which I hope will continue beyond this work. Dr. Linsey Marr, my teaching mentor, and Drs. Shelli Fowler and Karen DePauw, for their roles in shaping me as a teacher and mentor. Drs. Jactone Arogo Ogejo, Katharine Knowlton, Zhiyou Wen, and Biswarup Mukhopadhyay, for including me on collaborative proposal work and assisting with methods (Dr. Mukhopadhyay). Dr. E. M. Gregory, for the most challenging course of my life and useful discussions regarding anaerobic metabolism. Dr. Eric Wong and Elizabeth Gilbert, for allowing me access to the cryostat/microtome. Kristi DeCourcy, for her assistance and guidance in using the confocal scanning laser microscope. Julie Petruska, without whom nothing in our labs would be possible. Jody Smiley, who created the nitrous oxide analytical method for me and who keeps all the instruments in top shape. Tim Moore, for sharing the NOx analyzer. Lee Bryant, for graciously allowing me to use the picoammeter. Josh Williams, for assistance with PCR and clones. Dr. Zhaomin Yang and Wes Black for assistance with color photography of biofilm sections. Leon Downing, for useful advice on microsensors, reactor construction, and membrane-aerated biofilms in general.

To the laboratory research group of Nancy Love, I say thank you for creating an environment that not only allows successful research but is also a joy in which to work. Wendell Khunjar, for his selfless assistance and counsel regarding concepts, methods, and pedagogy; without whom I would not have completed this; Jeremy Guest, for his endless energy and dedication to friends; Chris Wilson, for assistance with methods and wonderful conversations. Ameet Pinto, for willingness to always take time to talk about research, forward papers, and share his extensive mastery of the literature. In addition, I thank Kaoru, Martin, Ines, Joy, Jason, Sam, Mert, K2, Romeo, Brian, Shoko, and many others for the experiences and memories.

To my mother and extended family, I thank you for your patience, support, and encouragement. To my children and especially my wife, Heidi, I owe a debt of gratitude for the opportunity to write this chapter in my life. I embarked on this journey later than most, and their sacrifices, understanding, and support have made this possible.

Organizations

This work was funded by the National Aeronautics and Space Administration (NASA) and a Marion Via Doctoral Fellowship from the Via Department of Civil and Environmental Engineering at Virginia Tech. Additional funding included a Sonny Roden Memorial Scholarship from the Virginia Water Environment Association (VWEA) and a William R. Walker Graduate Research Fellowship from the Virginia Water Resources Research Center (VWRRC). For the latter, I want to personally thank Loreta Walker and the late Dr. Bill Walker for their kindness and friendship to our family. He will be missed.

Contributions

While the author performed the research work herein and was the author of the written content, the intellectual contribution of co-authors listed in individual chapters is greatly appreciated and acknowledged.

TABLE OF CONTENTS

LIST OF TABLES

LIST OF FIGURES

1. EXECUTIVE SUMMARY

2. LITERATURE REVIEW

3. OXYGEN TRANSFER MODEL FOR A FLOW-THROUGH HOLLOW-FIBER MEMBRANE BIOFILM REACTOR

4. AUTOTROPHIC NITROGEN REMOVAL IN A HOLLOW-FIBER MEMBRANE-AERATED BIOFILM REACTOR

1. EXECUTIVE SUMMARY

1.1 Introduction

Biological processes for removal of nutrients from wastewater offer a means of preventing eutrophication of natural waters and producing effluents suitable for reuse, after polishing. However, resource requirements, namely the addition of oxygen and external organic carbon for nitrification and denitrification, respectively, are a burden to owners and operators of biological processes. Novel N removal systems that remove nitrogen autotrophically (using inorganic electron donors) offer a less resource-intensive alternative to conventional nutrient removal.

One such novel N removal process is partial nitrification to nitrite (termed 'nitritation'). The nitrite produced can be denitrified heterotrophically to N_2 gas or reduced to N_2 gas via anaerobic ammonium oxidation. While both systems offer reduced oxygen and organic carbon requirements, the coupling of nitritation and anaerobic ammonium oxidation has the lowest net resource requirement.

The success of a coupled nitritation-anaerobic ammonium oxidation process requires exclusion or control of nitrite-oxidizing bacteria (NOB) while allowing aerobic ammonia-oxidizing bacteria (AerAOB) and anaerobic ammonia-oxidizing bacteria (AnaerAOB) to grow. In biofilm systems, the use of washout to control NOB is not an option. However, the hollow-fiber membrane-aerated biofilm reactor (HFMBR) offer a means of manipulating oxygenation of the biofilm to the extent that NOB can be controlled. The membrane fibers or tubes within an HFMBR provide a support medium upon which a biofilm can grow, while at the same time also delivering oxygen to that biofilm. Aeration gas is passed through the inside of the fibers or tubes and oxygen diffuses across to the base of the biofilm in a bubbleless fashion with high transfer efficiency.

This dissertation presents the results of an experimental study with a HFMBR that was operated to achieve coupled nitritation and anaerobic ammonium oxidation for treatment of a high strength N wastewater. The wastewater was designed to mimic urine from a

confined space operation, although the work has broader application to high-strength N wastes on Earth, such as source-separated urine and recycle streams from wastewater treatment plant (WWTP) biosolids handling processes.

1.2 Oxygen Transfer Investigation, Model Formulation, and Comparison (Chapter 3)

Because the extent of oxygenation of a membrane-aerated biofilm determines the microenvironments and microbial community within the biofilm, oxygen transfer in an HFMBR was evaluated. This work is presented in Chapter 3 of this dissertation. When clean water oxygen transfer tests were conducted by measuring the increase in bulk liquid dissolved oxygen (DO) concentration over time, the overall mass transfer coefficient (K_{OL}) was calculated to be 4.0×10^{-4} cm/sec, which included both the membrane and liquid-phase boundary layer resistances. However, when the effect of the liquid-phase boundary layer was removed by monitoring the membrane-liquid interface DO concentration with oxygen microsensors, the membrane mass transfer coefficient was calculated to be 1.5×10^{-3} cm/sec. This microsensor-determined K_M was a more accurate predictor of the actual oxygen transfer occurring during operation with a biofilm present.

A mechanistic oxygen transfer model was developed to provide more versatility and utility in design and prediction of HFMBR aeration capabilities. The model was based on material properties, membrane and reactor geometries and dimensions, and operating conditions. Two primary models were created: Equation 1.1 expresses the gas-phase oxygen concentration as a function of distance along the length of the fiber/tube. Equation 1.2 predicts the flux of oxygen as a function of the same distance along the fiber (the reader is referred to Chapter 3 for a definition of the terms used in the equations).

$$y(x) = \left(y_0 - mC_{int}\right) \cdot \exp\left(-\frac{\pi d D K_g}{UA\delta} \cdot x\right) + mC_{int} \qquad \text{(eqn 1.1)}$$

$$J(x) = \frac{D}{\delta} \cdot \left(K_g \cdot y_0 - K_w \cdot C_{int}\right) \cdot \exp\left(-\frac{\pi d D K_g}{UA\delta} \cdot x\right) \qquad \text{(eqn 1.2)}$$

The model overpredicted oxygen transfer in the presence of a biofilm by a factor of only 1.3. While many previous studies have commented on the importance of gas-phase lumen pressure on oxygen transfer, our model simulation results show that velocity is also an important consideration, as it determines how much of the fiber is aerobic and available for transferring oxygen (Figure 1.1). It is evident from Figure 1.1 that as velocity increases, more of the lumen is aerobic and more oxygen is transferred (increasing oxygen flux, J_{O2}). However, as velocity continues to increase, the increase in oxygen flux slows (diminishing returns) and transfer efficiency drops to the range typical of conventional bubbled aeration systems.

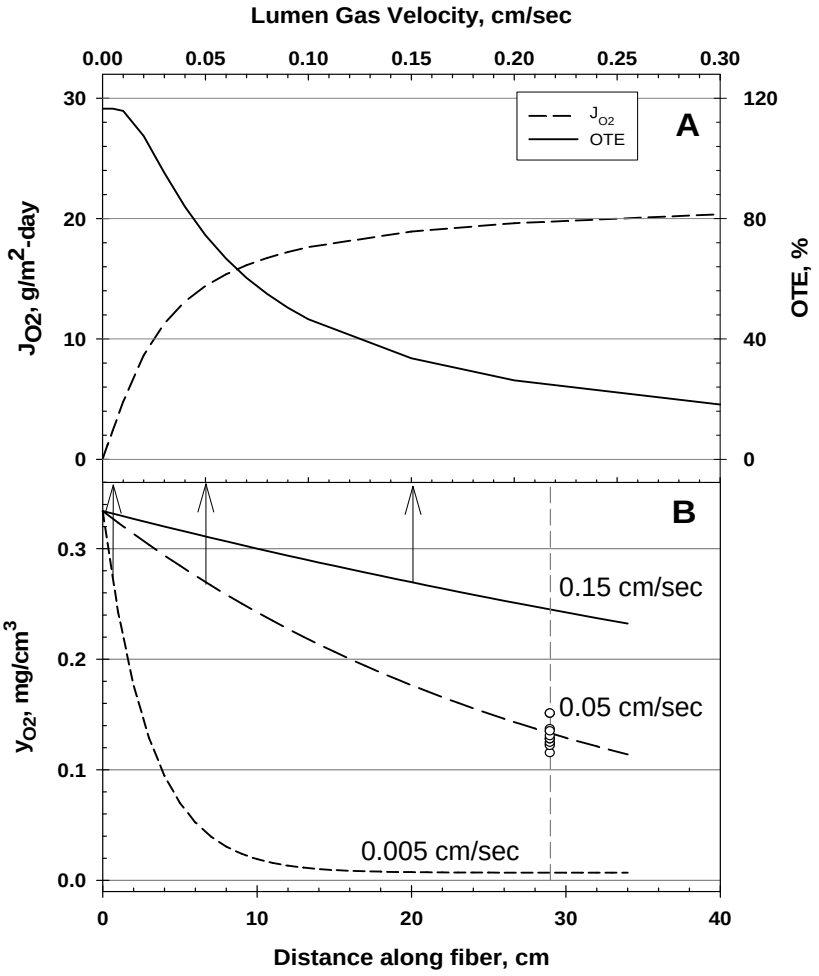

Figure 1.1. Mechanistic oxygen transfer model simulations. Panel A: Oxygen flux and OTE as a function of lumen gas velocity. Panel B: Gas-phase oxygen profile predicted along fiber length.

The mechanistic model requires assumption or measurement of the DO concentration at the membrane-biofilm interface, and predictions are most accurate when this DO concentration is small relative to the initial gas-phase oxygen concentration. Nonetheless, the mechanistic model offers a powerful tool for rapid evaluation of different membrane materials, geometries (diameter, wall thickness), and operating conditions (pressure, velocity, and membrane-biofilm interfacial DO concentration).

1.3 HFMBR Operation, Performance, Emissions, and Microbial Community Structure (Chapter 4)

Chapter 4 presents the results of research in which a laboratory-scale HFMBR was constructed and operated to achieve autotrophic N removal from a synthetic high-strength N waste. The HFMBR was operated for 550 days, the last 250 days of which demonstrated an average of 75% nitrogen lost from the system. Development of anaerobic ammonium oxidation activity and suppression of nitrite oxidation were primarily achieved through careful control of the ratio of oxygen flux to ammonium-nitrogen flux (J_{O2}/J_{NH4+}), which averaged 3.0 for the last 250 days. Prior to anaerobic ammonium oxidation (<Day 298), nitrogen balances showed significant emissions of the harmful gases NO and N_2O, which together accounted for up to 10% of the ammonium-nitrogen oxidized. These emissions could not be reduced by short-term increases in oxygenation or pH, but the onset of anaerobic ammonium oxidation coincided with the elimination of emissions from the system. This demonstrates a significant benefit of coupling these two autotrophic processes of nitritation and anaerobic ammonium oxidation in a single biofilm.

The microbial community in the biofilm, evaluated by fluorescence *in situ* hybridization (FISH), did not vary along the length of the reactor. However, clear spatial distribution of populations were evident with respect to radial distance from the membrane (Figure 1.2). AerAOB were found nearest the membrane (oxygen source), AnaerAOB were found

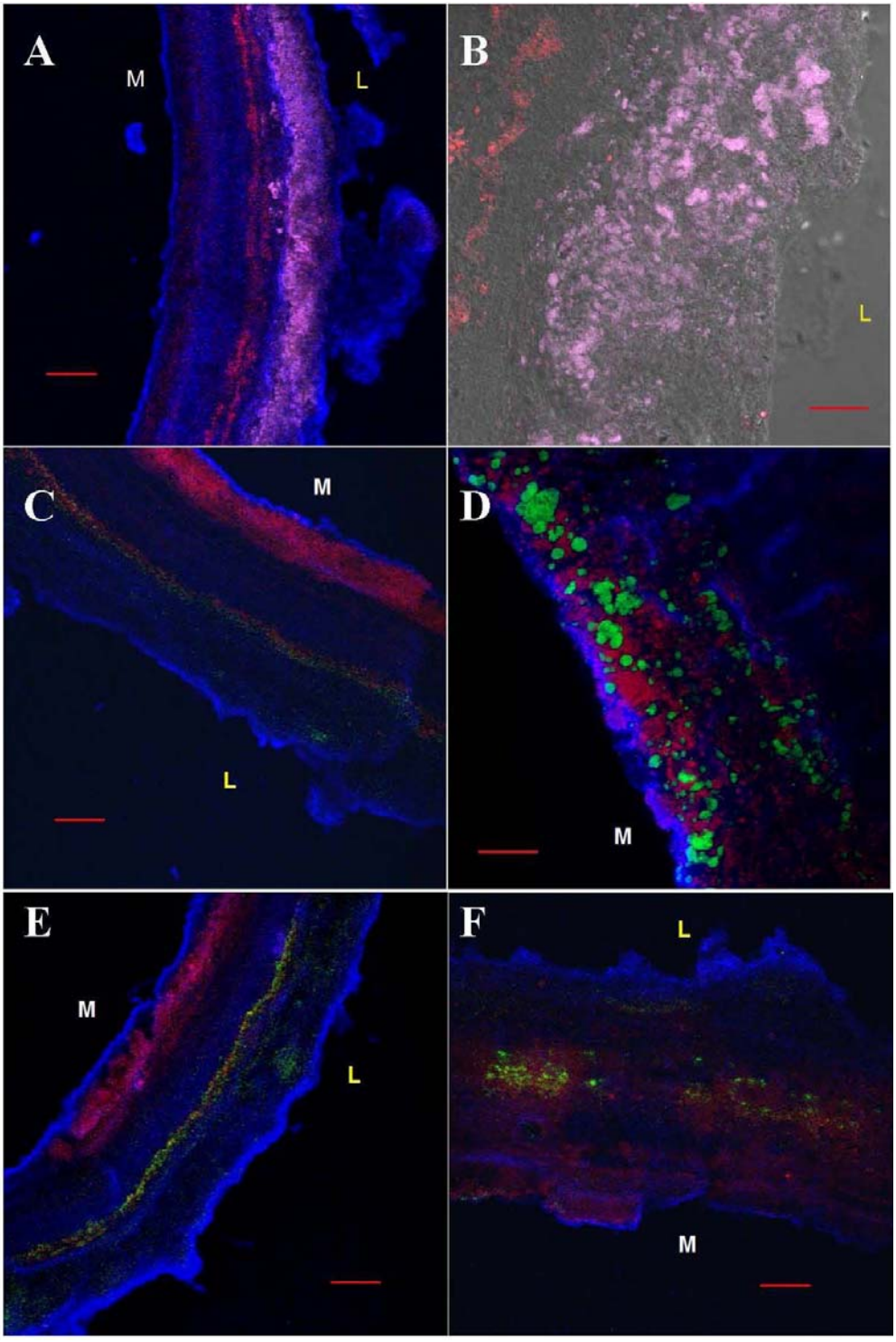

Figure 1.2. FISH confocal micrographs showing radial distribution of HFMBR microbial populations. M: Membrane side of biofilm; L: Liquid side of biofilm. Blue in all panels: all DNA; Panels A, B: AerAOB (Nso1225, red) and AnaerAOB (Pla46, magenta); C, D, E: AerAOB (Nso190, red) and NOB (Ntspa662, green); F: AerAOB (Nso190, red) and NOB (NIT3, green). Scale bars: A, C, E, F:100 μm. B, D:30 μm.

furthest from the membrane (near the anaerobic bulk liquid), and the intermediate region of the biofilm was less dense and less populated. The makeup of this region is unknown but could potentially be largely composed of exocellular polymeric substances (EPS). Both AerAOB and NOB were observed in this area, but oxygen microsensor profiles suggest negligible DO in this region. As a result, the observed community structure poses additional questions to be addressed in future research.

1.4 Engineering Significance (Chapter 5)

The application of HFMBRs to completely autotrophic nitrogen removal applications is new, and this approach offers great potential for significant cost savings on aeration and external organic carbon. Chapter 5 presents the engineering significance of the work, including a cost analysis comparing the completely autotrophic HFMBR to conventional nitrification and denitrification. The cost of the HFMBR is predicted to be approximately one-fifth the cost of conventional N removal systems while achieving nearly the same effluent quality. This cost savings is expected to drive further investigation of HFMBRs as a practical tool for treating high strength wastes using only autotrophic metabolisms. Future application of these systems will require further investigation of i) the time course over which microbial populations achieve the spatial distribution observed here, ii) start-up strategies to reduce the time required to reach the desired performance, and iii) evaluation of how organic carbon in wastewater affects performance and microbial community structure.

2. LITERATURE REVIEW

2.1 Nutrients in wastewater: Relevance, forms, and treatment

Treatment of anthropogenic wastes is and will continue to be one of the most critical challenges in sustaining our existence. As water resources are becoming increasingly scarce, biological technologies offer a renewable approach to treating wastewater, consuming fewer resources than many of the physical and chemical technologies that are often subsequently required to meet standards for direct and indirect potable reuse. Eutrophication of natural water bodies reduces the quality of drinking water sources and increases the extent and cost of treatment required to achieve potable water quality. As nutrients (primarily nitrogen and phosphorus) are the principle causes of eutrophication, nutrient removal from wastewater remains an important goal for environmental engineers today.

In municipal wastewater, the majority of nitrogen is in the reduced form (-3 oxidation state), such as organic amine groups ($R\text{-}NH_3$ or $R\text{-}NH_4^+$), ionized ammonium (NH_4^+), or free ammonia (NH_3). During collection, preliminary treatment, and primary treatment, most of the organic nitrogen in wastewater is hydrolyzed and ammonified to NH_4^+. This ammonium is taken into microbial cells and converted to unionized ammonia (NH_3) prior to oxidation; however, the terms ammonia and ammonium are use rather interchangeably in this dissertation to refer to the reduced form of inorganic nitrogen. Conventional secondary treatment involves biological oxidation from NH_3 to nitrate (NO_3^-) via nitrite (NO_2^-) (collectively, nitrification). Total nitrogen removal then requires subsequent denitrification to nitrogen gas (N_2), which is released to the atmosphere. These multi-step processes of nitrification and denitrification, illustrated in Table 2.1, have unique environmental and operational requirements, necessitating discrete environments either in time or in space. Addition of sufficient oxygen and organic carbon represent the majority of the resource demands associated with conventional nitrification and denitrification, respectively. As a result, novel processes such as anaerobic ammonium oxidation (Table 2.1) are being applied to achieve nutrient removal with fewer resources invested. While

these methods for nutrient 'removal' do not achieve nutrient 'recovery' for beneficial reuse, they are the current benchmark for treatment of nutrients in wastewater.

From the 1970s onward, research of biological nutrient removal processes led to the widespread implementation of full-scale systems to removal nitrogen and phosphorus, particularly at large publicly-owned treatment works (POTWs). Listings of impaired rivers and streams, classification of shellfish-sensitive estuaries, and hypoxia in sounds, bays, and gulfs continues to push nutrient removal regulations towards the limits of technology. These drivers underscore the need for improvements over conventional nutrient removal processes and application of novel solutions to wastewaters beyond simply the municipal realm.

Table 2.1. Nitrogen metabolisms relevant to wastewater treatment.

	N Oxidation State							
Process[a]	-3	-2	-1	0	+1	+2	+3	+5
Ammonia oxidation (nitritation)	NH_3 →		NH_2OH →				NO_2^-	
Nitrite oxidation (nitratation)							NO_2^- →	NO_3^-
Heterotrophic denitrification				N_2 ←	N_2O ←	NO ←	NO_2^- ←	NO_3^-
Autotrophic denitrification	NH_3 →		NH_2OH		N_2O ←	NO ←	NO_2^-	
Anaerobic ammonia oxidation[b]	NH_3 →	N_2H_4	NH_2OH →	N_2		NO ←	NO_2^- →	NO_3^-

[a] Blue: aerobic processes; red: anoxic processes; green: anaerobic processes.
[b] Hydroxylamine (NH_2OH) is shown in the anaerobic ammonium oxidation pathway as it was originally thought to participate in the metabolic pathway (van de Graaf et al., 1997), although the current metabolic model postulates direct oxidation of hydrazine (N_2H_4) to N_2 (Strous et al., 2006).

Several terms corresponding to the metabolisms in Table 2.1 are used throughout this dissertation, and these terms are defined here:

- AerAOB – Aerobic ammonia-oxidizing bacteria that oxidize ammonia to nitrite aerobically
- NOB – Nitrite-oxidizing bacteria that oxidize nitrite to nitrate aerobically
- AnaerAOB – Anaerobic ammonia-oxidizing bacteria that generate N_2 from the oxidation of ammonia and reduction of nitrite, generating some nitrate in the process

2.2 High-strength nitrogen-rich wastewaters

High strength wastewaters present a unique challenge for nutrient removal. Wastes such as those from space-based operations, biosolids stabilization and dewatering recycle streams, source-separated urine, and industrial wastewaters (pharmaceutical, food & beverage, chemical, etc.) often have nitrogen concentrations that are significantly higher than those encountered in municipal wastewaters. The category of industrial wastewaters is broad, and characteristics are industry- and site-specific. Therefore, such wastes are not discussed here. Characteristics and relevant literature for the other specialized wastewaters are discussed further.

2.2.1 Long-term confined space operations

Space-based operations represent a specialized area of wastewater treatment. Because of the limits of earth resupply, recovery and reuse of water is essential for long-term manned space missions. Water conservation practices during space missions result in minimal quantities of liquid wastewater (11.85 L/person-day) for an Early Planetary Base (EPB) crew (Verostko et al., 2004), which in turn leads to high concentrations of organic matter and nitrogen species, particularly ammonia and simple organic nitrogen (urea). The need for recovery and reuse, the high concentrations of pollutants, and the harsh environment of space, in which gravity, oxygen, and water are largely absent, all come together to present a unique challenge for water recovery.

Liquid wastewater sources aboard a long-term mission craft primarily include dehumidification condensate from ambient cabin air, water recovered from CO_2 scrubbing operations, hygiene water from hand-washing and limited bathing, and urine

and flush water. Table 2.2 lists the characteristics of these combined wastewater streams, as determined through monitoring of actual space missions as well as ground-based human biosphere-type experiments.

Table 2.2. Early planetary base ersatz wastewater characteristics[a].

Parameter	Value
Flow	11.85 L/cap-day
pH	8.9
Total Organic Carbon	631 mg/L
COD[b]	1,758 mg/L
NH_3-N	852 mg/L-N
NO_2^--N+ NO_3^--N	0 mg/L-N
SO_4^{2-}	88 mg/L

[a] Adapted from Verostko et al., 2004.
[b] Gilmore et al., 2006

Prior research aimed at treating this type of wastewater has involved processes targeting either the organic portion of the wastewater, the nitrogenous portion, or both. The primary organic constituent in the wastewater is a soap consisting of a mixture of fatty acid methyl taurates. Studies have demonstrated nearly complete degradation of this organic fraction under aerobic (Valadez et al.1998, Finger et al., 1999, Archer et al., 1999) and anoxic (Strayer et al., 1999, Pickering and Edeen, 1998, Supra et al., 1998) conditions. Less success has been demonstrated with anaerobic treatment (Gilmore et al., 2006, Finger et al., 1999). However, a wide variety of aerobic and facultative organisms can target the organic constituents in the wastewater.

The nitrogenous fraction of space-based wastewaters is largely urea, which readily hydrolyzes to ammonia via *ex vivo* urease in the wastewater collection vessel (Verostko, 2004). The anticipated ammonia concentration of 800+ mg/l-N results in a carbonaceous oxygen demand (COD) to total nitrogen mass ratio (COD:N) of approximately 2:1, much lower than what is typical of earth-based municipal wastewater. Various aerobic and anoxic biological processes have been applied to remove nitrogen from this wastewater formulation or carbon-free analogs, and some of these studies are listed in Table 2.3. However, no research to date has yet accomplished nitrogen removal from space-based wastewater by coupling partial ammonia oxidation to nitrite (nitritation) and anaerobic

ammonium oxidation, as described below. Given the extreme limitations associated with space operations, such autotrophic processes are attractive because they require less resources and generate minimal residuals.

Table 2.3. Selected studies treating space-based wastewater formulations.

Feed	Reactor configuration & oxic state	Reference
Planetary base ersatz wastewater	Anaerobic packed bed reactor, aerobic tubular reactor	Muirhead et al., 2003
Planetary base ersatz wastewater	Immobilized cell reactor (anoxic/ aerobic), trickling filter bioreactor (aerobic)	Pickering and Edeen, 1998
Space station ersatz wastewater	Hollow-fiber membrane biofilms in series: nitrification (aerobic) and denitrification (anoxic)	Finger et al., 1999
Carbon-free synthetic urine	Redox-controlled bioreactor; hollow-fiber membrane biofilms, aerobic (O_2) and anoxic (H_2) fibers	Smith et al., 2008

2.2.2 Wastewater treatment plant recycle streams

Although raw municipal sewage entering a treatment plant has a much higher COD:N ratio than space-based wastewater, additions to the influent flow can significantly increase the N load. Solids handling processes such as biosolids stabilization and dewater, make use of various technologies such as anaerobic digesters, belt filter presses, and centrifuges. These technologies, in turn, create recycle flow streams in the form of supernatant, filtrate, and centrate, respectively. Recycle flows are typically returned to the head of the treatment plant and, like space-based wastewaters, contain high concentrations of reduced nitrogen (ammonium). For instance, a study of several centrate streams in New York showed mean total Kjeldahl nitrogen (TKN) concentrations ranging from 555 to 1,782 mg/l as N, most of which was ammonium (Katehis et al., 1998). Other studies (Gu et al., 2007, Head and Oleszkiewicz, 2005) have found similar nitrogen concentrations in recycle streams, and these wastes often are too carbon-deficient for conventional denitrification.

Separate treatment of these recycle streams may be more efficient than treating the N load in the main liquid treatment train of the POTW. Sidestream treatment using

conventional processes is effective at completely nitrifying such waste streams (Chandrasekeran et al., 2007), though the cost of oxygenation can be prohibitive and drives the investigation of novel N removal systems. Both Fux et al. (2003) and Gu et al. (2007) showed effective treatment of a digester supernatant by nitritation and denitrification via nitrite (denitritation). However, the heterotrophic component of such systems still requires external carbon, whereas purely autotrophic systems circumvent this resource. The DEMON process (partial nitritation coupled with anaerobic ammonium oxidation in a suspended growth, low DO, pH-controlled reactor) has been shown to be effective in removing reduced N from an anaerobically-digested and dewatered biosolids stream prior to recycling to the head of a treatment plant (Wett, 2006). Others (van der Star, 2007) treated a digestion/dewatering recycle stream using nitritation (SHARON, see below) and anaerobic ammonium oxidation in series, achieving approximately 87% nitrogen removal (this author's calculation from apparent data). Others have used sidestream treatment as a means to select for ammonia and/or nitrite oxidizers and bioaugment the main liquid train. Such processes include the BioAugmentation reactor Batch Enhanced (BABE) (Berends et al., 2005), which attempts to enrich for nitrifiers without specificity between AerAOB or NOB, and Single reactor High activity Ammonium Removal Over Nitrite (SHARON) (Hellinga et al., 1998), which selects for AerAOB. For many of these waste streams, and for mesophilic and thermophilic digester supernatants in particular, the elevated temperature (>30°C) is useful for encouraging the growth of AerAOB and AnaerAOB, both of which grow well at elevated temperatures (Hellinga et al., 1998, Strous et al., 1999). The pervasiveness and composition of these recycle streams continues to be an area of application for such advanced N removal processes.

2.2.3 Source-separated urine

A third type of specialized wastewater is emerging as engineers and scientists consider more decentralized, on-site treatment. Such an approach lends itself well to water reuse, because the point of reuse is often closer to the point of generation than to a centralized treatment plant. The majority of both nitrogen and phosphorus in wastewater is derived from urine (approximately 75% and 50%, respectively) (Larsen and Gujer, 1996), and

reduced nitrogen concentrations have been reported in the range of 1 to 9 g/l (Maurer et al., 2006). Therefore, even more efficiency can be gained from decentralized treatment if this high-strength waste is treated separately from other wastewater sources that dilute it.

Biological N removal from source-separated urine has received limited study to date. Udert et al. (2003) demonstrated that nitritation in CSTR and SBR configurations could produce effluents with a 1:1 ratio of NH_4^+-N to NO_2^--N from enriched urine, and a batch experiment showed anaerobic ammonium oxidation to be possible thereafter. As advanced N removal processes become better understood, it is likely that source-separated urine will continue to be a good candidate for their application.

2.3 Novel nitrogen removal processes

Conventional nitrogen removal processes have been put to beneficial use in engineered systems for some time. However, these processes are often not ideal for treating specialized wastes with high concentrations of reduced N species, as they typically require spatial separation in the form of dedicated tanks and relatively high amounts of oxygen, organic carbon, and alkalinity. Some systems allow for simultaneous nitrification and denitrification (SND) with reduced resource requirements. However, in the past few decades, novel nitrogen removal processes have been discovered and developed, offering the possibility for significant resource reduction and cost savings relative to either conventional or SND systems. While many of these novel processes, some of which have been introduced previously and are discussed in more detail below, still reside in the realm of emerging science, they are beginning to be applied full-scale around the world.

2.3.1 Nitritation - Denitritation

During the 1970s and 1980s, the abbreviated process of nitritation followed by denitritation was recognized as requiring less oxygen, less organic carbon, and less alkalinity (Turk and Mavinic, 1989) than the conventional approach of nitrifying all the way to nitrate with subsequent denitrification**.** This approach was found to be especially well-suited for high-strength wastewaters with low organic carbon components (Turk and Mavinic, 1989). In addition, with some carbon sources the kinetics of denitrification via

nitrite have been shown to be faster than when nitrate was the electron acceptor (van Rijn et al., 1996).

As a result of these advantages, nitritation and denitritation became a viable option for treatment of high-strength wastewaters. While nitritation-denitritation is not specifically employed in this work, it is discussed in detail here due to the relevance of this body of literature with regard to controlling AerAOB and NOB populations in such systems.

This sequential process can be described by equations (2.1) (Love et al., 2008) and (2.2). Equation 2.1 assumes a biomass yield of 0.2 mg biomass formed as COD per mg NH_4^+-N oxidized, and Equation 2.2 assumes a yield of 0.4 mg COD per mg methanol as COD oxidized (Grady et al., 1999).

Nitritation:

$$NH_4^+ + 1.9\ O_2 + 0.069\ CO_2 + 0.017\ HCO_3^- \rightarrow 0.017\ C_5H_7O_2N + 0.98\ NO_2^- + 0.97\ H_2O + 1.8\ H^+ \quad (2.1)$$

Denitritation (assuming methanol as carbon source):

$$CH_3OH + 1.2\ NO_2^- + 1.2\ H^+ + 0.12\ NH_4^+ + 0.12\ HCO_3^- \rightarrow 0.12\ C_5H_7O_2N + 0.6\ N_2 + 2.46\ H_2O + 0.52\ CO_2 \quad (2.2)$$

The disadvantages of this approach are associated with the nitritation step and include the potential for nitrite toxicity to AerAOB, the need for pH control due to the high nitritation rates which produce acid quickly, and the difficulty in selectively inhibiting NOB to prevent complete nitrification to nitrate. The first two disadvantages are often addressed together: control of pH to above 7 favors the nitrite form over nitrous acid (pKa = 3.3). The third disadvantage has been addressed by different researchers who used methods to reduce NOB growth, such as maintaining a: high free ammonia (FA) concentration (Jenicek et al., 2004); low COD:N ratio (Jenicek et al., 2004); high pH (Jenicek et al., 2004); low solids retention time (SRT) (Hellinga et al., 1998); limited dissolved oxygen (DO) (Jenicek et al., 2004, Pollice et al., 2002); high temperature (Hellinga et al., 1998); or providing an internal denitrification component (Turk and Mavinic, 1989). The last of these strategies is unique in that NOB are out-competed for nitrite by heterotrophic

denitrifiers, resulting in complete nitrogen removal via the "short-cut" process of denitritation. Alternatively, the combination of low SRT with high temperature are characteristics of the SHARON process, which is best described as partial nitrification controlled by temperature and hydraulic retention time HRT (Hellinga et al., 1998). The effluent from this process is suitable for heterotrophic denitritation if the majority of ammonia is oxidized to nitrite, or autotrophic denitritation by AnaerAOB if approximately half of the ammonia is oxidized.

2.3.2 Anaerobic ammonium oxidation (often referred to as anammox)

Another novel nitrogen removal process dates back to 1977 when Broda (1977), based on thermodynamics, postulated a "missing lithotroph" capable of oxidizing ammonium to nitrogen gas with nitrite or nitrate as the electron acceptor. At the time such microorganisms had not been observed. In 1990, the first evidence of "anoxic" ammonium oxidation was presented based on the observation that up to 80% ammonium loss occurred in a denitrification reactor with nitrate as the electron acceptor (van de Graaf et al., 1990). More detailed investigation revealed that the reaction was biologically-mediated (van de Graaf, 1990, van de Graaf, 1995). Subsequent work by van de Graaf et al. (1996) showed that nitrite could also serve as the electron acceptor, that no COD was required, and that the responsible organisms grow very slowly (doubling time of approximately 40 days). Since then, researchers have identified the most likely reactions and pathways occurring in these AnaerAOB (van de Graaf et al., 1997, Schalk et al., 1998, Strous et al., 1999, Strous et al., 2006). The most current stoichiometric representation of anaerobic ammonia oxidation is as follows (Strous et al., 1998):

$$NH_4^+ + 1.32\ NO_2^- + 0.066\ HCO_3^- + 0.13\ H^+ \rightarrow 1.02\ N_2 + 0.26\ NO_3^- + 0.066\ CH_2O_{0.5}N_{0.15} + 2.03\ H_2O \quad (2.3)$$

The AnaerAOB responsible for this conversion were identified as belonging to the phylum *Planctomycetales* (Strous et al., 1999) and contained unique intracytoplasmic compartments called anammoxosomes (Niftrik et al., 2004). These compartments are bound by ladderdane lipids (Damste et al., 2005). The lipids are hypothesized to protect AnaerAOB from reactive intermediates such as hydrazine, which has been shown to be part of the metabolic pathway (Strous et al., 2006). The small amount of nitrate formed is

postulated to arise from the anaerobic oxidation of a fraction of the nitrite to nitrate, providing a source of electrons for carbon fixation via the Acetyl-CoA pathway (Strous et al., 2006). Nitric (NO) oxide is also thought to be an intermediate, formed by the reduction of nitrite by nitrite reductase. This NO then reacts with ammonia to form hydrazine via a novel hydrazine hydrolase (Strous et al., 2006). Clearly, AnaerAOB have complex metabolic capabilities with multiple novel N species as intermediates, and these low energy pathways result in the very low growth rates observed.

Anaerobic ammonium oxidation offers advantages over conventional nitrification and denitrification due to the lack of need for molecular oxygen and external organic carbon sources, lower sludge production, and lower alkalinity requirements. As a result, removal of nitrogen from wastewater was immediately recognized as an application for AnaerAOB.

2.3.3 Nitritation – Anaerobic ammonium oxidation

Almost as soon as anaerobic ammonium oxidation was discovered and elucidated it was put to work in engineered configurations. It is evident from equation 2.3 that a treatment process fed ammonium as the sole nitrogen source must oxidize approximately 57% to nitrite to achieve the appropriate stoichiometry for AnaerAOB. Hence, application to real wastewaters and representative surrogates has involved coupling of nitritation and anaerobic ammonium oxidation. The term Oxygen-Limited Autotrophic Nitrification and Denitrification (OLAND) was coined to describe such a combination (Kuai and Verstraete, 1998). typically when achieved in biofilm configurations. A similar process was termed Completely Autotrophic Nitrogen removal Over Nitrite, or CANON (Sliekers et al., 2002), which has been used to describe both biofilm and fixed film systems. Both of these processes consist of AerAOB and AnaerAOB co-existing in a single oxygen-limited reactor.

Systems with an anaerobic ammonium oxidation component are often seeded, at least in part, with an AnaerAOB enrichment. Due to the slow growth rates of the organisms and lack of pure cultures, much effort has been placed into studying the optimum reactor

configuration for AnaerAOB. Strous et al. (1997) compared fluidized bed and fixed bed configurations for culturing AnaerAOB. The fluidized bed performed better, largely due to less plugging/fouling, achieving up to 1 kg N/m^3 reactor volume per day in 100 days. The optimum pH was determined to be 7.8-8.2, and the optimum temperature to be 30ºC. The fluidized bed configuration was also applied to a real digester effluent and achieved 70% of the mass removal seen with synthetic wastewater in a lab controlled setting. Helmer et al. (2001) characterized AnaerAOB activity using seed sludge from a moving bed biofilm reactor (MBBR) pilot plant (Kaldnes media, HRT = 8 hours, DO <1 mg/l, pH>8, temp = 28ºC, 150 mg/l NH_3-N). They found that at a DO of 0.7 mg/L, both processes (nitritation and anaerobic ammonium oxidation) were well balanced. In batch tests that were relatively short (300 minutes) compared to AnaerAOB growth rates, they characterized several metabolic features of the biomass. Heterotrophic denitrification from nitrite was found to be only approximately 10% of the nitrite consumption attributable to AnaerAOB. Sliekers et al. (2003), starting with an 80% AnaerAOB enrichment culture, used a gas lift reactor with Ar/CO_2 sparging to maintain anaerobicity. Operating conditions included a neutral pH (7.5) and undetectable DO. This work yielded the best anaerobic ammonium oxidation performance to date (8.98 kg N/m^3 reactor volume per day).

Pynaert et al. (2004) used a novel approach of sequential seeding, consisting of the following: initial seeding of a rotating biological contactor (RBC) with a commercial enrichment of nitrifying bacteria (AerAOB and NOB), and after a biofilm development period a second seeding with granular anaerobic biomass as a potential source of AnaerAOB. The RBC was operated at 30ºC with a pH between 7.8 and 8.0, and a bulk DO of approx. 3.0 mg/l. The NH_4^+-N loading rate was increased from 0.06 to 0.30 kg N/m^3-day at which point anaerobic sludge was added. After a brief increase in nitrite, complete nitrification was quickly re-established. Subsequent N load increases led to transient effluent NO_2^- spikes, but overall performance recovered and ammonium oxidation rates were 1.2 and 0.86 kg N/m^3-day mg N/l/d for aerobic and anaerobic metabolisms, respectively. Use of this RBC system to treat a real sludge digester effluent was partially successful, as DO, temperature, and influent perturbations resulted in

performance that was variable and suboptimal. Aerobic and anaerobic ammonium oxidation rates were approximately one fifth of those seen under laboratory controlled conditions (above). Additional process and operational configurations have included both suspended growth (Sliekers et al., 2002, Mulder et al., 2001, Third et al., 2005) and attached growth (Furukawa et al., 2006, Fujii et al., 2002, Isaka et al., 2006) systems.

A common characteristic of these enrichment and culturing approaches is the need for biomass retention to allow sufficient time for AnaerAOB to grow. The ability of a hollow-fiber membrane-aerated biofilm reactor (HFMBR) to provide such biomass retention has not previously been demonstrated. This is one of the primary objectives of the work presented in this dissertation.

2.3.4 Operational challenges of nitritation-anaerobic ammonium oxidation

Processes coupling nitritation and anaerobic ammonium oxidation have achieved better than 85% nitrogen removal without adding external organic carbon and with significantly less aeration than is required for conventional nitrification-denitrification. However, disadvantages to this approach exist. AnaerAOB exhibit reversible inhibition to oxygen and light and potentially irreversible inhibition to nitrite concentrations >100 mg/l NO_2^--N (Strous et al., 1997 & 1999, van de Graaf, 1996). Furthermore, seed cultures of AnaerAOB require long enrichment periods, with published times ranging from 100 days to 18 months (Isaka et al., 2006, Strous et al., 1997, Third et al., 2005). In an isolated location such as space mission craft, restarting a failed system after a process upset could be difficult to achieve.

Just as in nitritation-denitritation systems, the growth of aerobic NOB in nitritation-anaerobic ammonium oxidation processes is undesirable. However, in this case the downside is no longer simply the loss of savings in oxygen and external carbon, but rather that NOB deprive AnaerAOB of substrate. Hence, control of NOB must be achieved for a duration at least long enough to allow establishment of an AnaerAOB population, and indeed indefinitely thereafter. In systems treating organic carbon-free wastewater formulations, denitrification is supported by the small amount of organic

carbon generated by decay and lysis processes. Hence, heterotrophs cannot be expected to keep the nitrite concentration low enough to prevent NOB growth. On the other hand, AerAOB can theoretically outcompete nitrite oxidizers based on three characteristics. First, AerAOB have higher specific growth rates at temperatures from 20-35ºC (Hellinga et al., 1998). Therefore, low SRTs at higher temperatures will result in retention of AerAOB but washout of NOB. Second, low DO concentrations favor AerAOB, which have an oxygen half-saturation coefficient (K_O) (0.6 mg/l) at least as low or lower than NOB (2.2 mg/l) (Hao et al. 2002, Dytczak et al., 2008). Third, AerAOB are more tolerant of FA than NOB (Vadivelu et al., 2006, 2007, Anthonisen et al., 1976). By making use of these differences, systems can be engineered to selectively grow AerAOB to accumulate nitrite. In fixed film systems, washout is not a viable control parameter, as SRT approaches a practical infinity. NOB have been shown to colonize such systems despite control efforts (Fux et al., 2004). FA and free nitrous acid (FNA) are not easily controlled due to concentration and pH fluctuations, and NOB can become acclimated to FA (Turk & Mavinic, 1989). Hence, the question of excluding NOB from nitritation-anaerobic ammonium oxidation systems becomes one of how to control temperature and dissolved oxygen. A solution for this challenge is described in the next section and is investigated as part of the present work in this dissertation.

2.4 Hollow-fiber membranes as wastewater treatment devices

Membranes are well established in the wastewater treatment field, particularly in the context of solids separation (microfiltration) or effluent reuse/polishing (ultrafiltration, nanofiltration, and reverse osmosis) (Brindle and Stephenson, 1996). The use of membranes as bubbleless aeration devices and as biofilm support media are more recent developments, each warranting discussion.

2.4.1 Oxygen transfer and hollow fiber membrane configurations

Bubbleless oxygen transfer has several benefits, including higher nominal transfer efficiencies, potential for reduced loss of volatile compounds to the atmosphere, and reduced foaming associated with surfactants (Brindle and Stephenson, 1996). Furthermore, membrane oxygenation decouples reactor depth from oxygen transfer

efficiency, because fiber lumen pressure can be varied (Cote et al., 1988). Membranes have been used to oxygenate laboratory-scale wastewater treatment reactors, achieving 100% oxygen transfer efficiency when pressurized with pure oxygen (Ahmed and Semmens, 1992a, Pankhania et al., 1994).

Hollow-fiber aeration membranes fall into the category of having the downstream end either sealed to prevent outlet gas from leaving ("sealed-end") or open to allow outlet gas to flow through ("flow-through"). While 100% oxygen transfer efficiency and zero emissions of volatile organic compounds (VOCs) may be achieved with sealed-end fibers (Ahmed and Semmens, 1992a), there are advantages to using a flow-through fiber configuration. Depending on gas velocity, such a configuration allows removal of condensate as well as a more consistent gas phase oxygen concentration along the length of the fibers. The diffusion coefficient of water vapor in poly(dimethylsiloxane) (PDMS) has been reported to range from 0.5×10^{-6} to 1×10^{-6} cm^2/sec (Yeom et al., 1999, Watson and Payne, 1990), which is comparable to the oxygen diffusivity. While the very low solubility of water vapor in PDMS (0.53% v/v, Yeom et al., 1999) reduces the actual permeation of water vapor to well below the rate of oxygen permeation, the potential for fiber plugging from water vapor transport is still significant when one considers the time span over which a membrane aeration system is expected to operate. Thus, accumulation of condensed water vapor must be anticipated, a symptom that can be lessened by using a flow-through configuration.

In a sealed-end configuration, the lumen oxygen profile often tapers from that in the original gas composition at the inlet to zero at the terminal fiber end (Ahmed and Semmens, 1992b, Ahmed et al., 2004), resulting in unevenly distributed biofilm growth and the potential for clogging and channeling near the inlet. A flow-through fiber configuration with back-pressure control provides benefits of both approaches: elevated lumen pressure for reasonable oxygen transfer efficiencies (although less than 100%), an oxygen gradient less severe than observed in sealed-end systems, and some degree of flushing of condensation and other gases in the lumen.

2.4.2 Predictive models for bubbleless oxygen transfer

The ability to predict oxygen transfer in membrane systems is a key factor in wastewater treatment design. Consequences of undersizing or oversizing aeration systems include incomplete treatment and wasted expense. Much research has been dedicated to developing predictive models for aeration. Ahmed and Semmens (1992b) developed a model to predict the gas phase concentration and pressure along the length of a sealed-end microporous fiber and observed that only the first 35% of the fiber length had enough oxygen partial pressure for rapid oxygen transfer. The authors suggested that a fiber that allowed continuous flow through the lumen would likely increase the length of the fiber's oxic region. Furthermore, the flushing of accumulated nitrogen was predicted to have a greater effect on the oxic length than flushing of condensed water in the flow-through fiber. Johnson et al. (1998) created a predictive model for sealed-end fibers that were attached only at one end, with the other end allowed to flow freely over a submerged liquid orifice. The goal of such 'unconfined' membranes was to reduce head loss and prevent fouling with solids. Casey et al. (1999) showed a three-dimensional, cylindrical-coordinate model for co-substrate diffusion and reaction to be a good predictor of oxygen flux and performance in a membrane-aerated biofilm. These models and others have been shown to be accurate, although all require either assumption or measurement of mass transfer coefficients.

Many of the models developed are suitable for microporous membranes, in which the gas phase is essentially in contact and in equilibrium with the pore liquid at the base of the biofilm (Shanahan and Semmens, 2004). Oxygen gradients may occur in the micropores of the membranes. However, because these membranes are typically an order of magnitude thinner than non-porous membranes, and because the diffusion coefficient of oxygen in air is orders of magnitude higher than in non-porous materials such as PDMS, the gradients are expected to be much less severe. In the case of microporous membranes, the DO concentration in the pore liquid is relatively high and near saturation. In contrast, a non-porous membrane material such as silicone rubber follows a sorption-dissolution-diffusion mechanism and exhibits an oxygen gradient across the thickness of the membrane. The resulting membrane-biofilm interface DO concentration may be much

lower than saturation, thus influencing the identity and metabolic state of the organisms present there. Models for non-porous membranes are available, but again, are based on empirically-determined mass transfer coefficients (Sidhoum et al, 2003, Rector et al., 2004). There exists a need for a fundamental mechanistic oxygen transfer model based on material properties and dimensional data such as length, diameter, wall thickness, and packing density. Such a model would be amenable to different materials, membrane geometries, and reactor operating conditions without the need for mass transfer coefficient testing, provided that material-specific diffusion and partitioning coefficients are available for the material(s) of interest. The work in this dissertation presents the development of such a predictive oxygen transfer model for a non-porous HFMBR system, a model which can be applied to different non-porous materials and reactor configurations without measurement of new mass transfer coefficients.

2.4.3 HFMBRs as biofilm treatment systems

Biofilms offer unique advantages over suspended growth wastewater treatment reactors. Long solids retention times (SRTs) via biomass retention, spatial metabolic coupling of organisms, and resistance to shock loads are all characteristics of biofilm systems. A more recent incarnation of fixed film processes are biofilms grown on aeration membranes. These systems have the advantage of providing counter-current mass transfer of oxygen (or other gaseous species) from the substratum of the biofilm, in the opposite direction of nutrient diffusion from the bulk liquid. This counter-diffusion allows independent manipulation of both fluxes, resulting in a powerful operational control parameter for operators of such systems (Terada et al., 2007).

The body of research dealing with the application of HFMBRs to wastewater treatment includes both conventional and novel metabolic configurations. Pankhania et al. (1994) demonstrated the concept by treating (COD removal only) a synthetic municipal wastewater with sealed-end microporous hollow-fiber membranes. Membrane aerated biofilm reactors have also been used in an attempt to shortcut traditional nitrification and denitrification processes. Hibiya et al. (2003), treating an artificial domestic wastewater, found AerAOB present in the biofilm and heterotrophic bacteria distributed in the liquid

phase surrounding the biofilm. Nitrification rate declined along the length of the fiber, due to the plug flow nature of the liquid phase and the sealed-end configuration of the microporous membranes fibers. Nitritation-denitritation was inferred from the lack of NOB detected by FISH. A similar system (Terada et al., 2003) achieved carbon and nitrogen removal from artificial swine wastewater, inferring nitritation-denitritation through calculation of free ammonia and stoichiometric analysis of the oxygen consumed in the reactor.

Because the counter-current delivery of electron donor and acceptor yields microenvironments quite different from conventional co-current biofilms, much research has been directed at determining the microbial communities that develop in HFMBRs. In the aforementioned HFMBR treating artificial swine wastewater, AerAOB were detected primarily in the first 300 μm of biofilm located closest to the membrane surface, the region shown to be aerobic (Terada et al., 2003). Cole et al. (2004) showed a stratified microbial population using quantitative PCR (qPCR) for ammonia monooxygenaseA (*amoA)*, copper-containing nitrite reductase (*nirK)*, and haem-cytochrome cd_1-type nitrite reductase (*nirS)*, the last of which has not been found in the sequenced genomes of AerAOB. They found that for a high-shear biofilm (14 cm/sec surface velocity), as distance progressed outward from the flat sheet microporous membrane, the target genes peaked in the same order as listed above. For a low-shear biofilm (2 cm/sec), only *nirS* was found in significant amounts, and the stratification was absent. From this observation they were able to infer that fluid hydrodynamics have an effect on microbial population dynamics and activity, although specific relationships or correlations between shear and community structure were not taken further than that inference. LaPara et al. (2006) reported that the COD:N ratio influenced the microbial populations and activities of AerAOB and heterotrophs: when the ratio was 10:1 AerAOB and heterotrophs did not coexist. A ratio of 4:1 was proposed for optimization of nitrification and denitrification. Electrochemical microsensor probing of membrane aerated biofilms has often shown relatively small regions (<30%) of the biofilm nearest the membrane to be aerobic (Cole et al., 2004, Terada et al., 2003, Schramm et al., 2000), thus characterizing the microenvironments that define microbial populations and activities. Multipopulation

models of membrane-aerated biofilms have also been developed (Shanahan and Semmens, 2004, Matsumoto et al., 2007, Lackner et al., 2008) to predict performance and operating conditions suitable for carbon and nitrogen removal. In summary, these and other experimental and modeling studies demonstrate influences of nutrient and oxygen gradients, free ammonia, oxygen flux, fluid shear, and C:N ratio on performance and community composition for membrane-aerated biofilms.

The application of stratified biofilms grown on aeration membranes is relatively new with respect to processes with an anaerobic ammonium oxidation component. Gong et al. (2007) achieved nitritation coupled with anaerobic ammonium oxidation by wrapping a nonwoven carrier around carbon aeration tubes. Partial nitritation occurred in the aerobic region near the tubes while AnaerAOB activity was observed in the region of the fabric closest to the bulk liquid, as illustrated by FISH and *ex situ* activity tests. The authors reported additional data elsewhere (Gong et al., 2008), namely that PCR and DGGE showed high enrichment of *Nitrosomonas*-like AerAOB and AnaerAOB of the Phylum Planctomycetes. However, the sequential seeding technique of Gong et al. (2007) allowed for deposition of seed organisms throughout the non-woven carrier matrix. This is in contrast to the manner in which a biofilm would grow in the absence of an external inert support matrix, in which initial attachment can only occur at the membrane surface. As a result, a true membrane-aerated nitritation-anaerobic ammonium oxidation biofilm with no supplemental structural element has not yet been reported. The research described in this dissertation may be the first successful coupling of these two autotrophic metabolisms in an HFMBR.

2.5 Nitrogen emissions

2.5.1 Metabolic pathways generating nitrogen oxide emissions

In 1964, Anderson demonstrated that whole cells of *Nitrosomonas* anaerobically converted hydroxylamine to a mixture of $NO_{(g)}$ and nitrous oxide $N_2O_{(g)}$. Although these gases were incorrectly postulated to be intermediates that formed between hydroxylamine (NH_2OH) and nitrite in the aerobic ammonia oxidation pathway, the findings of this work laid the foundation for much of the subsequent research characterizing the reactions

involved. Poth and Focht (1985) were the first to show that $N_2O_{(g)}$ was produced by *N. europaea* by a denitrification pathway rather than directly from ammonia oxidation.

In low dissolved oxygen (DO) conditions, AerAOB are capable of autotrophically denitrifying NO_2^- to $NO_{(g)}$ and $N_2O_{(g)}$ with ammonium as the electron donor (Poth and Focht, 1985, Schmidt and Bock, 1997, 1998, Kester et al. 1997). Genome sequencing of several AerAOB have confirmed the presence of genes coding for the enzymes responsible, nitrite reductase (Nir) and nitric oxide reductase (Nor) (Chain et al., 2003, Stein et al., 2007). Some research has also detected $N_{2(g)}$ production in cell-free extracts from *N. eutropha* (Schmidt and Bock, 1997) and whole cells of a Nitrosomonad (Poth, 1986), but AerAOB genomes sequenced to date have failed to reveal coding sequences for nitrous oxide reductase (Nos), indicating that AerAOB probably cannot generate $N_{2(g)}$ during autotrophic denitrification. Formation of $NO_{(g)}$ and $N_2O_{(g)}$ is also possible via denitritation/denitrification of NO_2^- and NO_3^- by heterotrophic microorganisms in anoxic conditions (Kester et al., 1997, Tallec et al., 2006b), though these are typically further reduced to $N_{2(g)}$. Even in carbon-limited systems, endogenous decay products are a potential carbon source for denitrification (Lackner et al., 2008), which can generate gaseous emissions of $NO_{(g)}$ and $N_2O_{(g)}$. Mixed cultures exhibit complex behaviors with respect to gaseous emissions. Kester et al. (1997) showed that co-culturing *N. europaea* with *Nitrobacter winogradsky* reduced emissions compared to *N. europaea* alone. The reactor conditions of conventional, fully aerobic secondary treatment systems are rarely conducive to the generation of appreciable emissions from autotrophic denitrification, but nutrient removal and advanced N processes that frequently invoke low DO conditions are susceptible to producing emissions.

2.5.2 Emissions source tracking

Ascertaining the source of biological emissions can be difficult in mixed culture systems, due to the diversity of metabolic groups for which these compounds are intermediates. Three methods that have been used in attempts to track sources are: kinetic modeling; isotope fractionation; and activity measurements using inhibitors that target selected microbial groups.

First, a modeling approach is founded in the apparent differences in kinetic parameters between autotrophic nitrification, autotrophic denitrification, and heterotrophic denitrification. By tracking the evolution of N oxides in lab-scale reactors and comparing results to model predictions, Kampschreur et al. (2007) determined that in a lab-scale reactor treating a carbon-free ammonium-based wastewater, autotrophic denitrification was the primary source of $NO_{(g)}$ emissions. However, broad application of such an approach may be limited, as $NO_{(g)}$ emissions patterns from autotrophic denitrification and heterotrophic denitrification were similar and may not be resolvable from the variability associated with full-scale operating data.

Second, fractionation between $^{14}N^{15}NO_{(g)}$ and $^{15}N^{14}NO_{(g)}$ has been hypothesized to be influenced by preference of enzymes for the lighter isotope at the alpha position ($^{\beta}N$-$^{\alpha}N$-O) in the molecule and, as a result, is an indicator of the source of biologically-produced $N_2O_{(g)}$. However, hypothetical models and observed fractionations diverge. A review by Stein and Yung (2003) describes these phenomena in detail. Nitric oxide reductase (Nor) enzymes can be classified as P-450nor (denitrifying fungi), cNOR (in the most common denitrifying bacteria), or qNOR (non-denitrifying pathogenic bacteria) (Stein and Yung, 2003). While the exact type of Nor enzyme in AerAOB is not known, qNOR is associated with detoxification of NO and does not require energy conservation at each step (Stein and Yung, 2003), properties that would seem appropriate for AerAOB denitrification. The reduction mechanisms of cNOR and qNOR are also unknown though they are likely to follow one of two mechanistic patterns. First, a sequential mechanism would involve one NO molecule binding before the other, creation of an N=N double bond, liberating 2 electrons, and, with the addition of 2 H^+, formation of water. In this mechanism, site preference for ^{14}N could lead to isotope fractionation. Second, a simultaneous mechanism would involve each NO molecule binding at the same time, followed by the same catalytic events. For this mechanism, no preference for the lighter isotope would be expected. It was hypothesized by Yoshida and Toyoda (2000), and subsequently described by Stein and Yung (2003), that in microbial systems dominated by nitrification, the ratio of $^{14}N^{15}NO_{(g)}$ to $^{15}N^{14}NO_{(g)}$ should be relatively low. This would be explainable by the preferential reduction of $^{14}NO_2^-$ over $^{15}NO_2^-$, leading to an enriched

fraction of $^{14}NO_{(g)}$.. The subsequent step, reduction of $NO_{(g)}$ to $N_2O_{(g)}$, would then enrich for the ^{14}N at the alpha position. Because genes for nitrous oxide reductase have yet to be found in AerAOB genome sequences, the nitrous oxide produced is likely the terminal step in this scenario and the off-gas would be enriched for $^{15}N^{14}NO_{(g)}$. On the other hand, for systems with heterotrophic denitrifiers, nitrous oxide is subsequently reduced to nitrogen gas by nitrous oxide reductase. If the assumption of preference for the lighter isotope holds for this enzyme, the $^{15}N^{14}NO_{(g)}$ will be preferentially reduced and the enrichment of $^{15}N^{14}NO_{(g)}$ over $^{14}N^{15}NO_{(g)}$ will be less pronounced, if at all.

Thirdly, activity measurements for N oxide emissions are a natural extension of methods used to parse parameters such as oxygen uptake rate among different populations. However, activity tests require a suitable source of biomass, and the tests are essentially destructive, meaning the biomass is rarely returned to the reactor. For biofilm systems especially, the biomass cannot be returned to its native state. Furthermore, in an HFMBR, removal of biomass from the substratum creates a new, high-DO niche environment that influences which microbial populations recolonize the membrane, affects the overall structure of the microbial community, and influences system performance. In summary, identification of the source of nitrogen oxide emissions is complex and is not investigated in this work. However, the quantities of gaseous emissions over time in an autotrophic N removal HFMBR is examined and compared to N removal performance and microbial community dominance during the same periods. This characterization provides insight into the operating conditions that lead to the net production of deleterious emissions in such systems.

2.5.3 Nitrogen oxides in the environment

Oxides of nitrogen, which are both natural and anthropogenic, have detrimental effects on the atmosphere and have toxic properties. $NO_{(g)}$, although not currently included in the U.S. National Ambient Air Quality Standards (NAAQS) for criteria pollutants, can be oxidized either through molecular oxygen or via reaction with hydroxyl radical and VOC to nitrogen dioxide ($NO_{2(g)}$). These two compounds ($NO_{(g)}$ and $NO_{2(g)}$) contribute to the formation of atmospheric nitric acid (HNO_3) and tropospheric (ground level) ozone,

which is also a criteria pollutant and causes respiratory impairment (Finlayson-Pitts and Pitts, 2000).

Nitrous oxide contributes to stratospheric ozone destruction as well as increased atmospheric radiation absorption ("greenhouse effect") in the 8 to 9 μm wavelength window. While $N_2O_{(g)}$ emissions are a small fraction of the total U. S. Greenhouse Gas Inventory (US D.O.E., 2005), the global warming potential of $N_2O_{(g)}$ is 300 times that of CO_2, due to its long life in the atmosphere (Finlayson-Pitts and Pitts, 2000). As a result, emissions of these compounds are of concern, and wastewater treatment systems have the potential to be significant sources, as discussed below.

2.5.4 Emissions from wastewater treatment systems

Only in recent years have researchers begun to investigate the impact of nitrogen oxide emissions from wastewater treatment systems, particularly in the context of $N_2O_{(g)}$ and its relationship to global climate change. While agricultural sources (nitrogen fertilization of soils, solid wastes of animals, crop residue burning) are by far the largest source of $N_2O_{(g)}$ (280 million metric tons in CO_2 equivalents, Mmt-CO_2), and CO_2 (6,000 Mmt-CO_2) and methane emissions (600 Mmt-CO_2) are an order of magnitude greater still, overall N_2O emissions from wastewater treatment facilities have increased over the past decade (U.S. Dept. of Energy, 2005), as shown in Figure 2.1. This increase may be related to the trend toward more advanced treatment (nitrification, total nitrogen removal) and also low-DO processes (nitritation, denitrification) at POTWs (Love et al., 2008). Regardless of the driver, the emissions trend requires engineers to direct more attention at characterizing and controlling these emissions.

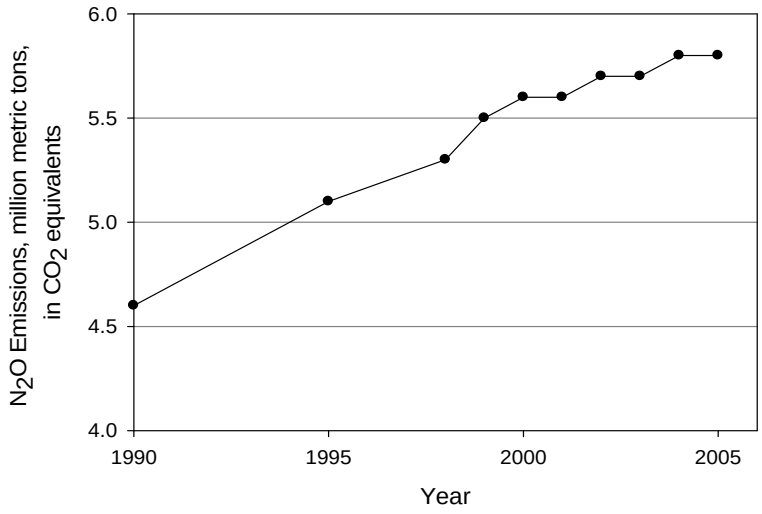

Figure 2.1. Trend in N_2O emissions from U. S. WWTPs. Created from data in: Energy Information Administration, U. S. DOE, Report#:DOE/EIA-0573(2005), Emissions of Greenhouse Gases in the United States, 2005.

Kampschreur et al. (2008) studied the $NO_{(g)}$, $NO_{2(g)}$, and $N_2O_{(g)}$ emissions from both a nitritation and an anaerobic ammonium oxidation reactor treating sludge digestion and dewatering recycle streams. Emissions of $N_2O_{(g)}$ were 1-2 orders of magnitude higher than those of $NO_{(g)}$, and $N_2O_{(g)}$ was attributed primarily to AerAOB. The most important factors influencing the rate of emissions were DO, NO_2^- concentration, and aeration rate. Based on comparison of reactor conditions with available literature, most of the $NO_{(g)}$ formed was speculated to be from AerAOB, but the potential for $NO_{(g)}$ emissions from AnaerAOB was not ruled out. In addition, the same study (Kampschreur et al., 2008) examined emissions from several full-scale nitritation and anaerobic ammonium oxidation systems and found $NO_{(g)}$ and $N_2O_{(g)}$ emissions ranging from negligible to over 60 ppm and 4,000 ppm, respectively (up to 0.3% and 7%, respectively, of the "N converted" in the reactor). In laboratory batch tests with varying oxygenation and methanol feed conditions, Tallec et al. (2006b) measured $N_2O_{(g)}$ emissions of up to 1% of the ammonia nitrogen oxidized using biomass from a full-scale immersed biofilter. Emissions peaked around a DO of approximately 1 mg/l. Emissions during denitrification were related to the methanol to nitrate ratio, peaking at 1.3% of the reduced nitrate-nitrogen. Another study (Tallec et al., 2006a) found that the $N_2O_{(g)}$ emissions from activated sludge batch tests were approximately 0.4% of the ammonia-nitrigen oxidized.

Again, peak emissions occurred at a DO of 1 mg/l. Using selective inhibitors, they attributed 58-83% of the total $N_2O_{(g)}$ emission to autotrophic denitrification as opposed to heterotrophic denitrification. Others have observed emissions that comprised 8-16% of the total N removed (Mao et al., 2006) and even 32-40% of the total N removed (Okayasu et al., 1997), both studies using a sequencing batch reactor. Although authors are not always clear as to whether these emissions percentages are based on reporting gas species 'as nitrogen,' these studies nonetheless illustrate the significance of $N_2O_{(g)}$ emissions from wastewater treatment systems, regardless of the source within the microbial community. The large range in reported percentages also underscores the complicated effects of multiple control variables on the types and quantities of emissions.

Control of N-oxide emissions is complicated due to the varied sources and contributing factors. This discussion will focus on control of emissions from autotrophic AerAOB. Dissolved oxygen concentration has been shown to have a significant impact on $N_2O_{(g)}$ generation in pure culture *Nitrosomonas* studies (Shrestha et al., 2001, Kester et al., 1997), implying that emissions can be eliminated by increasing oxygenation. However, this control will also strongly influence the predominant N removal metabolisms and microbial populations and, as such, may not be an option for some systems. More recently, nitrite concentration and pH have been implicated as factors contributing to $N_2O_{(g)}$ generation in an autotrophic wastewater treatment reactor (Shiskowski and Mavinic, 2006). The authors postulated that the increase in extracellular NO_2^- concentration resulted in saturation of enzyme active sites located in the periplasmic space, leading to increased activity of the periplasmic enzyme Nir and cytoplasmic membrane-bound enzyme Nor (active site on the periplasmic side) (Averill, 1996). In addition, their observations with respect to pH suggested that nitrous acid is the substrate for Nir, as opposed to NO_2^- itself. Finally, Beaumont et al. (2004) examined the effect of NO_2^- on N oxide production, finding that a nitrite-sensitive transcription repressor (NsrR) appeared to regulate expression of *nirK* in *N. europaea*. As nitrite concentration increased and bound to NsrR, de-repression occurred along with increased expression of *nirK*. This effect was less at pH 8.2 than at pH 7.2, suggesting that nitrous acid was binding with and influencing the activity of the regulatory enzyme. Together, these studies suggest that N

oxide emissions from mixed-culture wastewater treatment reactors can be minimized if, a) nitrite concentrations are minimized by coupling processes that produce and consume nitrite (e.g., nitritation-anaerobic ammonium oxidation), and b) the systems can be operated at pH levels above neutral to minimize nitrous acid. Investigation of these control strategies has received limited or no attention in HFMBR and nitritation-anammox processes.

2.6 Justification for this work

The need for sustainable nutrient removal led us to investigate the effectiveness of an oxygen-limited coupled nitritation-anaerobic ammonium oxidation hollow-fiber membrane-aerated biofilm system treating a synthetic high-nitrogen waste stream. Past work reported in the literature made it clear that the success of our system would rely on the precise control of oxygen delivery from the membrane to the biofilm. To assist with our desire to improve predictive oxygen transfer capabilities in HFMBRs, we created a new mechanistic oxygen transfer model, which is described in Chapter 3. Furthermore, a laboratory-scale HFMBR was built and operated to test the startup, performance, stability, and operating conditions of a nitritation-anaerobic ammonium oxidation biofilm community and is reported in Chapter 4. Because of their detrimental impact on atmospheric quality and climate change, nitrogen oxide emissions were monitored and strategies for controlling these emissions were evaluated. Biofilm structure and microbial community composition were investigated to further understand how biofilms with nitritation coupled to anaerobic ammonium oxidation in HFMBRs function, so that we can more effectively apply operational and control strategies to optimize performance.

References

United States. Dept. of Energy. Energy Information Administration. Emissions of Greenhouse Gases in the United States. DOE/EIA-0573 Washington: GPO, 2005.

Ahmed, T. and Semmens, M.J. (1992a) Use of sealed end hollow fibers for bubbleless membrane aeration: experimental studies. *J. Membr. Sci.* **69**(1-2):1-10.

Ahmed, T. and Semmens, M.J. (1992b) The use of independently sealed microporous hollow fiber membranes for oxygenation of water: model development. *J. Membr. Sci.* **69**(1-2):11-20.

Ahmed, T., Semmens, M.J. and Voss, M.A. (2004) Oxygen transfer characteristics of hollow-fiber, composite membranes. *Adv. in Environ. Res.* **8**(3-4):637-646.

Anthonisen, A.C., Loehr, R.C., Prakasam, T.B.S. and Srinatu, E.G. (1976) Inhibition of nitrification by ammonia and nitrous acid. *J. Wat. Pollut. Control Fed.* **48**:835-852.

Archer, S.D., Hitchens, D., Jabs, H.S., Campbell, A.K. and Edeen, M.A. (1999) A high efficiency magnetic activated sludge reactor for wastewater processing, SAE, 29th Intl. Conf. on Environ. Systems, Denver, CO.

Beaumont, H.J.E., Lens, S.I., Reijnders, W.N.M., Westerhoff, H.V. and van Spanning, R.J.M. (2004) Expression of nitrite reductase in *Nitrosomonas europaea* involves NsrR, a novel nitrite-sensitive transcription repressor. *Molec. Microbiol.* **54**(1):148-158.

Berends, D.H.J.G., Salem, S., van der Roest, H.F. and van Loosdrecht, M. (2005) Boosting nitrification with the BABE technology. *Water Sci. Technol.* **52**(4):63-70.

Brindle, K. and Stephenson, T. (1996) The application of membrane biological reactors for the treatment of wastewaters. *Biotechnol. Bioeng.* **49**(6):601-610.

Broda, E. (1977) Two kinds of lithotrophs missing in nature. *Zeit. Allg. Mikrobiol.* **17**(6):491-493.

Casey, E., Glennon, B. and Hamer, G. (1999) Oxygen mass transfer characteristics in a membrane-aerated biofilm reactor. *Biotechnol. Bioeng.* **62**(2):183-192.

Chain, P., Lamerdin, J., Larimer, F., Regala, W., Lao, V., Land, M., Hauser, L., Hooper, A., Klotz, M., Norton, J., Sayavedra-Soto, L., Arciero, D., Hommes, N., Whittaker, M. and Arp, D. (2003) Complete genome sequence of the ammonia-oxidizing bacterium and obligate chemolithoautotroph *Nitrosomonas europaea*. *J. Bacteriol.* **185**(9):2759-2773.

Chandrasekeran, P., Urgun-Demirtas, M. and Pagilla, K.R. (2007) Aerobic membrane bioreactor for ammonium-rich wastewater treatment. *Water. Environ. Res.* **79**(11):2352-2362.

Cole, A.C., Semmens, M.J. and LaPara, T.M. (2004) Stratification of activity and bacterial community structure in biofilms grown on membranes transferring oxygen. *Appl. Environ. Microbiol.* **70**(4):1982-1989.

Cote, P., Bersillon, J.-L. and Faup, G. (1988) Bubble free aeration using membranes: Process analysis. *J. Wat. Pollut. Contr. Fed.* **60**(11):1986-1992.

Damste, J.S.S., Rijpstra, W.I.C., Geenevasen, J.A.J., Strous, M. and Jetten, M.S.M. (2005) Structural identification of ladderdane and other membrane lipids of planctomycete capable of anaerobic ammonium oxidation (anammox). *FEBS J.* **272**:4270-4283.

Dytczak, M. A., Londry, K. L., Oleszkiewicz, J. A. (2008) Activated sludge operational regime has significant impact on the type of nitrifying community and its nitrification rates. *Water Res.* **42**:2320-2328.

Finger, B.W., Supra, L.N., DallBauman, L. and Pickering, K.D. (1999) Development and testing of membrane biological wastewater processors, SAE, 29th Intl. Conf. on Environ. Systems, Denver, CO.

Finlayson-Pitts, B.J. and Pitts, J.N. (2000) Chemistry of the upper and lower atmosphere: theory, experiments, and applications. Academic Press, San Diego.

Fujii, T., Sugino, H., Rouse, J.D. and Furukawa, K. (2002) Characterization of the microbial community in an anaerobic ammonium-oxidizing biofilm cultured on a nonwoven biomass carrier. *J. Bioscience Bioeng.* **94**(5):412-418.

Furukawa, K., Lieu, P.K., Tokitoh, H. and Fujii, T. (2006) Development of single-stage nitrogen removal using anammox and partial nitritation (SNAP) and its treatment performances. *Water Sci. Technol.* **53**(6):83-90.

Fux, C., Huang, D., Monti, A. and Siegrist, H. (2004) Difficulties in maintaining long-term partial nitritation of ammonium-rich sludge digester liquids in a moving-bed biofilm reactor (MBBR). *Water Sci. Technol.* **49**(11-12):53-60.

Fux, C., Lange, K., Faessler, A., Huber, P., Grueniger, B. and Siegrist, H. (2003) Nitrogen removal from digester supernatant via nitrite - SBR or SHARON? *Water Sci. Technol.* **48**(8):9-18.

Gilmore, K.R., Capuno, R.E., Love, N.G. and Smets, B.F. (2006) Anaerobic stabilization of early plantary base ersatz wastewater formulation. SAE Technical Paper Series 2006-01-2255, SAE, Norfolk, VA.

Gong, Z., Liu, S., Yang, F., Bao, H. and Furukawa, K. (2008) Characterization of functional microbial community in a membrane-aerated biofilm reactor operated for completely autotrophic nitrogen removal. *Biores. Technol.* **99**(8):2749-2756.

Gong, Z., Yang, F., Liu, S., Bao, H., Hu, S. and Furukawa, K. (2007) Feasibility of a membrane-aerted biofilm reactor to achieve single-stage autotrophic nitrogen removal based on anammox. *Chemosphere*. **69**:776-784.

Gu, A.Z., Pedros, P.B., Kristiansen, A., Onnis-Hayden, A. and Schramm, A. (2007) Nitrifying community analysis in a single submerged attached-growth bioreactor for treatment of high-ammonia waste stream. *Water Environ. Res.* **79**(13):2510-2518.

Hao, X., Heijnen, J.J. and van Loosdrecht, M.C.M. (2002) Sensitivity analysis of a biofilm model describing a one-stage completely autotrophic nitrogen removal (CANON) process. *Biotechnol. Bioeng.* **77**(3):266-277.

Head, M.A. and Oleszkiewicz, J. (2005) Bioaugmentation with nitrifying bacteria acclimated to different temperatures. *J. Environ. Eng.* **131**(7):1046-1051.

Hellinga, C., Shellen, A.A.J.C., Mulder, J.W., van Loosdrecht, M.C.M. and Heijnen, J.J. (1998) The SHARON process: an innovative method for nitrogen removal from ammonium-rich waste water. *Water Sci. Technol.* **37**(9):135-142.

Helmer, C., Tromm, C., Hippen, A., Rosenwinkel, K.-H., Seyfried, C.F. and Kunst., S. (2001) Single stage biological nitrogen removal by nitritation and anaerobic ammonium oxidation in biofilm systems. *Water Sci. Technol.* **43**(1):311-320.

Hibiya, K., Terada, A., Tsuneda, S. and Hirata, A. (2003) Simultaneous nitrification and denitrification by controlling vertical and horizontal microenvironment in a membrane-aerated biofilm reactor. *J. Biotechnol.* **100**:23-32.

Isaka, K., Date, Y., Sumino, T., Yoshie, S. and Tsuneda, S. (2006) Growth characteristic of anaerobic ammonium-oxidizing bacteria in an anaerobic biological filtrated reactor. *Appl. Microbiol. Biotechnol.* **70**(1):47-52.

Jenicek, P., Svehla, P., Zabranska, J. and Dohanyos, M. (2004) Factors affecting nitrogen removal by nitritation/denitritation. *Water Sci. Technol.* **49**(5-6):73-79.

Johnson, D.W., Semmens, M.J. and Gulliver, J.S. (1998) Unconfined membranes: transfer performance and module design. *J. Membr. Sci.* **140**:13-25.

Kampschreur, M.J., Picioreanu, C., Tan, N., Kleerebezem, R., Jetten, M.S.M. and van Loosdrecht, M.C.M. (2007) Unraveling the source of nitric oxide emission during nitrification, IWA, Nutrient Removal 2007, Baltimore, MD.

Kampschreur, M.J., van der Star, W.R.L., Wielders, H.A., Mulder, J.W., Jetten, M.S.M. and van Loosdrecht, M.C.M. (2008) Dynamics of nitric oxide and nitrous oxide emission during full-scale reject water treatment. Water Research **42**(3), 812-826.

Katehis, D., Diyamandoglu, V. and Fillos, J. (1998) Stripping and recovery of ammonia from centrate of anaerobically digested biosolids at elevated temperatures. *Water Environ. Res.* **70**(2):231-240.

Kester, R.A., de Boer, W. and Laanbroek, H.J. (1997) Production of NO and N_2O by pure cultures of nitrifying and denitrifying bacteria during changes in aeration. *Appl. Environ. Microbiol.* **63**(10):3872-3877.

Kuai, L. and Verstraete, W. (1998) Ammonium removal by the oxygen-limited autotrophic nitrification-denitrification system. *Appl. Environ. Microbiol.* **64**(11):4500-4506.

Lackner, S., Terada, A. and Smets, B.F. (2008) Heterotrophic activity compromises autotrophic nitrogen removal in membrane-aerated biofilms: Results of a modeling study. *Water Res.* **42**(4-5):1102-1112.

Lai, E., Senkpiel, S., Solley, D. and Keller, J. (2004) Nitrogen removal of high strength wastewater via nitritation/denitritation using a sequencing batch reactor. *Water Sci. Technol.* **50**(10):27-33.

LaPara, T.M., Cole, A.C., Shanahan, J.W. and Semmens, M.J. (2006) The effects of organic carbon, ammoniacal-nitrogen, and oxygen partial pressure on the stratification of membrane-aerated biofilms. *J. Ind. Microbiol. Biotechnol.* **33**:315-323.

Larsen, T.A. and Gujer, W. (1996) Separate management of anthropogenic nutrient solutions (human urine). *Water Sci. Technol.* **34**(3-4):87-94.

Love, N.G., Bronk, D. and Mulholland, M.R. (2008) Nutrients and their effects on the environment. In *Biological and Chemical Systems for Nutrient Removal*. WEF, Alexandra, VA.

Mao, J., Jiang, X.-Q., Yang, L.-Z., Zhang, J., Qiao, Q.-Y., He, C.-D. and Yin, S.-X. (2006) Nitrous oxide production in a sequence batch reactor wastewater treatment system using synthetic wastewater. *Pedosphere*. **16**(4):451-456.

Matsumoto, S., Terada, A. and Tsuneda, S. (2007) Modeling of membrane-aerated biofilm: Effects of C/N ratio, biofilm thickness and surface loading of oxygen on feasibility of simultaneous nitrification and denitrification. *Biochem. Eng. J.* **37**(1):98-107.

Maurer, M., Pronk, W. and Larsen, T.A. (2006) Treatment processes for source-separated urine. *Water Res.* **40**(17):3151-3166.

Muirhead, D., Rector, T., Jackson, W.A., Keister, H., Morse, A., Rainwater, K. and Pickering, K.D. (2003) Performance of a small scale biological water recovery system., SAE, 33rd Intl. Conf. on Environ. Systems, Vancouver, B.C.

Mulder, J.W., van Loosdrecht, M.C.M., Hellinga, C. and van Kempen, R. (2001) Full-scale application of the SHARON process for treatment of rejection water of digested sludge dewatering. *Water Sci. Technol.* **43**(11):127-134.

Okayasu, Y., Abe, I. and Matsuo, Y. (1997) Emission of nitrous oxide from high-rate nitrification and denitrification by mixed liquor circulating process and sequencing batch reactor process. *Water Sci. Technol*. **36**(12):39-45.

Pankhania, M., Stephenson, T. and Semmens, M.J. (1994) Hollow-fiber bioreactor for waste-water treatment using bubbleless membrane aeration. *Water Res.* **28**(10):2233-2236.

Pickering, K.D. and Edeen, M.A. (1998) Lunar-Mars life support test project phase III water recovery system operation and results., SAE, 28th Intl. Conf. on Environ. Systems, Danvers, MA.

Pollice, A., Tandoi, V. and Lestingi, C. (2002) Influence of aeration and sludge retention time on ammonium oxidation to nitrite and nitrate. *Water Res.* **36**:2541-2546.

Poth, M. (1986) Dinitrogen production from nitrite by a *Nitrosomonas* isolate. *Appl. Environ. Microbiol.* **52**(4):957-959.

Poth, M. and Focht, D.D. (1985) ^{15}N Kinetic analysis of N_2O production by *Nitrosomonas europaea*: an examination of nitrifier denitrification. *Appl. Environ. Microbiol.* **49**(5):1134-1141.

Pynaert, K., Smets, B.F., Beheydt, D. and Verstraete, W. (2004) Start-up of autotrophic nitrogen removal reactors via sequential biocatalyst addition. *Environ. Sci. Technol.* **38**:1228-1235.

Rector, T., Garland, J., Strayer, R.F., Levine, L., Roberts, M. and Hummerick, M. (2004) Design and preliminary evaluation of a novel gravity independent rotating biological membrane reactor, SAE, Colorado Springs, CO.

Schalk, J., Oustad, H., Kuenen, J.G. and Jetten, M.S.M. (1998) The anaerobic oxidation of hydrazine: a novel reaction in microbial nitrogen metabolism. *FEMS Microbiol. Lett.* **158**(1):61-67.

Schmidt, I. and Bock, E. (1997) Anaerobic ammonia oxidation with nitrogen dioxide by *Nitrosomonas eutropha*. *Arch. Microbiol*. **167**:106-111.

Schmidt, I. and Bock, E. (1998) Aerobic ammonia oxidation by cell-free extracts of *Nitrosomonas eutropha. Antonie van Leeuwenhoek.* **73**:271-278.

Schramm, A., Beer, D.D., Gieseke, A. and Amann, R. (2000) Microenvironments and distribution of nitrifying bacteria in a membrane-bound biofilm. *Environ. Microbiol.* **2**(6):680-868.

Shanahan, J.W. and Semmens, M.J. (2004) Multipopulation model of membrane-aerated biofilms. *Environ. Sci. Technol.* **38**(11):3176-3183.

Shiskowski, D.M. and Mavinic, D.S. (2006) The influence of nitrite and pH (nitrous acid) on aerobic-phase, autotrophic N_2O generation in a wastewater treatment bioreactor. *J. Environ. Eng. Sci.* **5**(4):273-283.

Shrestha, N.K., Hadano, S., Kamachi, T. and Okura, I. (2001) Conversion of ammonia to dinitrogen in wastewater by *Nitrosomonas europaea*. *Appl. Biochem. Biotechnol.* **90**(3):221-232.

Sidhoum, M., Christodoulatos, C., Ponce-Garcia, E. and Koutsospyros, A. (2003) Grey water treatment under microgravity conditions: mass transfer and kinetic studies, SAE, Vancouver, B.C.

Sliekers, A.O., Third, K.A., Abma, W., Kuenen, J.G. and Jetten, M.S.M. (2003) CANON and anammox in a gas-lift reactor. *FEMS Microbiol. Lett.* **218**:339-344.

Sliekers, O.A., Derwort, N., Gomez, J.L.C., Strous, M., Kuenen, J.G. and Jetten, M.S.M. (2002) Completely autotrophic nitrogen removal over nitrite in one single reactor. *Water. Res.* **36**:2475-2482.

Smith, D.P., Rector, T., Reid-Black, K., Hummerick, M., Strayer, R., Birmele, M., Roberts, M.S. and Garland, J.L. (2008) Redox control bioreactor: A unique biological water processor. *Biotechnol. Bioeng.* **99**(4):830-845.

Stein, L.Y., Arp, D.J., Berube, P.M., Chain, P.S.G., Hauser, L., Jetten, M.S.M., Klotz, M.G., Larimer, F.W., Norton, J.M., Op den Camp, H.J.M., Shin, M. and Wei, X. (2007) Whole-genome analysis of the ammonia-oxidizing bacterium, *Nitrosomonas eutropha* C91: implications for niche adaptation. *Environ. Microbiol.* **9**(12):2993-3007.

Stein, L.Y. and Yung, Y.L. (2003) Production, isotopic composition, and atmospheric fate of biologically produced nitrous oxide. *Annu. Rev. Earth Planet. Sci.* **31**(1):329-356.

Strayer, R.F., Alazraki, M.P., Judkins, J., Adams, J., Garland, J. and Hsu, V. (1999) Development and testing of inocula for biodegradation of Igepon under denitrifying conditions., SAE, 29th Intl. Conf. on Environ. Systems, Denver, CO.

Strous, M., Pelletier, E., Mangenot, S., Rattei, T., Lehner, A., Taylor, M. W., Horn, M., Daims, H., Bartol-Mavel, D., Wincker, P., Barbe, V., Fonknechten, N., Vallenet,

D., Segurens, B., Schenowitz-Truong, C., Medigue, C., Collingro, A., Snel, B., Dutilh, B. E., Op den Camp, H. J. M., van der Drift, C., Cirpus, I., van de Pas-Schoonen, K. T., Harhangi, H. R., van Niftrik, L., Schmid, M., Keltjens, J., van de Vossenberg, J., Kartal, B., Meier, H., Frishman, D., Huynen, M. A., Mewes, H.-W., Weissenback, J., Jetten, M. S. M., Wagner, M., Le Paslier, D. (2006) Deciphering the evolution and metabolism of an anammox bacterium from a community genome. *Nature.* **440**(7085):790-794.

Strous, M., Kuenen, J.G. and Jetten, M.S.M. (1999) Key physiology of anaerobic ammonium oxidation. *Appl. Environ. Microbiol.* **65**(7):3248-3250.

Strous, M., Fuerst, J.A., Kramer, E.H.M., Logemann, S., Muyzer, G., van de Pas-Schoonen, K.T., Webb, R., Kuenen, J.G. and Jetten, M.S.M. (1999) Missing lithotroph identified as new planctomycete. *Nature*. **400**(6743):446-449.

Strous, M., Gerven, E.V., Zheng, P., Kuenen, J.G. and Jetten, M.S.M. (1997) Ammonium removal from concentrated waste streams with the anaerobic ammonium oxidation (Anammox) process in different reactor configurations. *Water Res.* **31**(8):1955-1962.

Strous, M., Heijnen, J.J., Kuenen, J.G. and Jetten, M.S.M. (1998) The sequencing batch reactor as a powerful tool for the study of slowly growing anaerobic ammonium-oxidizing microorganisms. *Appl. Microbiol. Biotechnol.* **50**:589-596.

Supra, L.N., Reddig, M.A., Finger, B.W., Zhou, S.J. and DallBauman, L. (1998) Membrane-based bioprocessor for life support wastewater reclamation, SAE, 28th Intl. Conf. on Environ. Systems, Danvers, MA.

Tallec, G., Garnier, J., Billen, G. and Gousailles, M. (2006a) Nitrous oxide emissions from secondary activated sludge in nitrifying conditions of urban wastewater treatment plants: effect of oxygenation level. *Water Res.* **40**:2972-2980.

Tallec, G., Garnier, J. and Gousailles, M. (2006b) Nitrogen removal in a wastewater treatment plant through biofilters: nitrous oxide emissions during nitrification and denitrification. *Bioprocess Biosyst. Eng.* **29**:323-333.

Terada, A., Hibiya, K., Nagai, J., Tsuneda, S. and Hirata, A. (2003) Nitrogen removal characteristics and biofilm analysis of a membrane-aerated biofilm reactor applicable to high-strength nitrogenous wastewater treatment. *J. Bioscience Bioeng.* **95**(2):170-178.

Third, K.A., Paxman, J., Schmid, M., Strous, M., Jetten, M.S.M. and Cord-Ruwisch, R. (2005) Enrichment of anammox from activated sludge and its application in the CANON process. *Microbial Ecology*. **49**:236-244.

Turk, O. and Mavinic, D.S. (1989) Maintaining nitrite build-up in a system acclimated to free ammonia. *Water Res.* **23**(11):1383-1388.

Udert, K.M., Fux, C., Munster, M., Larsen, T.A., Siegrist, H. and Gujer, W. (2003) Nitrification and autotrophic denitrification of source-separated urine. *Water Sci. Technol.* **48**(1):119-130.

Vadivelu, V.M., Keller, J. and Yuan, Z. (2006) Effect of free ammonia and free nitrous acid concentration on the anabolic and catabolic processes of an enriched *Nitrosomonas* culture. *Biotechnol. Bioeng.* **95**(5):830-839.

Vadivelu, V.M., Keller, J. and Yuan, Z. (2007) Effect of free ammonia on the respiration and growth processes of an enriched *Nitrobacter* culture. *Water Res.* **41**(4):826-834.

Valadez, V.A., Koenig, D.W. and Pierson, D.L. (1998) Utilization of the space station detergent IGEPON by a candidate organism for use in a space biological waste reactor., SAE, 28th Intl. Conf. on Environ. Systems, Danvers, MA.

van de Graaf, A.A., de Bruijn, P., Robertson, L.A., Jetten, M.S.M. and Kuenen, J.G. (1996) Autotrophic growth of anaerobic ammonium-oxidizing micro-organisms in a fluidized bed reactor. *Microbiology.* **142**:2187-2196.

van de Graaf, A.A., de Bruijn, P., Robertson, L.A., Jetten, M.S.M. and Kuenen, J.G. (1997) Metabolic pathway of anaerobic ammonium oxidation on the basis of ^{15}N studies in a fluidized bed reactor. *Microbiology.* **143**:2415-2421.

van de Graaf, A.A., Mulder, A., Bruijn, P.d., Jetten, M.S.M., Robertson, L.A. and Kuenen, J.G. (1995) Anaerobic oxidation of ammonium is a biologically mediated process. *Appl. Environ. Microbiol.* **61**(4):1246-1251.

van de Graaf, A.A., Mulder, A., Slijkhuls, H., Robertson, L.A. and Kuenen, J.G. (1990) Anoxic ammonium oxidation. Christiansen, C., Munck, L. and Villadsen, J. (eds), pp. 338-391, Munksgaard, Copenhagen.

van der Star, W.R.L., Abma, W.R., Blommers, D., Mulder, J.-W., Tokutomi, T., Strous, M., Picioreanu, C. and van Loosdrecht, M.C.M. (2007) Startup of reactors for anoxic ammonium oxidation: Experiences from the first full-scale anammox reactor in Rotterdam. *Water Res.* **41**(18):4149-4163.

van Niftrik, L.A., Fuerst, J.A., Damste, J.S.S., Kuenen, J.G., Jetten, M.S.M. and Strous, M. (2004) The anammoxosome: an intracytoplasmic compartment in anammox bacteria. *FEMS Microbiol. Lett.* **233**:7-13.

van Rijn, J., Tal, Y. and Barak, Y. (1996) Influence of volatile fatty acids on nitrite accumulation by a *Pseudomonas stutzeri* strain isolated from a denitrifying fluidized bed reactor. *Appl. Environ. Microbiol.* **62**(7):2615-2620.

Verostko, C.E., Carrier, C. and Finger, B.W. (2004) Ersatz wastewater formulations for testing water recovery systems. SAE Technical Paper Series 2004-01-2448., SAE, 34th Intl. Conf. on Environ. Systems, Colorado Springs, CO.

Watson, J.M. and Payne, P.A. (1990) A study of organic compound pervaporation through silicone rubber. *J. Membr. Sci.* **49**:171-205.

Wett, B. (2006) Solved upscaling problems for implementing deammonification of rejection water. *Water Sci. Technol.* **53**(21):121-128.

Yeom, C.K., Kim, B.S. and Lee, J.M. (1999) Precise on-line measurements of permeation transients through dense polymeric membranes using a new permeation apparatus. *J. Membr. Sci.* **161**:55-66.

Yoshida, N. and Toyoda, S. (2000) Constraining the atmospheric N_2O budget from intramolecular site preference in N_2O isotopomers. *Nature.* 405(6784):330-334.

3. OXYGEN TRANSFER MODEL FOR A FLOW-THROUGH HOLLOW-FIBER MEMBRANE BIOFILM REACTOR

Kevin R. Gilmore[1], John C. Little[2], Barth F. Smets[3], Nancy G. Love[4,*]

[1]Department of Civil and Environmental Engineering, Virginia Polytechnic Institute and State University, 418 Durham Hall (0246), Blacksburg, VA 24061

[2]Professor, Charles E. Via Department of Civil and Environmental Engineering, 418 Durham Hall (0246), Virginia Tech, Blacksburg, VA 24061, USA

[3]Professor, Department of Environmental Engineering, Miljøvej, Building 115, Technical University of Denmark,
DK-2800 Kgs. Lyngby, Denmark

[4]Professor, Department of Civil and Environmental Engineering, University of Michigan, 2350 Hayward, 2340 G.G. Brown Building, Ann Arbor, MI 48109-2125
*Corresponding Author

Currently revised following reviewer comments,
submitted for consideration for publication in the

Journal of Environmental Engineering
ASCE

3.1 ABSTRACT

A mechanistic oxygen transfer model was developed based on material properties and applied to a flow-through hollow-fiber membrane-aerated biofilm reactor (HFMBR). Model results are compared to conventional clean water testing and performance data when an actively nitrifying biofilm was present on the fibers. With the biofilm present, oxygen transfer efficiencies between 30% and 55% were calculated from measured data including outlet gas oxygen concentration, ammonia consumption stoichiometry, and oxidized nitrogen production stoichiometry, all of which were in reasonable agreement. The mechanistic model overpredicted oxygen transfer by a factor of 1.3 relative to the result calculated from outlet gas oxygen concentration, which was considered the most accurate of the measured benchmarks. A mass transfer coefficient derived from clean water testing with oxygen sensors at the membrane-liquid interface was the most accurate of the predictive models (overpredicted by a factor of 1.1), while a coefficient determined by measuring bulk liquid dissolved oxygen (DO) underpredicted oxygen transfer by a factor of 3. The mechanistic model was found to be an adequate tool for design and prediction of oxygen transfer in HFMBRs, because it used published diffusion and partitioning coefficients and avoided use of cumbersome small-scale tests to determine system-specific mass transfer coefficients.

KEYWORDS

Wastewater treatment, oxygen, mass transfer, hollow-fiber membrane biofilm reactor, modeling

ALPHABETICAL LIST OF TERMS AND VARIABLES

A = cross-sectional area of one membrane fiber, cm^2
a = specific inner surface area of membrane fibers relative to volume, cm^2/cm^3
C = bulk aqueous phase dissolved oxygen (DO) concentration, g/cm^3
C_{int} = membrane/water or membrane/biofilm interface DO concentration, g/cm^3
C^*_{sat} = saturation DO concentration in equilibrium with gas phase, g/cm^3
C^*_{∞} = equilibrium DO concentration as time approaches infinity, g/cm^3
C_0 = bulk aqueous phase DO concentration at beginning (t=0) of clean water test, g/cm^3
d = inside diameter of fibers (lumen diameter), cm
D = diffusion coefficient of oxygen in poly(dimethylsiloxane), cm^2/sec
J = oxygen flux, g O_2/cm^2-sec
K_g = air/membrane partitioning coefficient (concentration of O_2 in membrane / concentration of O_2 in air), dimensionless
K_w = water/membrane partitioning coefficient (concentration of O_2 in membrane / concentration of O_2 in water), dimensionless
K_{OL} = overall resistance mass transfer coefficient, cm/sec
K_L = liquid boundary layer resistance mass transfer coefficient, cm/sec
K_M = membrane resistance mass transfer coefficient, cm/sec
m = Henry's constant, O_2 equilibrium concentration in gas/O_2 equilibrium concentration in water, dimensionless
n = number of membrane fibers
OTE = oxygen transfer efficiency, %
OTR = oxygen transfer rate, g O_2/sec (as derived), also presented as mg O_2/min
P = permeability, cm^2/sec
t = time, sec
U = lumen gas velocity, cm/sec
V = bulk liquid volume, cm^3
x = distance along fiber length, cm
y = gas-phase oxygen concentration in fiber lumens, g/cm^3
y_0 = initial gas-phase oxygen concentration at fiber lumen entrance, g/cm^3
Z = length of fibers, cm
δ = fiber wall thickness, cm

3.2 INTRODUCTION

Tertiary wastewater treatment processes typically require full or partial oxygenation to meet treatment goals. To this end, membranes have been used to oxygenate laboratory-scale wastewater treatment reactors in a bubbleless manner, achieving up 100% oxygen transfer efficiency when pressurized with pure oxygen (Ahmed and Semmens, 1992a, Pankhania et al., 1994). Bubbleless oxygen transfer has several benefits, including higher nominal transfer efficiencies, the potential for reduced loss of volatile compounds to the atmosphere, and reduced

foaming associated with surfactants (Brindle and Stephenson, 1996). Furthermore, membrane oxygenation decouples reactor depth from oxygen transfer efficiency, because fiber lumen pressure can be varied (Cote et al., 1988). More recently, low dissolved oxygen membrane-aerated biofilm reactors have been used in an attempt to shortcut traditional biological nitrification and denitrification processes (Hibiya et al., 2003). This approach allows precise control of oxygen delivery and the capability to create redox-stratified biofilms for novel metabolic configurations (Terada et al., 2007).

Measurement of oxygen transfer by aeration devices has traditionally been performed with clean water testing (ASCE, 1993, Leung et al., 2006). This approach allows measurement of the liquid phase oxygen concentration in an abiotic setting, as opposed to the more elaborate instrumentation associated with off-gas analysis in the presence of active biomass. However, clean water testing to quantify oxygen transfer in microporous and composite membrane aeration systems has been shown to underestimate the transfer capabilities of the oxygenation device (Shanahan and Semmens, 2006). As a result, more representative measurement techniques and predictive models are required to enable more widespread application of non-porous and microporous membrane aeration and membrane biofilm treatment processes.

Because of the importance of oxygen in creating biofilm microenvironments, predictive models have been developed to calculate oxygen fluxes in non-porous HFMBR systems (Ahmed and Semmens, 1992b, Johnson et al., 1998, Shanahan and Semmens, 2004). However, the majority of available models require either assumption or measurement of the mass transfer coefficient. Currently there are no mechanistic models for predicting oxygen transfer in HFMBRs based on material properties such as diffusion and partitioning coefficients, which are available for some, but not all, commonly-used membrane materials. Mechanistic models are desirable, because they would allow for oxygen transfer efficiency to be predicted across a range of materials and geometries.

This study presents a mechanistic oxygen transfer model that is based on material properties and reactor configuration. The oxygen transfer characteristics of a non-porous HFMBR with a flow-through fiber configuration are investigated. Reactor hydrodynamics are discussed, followed by clean water oxygen transfer experiments at varying lumen pressures and gas flow rates. The

model is compared with other predictors and indicators of oxygen transfer. Bulk liquid oxygen consumption data and oxygen microsensor profiles were collected during operation in the presence of an active biofilm present and are used to illustrate the capabilities and limitations of the proposed model.

3.3 METHODS

Hollow-fiber membrane-aerated biofilm reactor. Aeration occurs in HFMBRs (Figure 3.1, Table 3.1) by flowing aeration gas through the lumen fibers, which are clustered in an immersible bundle. Oxygen diffuses through the non-porous membranes to the surrounding liquid-filled reactor shell. The HFMBR reactor used in this study was modeled after Rector et al. (2004) without rotation of the membrane module and housed 98 fibers (0.29 m^2 total membrane surface area). Fibers were Silastic laboratory tubing (Dow Corning 508-009), 3.18 mm outer diameter, 1.98 mm inner diameter, potted in CPVC end caps with Silastic® E RTV Silicone Rubber Base and Curing Agent (Dow Corning) and Bio-Clear 810 epoxy (RTC011-A, RTC011-B, Progressive Epoxy Pittsfield, NH) (Garland, 2005). The reactor vessel was constructed of an acrylic tube, 9.4 cm diameter, 63.0 cm flange-to-flange height, and was oriented vertically. Four ports were tapped in the side of the reactor shell for dissolve oxygen microsensor profiling and biomass sampling, as described in Chapter 4. Ports 1 through 4 were located at distances 2.5, 10.2, 17.8, and 25.4 cm from the bottom of the 29.2 cm membrane module. Total reactor volume, including associated external tubing and instrument cells, was 4.5 L. Liquid flow was recycled at 500 mL/min to promote well-mixed conditions and minimize boundary layer resistance at the membrane fiber surfaces. Additional mixing was achieved with a magnetic stir plate and a magnetic stir bar in the base of the reactor. Air was used as the oxygen source and was controlled by a mass flow controller (Aalborg GFC-17, Orangeburg, NY). Lumen pressure was maintained manually by a backpressure needle valve on the gas outlet. Tracer tests were performed with distilled water and NaCl tracer, and tracer concentration was measured independently as both chloride ion and as conductivity. The results revealed that the hydrodynamics approached completely mixed conditions in the reactor and could be modeled as 1 to 2 completely-mixed stirred tank reactors (CSTRs) in series (Appendix A).

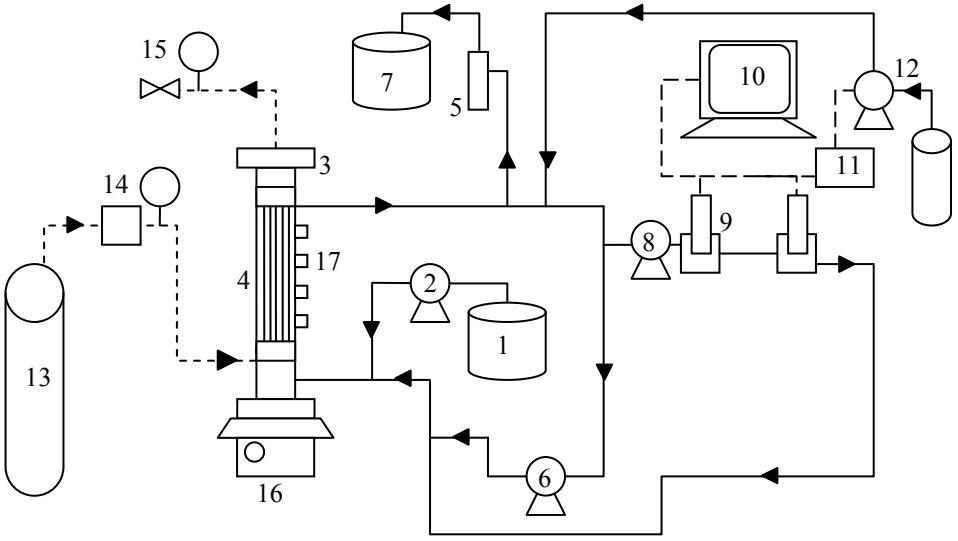

Figure 3.1. HFMBR Schematic. 1. deoxygenated feed, 2. feed pump, 3. reactor vessel, 4. membrane module, 5. gas/liquid separator, 6. recirculation pump, 7. effluent (overflow), 8. instrumentation pump, 9. pH & ORP flow cells, 10. data acquisition, 11. pH controller, 12. base supply and base pump, 13. air source, 14. mass flow controller and pressure gauge, 15. backpressure valve and pressure gauge, 16. magnetic mixer, 17 sampling ports. Solid lines – liquid; short dash lines – gas; long dash lines – instrument signal.

Table 3.1. HFMBR design and operating parameters.

Parameter	Value
Reactor vessel dimensions	9.4 cm diam. X 63 cm height
Empty bed reactor volume	4.0 L
Membrane module displacement volume	0.53 L
Nominal liquid volume	3.47 L
Membrane material	Silastic (PDMS, DOW Corning 508-009)
Membrane fiber diameter	3.18 mm outer, 1.98 mm inner
Membrane length	30.5 cm
Specific inner surface area of membrane in reactor	0.553 cm^2/cm^3 system volume, 0.393 cm^2/cm^3 vessel volume
Total liquid volume, including tubing, etc.	4.5 L
Influent flow rate range	0.2 mL/min – 2.0 mL/min
Nominal hydraulic retention time range	12.0 days – 1.2 days
Reactor recirculation rate range (x)	2,500x – 250x
Ammonia loading rate range	0.07 – 0.53 kg N/m^3-day
Range of gas loading	0.025 to 0.10 cm/sec

Bulk liquid clean water oxygen transfer experiments. Clean water oxygen transfer tests were conducted *in situ* at the intended reactor operation temperature of 30°C. Tests were conducted in general accordance with ASCE method 002-91: Measurement of Oxygen Transfer in Clean Water (A-91) (ASCE, 1984), with the following exceptions: total dissolved solids (TDS) and soluble cobalt were not measured between tests since virgin distilled water was used each time; and the equilibrium DO concentration as time approaches infinity, C^*_∞, was assumed to be equal to C^*_{sat}, the saturation concentration at the measured lumen pressure and temperature, rather than being determined from the nonlinear regression of each test condition. The reactor vessel and tubing were deoxygenated with sodium sulfite and cobalt chloride. Dissolved oxygen was monitored by an Orion Model 97-08 oxygen electrode (Thermo Fisher Scientific, Waltham, MA) located in a flow-through cell external to the reactor. The signal was analyzed by an Accumet® AR25 dual channel pH/ion meter (Thermo Fisher Scientific, Waltham, MA) and recorded at 30 second intervals on a computer using LabView7 (National Instruments Corp., Austin, TX). The mass transfer coefficient (K_{OL}) was then determined by non-linear regression of equation 3.1 (ASCE, 1984) with a spreadsheet solver (Excel, Microsoft Corp., Redmond, WA):

$$C = C^*_\infty - (C^*_\infty - C_0)\exp(-K_{OL}a \cdot t) \qquad \text{(eqn 3.1)}$$

C_0 in equation 3.1 was the measured bulk liquid DO concentration at time=0 when the air flow to the membrane lumens was initiated. $K_{OL}a$ was divided by the specific membrane surface area (a) to obtain K_{OL}. Because these tests included the external recirculation loop, 'a' was equal to the inner membrane surface area (1,770 cm^2) divided by the whole system volume (4,500 cm^3), or 0.393 cm^2/cm^3. Goodness of fit for regression of each test condition was determined as 1 – (residual sum of squares/total sum of squares) for the data (Montgomery et al., 2004). Clean water oxygen transfer efficiency was calculated by dividing oxygen transfer rate ($K_{OL}a \times (C^*_{sat} - 0) \times$ reactor volume) by mass input rate of oxygen as controlled by the mass flow controller for each flow/pressure condition tested (ASCE, 1993). At the time of clean water testing, the method for off-gas oxygen analysis by GC was not yet fully developed. Hence, outlet oxygen mass flow rates were not available for confirming the oxygen transfer efficiency calculations.

Membrane interface clean water oxygen transfer experiments. To determine the effect of the liquid phase boundary layer when estimating the clean water mass transfer coefficient, clean

water tests were performed with oxygen microsensors positioned at the membrane-water interface. Sensors were manipulated to the surface of the membrane (as described below for biofilm measurements), at which time the water was deoxygenated and the flow of air to the membranes was turned on. Again, tests were in accordance with ASCE Method 002-91, except that TDS and cobalt were not measured. DO at the membrane interface (C_{int}) was monitored over time until a stable reading was obtained, and this value was used as C^*_∞. One test was performed at each port in the reactor, and during two of those tests a second microsensor was positioned to measure bulk liquid DO concurrently. Again, $K_{OL}a$ was determined using non-linear regression and equation 3.1. Reactor recirculation was turned off for these tests to prevent leaking water through the reactor ports. The volume of the reactor vessel without recirculation tubing was 3.2 L, leading to a specific surface area of 0.553 cm^2 membrane inner surface area per cm^3 reactor volume during these tests.

Operating oxygen transfer experiments. Oxygen transfer efficiencies during biofilm operation were measured by gas chromatography (GC) of collected outlet gas. Outlet gas was collected in a 1L Tedlar bag and analyzed the same day for nitrogen and oxygen on a GOW-MAC gas chromatograph (Model 69-580-TCD, GOW-MAC Instrument Co., Bethlehem, PA) with a stainless steel column packed with molecular sieve 5A (Supelco/Sigma-Aldrich Group, Bellefonte, PA) and TCD detector (isocratic, column = 35°C, injector = 70°C, detector = 70°C, TCD current = 200 mA, 100µL injection volume).

Reactor operation with active biofilm. The HFMBR was operated for 220 days treating a high-strength synthetic wastewater (Hummerick, 2005) lacking organic carbon. The wastewater was designed to mimic a urine wastewater from a confined human operation such as a long-term space exploration mission: 47.1 mM NH_3-N (added as NH_4HCO_3), 14.3 mM NaCl, 3.7 mM $KHCO_3$, 0.8 mM $KHSO_4$, 1.25 mM KH_2PO_4, 0.83 mM $MgSO_4$, 1.23 mM $CaCl_2$, 0.11 mM $FeCl_2$, in distilled water. Ammonia removal rates were 95% and 78% at influent NH_3-N loads of 1.6 and 2.3 g NH_3-N per m^2 outer membrane area per day, respectively (flux of all non-O_2 substrates is reported as g/m^2 of outer membrane area). At 1.6 g NH_3-N/m^2-day, nitrite (NO_2^-) was the predominant product, ranging from 66% to 84% of the influent ammonia load, with 0% to 22% of the influent ammonia load recovered as nitrate (NO_3^-). At 2.3 g NH_3-N/m^2-day, effluent NO_2^- ranged from 49% to 62% of the influent ammonia load, and effluent NO_3^- was 8%

to 13% of the influent ammonia load. Ammonia nitrogen was analyzed spectrophotometrically using the phenate method (640 nm). Nitrite was analyzed spectrophotometrically using the colorimetric method (543 nm), and nitrate was analyzed by ion chromatography with a Dionex AS9-HC anion column (Dionex, Sunnyvale, CA). All analyses were performed in accordance with procedures outlined in Standard Methods for the Examination of Water and Wastewater (APHA, et al., 1998). All chemicals were obtained from Fisher Scientific (Pittsburgh, PA).

Oxygen microsensor profiles. Oxygen profiles were measured on operation day 204 using an OX-10 Clark-type oxygen microsensor (Unisense, Aarhus, Denmark) with a specified nominal tip diameter between 8 and 12 μm, 150-200 mm total sensor length. A two-point calibration was performed according to the manufacturer's instructions in reactor effluent (to ensure representative ionic strength) sparged for 15 minutes with N_2 or air for zero- or saturated-calibrations, respectively. Oxygen concentrations were measured at 10 μm intervals controlled manually by a micromanipulator (Narishige International, East Meadow, NY). Microsensor signals were processed by a PA2000 Picoammeter (Unisense, Aarhus, Denmark) and recorded with Profix software (Unisense, Aarhus, Denmark). An arbitrary sensor tip location near the biofilm/membrane was chosen as the longitudinal datum. The oxygen concentration was monitored in real-time as the microsensor was manipulated towards the membrane, and distance was tracked relative to the datum. The oxygen concentration increased as the tip approached the surface before stabilizing briefly. The beginning of this concentration plateau was presumed to be the membrane surface. The distance required to reach the membrane surface relative to the datum was then inverted to set the membrane surface as the zero distance.

As the sensor was advanced further, it was rigid enough to visibly deflect the flexible fibers, and stable DO concentrations were associated with this period of deflection. The sensor tip was then able to pierce the PDMS material. A slower and linear increase in DO appeared to be associated with this phenomenon, although the sensor is not designed to provide accurate measurements within such a matrix. During profiling, the recycle pump had to be turned off and the reactor vessel isolated with valves to prevent leakage from the vessel. Without recirculation pumping, surface tension was sufficient to minimize leakage through the small-diameter (~0.9 cm) sampling ports. The internal magnetic mixer remained operational during profiling. The lack of

recirculation likely affected the liquid-phase boundary layer, especially at the top of the membrane module, which was far from the magnetic stir bar and was more dependent on fluid recirculation for surface velocity.

Oxygen transfer model formulation. An oxygen transfer model, based on material properties rather than experimental mass transfer coefficients, was developed and compared to experimental data. The model employs the simplifying assumption of a flat sheet membrane with a unit surface area equivalent to the inner surface area of the cylindrical fiber type used in the reactor (i.e., the inside diameter was used to calculate surface area available for mass transfer).

The model was developed to express oxygen flux, J(x), as a function of the distance x along the fiber. Inputs to the model include both membrane material parameters such as the diffusion coefficient of oxygen in poly(dimethylsiloxane) (D), air/membrane partitioning coefficient (K_g), amd water/membrane partitioning coefficient (K_w), and reactor dimensional and operating properties, such as gas velocity (U), cross-sectional fiber area (A), fiber wall thickness (δ), Henry's constant (m), and the initial gas-phase oxygen concentration at the fiber inlet (y_0). It incorporates a nested sub-model for gas-phase oxygen concentration, y, along the length of the fiber, which was developed using a mass balance for oxygen about a differential element of fiber (Figure 3.2):

$$U_1 \cdot A \cdot y(x) - \pi d \cdot \Delta x \cdot J(x) = U_2 \cdot A \cdot y(x + \Delta x) \qquad \text{(eqn 3.2)}$$

where:

$$J(x) = \frac{D \cdot \left(K_g \cdot y(x) - K_w \cdot C_{int}(x)\right)}{\delta} \quad \text{(eqn 3.3)} \qquad \text{and} \qquad \frac{K_w}{K_g} = m \quad \text{(eqn 3.4)}$$

At this point, the DO concentration used in the model is assumed to be at the interface between the membrane and the liquid (C_{int}). As biofilms are heterogenous structures with pores and channels, water is present in the matrix and this is still assumed to be an aqueous phase concentration. To simplify the model, C_{int} in the expression for flux above (eqn 3.3) was assumed not to vary with distance along the fibers and, hence, to be a user-defined constant. The fact that tracer tests confirmed relative homogeneity of the liquid phase supports this assumption. Furthermore, the velocity out of the differential element, U_2, was assumed to be equal to the

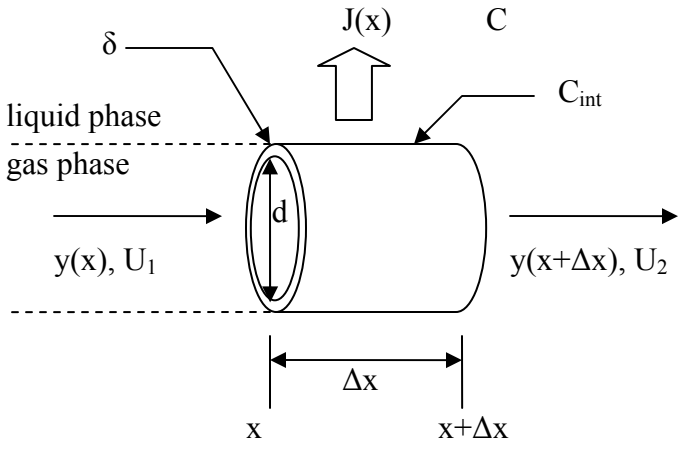

Figure 3.2. Diagram of a differential hollow fiber element.

velocity in, U_1, by neglecting the change in gas volume as a result of flux across the fiber. Thus, setting C_{int}=constant and substituting the simplified expression for flux yields the expression for gas-phase oxygen concentration versus distance along the fiber:

$$y(x) = \left(y_0 - mC_{int}\right) \cdot \exp\left(-\frac{\pi dDK_g}{UA\delta} \cdot x\right) + mC_{int} \qquad \text{(eqn 3.5)}$$

Substitution of this expression for y (eqn 3.5) back into the equation for flux (eqn 3.3) yields the expression for flux as a function of distance along the fiber:

$$J(x) = \frac{D}{\delta} \cdot \left(K_g \cdot y_0 - K_w \cdot C_{int}\right) \cdot \exp\left(-\frac{\pi dDK_g}{UA\delta} \cdot x\right) \qquad \text{(eqn 3.6)}$$

Integrating this expression for flux (eqn 3.6) over the length, Z, of a single fiber yields the mass of oxygen transferred per unit perimeter per fiber per unit time. Introducing the number of fibers, n, and simplifying gives the mass of oxygen transferred per unit time (the oxygen transfer rate) for the HFMBR:

$$OTR = nUA\left(mC_{int} - y_0\right) \cdot \left[\exp\left(-\frac{\pi dDK_g}{UA\delta} \cdot Z\right) - 1\right] \qquad \text{(eqn 3.7)}$$

3.4 RESULTS AND DISCUSSION

Bulk liquid clean water oxygen transfer tests. As shown in Figure 3.3, bulk liquid clean water testing predicts an oxygen transfer efficiency (OTE) ranging from 6% to 14% at higher air flow rates (62.5 $cm^3/min\text{-}m^2$) and between 20% and 35% at lower air flow rates (15.6 $cm^3/min\text{-}m^2$). These OTE values were determined from maximum aeration rates in mg/l-min (slope of DO vs.

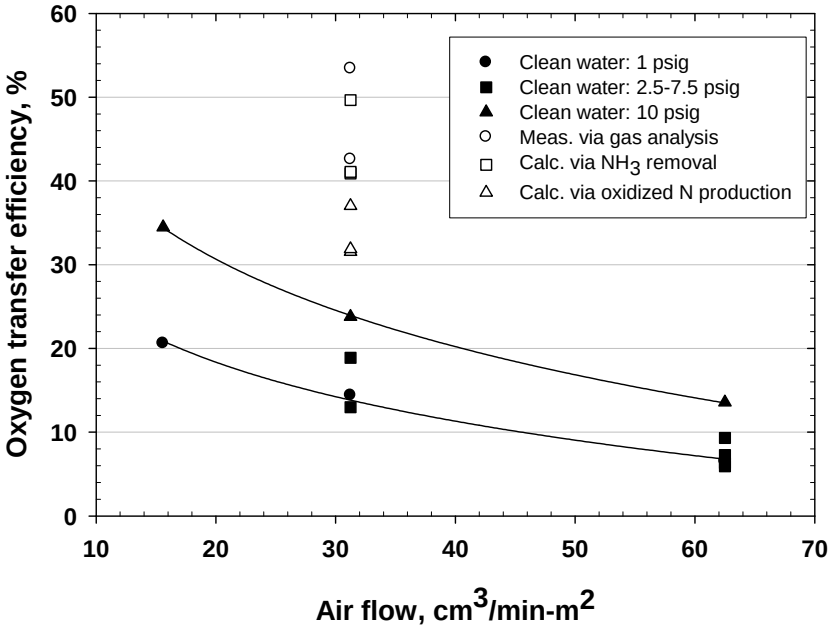

Figure 3.3. Oxygen transfer efficiencies during clean water tests and with active biofilm present. Curves on graph are logarithmic models fit to data to illustrate approximate upper (10 psig) and lower (1 psig) bounds of predicted OTE region ($R^2 > 0.99$ for both curve fits).

time) during tests, extrapolated to the entire system volume. The shapes of the curves correctly suggest increasing efficiencies as volumetric air flows approach zero (a sealed-end fiber condition). A maximum oxygenation rate of 1.25×10^{-6} mol O_2/m^2-sec (0.64 mg/min) was observed at a lumen pressure of 10 psi and an air flow of 62.5 cc/min-m^2. This is lower than literature values of 1.5×10^{-5} mol O_2/m^2-sec for a pure oxygen flow-through system at 28-30 psi (Rector et al., 2004) and 5.7×10^{-6} mol O_2/m^2-sec for a sealed-end system at 1.5 psi (Hibiya et al., 2003). However, when the much higher lumen pressure in the first reference (28-30 psi) and

the sealed-end configuration in the second reference are considered, the observed oxygenation rate compares reasonably well.

In oxygen transfer modeling, the mass transfer coefficient (K) describes the individual or cumulative resistances of the gas-phase boundary layer, liquid-phase boundary layer, or membrane itself. Once determined through clean water testing, K can be used to predict oxygen flux and transfer rate for a particular system under a narrow range of operating conditions. Like the oxygen transfer rate, the average K_{OL} of 4.0×10^{-4} cm/sec (Figure 3.4) for this HFMBR was also comparable to that observed previously for a siloxane fiber flow-through system (7.71×10^{-4} cm/sec, Rector et al., 2004), and was approximately an order of magnitude lower than for a 0.4 mm diameter sealed-end microporous fiber (80×10^{-4} cm/sec, Voss et al., 1999). The lower K_{OL} found for the present study is expected, as the resistance is higher for a non-porous membrane in which the oxygen must partition into and diffuse across the fiber wall. It is expected that mass transfer would be

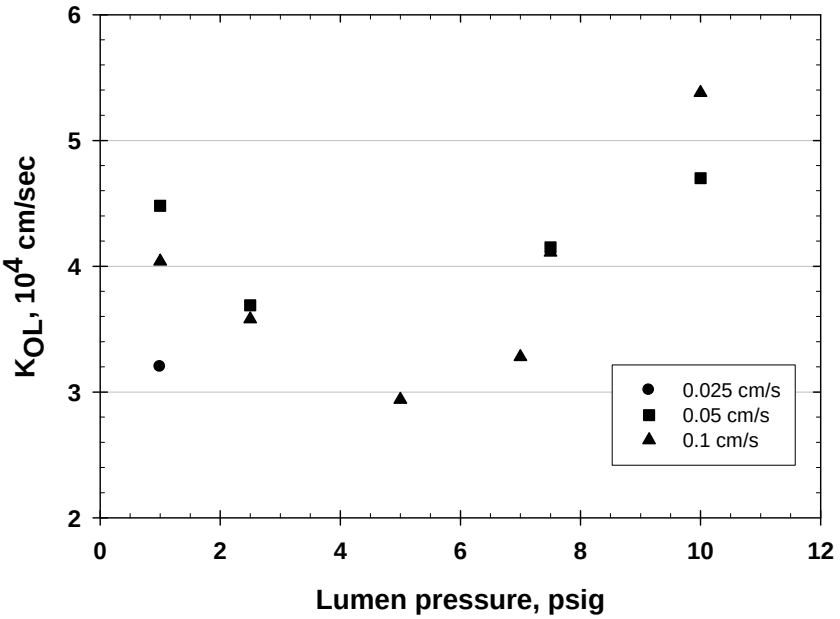

Figure 3.4. Mass transfer coefficients (K_{OL}) calculated from bulk liquid clean water testing. Values were calculated by non-linear regression fit of equation 1 to data. Goodness of fit (R^2) values ranged from 0.911 to 0.998.

dependent only on driving force as determined by the lumen pressure and resulting equilibrium aqueous phase dissolved oxygen concentration. However, K_{OL} (Figure 3.4) was found to show a weak positive correlation (Pearson's product-moment correlation coefficient = 0.35, t=1.19), slightly increasing with increasing lumen pressure. Although this was only significant between an 85% and 90% level (t_{crit} = 1.093 and 1.372, respectively), this positive correlation has also been observed by others for a membrane with a non-porous component (Ahmed et al., 2004). This potential pressure dependence is not currently understood but may be due to material properties or stretching of the membrane under the increased pressure. Stretching would result in a thinner membrane with a higher surface area, allowing greater mass transfer flux. More controlled experiments are needed to elucidate the relationship between membrane deformation and oxygen transfer with this material. Goodness of fit ($R^2 = 1\text{-}SS_{res}/SS_{tot}$) for K_O regressions of equation 3.1 to clean water test DO data were greater than 0.979 with the exception of the 5 and 7 psig tests, for which R^2 = 0.922 and 0.911, respectively. In both those cases, the measured DO tailed off after ~60 minutes and caused the poor fit and lower calculated K_{OL} value. The cause for this observation was not determined. K_{OL} did not correlate with lumen velocity, indicating that gas phase boundary layer resistance is negligible.

Membrane interface clean water oxygen transfer tests. Tests in which the effect of the liquid boundary layer was removed yielded an average K_M of 1.5×10^{-3}cm/sec (standard deviation 0.53×10^{-4} cm/sec, approximately 4-fold higher than the transfer coefficient obtained by measuring bulk liquid DO. The term K_M is used to describe this transfer coefficient because the influence of the liquid boundary layer is eliminated by measuring the DO at the membrane surface. K_M did not vary along different ports in the reactor. Using this average K_M, and under conditions in which K_M was determined (5 psig, 31 cm^3/min-m^2, C_{int}=0.2 mg/L), the calculated OTE was approximately 42%, compared to approximately 19% calculated using the bulk liquid DO-determined K_{OL} (Figure 3.3). This disparity indicated that the liquid boundary layer played a significant role in mass transfer resistance.

Oxygen transfer with biofilm present. Examination of operating data when a biofilm was present and active on the membrane surface revealed oxygen transfer efficiencies significantly higher than those predicted by bulk liquid clean water tests at the same air flow rate and lumen

pressure but similar to that calculated from the membrane interface-determined K_M. From measured outlet oxygen concentrations, transfer efficiencies between 40% and 55% at pressures ranging from 5 psi to 8 psi were calculated (Figure 3.3). Theoretical oxygen consumption calculated from ammonia oxidation to nitrite (3.43 g O_2/g NH_3-N oxidized) and oxidized nitrogen production (3.43 g O_2/g NO_2^--N+NO_3^--N + 1.14 g O_2/g NO_3^--N), also shown in Figure 3.3, support these higher measured efficiencies. Calculated OTEs differ depending on whether ammonia removal or oxidized nitrogen production is used as the basis. This is likely explained by the reduction of NO_2^- to $NO_{(g)}$ and $N_2O_{(g)}$ via autotrophic denitrification, as both these nitrogen compounds have been measured in the outlet gas in proportions totaling up to 9.8% of the ammonia nitrogen (see Chapter 4).

The liquid-phase boundary layer could be further characterized by examining the oxygen microsensor profiles (Figure 3.5). Oxygen microsensor profiles demonstrate the effect of attached biofilm on oxygen transfer and, in particular, the mass transfer driving force at the membrane surface. All profiles were taken on the same day, and one profile was made at reactor Port 2 on a portion of the fiber that was scoured clean during biomass sampling for fluorescence *in situ* hybridization (FISH) analysis. As a result, this location offered a side-by side comparison of oxygen transfer into a biofilm versus transfer directly into the bulk liquid. The interface oxygen concentration (C_{int}) of the bare membrane (0.90 mg/L) was nearly five times the surface concentration under a biofilm (0.19 mg/L) at the same reactor port, illustrating the substantial difference between oxygen transfer in abiotic and biotic systems. The bare fiber profile also suggests a liquid boundary layer thickness between 500 and 600 μm, the distance at which the DO reaches negligible concentration. The presence of such a boundary layer has been observed by others to be a critical factor in determining mass transfer, requiring turbulent conditions to minimize the resistance (Brindle and Stephenson, 1996). However, it must be recognized that the boundary layer thickness is overestimated by the method used, as the liquid recirculation flow had to be discontinued during microsensor measurements to prevent draining through the sensor port. While the membrane surface DO concentrations do not suggest the presence of a longitudinal oxygen gradient along the length of the membrane fibers, a gradient existed nonetheless, as biofilm on the fibers is thicker and more prevalent by visual inspection near the

bottom of the membrane module (gas entrance) and as evidenced by the measured outlet oxygen concentrations (Figure 3.6).

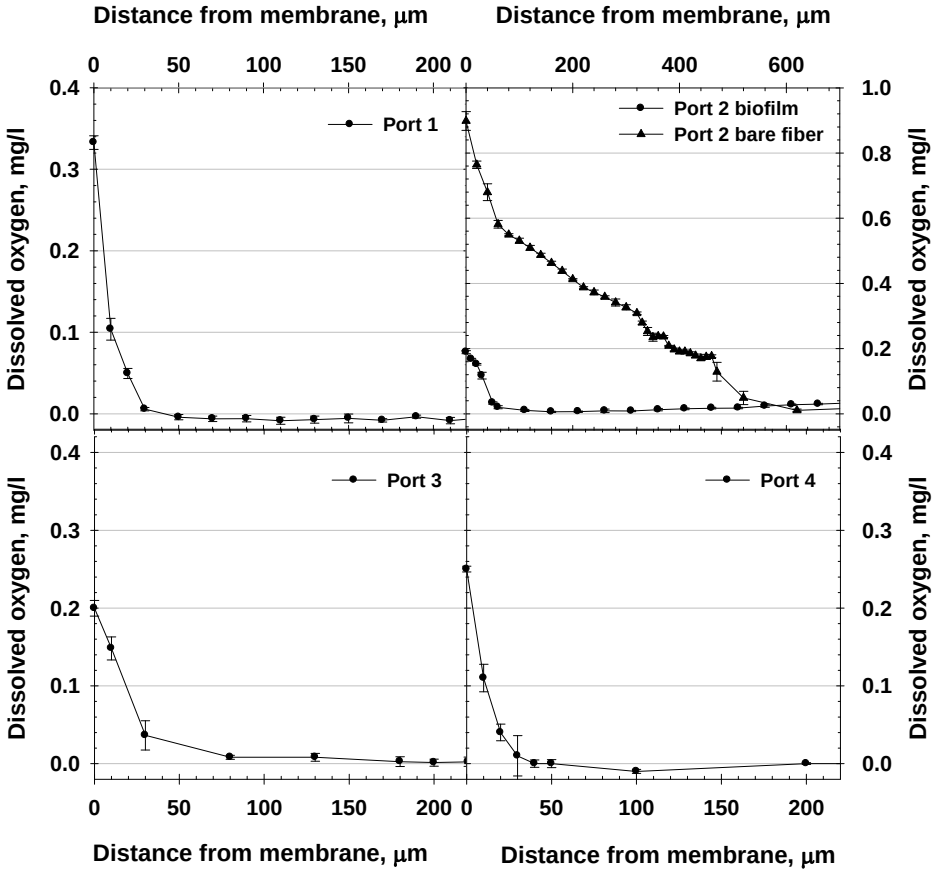

Figure 3.5. Oxygen microsensor profiles during operation with active biofilm on fibers. Port number refers to reactor location, with Port 1 near bottom of reactor (feed+recycle inlet) to Port 4 near top of reactor (effluent+recycle outlet) The "bare fiber" profile was taken at Port 2 on a region of bare fiber exposed during biomass sampling. Note differences in scales of Port 2 axes.

Mechanistic oxygen transfer model. The key parameters to which the model was most sensitive were y_0, D, and K_g. Initial gas-phase oxygen concentration, y_0, affects the model most significantly at extremely low lumen velocities. The diffusion coefficient was taken from Lu et al. (2001), who measured D of oxygen in PDMS with varied content of 10 nm diameter silica nanospheres, from 0% to 30% by weight. The value for silica-free PDMS was used (2.22×10^{-5} cm^2/sec), although the manufacturer reports that the proprietary formulation includes a "small" amount of silica. This value is comparable to other sources (Lee et al., 2006, Merkel et al., 2000).

Using this value for D, K_g was calculated from O_2 permeability (P) using $P = D \times K_g$. The manufacturer's reported oxygen permeability is 4.88×10^{-6} cm^2/sec, yielding $K_g = 0.22$. This value is consistent with Merkel et al. (2000) (0.20) and Blume et al. (1991) (0.21). De Bo et al. (2002) measured K_g of 0.44, but the variability was high (+/- 0.3) due to their measurement technique, which was better suited for VOCs.

Model predictions of oxygen transfer (mass and efficiency) with respect to velocity at a fixed pressure (5 psig) are shown in Figure 3.6A. Figure 3.6B illustrates the gas phase oxygen profile along the length of the fiber at three velocity conditions. Mass transfer increases with increasing velocity, as more of the fiber length is aerobic. An additional improvement may also be realized by a thinner gas-phase boundary layer, although this layer does not control mass transfer because the diffusion coefficient of oxygen in air is orders of magnitude higher than in the membrane and water. At very low velocities, all of the oxygen transfers across the membrane early in the fiber, and OTE is flat at ≥100%. The 116% OTE shown in Figure 3.6A reflects the best model prediction based on current parameter estimates and concentration calculations, and this artifact illustrates an area where future refinement will improve the model. As the velocity increases sufficiently to extend the oxic length to at least the end of the fiber, transfer efficiency begins to decrease as residual oxygen is lost in the outlet. It is evident that while higher lumen velocities yield higher mass transfer rates, diminishing returns and reduced transfer efficiency suggest little additional economic benefit of oeprating at velocities higher than 0.15 cm/sec for this system (which corresponded to a gas residence time of ~3 minutes in this system).

Table 3.2 shows the oxygen fluxes predicted by the fundamental model (eqn 3.7) in comparison to the empirical K_L–based models, stoichiometric calculations, and off-gas analysis. Compared to the off-gas oxygen analysis, which is considered to be the most reliable benchmark, the model overpredicted oxygen transfer by a factor of only 1.3. Inspection of the gas phase oxygen concentration (Figure 3.6B) predicted at the end of the fibers (x=29.2 cm, 0.5 cm/sec) shows that the model accurately predicts the outlet oxygen concentration (0.126 mg/cm^3) when compared to off-gas oxygen analysis (average = 0.131 mg/cm^3). Calibration of this model requires measurement of the actual oxygen concentration at the membrane/biofilm interface (C_{int}), which requires delicate instrumentation. Sensitivities to the parameters D and K_g suggest that

differences between model predictions and observed conditions may be due to variability in estimation of these parameters, both of which are not easy to measure. Furthermore, the unknown silica content of the material adds uncertainty to D. Increasing amounts of silica filler leads to a decrease in D (Lu et al., 2001) and a corresponding decrease in oxygen transfer.

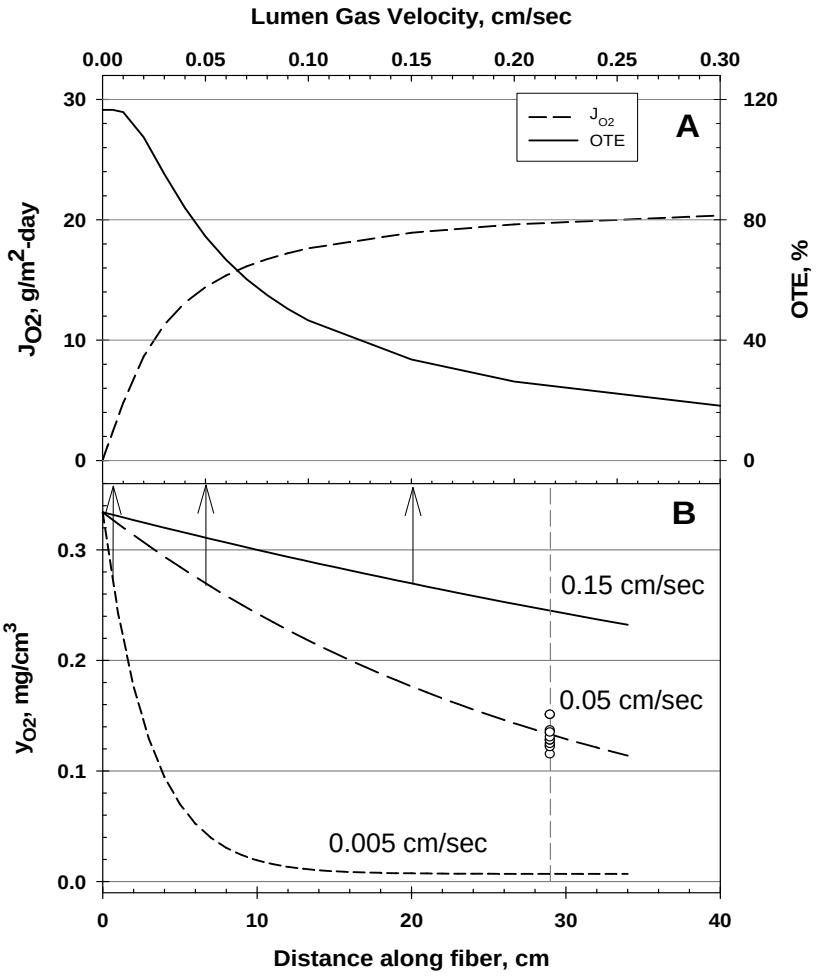

Figure 3.6. Model characterization of oxygen transfer performance. Panel A: Oxygen flux and OTE as a function of lumen gas velocity. Flux is normalized to inner membrane surface area, in accordance with model parameters. 5 psig lumen pressure, C_{int} = 0.2 mg/l, 30°C. Panel B: Gas-phase oxygen profile predicted along fiber length. Each curve represents velocity indicated by arrow toward Panel A axis, and off-gas data is shown for 0.05 cm/sec. Vertical line at 29.2 cm in Panel B represents length of fibers in this study.

Table 3.2. Comparison of predicted and measured oxygen fluxes for the HFMBR[a].

Method	J_{O2}, g O_2/m^2-day
Experimental	
Off-gas analysis	10.7
Predicted	
K_{OL} Model fit to bulk liquid clean water data	3.1
K_M model fit to membrane interface clean water data	11.8
NH_3 removal rate + NO_3^- formation rate	12.0
Mechanistic Model[b]	14.4

[a] Clean water test conditions and biofilm operating conditions: 5 psi lumen pressure and 0.05 cm/sec inlet air velocity. J values are are normalized to inner surface area of membrane fibers, in accordance with the mechanistic model convention.
[b] A surface DO concentration (C_{int}) of 0.2 mg/L is assumed at membrane-biofilm interface, per microsensor profiles with biofilm present.

Despite these limitations, the proposed model has two primary benefits over previous models. First, equations 3.5, 3.6, and 3.7 are straightforward to solve with simple spreadsheet software without the use of more advanced mathematical tools, making the model more accessible to practitioners, designers, and operators of such systems. Second, more complex models still require measurement or assumption of key parameters such as K_L (Ahmed and Semmens, 1992b). In contrast, the present model is instead based on material properties, reactor dimensional data, and the assumption of an interfacial DO concentration at the surface of the membrane. The model can be applied across materials by drawing on the literature for diffusion and partitioning coefficients. Also, C_{int} can be selected or assumed based on the desired oxic state of the membrane-biofilm interface without measurement of K_M or K_{OL} using small-scale tests. It is important to note that the variable C_{int} is independent from other model parameters such as pressure and velocity. At the same time, the structure and activity of a biofilm will influence C_{int}, as will the availability of substrate from the bulk liquid side. Therefore, assumption of a very low C_{int} will be erroneous if the biofilm is substrate-limited from the liquid phase. The model is most accurate and applicable to oxygen-limited biofilms in which y_0 is much greater (>100-200X) than C_{int}. Therefore, the model is especially useful when designing a redox-stratified HFMBR in which the metabolisms associated with the membrane-biofilm interface are of key importance.

3.5 CONCLUSIONS

The mechanistic model proposed is a reasonable predictor of oxygen transfer rate in an HFMBR with an active biofilm present. Oxygen transfer rates with an actively nitrifying biofilm present were significantly higher than those predicted by bulk liquid clean water testing, and the DO-consumption effect of the biofilm replacing the liquid-phase boundary layer explained this discrepancy. Measured mass transfer coefficients displayed a slight positive correlation with fiber lumen pressure but were independent of air flow rate in the range of flows measured, supporting the hypothesis that gas phase boundary layer resistance is negligible. The model based on material properties was representative of oxygen transfer conditions when biofilms are present on the membrane surface, but it requires measurement or assumption of the actual membrane-biofilm interface DO concentration (C_{int}). Furthermore, these models are sensitive to material property parameters. However, the model maintains two advantages over other predictors of oxygen transfer rate in such systems: 1) simplicity of solving, and 2) utility in design of redox-stratified biofilms (by selection of the membrane-biofilm interfacial DO concentration as opposed to less intuitive parameters). We hope that application of this model to future lab-scale systems with different materials and reactor configurations will help to refine its accuracy and applicability to the design of membrane-aerated biofilm reactors.

3.6 ACKNOWLEDGEMENTS

Funding was provided by the National Aeronautics and Space Administration (NASA) and a Charles Via Doctoral Fellowship to the first author from the Charles E. Via, Jr. Department of Civil and Environmental Engineering at Virginia Tech. The authors also thank Dr. Jay Garland, Kristina Reid-Black, and Mary Hummerick of Dynamac Corp./NASA Kennedy Space Center for assistance in constructing the membrane module and with wastewater formulation, Julie Petruska and Jody Smiley of Virginia Tech for assistance with facilities, instrumentation, and experimental methods, Lee Bryant of Virginia Tech for use of the picoammeter, and the journal editor and two anonymous reviewers for their helpful comments.

3.7 REFERENCES

Ahmed, T., Semmens, M. J. 1992a. Use of sealed end hollow fibers for bubbleless membrane aeration: experimental studies. *J. Membr. Sci.* **69**(1-2):1-10.

Ahmed, T., Semmens, M. J. 1992b**.** The use of independently sealed microporous hollow fiber membranes for oxygenation of water: model development. *J. Membr. Sci.* **69**(1-2):11-20.

Ahmed, T., Semmens, M. J., Voss, M. A. 2004. Oxygen transfer characteristics of hollow-fiber, composite membranes. *Adv. Environ. Res.* **8**(3-4):637-646.

APHA, AWWA, WEF. *Standard Methods for the Examination of Water and Wastewater*. 20th ed.; APHA: New York, 1998.

ASCE. *Standard for Measurement of Oxygen Transfer in Clean Water.* ASCE, New York, 1993.

Blume, I., Schwering, P. J. F., Mulder, M. H. V., Smolders, C. A. 1991. Vapour sorption and permeation properties of poly(dimethylsiloxane) films. *J. Membr. Sci*. **61**:85-97.

Brindle, K., Stephenson, T. 1996. The application of membrane biological reactors for the treatment of wastewaters. *Biotechnol. Bioeng.* **49**:601-610.

Cote, P., Bersillon, J.-L., Faup, G. 1988. Bubble free aeration using membranes: Process analysis. *J. Water Pollut. Contr. Fed.* **60**(11):1986-1992.

De Bo, I., Van Langenhove, H. De Keijser, J. 2002. Application of vapour phase calibration method for determination of sorption of gases and VOC in polydimethylsiloxane membranes. *J. Membr. Sci.* **209**:39-52.

Garland, J., Personal communication. 2005.

Gilmore, K. R., Smets, B. F., Terada, A., Garland, J. L., Love, N. G. Autotrophic nitrogen removal in a hollow-fiber membrane-aerated biofilm reactor. In preparation.

Hummerick, M., Personal communication. 2005.

Lee, H. L. T., Boccazzi, P., Ram, R. J., Sinskey, A. J. 2006. Microbioreactor arrays with integrated mixers and fluid injectors for high-throughput experimentation with pH and dissolved oxygen control. *Lab on a Chip*. **6**:1229-1235.

Leung, S. M., Little, J. C., Holst, T., and Love, N. G. 2006. Oxygen transfer in a biological aerated filter. *J. Environ. Eng.* ASCE. **132**:181-189.

Lu, X., Manners, I., and Winnik, M. A. 2001. Polymer/silica composite films as luminescent oxygen sensors. *Macromolecules*. **34**(6):1917-1927.

Merkel, T. C., Bondar, V. I., Nagai, K., Freeman, B. D., and Pinnau, I. 2000. Gas sorption, diffusion, and permeation in poly(dimethylsiloxane). *J. Polymer Sci.: Part B: Polymer Physics*. **38**:415-434.

Montgomery, D. C., Runger, G. C., Hubele, N. F. *Engineering Statistics*. 3rd ed.; John Wiley & Sons, Inc.: New York, 2004.

Pankhania, M., Stephenson, T., Semmens, M. J., 1994. Hollow-fiber bioreactor for waste-water treatment using bubbleless membrane aeration. *Water Res.* **28**(10):2233-2236.

Rector, T., Garland, J., Strayer, R. F., Levine, L., Roberts, M., Hummerick, M. 2004. Design and preliminary evaluation of a novel gravity independent rotating biological membrane reactor. In *34th International Conference on Environmental Systems*, SAE: Colorado Springs, CO.

Shanahan, J. W., Semmens, M. J. 2006. Influence of a nitrifying biofilm on local oxygen fluxes across a micro-porous flat sheet membrane. *J. Membr. Sci.* **277**(1-2):65-74.

Terada, A., Lackner, S., Tsuneda, S., and Smets, B. F. 2007. Redox-stratification controlled biofilm (ReSCoBi) for completely autotrophic nitrogen removal: The effect of co- versus counter-diffusion on reactor performance. *Biotechnol. Bioeng.* **97**(1):40-51.

Voss, M. A., Ahmed, T., Semmens, M. J. 1999. Long-term performance of parallel-flow, bubbleless, hollow-fiber membrane aerators. *Water Environ. Res.* **71**(1):23-30.

4. AUTOTROPHIC NITROGEN REMOVAL IN A HOLLOW-FIBER MEMBRANE-AERATED BIOFILM REACTOR

Kevin R. Gilmore[1], Barth F. Smets[2], Akihiko Terada[2], Jay L. Garland[3], Nancy G. Love[4,*]

[1] Department of Civil and Environmental Engineering, 418 Durham Hall, Virginia Polytechnic Institute and State University, Blacksburg, VA 24061

[2]Department of Environmental Engineering, Miljøvej, Building 115, Technical University of Denmark,
DK-2800 Kgs. Lyngby, Denmark

[3]Dynamac Corporation, NASA Kennedy Space Center

[4]Department of Civil and Environmental Engineering, University of Michigan, 2350 Hayward, 2340 G.G. Brown Building, Ann Arbor, MI 48109-2125
*Corresponding Author

4.1 ABSTRACT

This work presents the successful application of a hollow-fiber, membrane-aerated biofilm reactor in treating an organics-free synthetic wastewater via partial nitrification (nitritation) and anaerobic ammonium oxidation over 550 days. Elevated temperature (30°C) and careful control of the relative fluxes of oxygen and ammonia prevented complete nitrite oxidation long enough to allow a population of anaerobic ammonia-oxidizing bacteria (AnaerAOB) to develop and be retained for >250 days of operation. During nitritation, nitrogen oxide ($NO_{(g)}$, $NO_{2(g)}$, $N_2O_{(g)}$) emissions comprised up to 10% of the nitrogen balance, but emissions gradually disappeared preceding the detectable proliferation of AnaerAOB. The biofilm was approximately equivalent to 4% solids, and oxygen microsensor measurements showed that only 16% of the biofilm depth was microaerobic (DO<0.8 mg/l). No trends in microbial community were observed with respect to length along the reactor, but patterns of radial distribution were marked, with aerobic ammonia-oxidizing bacteria (AerAOB) colonizing nearest the membrane and AnaerAOB furthest from it. Sloughing and uneven membrane colonization provided niche environments for growth of undesirable nitrite-oxidizing bacteria (NOB). This

work demonstrates the ability of this HFMBR configuration to couple these autotrophic processes in a single biofilm.

Keywords: membrane aerated biofilm reactor, hollow fiber, nitritation, anammox, nitrous oxide, FISH, ammonia oxidizing bacteria, nitrite oxidizing bacteria

4.2 INTRODUCTION

Nitrogen removal from wastewater remains an important goal for preventing eutrophication and preserving source water quality. To this end, conventional nitrification and denitrification are widely applied to municipal and industrial wastewaters worldwide. However, novel processes have been developed to reduce the impact of the most costly and least sustainable aspects of these processes (supplying oxygen and external organic carbon). By coupling two autotrophic processes, partial nitrification to nitrite (NH_3 to NO_2^-) and subsequent anaerobic ammonia oxidation ($NH_3 + NO_2^-$ to N_2 and NO_3^-), fewer resources are required (less oxygen, no external organic carbon, and less alkalinity) and less biomass is produced. Reducing the concentration of nitrite oxidizing bacteria (NOB) is key to the success of the process and is often accomplished by exploiting the higher growth rate of the K-strategist AerAOB relative to the r-strategist NOB at elevated temperature (Hellinga et al., 1998), and the higher oxygen affinity of AerAOB relative to NOB (Blackburne et al., 2007, Hao et al., 2002). AerAOB selection over NOB is accomplished by washout with suspended growth cultures (Hellinga et al., 1998, Fux et al., 2002), but use of washout to establish a selective pressure is not feasible with fixed-film processes due to the high solids retention time. Some studies have demonstrated that nitrite oxidation can be successfully avoided in co-current biofilms by establishing low dissolved oxygen (DO) and/or elevated temperature (Picioreanu et al., 1997, Helmer et al., 2001, Pynaert et al., 2004, Furukawa et al., 2006) conditions. Unfortunately, because co-current biofilms provide the electron donor and acceptor from the same phase (liquid), it is not possible to independently control the flux of each substrate.

The hollow-fiber membrane-aerated biofilm reactor (HFMBR) is a recent process configuration that offers counter-current delivery of electron donor and acceptor

(typically oxygen), which allows for independent control of each. The benefits of the HFMBR configuration include: precise oxygen control, high transfer efficiency, high substrate utilization rates, reduced VOC emission due to bubbleless oxygenation, and redox stratification of the biofilm. HFMBRs have been successfully demonstrated for treatment of carbonaceous wastewaters (Cole et al., 2004, Lapara et al., 2006), nitrification (Hibiya et al., 2000, Terada et al., 2006), and total nitrogen removal (Hibiya et al., 2003). Very recent work has also demonstrated the coupling of partial nitritation and anaerobic ammonium oxidation in a completely autotrophic nitrogen removal HFMBR with a supplemental biomass support matrix (Gong et al., 2007, 2008). In addition to these experimental demonstrations, evaluations of these systems *in silico* suggest that this type of reactor is capable of higher nitrogen removal efficiency via completely autotrophic metabolisms than co-current diffusion biofilms, especially at higher specific N loadings (Terada et al., 2007, Lackner et al., 2008). As a result, HFMBRs hold promise as a solution to the resource-intensive aspects of nitrogen removal from wastewater. Previous work, however, has shown that complete exclusion of NOB from counter-current biofilms remains difficult (Terada et al., 2006), preventing HFMBRs from realizing their full potential in N removal applications. As with suspended growth and co-current biofilm systems, the most effective control approaches for preventing NOB growth have involved using an elevated temperature, low DO, concentrations or, most often, both.

Although low DO concentrations help generate the selective pressure needed to prevent NOB proliferation in HFMBRs, there are unintended consequences of low DO concentrations that accompany novel N removal processes. In low DO environments, AerAOB are capable of autotrophically denitrifying nitrite (NO_2^-) to nitric oxide ($NO_{(g)}$) and nitrous oxide ($N_2O_{(g)}$) with ammonium as the electron donor (Poth and Focht, 1985, Schmidt and Bock, 1997, 1998, Kester et al. 1997). Genome sequencing of several AerAOB have confirmed the presence of nitrite reductase (*nir*) and nitric oxide reductase (*nor*) genes (Chain et al., 2003, Stein et al., 2007). $N_{2(g)}$ production was detected in *N. eutropha* cell-free extracts (Schmidt and Bock, 1997), but AerAOB genomes sequenced to date have failed to provide evidence of the presence of a nitrous oxide reductase (*nos*)

gene. Formation of these gases also occurs via denitritation/denitrification of NO_2^- and NO_3^- by heterotrophic microorganisms (Kester et al., 1997, Tallec et al., 2006). Emissions of $NO_{(g)}$ and $NO_{2(g)}$, the latter of which is not a biologically produced compound, contribute to the formation of atmospheric nitric acid (HNO_3) and tropospheric ozone, which is also a criteria pollutant and causes respiratory impairment (Finlayson-Pitts and Pitts, 2000). Nitrous oxide has a two-fold effect on the atmosphere: 1) catalyzing stratospheric ozone destruction, and 2) absorbing infrared radiation in the 8 to 9 μm wavelength window, thus acting as a greenhouse gas with a global warming potential 300 times that of CO_2 (Finlayson-Pitts and Pitts, 2000). Because of the detrimental effects of these emissions, implementation of N removal processes must be accompanied by strategies to control the environmental conditions that cause the emissions or control the microbial groups responsible for their generation. To this end, we have investigated the generation and control of nitrogen oxide emissions from an autotrophic N-removal HFMBR, neither of which have been previously reported.

Evaluation of microbial populations, defined as the relative quantity of target metabolic groups of interest (e.g. ammonia oxidizers, nitrite oxidizers, etc.) and activities has been performed for numerous biofilm configurations using methods such as fluorescence *in situ* hybridization (FISH) (Schramm et al., 2000, Smith et al., 2008), quantitative real-time polymerase chain reaction (qPCR) (Kindaichi et al., 2006), electrochemical microsensors (Schramm et al., 2000, Gieseke et al., 2005), microautoradiography (Gieseke et al., 2005), and PCR-DGGE (Cole et al., 2004). These studies have examined ammonia- and nitrite-oxidizing populations or activities with respect to radial distance from the membrane surface (Schramm et al., 2000 , Smith et al., 2008) or along the length of the fiber (Hibiya et al., 2003), but few have evaluated microbial communities, defined as the quantitative and spatial consortia made up of individual populations, with respect to all of these spatial and temporal variables.

The present study examines the capability of an HFMBR to achieve stable nitritation coupled with anaerobic ammonium oxidation while treating a synthetic high-strength nitrogenous wastewater. Performance is presented along with operational and control strategies related to oxygen and ammonium fluxes (J_{O2} and J_{NH4+}) to achieve desired

metabolic outcomes. Complete nitrogen mass balances are performed to examine the fate of influent nitrogen. The production of gaseous oxides of nitrogen is quantified, and the effects of short-term control strategies on the production of these gases are examined. Finally, microbial populations of AerAOB, NOB, and AnaerAOB are examined as a function of three variables: time, distance along the hollow fiber, and radial proximity to the membrane.

4.3 METHODS

Reactor configuration and operation. The HFMBR was modeled after Rector et al. (2004) without rotation of the membrane module and housed 98 fibers (0.285 m^2 total membrane surface area). Fibers were Silastic laboratory tubing (Dow Corning 508-009), 3.18 mm outer diameter, 1.98 mm inner diameter, potted in CPVC end caps. The HFMBR was operated for 555 days treating a synthetic wastewater designed to mimic urine from a confined human operation such as a long-term space exploration mission: 47.1 mM NH_3-N (added as NH_4HCO_3), 14.3 mM NaCl, 3.7 mM $KHCO_3$, 0.8 mM $KHSO_4$, 1.25 mM KH_2PO_4, 0.83 mM $MgSO_4$, 1.23 mM $CaCl_2$, 0.11 mM $FeCl_2$, in distilled water. (Hummerick, 2005, Smith et al., 2008). For feed batches on Days 274, 283, and 292, the $FeCl_2$ was replaced with 0.2 ml/l each of Trace Element Solutions I and II, slightly modified from van de Graaf et al. (1996). Trace Elements Solution I contained (per l distilled water): 1 g EDTA, 5 g $FeSO_4$; and Trace Element Solution II contained (per l distilled water): 0.43 g $ZnSO_4.7H_2O$, 0.24 g $CoCl_2.6H_20$, 0.99 g $MnCl_2.4H_2O$, 0.25 g $CuSO_4.5H_2O$, 0.22 g $NaMoO_4.2H_2O$, 0.19 g $NiCl_2.6H_2O$, 0.21 g $NaSeO_4.10H_2O$, 0.014 g H_3BO_4. EDTA was eliminated from Trace Element Solution II; acidification to pH<2 was sufficient to solubilize the constituents. Feed was restored to the original composition on Day 299.

The reactor configuration is described elsewhere (Chapter 3). Hydraulic residence time (HRT) at the highest volumetric loading rate was approximately 3.4 days, not including tubing external to the reactor for recirculation, etc. Feed and recycle entered the bottom of the upflow reactor, and inlet aeration gas (either air or 80% argon/20% oxygen)

entered at the bottom of the membrane module. Bulk liquid dissolved oxygen was checked by an Orion Model 97-08 oxygen electrode (Thermo Fisher Scientific, Waltham, MA) inserted into a flow-through cell external to the reactor. The DO electrode was inserted only during measurements to prevent sensor drift. Sample Ports 1-4 were located at 2.5, 10.2, 17.8, and 25.4 cm along the length of the 29.2 cm membrane fibers.

The reactor was inoculated only once, at startup. Two sources made up the 1 g of biomass inoculum. Two-thirds of the inoculum came from a nitrifying activated sludge that was fed an organic-carbon free ammonium-based feed (20 mM) with micronutrients for 9 days at 30°C with intermittent aeration to enrich for low-DO AerAOB. pH was adjusted every 1-2 days with sodium bicarbonate to maintain neutral pH. The remaining HFMBR inoculum was a mixture of two seed sludge sources taken from a lab-scale bioreactor performing oxygen-limited autotrophic nitrification and denitrification (OLAND) and a full-scale plant achieving anaerobic ammonium oxidation. The lab reactor was a rotating biological contactor (RBC) in Belgium (Courtesy of W. Verstraete, Ghent, Belgium), while the full scale plant was documented to perform the deammonification process treating a biosolids processing recycle stream in Strass, Austria (Courtesy of B. Wett, Strass, Austria). After attempts to culture AnaerAOB from this mixture in a sequencing batch reactor (SBR), the mixture was transferred to an anaerobic glove bag for approximately 18 months prior to HFMBR inoculation. This mixed inoculum was fed weekly with ammonium and nitrite in a 1:1.3 ratio as specified by anaerobic ammonium oxidation stoichiometry (Strous et al., 1998) along with 1 ml/l of each Trace Element Solution described above (van de Graaf et al., 1996).

Nitrogen oxide emissions. Between Days 56 and 405, outlet gas was collected approximately monthly during normal operation and more frequently (7 to 8 samples over 4 days) during perturbation experiments. Gas was collected by connecting an evacuated 1 liter Tedlar bag to the membrane module outlet. Analyses were performed as soon as possible after collection but usually within 2 hours. $N_2O_{(g)}$ was analyzed with a Shimadzu GC14A gas chromatograph (GC) with TCD detector and a 6' long stainless steel column packed with Hayesep D. The column temperature was 40°C (isocratic)

while the injector temperature and detector temperature were both held at 70°C. The detector current was set at 175 mA, and helium was used as the carrier gas at 40 kPa. Nitric oxide ($NO_{(g)}$) and $NO_{X(g)}$ ($NO_{2(g)}$ + $NO_{(g)}$) were analyzed using a chemiluminescent NO_X analyzer (Ecophysics AG, Duernten, Switzerland), model CLD88Yl. $NO_{2(g)}$ was calculated by subtracting the $NO_{(g)}$ concentration from the $NO_{X(g)}$ total concentration. Perturbation experiments were performed with the HFMBR by increasing the lumen air pressure for periods of 12 hours or increasing the feed pH for 12 hours.

Fluorescence in-situ hybridization (FISH). For all biomass samples collected prior to shutdown, a Pasteur pipette was inserted through a reactor port and biomass was extracted by suction from the surface of one or two membrane fibers. The biomass sample was homogenized by passing through a 26Ga needle 25 times, and fixed at a final concentration of 3% fresh paraformaldehyde (PFA) for 4 hours at 4°C. Following two centrifugations and washes with phosphate-buffered saline (PBS, 130 mM NaCl, 10 mM phosphate buffer, pH 7.2), biomass was resuspended in 50% PBS-50% ethanol and stored at -20°C until hybridization was performed. For quantitative FISH, only one probe was used in conjunction with 4',6-diamidino-2-phenylindole (DAPI) for each slide. For qualitative FISH, sequential hybridization was performed in order of decreasing stringency. Probes were obtained from Integrated DNA Technologies (Coralville, IA), and FISH was performed according to standard protocols (Daims et al., 2006, Manz et al., 1992) using the conditions shown in Table 4.1. Dry slides were mounted in one part Vectashield® H-1000 (Vector Laboratories, Burlingame, CA) mixed with two parts Citifluor AF-1 (Electron Microscopy Sciences, Hatfield, PA). Full-length cover slips were sealed on hybridized slides using nail polish, and edges were then wrapped in thin strips of Parafilm® M. Pure cultures of *Nitrosomonas europaea* (ATCC 19718) were used as positive controls for Nso190 and Nso1225. A nitrifying activated sludge and two lab cultures oxidizing NH_4^+ to NO_3^- were used as positive controls for NIT3 and Ntspa662. Red granules of the seed sludge from Strass, Austria were homogenized by crushing and dispersing with a needle for use as a positive control for Pla46. Pure culture *Pseudomonas aeruginosa* was used as a negative control for all probes (ranging from four to eight mismatches) except EUB338mix.

Table 4.1. Oligonucleotide probes used for microbial community analysis.

Probe Name	Sequence (5'-3')	Label	% FA[1]	mM NaCl	Reference
Nso190	CGATCCCCTGCTTTTCTCC	Cy3	30[2]	112	Mobarry et al. 1996, Rittmann et al. 1999, Konuma et al. 2000
Nso1225	CGCCATTGTATTACGTGTGA	Cy5	35	77	Mobarry et al. 1996
Pla46	GACTTGCATGCCTAATCC	Cy3	30	112	Neef et al., 1998
NIT3	CCTGTGCTCCATGCTCCG	Cy5	40	56	Wagner et al., 1996
cNIT3	CCTGTGCTCCAGGCTCCG	- -	40	56	Wagner et al., 1996
Ntspa662	GGAATTCCGCGCTCCTCT	Cy5	35	77	Daims et al., 2001
cNtspa662	GGAATTCCGCTCTCCTCT	- -	35	77	Daims et al., 2001
EUB338	GCTGCCTCCCGTAGGAGT	Cy5	30	112	Amann et al., 1990
EUB338II	GCAGCCACCCGTAGGTGT	Cy5	30	112	Daims et al., 1999
EUB338III	GCTGCCACCCGTAGGTGT	Cy5	30	112	Daims et al., 1999

[1]FA = Formamide.
[2]Nso190 FA concentration was reduced to 30% as an average of 35% (Rittmann et al., 1999) and 25% (Konuma et al., 2000).

Slides were imaged on a Zeiss LSM510 confocal scanning laser microscope with Meta detector. A minimum of 10 images were exported from LSM Image Browser (v. 4.2.0.121, Carl Zeiss MicroImaging, Inc., Thornwood, NY) as single channel images (e.g., one image each for DAPI, Cy3, and Cy5) and processed in ImageJ software (v 1.40, NIH, USA). Briefly, images were opened, background subtracted with a rolling ball radius of 50 pixels, converted to 8-bit grayscale, thresholded based on no-probe controls and no-DAPI controls, and areas were calculated by the software. The relative area that hybridized with the probe of interest was expressed as a fraction of the area stained with DAPI. Because distribution of percentages ranged from normal to lognormal, a normal distribution was assumed for all port-probe combinations, and arithmetic means and confidence intervals were used assuming a normal distribution of data. To check the suitability of DAPI as a normalizing control, biofilm samples were hybridized with EUB338 mix (I,II,III) and post-stained with DAPI. The areal fraction of DAPI signal also stained by EUB338mix was 88.7% (95% confidence interval = ±19.2%, N=30). Therefore, DAPI was deemed an acceptable control to which probe area could be normalized.

Biofilm sectioning for FISH and thickness measurement. HFMBR biofilm was fixed *in situ* (in the reactor vessel while still attached to the membranes) for analysis by FISH. Briefly, 75% of the reactor volume was drained and replaced with 4% PFA in PBS. The

reactor was incubated at 4°C for 4 hours, after which the contents were drained and replaced with PBS, which was also then fed to the system continuously for 24 hours at 2.5 ml/min. Biofilm sections were obtained at four points along the length of a single fiber. The module was positioned so as to soak several fibers in OCT compound (EMS, Hatfield, PA) for 6 hours at 4°C to allow the compound to permeate the biofilm and pores (Kindaichi et al., 2006, Okabe et al., 1999). The module was then positioned over a block of dry ice covered in foil, and a section of fiber was immersed in embedding compound and allowed to harden (approximately 15 minutes). The frozen block containing biofilm was removed by hand, backfilled with embedding compound, and placed at -80°C until sectioning. Sectioning was performed on a cryostat microtome (Microm HM550 OMP, Microm Intl. GmbH, Walldorf). For biofilm thickness measurement (thickness perpendicular to the membrane), slices ranging from 50-100 μm across (parallel to membrane surface) were analyzed by microscopy at 40X and 100X on an Axioskop 2 Plus (Carl Zeiss MicroImaging, Inc., Thornwood, NY). Thinner sections lost integrity when slicing. For FISH, slices between 50 and 100 μm across were used and analyzed by confocal microscopy as described above.

Oxygen microsensor measurements. Oxygen profiles were performed on Days 204 and 458 using an OX-10 Clark-type oxygen microsensor (Unisense, Aarhus, Denmark) with a specified nominal tip diameter between 8 and 12 μm. Calibrations and profiling were performed as described previously (Chapter 3). During profiling, the recycle pump had to be turned off and the reactor isolated with valves to prevent leakage from the vessel. However, the internal magnetic mixer remained operational during profiling and surface tension was sufficient to minimize leakage through the small diameter (~0.9 cm) sampling ports. With no recirculation pumping, estimates of boundary layer distances of 600 to 1,000 μm (Chapter 3 and Appendix G) may not be representative of what existed when recirculation was employed, although trends are still applicable.

Analytical methods. Samples for soluble analysis were filtered through 0.45 μm nitrocellulose membrane filters. Ammonia nitrogen was analyzed spectrophotometrically using the phenate method (640 nm). Nitrite was analyzed spectrophotometrically using

the colorimetric method (543 nm), and nitrate and nitrite were analyzed by ion chromatography (Dionex AS9-HC anion column). All analyses were performed in accordance with procedures outlined in Standard Methods for the Examination of Water and Wastewater (APHA, et al., 1998). Hydroxylamine was analyzed by derivatization via acetone to acetone oxime, followed by GC analysis on an HP5890 with FID detector and a SupelcoWax10 column (30m x 0.32mm x 100μm). A splitless injection (1μl) was used. The column temperature was maintained at 60°C for one minute, then ramped at 20°C/min for 7 minutes. The injector and detector temperatures were 130°C and 220°C, respectively. Helium was used as the carrier gas and flowed at 5 ml/min. For the FID gases, N_2 was used as makeup gas at 30 ml/min and flame gases were H_2 at 35 ml/min and air at 350 ml/min.

4.4 RESULTS

Controlling temperature and J_{O2}/J_{NH4+} allows control of NOB long enough to establish AnaerAOB activity. Performance was categorized into four phases: I: Startup, II: Nitritation, III: Nitritation and Partial Nitrite Oxidation, and IV: Nitritation + Anaerobic Ammonium Oxidation, as shown in Figure 4.1. To illustrate the effects of operating conditions on performance, fluxes of oxygen and ammonia are given for selected operating periods in Table 4.2.

Phase I, Days 0-23, Startup: Nitritation was rapidly established during Phase I at the startup loading of 0.82 g NH_4^+-N/m^2-day (normalized to membrane surface area), depleting the initial pool of DO contained in the media within the first five days. After the initial ammonia was consumed by Day 20, bulk liquid DO increased rapidly from <0.2 to 3.2 mg/l. Decreasing the lumen pressure from the initial setting of 9 psig to 8 psig, and doubling the influent loading on Day 23 restored the bulk DO to microaerophilic conditions (<0.3 mg/l). Ammonia was never limiting (< 1 mg/l N) again during the experiment.

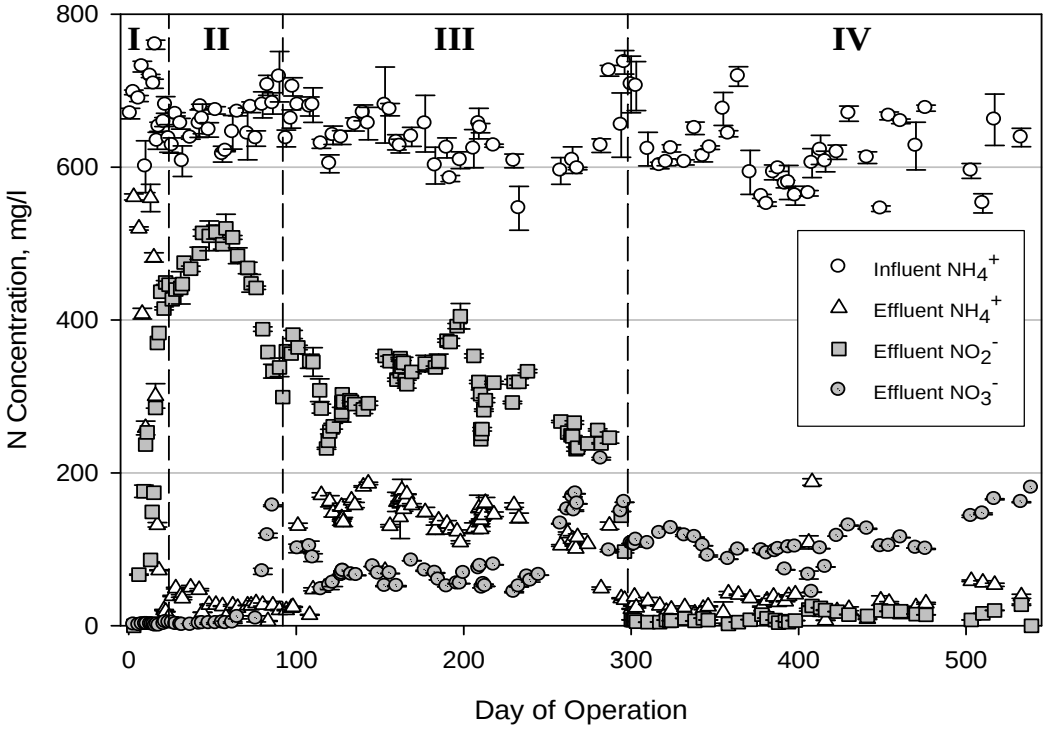

Figure 4.1. Reactor performance. Soluble nitrogen species in the reactor effluent over the duration of operation. Nitrogen in the feed was composed entirely of ammonium.

Phase II, Days 24-92, Nitritation: Stable nitritation was achieved in the HFMBR from Day 24 to 70 at a loading of 1.63 g NH_4^+-N/m^2-day. Due to an initial underestimation of the mass transfer coefficient, J_{O2}/J_{NH4+} exceeded the amount required for complete nitrification (4.57 g O_2/g NH_4^+-N). Despite this, NOB activity was not observed for most of this phase, likely due to the elevated temperature. The bulk liquid DO concentration measured with a macroelectrode averaged 0.26 $\pm$ 0.14 mg/l with the exception of one reading at 2.35 mg/l after a feed tube blockage on Day 83. However, DO concentrations measured later in the study with more sensitive microsensors suggest the DO was much lower than this in the bulk liquid (<0.05 mg/l). The complete oxidation of ammonia, plus the predominance of nitrite relative to nitrate, are evidence of nitritation as the dominant metabolism during this phase.

Table 4.2. Fluxes of oxygen transferred and ammonia removed for selected operating periods.

Period	Aeration Source[a]	Lumen Pressure, kPa (psig)	J_{O2}[b], g O_2/m^2-day	J_{NH4+}[c], g N/m^2-day	J_{O2}/J_{NH4+}
II, Day 24-92	Air	55.2 (8)	8.22	1.52	5.41
IIIa, Day 93-108	Air	34.5 (5)	7.09	1.51	4.70
IIIb, Day 109-152	Air	34.5 (5)	7.09	1.75	4.05
IIIc, Day 152-297	Argon:O_2	34.5 (5)	6.77	1.86	3.64
IV, Day 298-550	Argon:O_2	27.6 (4)	6.42	2.12	3.03

[a] Argon:O_2 = 80% argon, 20% O_2.
[b] J_{O2} calculated as $J_{O2} = K_{OL}$ (C* - C). $K_{OL} = 9.17 \times 10^{-4}$ cm/sec (Chapter 3), C = 0.42 mg/l, average of membrane-biofilm interface DO concentrations measured on Day 458.
[c] J_{NH4+} is based on ammonia removed (flux into the biofilm), not N loaded to the reactor.

Phase III, Days 93-297, Nitritation and Partial Nitrite Oxidation: After day 70, the drop in effluent NO_2^- and increase in effluent NO_3^- suggested proliferation of NOB. On Day 92, oxygen supply was reduced by lowering the air pressure in the fiber lumens from 8 psig to 5 psig, resulting in a rapid stabilization of effluent NO_2^- and effluent NO_3^- concentrations. On Day 108, a load increase to 2.3 g NH_4^+-N/m^2-day resulted in a decrease in J_{O2}/J_{NH4+} to below the value required for nitrification of all influent ammonia. As a result, oxygen-limiting conditions were established and residual NH_4^+ stabilized at concentrations approximately 20% of the influent. Replacement of the external nylon recirculation tubing (and removal of the associated biofilm) on Day 115 did not cause any change in performance, suggesting that although the tubing is slightly permeable to oxygen, the biofilm growing within was not achieving a significant amount of nitrite oxidation. The presence of both nitrite and nitrate for the remainder of this phase indicated that a combination of nitritation with partial nitrite oxidation to nitrate occurred.

A significant sloughing event occurred on Day 196, followed by an increase in effluent NH_4^+ and a decrease in effluent NO_2^- which was not accompanied by a stoichiometric increase in effluent NO_3^- that would have indicated NOB activity. This suggests that separation of a portion of AerAOB from the oxygen source may have caused the initial nitrite decrease rather than growth of new NOB. No discrete event or operating condition could be identified as the cause of the sloughing event; increasing biofilm thickness

under the influence of liquid turbulence was the likely cause. From Day 200 to 275, the effluent NO_2^-:NO_3^- ratio continued to decrease.

Phase IV, Days 298-550, Nitritation + Anaerobic Ammonium Oxidation: Between Day 287 and 298, concentrations of NH_4^+ and NO_2^- decreased drastically to below 30 mg/l and 10 mg/l, respectively, with no preceding change in ammonia or oxygen flux. It was during this period that the feed composition was altered briefly to include additional micronutrients, and was returned to the original composition on Day 299. The lumen pressure was decreased by 20% on Day 298 to further lower J_{O2}/J_{NH4+} to 3.03 g O_2/g NH_4^+-N. An anaerobic perturbation on Day 405 due to an empty aeration gas tank resulted in transient NH_4^+ accumulation and a drop in NO_3^-, the latter of which signified the presence of heterotrophic denitrifiers. After the tank was replaced, performance was rapidly restored and stabilized. Disregarding the contribution of heterotrophic denitrification and neglecting biomass N (see below), a mass balance of N species during Phase IV suggests that up to 89% of the ammonia flux (2.12 g N/m^2-d) proceeded through nitritation and anaerobic ammonia oxidation, with only 11% recovered as NO_2^- and NOB-produced NO_3^- (0.046 g N/m^2-d and 0.20 g N/m^2-d, respectively). Hence, the predominant metabolisms in the reactor at this time were aerobic nitritation and anaerobic ammonium oxidation.

Coupling anaerobic ammonium oxidation with low-DO nitritation eliminates N-oxide emissions, which short-term operational controls could not accomplish. Nitrogen balances were conducted for one day's data approximately every month between Day 56 and Day 405 during system operation. Figure 4.2 illustrates the cumulative effluent nitrogen speciation relative to the influent N load to the reactor. Biomass N was calculated from the total 'suspended' solids of the biofilm (7.36 g TSS) and TKN of the biomass (0.13 g N/g TSS), both of which were measured after shutdown. Assuming linear accumulation of biomass over the 550 days of operation (0.0017 g biomass N/day), biomass N was always less than 1% of the daily total influent N and is thus not included in Figure 4.2. An average of 16% of the influent nitrogen load (95% C.I.=13%-19%) was unaccounted for during Phase II using only NH_3, NO_2^-, NO_3^-, and biomass N, which motivated the decision to measure the following non-traditional N

species: $NH_2OH_{(aq)}$, $NO_{(g)}$, $N_2O_{(g)}$, $NO_{2(g)}$, and $N_{2(g)}$. Hydroxylamine was not detected early in the operation and monitoring was discontinued. Measurements of $N_{2(g)}$ resulted in N balances >100% due to sample contamination with ambient N_2. However, the contribution of $NO_{x(g)}$ and $N_2O_{(g)}$ to the N balances was significant. Between Days 93

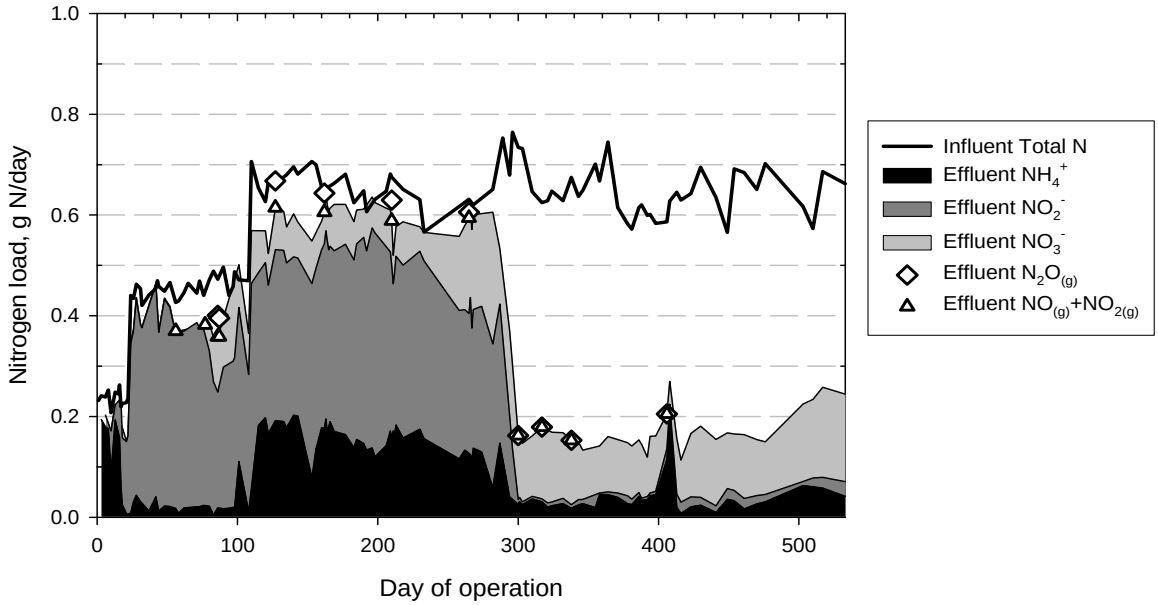

Figure 4.2. Aqueous and gaseous effluent nitrogen speciation (cumulative) from N balances. Influent contained only NH_4^+. All effluent species are cumulative. Gaseous species are marked with $_{(g)}$, all others are aqueous.

and 265, $NO_{x(g)}$ and $N_2O_{(g)}$ concentrations averaged 56 ppm and 2,540 ppm, respectively. The highest $N_2O_{(g)}$ concentration of 3,650 ppm was measured on Day 127, and was accompanied by $NO_{(g)}$ and $NO_{2(g)}$ concentrations of 27 and 49 ppm, respectively.

Two experiments were conducted to determine if short-term operational changes could reduce or eliminate emissions. During the first experiment, the lumen pressure was increased for 12 hours to promote a shift toward aerobic metabolism. The shift decreased $N_2O_{(g)}$ emissions (Figure 4.3), but the decrease was consistent with what was predicted by Henry's Law (Figure 4.3C, horizontal dashed line) and could be explained by physical phenomena rather than biological changes. During the second experiment, the pH (>8) was increased for 12 hours. It was expected that this pH shift would reduce expression of the nitrite reductase gene (*nirK*) in AerAOB, based on work by Beaumont and colleagues

(2004). While $NO_{(g)}$ and $NO_{2(g)}$ decreased, $N_2O_{(g)}$ emissions increased (Figure 4.4). This result was the opposite of what was expected. The results from both experiments imply that short term changes are not sufficient to reduce gaseous emissions.

As shown in Figure 4.2, the shift towards anaerobic ammonium oxidation was accompanied by a remarkable decrease in gaseous emissions (99.9% decrease compared to Day 210 emissions). $NO_{(g)}$ and $NO_{2(g)}$ concentrations, while still detectable, fell to below 7 ppm each following Day 300. The concentration of $N_2O_{(g)}$ fell below the detection limit of 100 ppm. Thus, when AnaerAOB activity was established in the system which was achieving nitritation, N-oxide emissions were significantly reduced.

Biofilm structure shows clear differences in morphology, density and color with distance from the membrane. Despite high liquid recirculation (0.5 l/min) and mechanical mixing from below the module, some of the inoculum biomass settled into the base of the vertical membrane modules, resulting in colonization of the lowest region of the fibers first and the highest region of the fibers last. Biofilm thickness measurements were performed after harvesting the biofilm on Day 555, and revealed that thickness generally decreased along the length of the reactor (Table 4.3). Microscopic observation of biofilm sections taken after harvesting revealed regions of different morphology across the depth

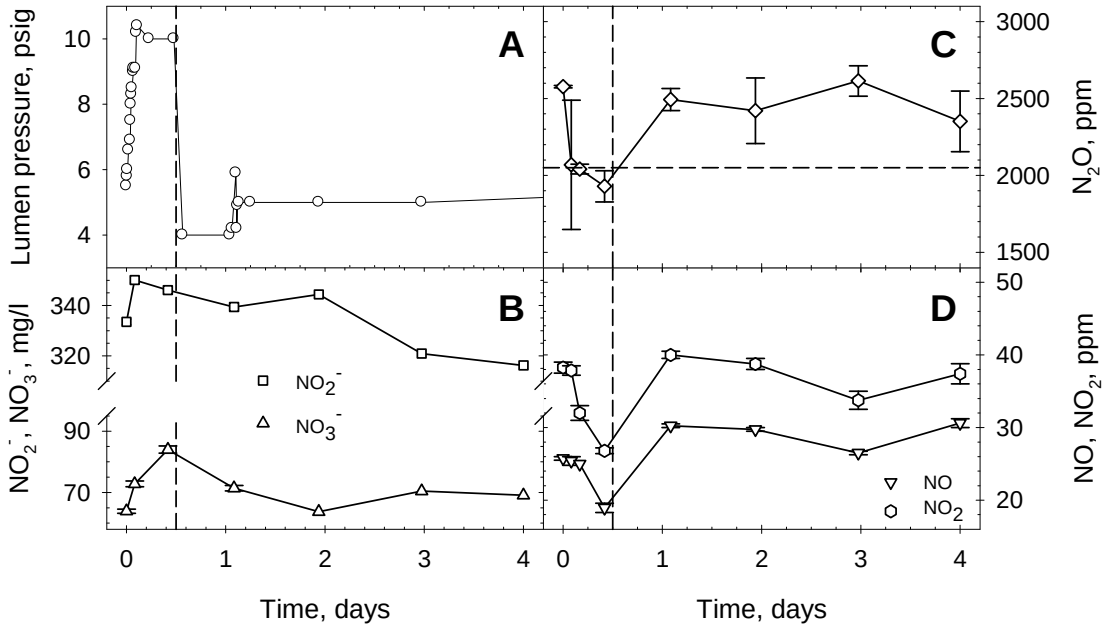

Figure 4.3. Effects of oxic perturbation experiment on gaseous emissions. Vertical line represents duration of elevated lumen pressure. Horizontal line in Panel C represents N_2O concentration predicted by Henry's law based on lumen pressure.

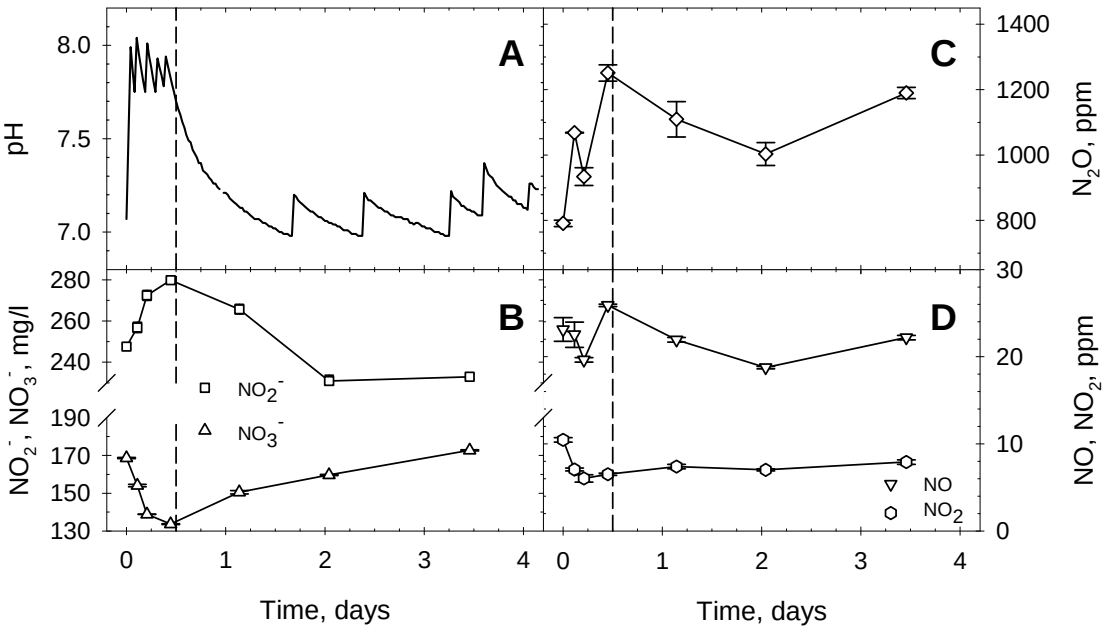

Figure 4.4. Effects of elevated pH perturbation experiment on gaseous emissions. Vertical line represents duration of elevated pH.

of the biofilm. Contrast within the biofilm, considered representative of density, decreased with distance from the membrane surface (Figure 4.5, M) until the region located 100-200 µm from the biofilm-liquid interface (Figure 4.5, L), which had an orange-rust color similar to that typically observed in cultures enriched for AnaerAOBs (Wett, 2006, Strous et al., 1998). During slicing, biofilm sections often tore in the middle 200 µm region, suggesting less cohesive structure. The biofilm-liquid surface (Figure 4.5, L) ranged from clearly defined to fibrous and loose.

Table 4.3. Measured biofilm thickness at Day 555.

Reactor Port	Distance from fiber inlet, cm	Biofilm Thickness, µm[a]	No of images (measurements)[b]
1	2.54	674 ± 29	15 (31)
2	10.16	625 ± 25	14 (31)
3	17.78	443 ± 12	15 (40)
4	25.40	526 ± 17	14 (31)

[a] ± values = 95% confidence intervals.
[b]Multiple measurements were taken from each biofilm image.

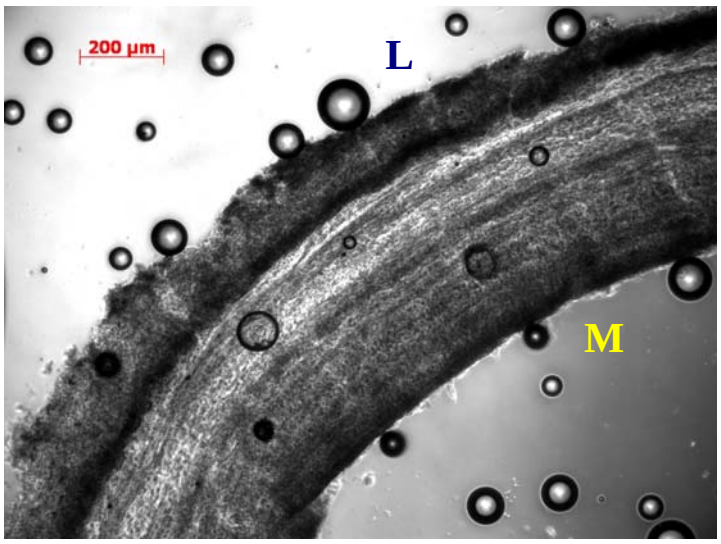

Figure 4.5. Biofilm morphology. Transmitted light image, 100 µm thick (into page) slice, 40X. (M) membrane-biofilm interface, (L) biofilm-liquid surface. Bubbles are visible in thawed embedding compound, which was used as mounting medium.

Inter-fiber growth was not observed when inspected after shutdown. The membrane fibers harbored 6.84 g biomass VSS (7.36 g of biomass TSS), equivalent to a specific biomass coverage of 23.9 g biomass VSS/m^2 surface area. Biomass in the external recirculation tubing was quantified, extrapolated to the entire tubing system, and calculated to be approximately 0.93 g VSS (1.11 g TSS). Hence, up to 13% of the total biomass in the system was external to the vessel. Using the fiber radius (1.59 mm) and the measured thicknesses in Table 4.3, a mathematical solid of rotation was integrated to calculate a biofilm volume of 189 cm^3 (0.066 cm^3/cm^2 fiber surface area). Using this value and the measured biomass TSS, biofilm density was calculated to be 0.038 g TSS / cm^3 (~4% solids, 93% volatile). DO microsensor profiles on Day 204 (Chapter 3) and Day 458 (Appendix G) revealed that a microaerobic region extended at most 90 μm from the membrane, with membrane surface DO concentrations ranging from 0.80 mg/l at Port 1 to 0.20-0.40 mg/l at Ports 2-4. This microaerobic region may have contributed to the increased density of biomass nearest the membrane, due to the higher yield of aerobic growth relative to anoxic growth.

Low-DO microenvironments generate radial stratification of microbial communities in the biofilm. Table 4.4 shows populations of FISH-targeted groups in homogenized samples relative to three sample dates and port locations in the reactor. On Day 192, AerAOB were the dominant organisms of all the target groups at all ports. Although the average percentage increased along the length of the fiber, the increase was not significant using a linear regression to test significance of distance as a variable (P=0.12) nor was the regression model a good predictor of AerAOB prevalence (R^2=0.06). Despite using a syringe to homogenize samples, microcolonies of AerAOB were prevalent. The formation of microcolonies by AerAOB is a common phenomenon (Coskuner et al, 2005), and these results suggest that a large fraction of the AerAOB may have existed as microcolonies within the undisturbed biofilm. AnaerAOB were detected sparsely but were not a substantial component of the microbial community on Day 192.

Table 4.4. Relative microbial populations (%) over time and along length of fibers.[a]

Day and Port	AerAOB (Nso190)	*Nitrobacter*-like NOB (NIT3)	*Nitrospira*-like NOB (Ntspa662)	AnaerAOB (Pla46)	Non-target organisms[b]
Day 192					
Port 1	22.7 (11.2)	5.3 (2.8)	9.1 (7.2)	0.53 (0.79)	62.4
Port 2	30.9 (14.5)	2.4 (2.0)	19.0 (12.5)	0.24 (0.18)	46.4
Port 3	33.2 (13.0)	9.6 (7.7)	4.4 (2.6)	0.57 (0.40)	52.3
Port 4	37.1 (11.3)	25.6 (15.3)	11.4 (9.8)	0.27 (0.16)	25.6
Day 325					
Port 1	26.7 (20.3)	0.3 (0.2)	1.6 (2.2)	0.37 (0.32)	71.0
Port 2	7.0 (5.4)	1.3 (2.2)	2.1 (1.8)	0.11 (0.11)	89.5
Port 3	15.1 (13.8)	7.1 (3.6)	10.1 (4.6)	0.30 (0.20)	67.4
Port 4	7.0 (5.2)	4.8 (2.7)	12.9 (6.3)	0.57 (0.42)	74.6
2-regrowth	4.4 (2.0)	9.2 (4.9)	17.1 (9.3)	2.3 (2.56)	67.0
Day 538					
Port 1	18.3 (8.0)	12.8 (9.6)	3.5 (3.5)	3.7 (2.0)	61.8
Port 2	4.9 (3.4)	12.5 (9.2)	6.9 (6.3)	16.4 (14.4)	59.3
Port 3	5.9 (1.9)	3.3 (2.4)	5.2 (2.7)	5.6 (2.8)	80.1
Port 4	21.8 (8.2)	1.9 (1.0)	7.2 (3.9)	10.3 (12.5)	58.9

[a] Numbers represent probe-conferred fluorescence area as a percentage of DAPI-conferred fluorescence area (95% confidence intervals).
[b] Non-target organisms calculated by 100% minus sum of target organisms.

On Day 325, the average percent of both NOB groups increased with respect to distance along the reactor. Distance was a significant variable for both (i) NIT3-positive organisms ($P=0.003$), and (ii) Ntspa662-positive organisms ($P=8\times10^{-5}$). Biofilm regrowth on a Port 2 fiber previously made bare by biomass sampling on Day 192 revealed a significant increase in the relative percentage of NOB on Day 325 ($P= 0.01$ for both Ntspa662 and NIT3) compared to the undisturbed Port 2 biofilm sample.. Again, only minimal AnaerAOB were detected on Day 325, despite observed performance stoichiometry that was consistent with anaerobic ammonium oxidation activity at that time.

AnaerAOB were detected in significant amounts on Day 538, typically in clusters ranging in size from <5 μm to >30 μm. No strong trends in microbial community were observed with respect to distance along the fibers, with the exception that AerAOB were more numerous at Ports 1 and 4 than Ports 2 and 3 ($P<0.005$).

Although structural community patterns were not observed to be different along the length of the fibers, interrogation of the community structure in the radial direction revealed a more clear pattern. Using structurally intact biofilm sections, a band of AnaerAOB was visible in the outer region of the biofilm using FISH (Figure 4.6A). Confocal micrographs show this band to be composed of dense clusters (Figure 4.6B) that were typically located 65% to 90% of the biofilm depth away the membrane (dehydration process caused shrinking of the biofilm slice, so absolute distance is not relevant in Figure 4.6). AerAOB were found most often near the membrane surface (Figure 4.6C-E) either in microcolonies or in striated bands. In some samples, a second region of AerAOB was visible midway through the biofilm (Figure 4.6C, E), and signals here were more intense with the probe Nso1225 than with Nso190 (See Figure 4.6A), suggesting that the majority of these AerAOB were groups with higher Nso1225 specificity. These mid-depth AerAOB were also often associated with microcolonies of NOB (Figure 4.6C, E, F). The microcolony association of *Nitrospira*-like NOB with Nso190-positive AerAOB at the membrane surface was only observed at Port 1 (Figure 4.6D), with no other NOB detected throughout the biofilm. At Ports 2 through 4, both *Nitrospira* and *Nitrobacter* (Figures 4.6 E and F, respectively) were found primarily in the mid-region of the biofilm, associated with Nso190-positive AerAOB. This observation was the only difference in radial distribution observed with respect to the four ports and their location along the reactor, although some port-probe combinations could not be observed due to repeated destruction or detachment of the biofilm during the hybridization process.

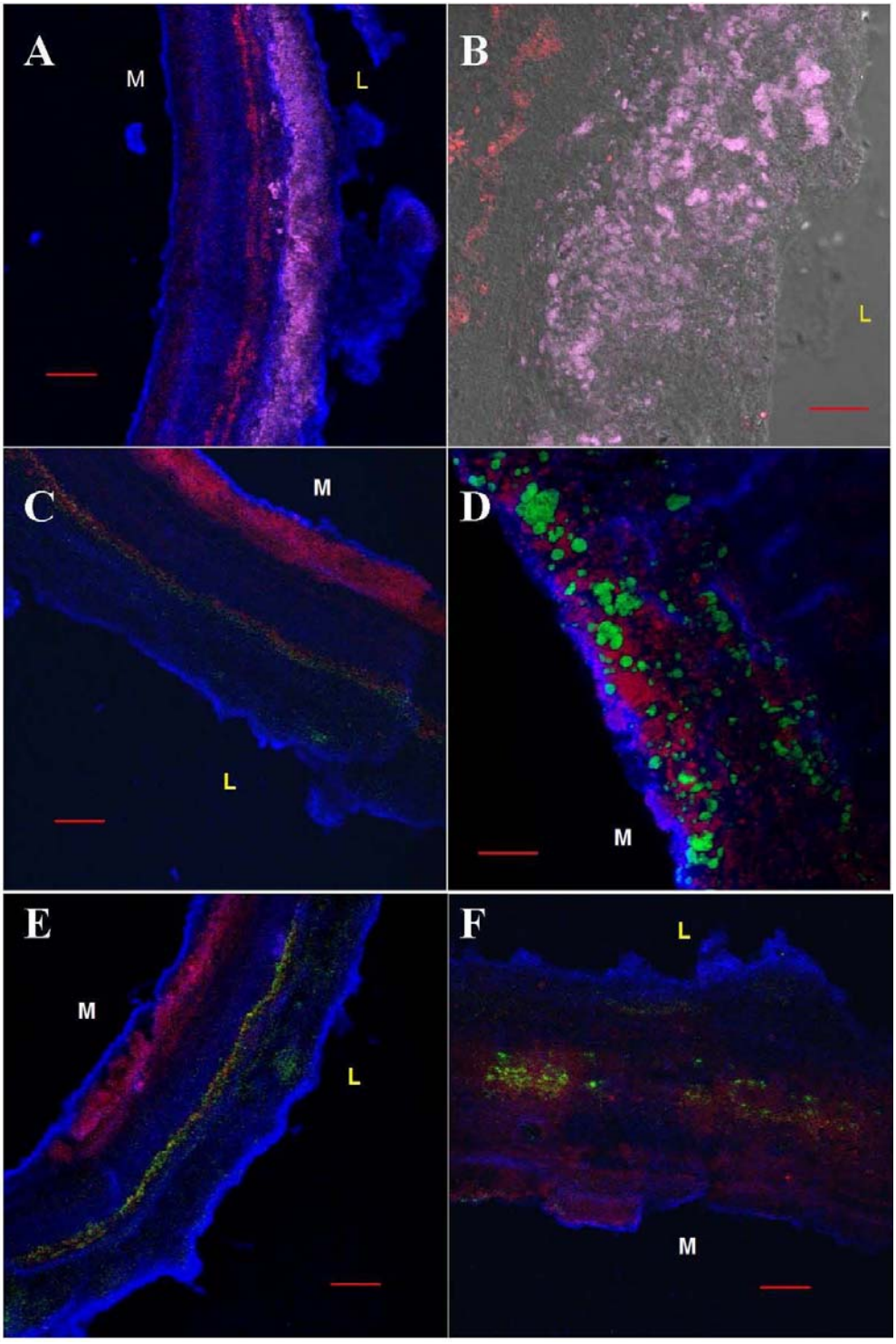

Figure 4.6. Radial distribution of microbial populations. M: Membrane side of biofilm; L: Liquid side of biofilm. Blue in all panels: DAPI; Panels A, B: Nso1225 (red) and Pla46 (magenta); C, D, E: Nso190 (red) and Ntspa662 (green); F: Nso190 (red) and NIT3 (green). Scale bars: A, C, E, F:100 µm. B, D:30 µm. Panel B: transmitted light image shown instead of DAPI channel.

4.5 DISCUSSION

Reactor performance and control. Nitritation was rapidly established in the HFMBR, and was also observed by others in similar systems (Hibiya et al., 2003, Kindaichi et al., 2006). Likewise, the appearance of NOB was observed in membrane biofilm or biomass retention systems (Terada et al., 2006, Sliekers et al., 2005). Terada et al. (2006) suggested two control approaches for minimizing NOB activity: (i) use an inoculum acclimated to low DO conditions in order to select for AerAOB with low K_{O2} values, and/or (ii) precisely control the ammonium/oxygen flux ratio. The seed used in the present study was a mixture of two sources, the first being a nitrifying activated sludge subjected to 9 days of carbon-free feed and intermittent aeration to select for AerAOB amenable to low DO conditions, and the second being an anaerobic glove bag culture intended to enrich for AnaerAOB. The appearance of NOB in the reactor suggests that low-DO, elevated-temperature seed sludge acclimation alone is not sufficient to exclude nitrite oxidizers.

Performance data demonstrate that establishing conditions to favor AerAOB over NOB, with low DO (achieved through appropriate J_{O2}/J_{NH4+}) and elevated temperature as the primary control parameters, can be successful at maintaining stable nitritation. The initially high values of J_{O2}/J_{NH4+} (Table 4.1) were a result of underestimation of the mass transfer coefficient for the system, and the excess oxygen flux likely contributed to NOB proliferation. Reduction of this ratio after Day 109 to below the nitrification threshold ($J_{O2}/J_{NH4+} = 4.57$) was successful in controlling, if not eliminating further proliferation of NOB. This flux ratio has been shown by others through modeling and experimental studies to be a key parameter for achieving partial nitritation (Bernet et al, 2005, Matsumoto et al., 2007, Terada et al., 2007). Even though J_{O2}/J_{NH4+} was in excess of that required for nitritation, incomplete ammonia oxidation was observed, suggesting localized oxygen-limited microenvironments likely due to competing oxygen consumption by NOB and/or heterotrophs. A free ammonia (FA) concentration of 1.6 mg/l-N between days 115 and 230 was unlikely to inhibit NOB (Vadivelu et al., 2006, 2007, Kim et al., 2006, Anthonisen et al., 1976); furthermore, free nitrous acid (FNA) was not significant. For the current study, both elevated temperature and oxygen

limitation are assumed to be the operational controls that prevented complete nitrite oxidation in the HFMBR.

The appearance of AnaerAOB activity after 300 days of operation is consistent with the slow growth rates published for these bacteria by others (Gong et al., 2008, Strous and Jetten, 2004), though some have reported more rapid onset (Gong et al. 2008). It is possible that AnaerAOB were micronutrient-limited prior to this point, and the change in micronutrient solution on Day 274 provided sufficient micronutrients for their growth. This infusion of nutrients may also explain the relatively rapid onset of AnaerAOB activity. The optimum J_{O2}/J_{NH4+} for completely autotrophic removal of nitrogen is 1.96 g O_2/g NH_4^+, based on oxidizing 57% of the influent NH_4^+ to NO_2^- to achieve anaerobic ammonium oxidation stoichiometry (Strous et al., 1998). The present work demonstrated that performance can be achieved at a flux ratio as high as 3.0 (Phase IV), but NOB and heterotrophs will be present in the community. This observation is consistent with modeling predictions that AnaerAOB activity can occur at J_{O2}/J_{NH4+} as high as 3.7, especially in thicker biofilms (Terada et al., 2007).

The presence of heterotrophic denitrifiers was evident from the decrease in nitrate on Day 405 during the lapse in aeration. Multipopulation modeling of a similar system suggests that at higher ammonium loading rates (>3 g N/m^2-day), nitrogen removal performance decreases due to increased growth of heterotrophs and oxygen inhibition of AnaerAOB (Lackner et al., 2008). More specifically, the higher N load to the system requires such an increase in oxygen flux for nitritation that DO penetration into the biofilm reaches the location of AnaerAOB. However, loading rates above 2.3 g N/m^2-day were not evaluated in the present work. The trends in performance nearing shutdown (increasing NO_3^-, higher NH_4^+ concentrations) also suggest that the microbial community may have been continuing to evolve in the system towards heterotrophic and nitrite-oxidizing groups.

Nitrogen balancing and N oxides. The combination of consumptive and productive processes that contribute to nitrogen oxide emissions make it difficult to infer their source(s) from concentrations alone (Stein and Yung, 2003). However, it is hypothesized that the NO and N_2O in this study were primarily attributable to autotrophic

denitrification, for several reasons. First, emissions were present only in the first 300 days of the study and highest at Day 127, when autotrophic metabolisms dominated the reactor. Second, high nitrite concentrations such as those observed here have been shown to cause a nitrite-sensing transcription repressor (NsrR) to reverse its repression of *nirK* in *N. europaea* (Beaumont et al., 2004). Those authors found this derepression is particularly marked in the neutral pH range (~7.2), in which this HFMBR was operated, suggesting this mechanism may have been active during Phases II and III. Third, nitrite buildup from AerAOB can inhibit N_2O production by heterotrophs (Stein and Yung, 2003, Averill, 1996, Payne et al., 1971). These supporting studies point towards autotrophic denitrification as the primary source of N-oxide emissions from the HRMBR. The short-term perturbation experiments were largely unsuccessful at reversing these emission trends.

The disappearance of N-oxide emissions coinciding with the establishment of anaerobic ammonium oxidation demonstrates an advantage of coupling the two autotrophic processes in a single reactor. This may be due to the subsequent absence of NO_2^- available for NsrR-mediated regulation of *nirK* in AerAOB. In addition, AnaerAOB may have a higher affinity for NO_2^- (lower K_{NO2-}) than NsrR in AerAOB or the nitrite reductase enzymes of either autotrophic AerAOB or heterotrophic denitrifiers. Very low K_{NO2-} values have been reported in the range of 0.05 to 0.1 mg NO_2^--N/l for AnaerAOB (Hao et al., 2002, Strous et al., 1999), significantly lower than K_{NO2-} for aerobic NOB (5.5 mg NO_2^--N/l, Weismann, 1994). Quantitative comparison of affinities cannot be made from the present study. However, the elimination of emissions reduces the global warming potential of this coupled process configuration.

Biofilm structure. The specific biomass coverage (23.9 g VSS/m^2) compares well to values reported previously (Terada et al., 2006, Brindle et al., 1998, Smith et al., 2008). In general, the calculated biofilm solids density of 0.038 g/cm^3 is also reasonable when compared to available literature (0.05 – 0.20 g/cm^3, Celmer et al., 2006, 0.03 – 0.06 g/cm^3, Ong et al., 2006, 0.02 – 0.15 g/cm^3, Zahn et al., 2006). The biofilm exhibited a trend of decreasing thickness (Table 4.3) from gas inlet to outlet, although the microbial

community was not observed to vary along the fibers. The low degree of oxygen penetration into the biofilm (9.0% to 16% of biofilm depth) was lower than comparable studies (Schramm et al., 2000, Terada et al., 2003). The latter study used similar lumen pressures but a microporous membrane and had significantly higher membrane surface DO concentrations (3-5 mg/l), illustrating the effect of membrane material on oxygen transfer. Specifically, the sorption-dissolution-diffusion mechanism of non-porous membranes imparts an oxygen gradient across the fiber wall, as opposed to microporous membranes where oxygen is in the gas phase all the way up to the biofilm base and yields higher DO concentrations. This suggests an important consideration in the application of HFMBR systems: the membrane material selected may have a significant impact on the DO concentration at the membrane biofilm interface and, hence, the microbial metabolisms occurring there. If the membrane material and operating conditions result in DO concentrations that are too high, the resulting microenvironments may select for undesired populations within the microbial community.

Microbial population dynamics and distribution. In general, distance along the membrane fiber did not substantially influence microbial community. Tracer tests support this observation, as reactor hydrodynamics were shown to model as 1 to 2 completely-mixed stirred tank reactors (CSTRs) in series. An oxygen gradient along the fibers, as predicted by both a mechanistic model and outlet oxygen gas analyses (Chapter 3), appears not to be a strong determinant of microbial community, at least at this scale. The higher presence of NOB at regrowth locations (Table 4.4) suggests a weakness of the HFMBR configuration: sloughing creates conditions of relatively high-DO at the exposed membrane. If NO_2^- is present in the bulk liquid, a niche environment favorable for NOB growth develops.

Radial stratification of microbial groups across the biofilm was consistent with both experimental and modeling studies (Smith et al., 2008, Terada et al., 2003, Lackner et al., 2008) and with intuition considering the oxygen source. In addition, the lack of target organisms between the AerAOB and AnaerAOB layers is consistent with computational models that predict the middle region selects for heterotrophic bacteria feeding on

organic decay products (Lackner et al., 2008). The presence of AerAOB and NOB at significant distances from the membrane (Figure 4.6A & C) was unexpected, as DO was negligible in this region. These organisms may have grown near the biofilm and been displaced outward over time. Alternatively, they may have grown at the liquid interface by scavenging minute quantities of oxygen from the bulk liquid, prior to being enveloped by the AnaerAOB layer. The observation of stronger signals here with Nso1225, which has a higher specificity than Nso190 for *N. oligotropha* and *N. marina* AerAOB clusters, could suggest that perhaps they are enriched as the biomass is displaced further from the membrane and oxygen becomes more scarce. The observation that NOB were found near the membrane only at Port 1 was also unexpected. At all subsequent ports, *Nitrobacter* sp. and *Nitrospira* sp. were found only in the mid-region of the biofilm and with approximately equal frequency (not quantified). The presence of these NOB species in the oxygen-poor region of the biofilm may be due to displacement by underlying growth of AerAOB and heterotrophs, as discussed above. Further study is needed on systems with the ability to remove biofilm sections for community analysis at different times over the life of the system to determine the nature of these dynamics.

4.6 CONCLUSIONS

Control of temperature and the relative fluxes of oxygen and ammonia allowed successful coupling of partial nitrification and anaerobic ammonium oxidation in an HFMBR. The HFMBR successfully achieved sustained nitrogen removal from an organic carbon-free synthetic wastewater, realizing significant resource savings in the form of oxygen supplied, biomass produced, and alkalinity consumed. The emergence of anaerobic ammonium oxidizing activity coincided with the disappearance of nitrogen oxide emissions, demonstrating an additional benefit of coupling these autotrophic metabolisms in a single reactor.

Analysis of the microbial community revealed few consistent trends with respect to length along the reactor, but patterns of radial population distribution were clearly evident, suggesting the microenvironments in this dimension are the more significant determinants of microbial community structure. The results presented herein establish a

foundation for application of nitritation-anaerobic ammonium oxidation HFMBRs to a broad range of wastewaters. Future studies should focus on i) determination of spatial population distribution within the biofilm community over time, ii) more rapid startup through sequential seeding techniques, and iii) application to more representative waste streams containing varying concentrations and forms of organic carbon.

4.7 REFERENCES

Anthonisen, A.C., Loehr, R.C., Prakasam, T.B.S. and Srinatu, E.G. (1976) Inhibition of nitrification by ammonia and nitrous acid. *J. Wat. Pollut. Control Fed.* **48**:835-852.

APHA, AWWA, and WEF (1998) Standard Methods for the Examination of Water and Wastewater, APHA, New York.

Averill, B.A. (1996) Dissimilatory nitrite and nitric oxide reductases. *Chem. Rev.* **96**:2951-2964.

Bernet, N., Sanchez, O., Cesbron, D., Steyer, J.P. and Delgenès, J.P. (2005) Modeling and control of nitrite accumulation in a nitrifying biofilm reactor. *Biochem. Eng. J*. **24**(2):173-183.

Brindle, K., Stephenson, T. and Semmens, M.J. (1998) Nitrification and oxygen utilisation in a membrane aeration bioreactor. *J. of Membr. Sci.* **144**(1-2):197-209.

Celmer, D., Oleszkiewicz, J., Cicek, N. and Husain, H. (2006) Hydrogen limitation - a method for controlling the performance of membrane biofilm reactor for autotrophic denitrification of wastewater. *Water Sci. Technol.* **54**(9):165-172.

Chain, P., Lamerdin, J., Larimer, F., Regala, W., Lao, V., Land, M., Hauser, L., Hooper, A., Klotz, M., Norton, J., Sayavedra-Soto, L., Arciero, D., Hommes, N., Whittaker, M. and Arp, D. (2003) Complete genome sequence of the ammonia-oxidizing bacterium and obligate chemolithoautotroph *Nitrosomonas europaea*. *J. Bacteriol.* **185**(9):2759-2773.

Cole, A.C., Semmens, M.J. and LaPara, T.M. (2004) Stratification of activity and bacterial community structure in biofilms grown on membranes transferring oxygen. *Appl. Environ. Microbiol.* **70**(4):1982-1989.

Coskuner, G., Ballinger, S.J., Davenport, R.J., Pickering, R.L., Solera, R., Head, I.M. and Curtis, T.P. (2005) Agreement between theory and measurement in quantification of ammonia-oxidizing bacteria. *Appl. Environ. Microbiol.* **71**(10):6325-6334.

Finlayson-Pitts, B.J. and J. N. Pitts, J. (2000) Chemistry of the upper and lower atmosphere: theory, experiments, and applications. Academic Press, San Diego.

Furukawa, K., Lieu, P.K., Tokitoh, H. and Fujii, T. (2006) Development of single-stage nitrogen removal using anammox and partial nitritation (SNAP) and its treatment performances. *Water Sci. Technol.* **53**(6):83-90.

Fux, C.M., Boehler, M., Huber, P., Brunner, I. and Siegrist, H. (2002) Biological treatment of ammonium-rich wastewater by partial nitritation and subsequent anaerobic ammonium oxidation (anammox) in a pilot plant. *J. Biotechnol.* **99**: 295-306.

Gieseke, A., Nielsen, J.L., Amann, R., Nielsen, P.H. and de Beer, D. (2005) In situ substrate conversion and assimilation by nitrifying bacteria in a model biofilm. *Environ. Microbiol.* **7**(9):1392-1404.

Gilmore, K.R., Little, J.C., Smets, B.F. and Love, N.G. (In review) Oxygen transfer model for a flow-through hollow-fiber membrane biofilm reactor.

Gong, Z., Liu, S., Yang, F., Bao, H. and Furukawa, K. (2008) Characterization of functional microbial community in a membrane-aerated biofilm reactor operated for completely autotrophic nitrogen removal. *Biores. Technol.* **99**(8):2749-2756.

Hao, X., Heijnen, J.J. and van Loosdrecht, M.C.M. (2002) Sensitivity analysis of a biofilm model describing a one-stage completely autotrophic nitrogen removal (CANON) process. *Biotechnol. Bioeng.* **77**(3):266-277.

Hellinga, C., Shellen, A.A.J.C., Mulder, J.W., van Loosdrecht, M.C.M. and Heijnen, J.J. (1998) The SHARON process: an innovative method for nitrogen removal from ammonium-rich waste water. *Water Sci. Technol.* **37**(9):135-142.

Helmer, C., Tromm, C., Hippen, A., Rosenwinkel, K.-H., Seyfried, C.F. and Kunst., S. (2001) Single stage biological nitrogen removal by nitritation and anaerobic ammonium oxidation in biofilm systems. *Water Sci. Technol.* **43**(1):311-320.

Hibiya, K., Terada, A., Tsuneda, S. and Hirata, A. (2003) Simultaneous nitrification and denitrification by controlling vertical and horizontal microenvironment in a membrane-aerated biofilm reactor. *J. Biotechnol*. **100**:23-32.

Hibiya, K., Tsuneda, S. and Hirata, A. (2000) Formation and characteristics of nitrifying biofilm on a membrane modified with positively-charged polymer chains. *Colloids and Surfaces B: Biointerfaces.* **18**(2):105-112.

Hummerick, M. (2005) Personal communication.

Kester, R.A., Meijer, M.E., Libochant, J.A., De Boer, W. and Laanbroek, H.J. (1997) Contribution of nitrification and denitrification to the NO and N_2O emissions of an acid forest soil, a river sediment and a fertilized grassland soil. *Soil Biol. Biochem.* **29**(11-12):1655-1664.

Kim, D.-J., Lee, D.-I. and Keller, J. (2006) Effect of temperature and free ammonia on nitrification and nitrite accumulation in landfill leachate and analysis of its nitrifying bacterial community by FISH. *Biores. Technol.* **97**(3):459-468.

Kindaichi, T., Kawano, Y., Ito, T., Satoh, H. and Okabe, S. (2006) Population dynamics and in situ kinetics of nitrifying bacteria in autotrophic nitrifying biofilms as determined by real-time quantitative PCR. *Biotechnol. Bioeng.* **94**(6):1111-1121.

Lackner, S., Terada, A. and Smets, B.F. (2008) Heterotrophic activity compromises autotrophic nitrogen removal in membrane-aerated biofilms: Results of a modeling study. *Water Res.* **42**(4-5):1102-1112.

LaPara, T.M., Cole, A.C., Shanahan, J.W. and Semmens, M.J. (2006) The effects of organic carbon, ammoniacal-nitrogen, and oxygen partial pressure on the stratification of membrane-aerated biofilms. *J. Ind. Microbiol. Biotechnol.* **33**:315-323.

Matsumoto, S., Terada, A. and Tsuneda, S. (2007) Modeling of membrane-aerated biofilm: Effects of C/N ratio, biofilm thickness and surface loading of oxygen on feasibility of simultaneous nitrification and denitrification. *Biochem. Eng. J.* **37**(1):98-107.

Okabe, S., Satoh, H. and Watanabe, Y. (1999) In situ analysis of nitrifying biofilms as determined by in situ hybridization and the use of microelectrodes. *Appl. Environ. Microbiol.* **65**(7):3182-3191.

Ong, S.L., Sarkar, S.K., Lee, L.Y., Hu, J.Y., Ng, H.Y. and van Loosdrecht, M. (2006) Effect of formaldehyde on biofilm activity and morphology in an ultracompact biofilm reactor for carbonaceous wastewater treatment. *Water Environ. Res.* **78**:372-380.

Payne, W.J., Riley, P.S. and Cox, Jr., C.D. (1971) Separate nitrite, nitric oxide, and nitrous oxide reducing fractions from *Pseudomonas perfectomarinus*. *J. Bacteriol.* **106**(2):356-361.

Picioreanu, C., van Loosdrecht, M.C.M. and Heijnen, J.J. (1997) Modelling the effect of oxygen concentration on nitrite accumulation in a biofilm airlift suspension reactor. *Water Sci. Technol.* **36**(1):147-156.

Poth, M. and Focht, D.D. (1985) 15N Kinetic analysis of N_2O production by *Nitrosomonas europaea*: an examination of nitrifier denitrification. *Appl. Environ. Microbiol.* **49**(5):1134-1141.

Pynaert, K., Smets, B.F., Beheydt, D. and Verstraete, W. (2004) Start-up of autotrophic nitrogen removal reactors via sequential biocatalyst addition. *Environ. Sci. Technol.* **38**:1228-1235.

Schmidt, I. and Bock, E. (1997) Anaerobic ammonia oxidation with nitrogen dioxide by *Nitrosomonas eutropha*. *Arch. Microbiol*. **167**:106-111.

Schmidt, I. and Bock, E. (1998) Aerobic ammonia oxidation by cell-free extracts of *Nitrosomonas eutropha*. *Antonie van Leeuwenhoek* **73**:271-278.

Schramm, A., Beer, D.D., Gieseke, A. and Amann, R. (2000) Microenvironments and distribution of nitrifying bacteria in a membrane-bound biofilm. *Environ. Microbiol.* **2**(6):680-868.

Sleikers, A.O., Haaijer, S.C.M., Stafsnes, M.H., Kuenen, J.G. and Jetten, M.S.M. (2005) Competition and coexistence of aerobic ammonium- and nitrite-oxidizing bacteria at low oxygen concentrations. *Appl. Microbio. Biotechnol.* **68**:808-817.

Smith, D.P., Rector, T., Reid-Black, K., Hummerick, M., Strayer, R., Birmele, M., Roberts, M.S. and Garland, J.L. (2008) Redox control bioreactor: A unique biological water processor. *Biotechnol. and Bioeng.* **99**(4):830-845.

Stein, L.Y., Arp, D.J., Berube, P.M., Chain, P.S.G., Hauser, L., Jetten, M.S.M., Klotz, M.G., Larimer, F.W., Norton, J.M., Op den Camp, H.J.M., Shin, M. and Wei, X. (2007) Whole-genome analysis of the ammonia-oxidizing bacterium, *Nitrosomonas eutropha* C91: implications for niche adaptation. *Environ. Microbiol.* **9**(12):2993-3007.

Stein, L.Y. and Yung, Y.L. (2003) Production, isotopic composition, and atmospheric fate of biologically produced nitrous oxide. *Annu. Rev. Earth Plan. Sci.* **31**(1):329-356.

Strous, M. and Jetten, M.S.M. (2004) Anaerobic oxidation of methane and ammonium. *Annu. Rev. Microbiol.* **58**:99-117.

Strous, M., Kuenen, J.G. and Jetten, M.S.M. (1999) Key physiology of anaerobic ammonium oxidation. *Appl. Environ. Microbiol.* **65**(7):3248-3250.

Tallec, G., Garnier, J. and Gousailles, M. (2006) Nitrogen removal in a wastewater plant through biofilters: nitrous oxide emissions during nitrification and denitrification. *Bioprocess Biosyst. Eng.* **29**:323-333.

Terada, A., Hibiya, K., Nagai, J., Tsuneda, S. and Hirata, A. (2003) Nitrogen removal characteristics and biofilm analysis of a membrane-aerated biofilm reactor applicable to high-strength nitrogenous wastewater treatment. *J. Bioscience & Bioeng.* **95**(2):170-178.

Terada, A., Lackner, S., Tsuneda, S. and Smets, B.F. (2007) Redox-stratification controlled biofilm (ReSCoBi) for completely autotrophic nitrogen removal: The effect of co- versus counter-diffusion on reactor performance. *Biotechnol. Bioeng*. **97**(1):40-51.

Terada, A., Yamamoto, T., Igarashi, R., Tsuneda, S. and Hirata, A. (2006) Feasibility of a membrane-aerated biofilm reactor achieve controllable nitrification. *Biochem. Eng. J.* **28:**123-130.

Vadivelu, V.M., Keller, J. and Yuan, Z. (2006) Effect of free ammonia and free nitrous acid concentration on the anabolic and catabolic processes of an enriched *Nitrosomonas* culture. *Biotechnol. Bioeng.* **95**(5):830-839.

Vadivelu, V.M., Keller, J. and Yuan, Z. (2007) Effect of free ammonia on the respiration and growth processes of an enriched *Nitrobacter* culture. *Water Res.* **41**(4):826-834.

van de Graaf, A.A., Bruijn, P.d., Robertson, L.A., Jetten, M.S.M. and Kuenen, J.G. (1996) Autotrophic growth of anaerobic ammonium-oxidizing micro-organisms in a fluidized bed reactor. *Microbiol.* **142**:2187-2196.

Weismann, U. (1994) Advances in biochemical engineering/biotechnology. Feichter, A. (ed), pp. 113-154, Springer-Verlag Berlin Heidelberg, Berlin.

Wett., B. (2006) Solved upscaling problems for implementing deammonification of rejection water. Water Sci. Technol. **53**(12):121-128.

5. ENGINEERING SIGNIFICANCE

Installation of novel N removal processes for wastewater treatment are expected to proliferate along with efforts to protect water quality and reduce resource consumption associated with treatment of wastes. HFMBR technology has been shown previously to achieve N and COD removals comparable to conventional technologies, while offering reduced aeration costs and lower solids production without advanced or complicated operating requirements (Dahm et al., 2000). Coupling this technology with completely autotrophic processes for N removal realizes the benefits of both components.

To illustrate these benefits, a cost comparison using the method of Semmens (2005) was performed, wherein the power and external organic carbon requirements for a scaled-up version of the HFMBR system were compared to a conventional nutrient removal activated sludge system. Because the HFMBR produces some effluent nitrate, it was assumed that a post-denitrification process would be required after the HFMBR prior to discharge or reuse. Similarly, the nutrient removal activated sludge system was assumed to have denitrification with external organic carbon (methanol). Assumptions for both systems are shown in Appendix L. Briefly, these assumptions included an influent flow of 1 MGD (3,780 m^3/day), 620 mg/l influent NH_4^+-N, 85% of which becomes effluent nitrate to be denitrified, 4.57 kg O_2 required per kg N, 1.5 kg COD per kg methanol, methanol density of 791.3 kg/m^3, $1.00 cost per gallon of methanol, and $0.05 per kW-h. Assumptions specific to the scaled-up HFMBR system included a temperature of 30°C, 110 mg/l effluent NO_3^--N to be denitrified (from performance data), 1.5 psig losses across membrane module, and head loss was assumed to be independent of transfer efficiency for the purposes of the analysis. Assumptions for a suspended growth system to achieve the same degree of nitrogen removal via complete nitrification and denitrification with external carbon included a temperature of 20°C, tank depth of 5.5 m, oxygen transfer efficiency of 25%, 1 psig aeration piping head losses, 85% of influent N load converted to NO_3^--N to be denitrified.

The equation used for power requirement (Semmens, 2005) was:

$$P_w = \frac{wRT}{29.7ne}\left[\left(\frac{p_2}{p_1}\right)^{0.283} - 1\right] \qquad \text{(eqn 5-1)}$$

Where:

P_w = power requirement, kW
w = mass rate of air flow, kg/sec
R = universal gas constant, 8.314 kJ/(mol-K)
T = temperature, 303K
p_1 = inlet pressure, 101.325 kPa absolute
p_2 = outlet pressure, p_1 + head losses, kPa absolute
n = constant, 0.283
e = blower efficiency, assumed 0.8

The costs associated with each type of system are shown in Table 5-1. The power requirement for the HFMBR system is dependent on the oxygen transfer efficiency realized, which was examined at 25%, 50% and 75%. It is apparent that the aeration cost associated with HFMBR technology is approximately an order of magnitude lower than conventional diffused aeration in a deep tank, with the difference due to the lack of hydrostatic head and increased transfer efficiency of the HFMBR configuration.

Table 5-1. Aeration and external organic carbon cost analysis of autotrophic HFMBR technology and conventional activated sludge.

Parameter	**Activated Sludge System**	**HFMBR System with Indicated Oxygen Transfer Efficiency**		
Transfer efficiency, %	25	25	50	75
Air flow required m^3/day	150,000	150,000	75,000	50,000
Temperature, C	20	30	30	30
Head loss, kPa	60.8	10.3	10.3	10.3
Power required	107.8	21.1	10.6	7.0
Annual power cost	**$47,000**	**$9,000**	**$5,000**	**$3,000**
Nitrate produced, kg/d	2,000	420	420	420
Methanol required, m3/d	4.8	1	1	1
Annual methanol cost	**$463,000**	**$97,000**	**$97,000**	**$97,000**
Total annual cost	**$510,000**	**$106,000**	**$102,000**	**$100,000**

The autotrophic nature of the nitritation-anaerobic ammonium oxidation HFMBR offers another benefit, illustrated in the cost of external carbon. The conventional system produces very high quantities of nitrate to be denitrified. Assuming both configurations lack indigenous carbon for an electron donor, the methanol costs associated with the autotrophic HFMBR system is approximately one fifth that for the conventional system that nitrifies all the way to nitrate. Furthermore, this outcome is conservative, because in full-scale implementation it is likely that autotrophic HFMBR systems would be staged in series to realize a further reduction of effluent nitrate load, thereby reducing the external carbon requirement. Of the two costs evaluated in this analysis, the cost of external carbon dominates, demonstrating the benefit of using autotrophic metabolisms to achieve nitrogen removal from high strength N wastes.

Several other aspects of the work herein contribute to the body of knowledge related to application of HFMBR technology to wastewater treatment. The mechanistic oxygen transfer model shows promise for design and operation of redox-stratified HFMBRs. The model's overprediction implies the need for further refinement. However, its utility lies in its simplicity and portability. For example, different membrane materials and cylindrical geometries (diameter, wall thickness) can be evaluated rapidly by simulation, without the need for laboratory mass transfer coefficient determination. Operating conditions can also be compared by varying flows, pressures, and velocities to optimize the balance between transfer efficiency and uniformity along the fibers. In the future, expansion of the model into 3-dimensions (cylindrical coordinates) will further increase the predictive capabilities of oxygenation of biofilms in HFMBRs.

Oxygen gradients are predicted by the model to occur in flow-through fibers, especially at low lumen velocities. However, molecular analysis did not reveal consistent trends in microbial populations along the length of the fibers. The disparity of these two observations may be related to the scale of this system. As the technology is scaled up for real-world applications and longer fibers are used, the potential for lumen gradients increases. The model illustrates the effect of using increased velocity to make the lumen oxygen profile more aerobic and more uniform, but oxygen transfer efficiency decreases

as more oxygen is wasted in the outlet gas. A possible solution to this engineering challenge is high-rate recirculation of the lumen gas to balance transfer efficiency with concentration uniformity. An area of future research is to investigate this and other approaches strategies for optimizing oxygen mass transfer in HFMBRs.

The demonstration of the oxygen:ammonia flux ratio for controlling microbial populations is not new. However, this is one of the first, if not the first, successful demonstrations of coupling nitritation with anaerobic ammonium oxidation in an HFMBR. The observations related to flux are applicable to larger scale HFMBR systems as well as other biofilm configurations achieving autotrophic nitrogen removal.

Microbial community analysis revealed trends in radial distribution, some of which were expected (AerAOB near the membrane, AnaerAOB near the liquid) and some of which were not (AerAOB and NOB at mid-depth in the biofilm). The scale and design of the reactor in this study did not allow side-by-side testing of multiple conditions and removal of structurally-intact biofilm sections over time. Future work that allows looking at fluxes, performance, and intact biofilm communities over time is needed to determine how these microbial communities came to arrive in the locations they were found, and why.

In scaling up of this process, nitrogen oxide emissions must be addressed, particularly during startup and prior to stable anaerobic ammonium oxidation. This process relies on maintaining the low-DO conditions that will encourage generation of emissions and, because the outlet gas stream is more concentrated than that from open aeration tanks, safety of operators and ambient air quality must be considered. The observation of NOB preferentially colonizing bare fiber regions also represents an important issue for scaling up, as nitrite oxidation will compromise the resource efficiency of the system.

The application of this technology to organic carbon-containing wastewaters introduces an additional dimension of heterotrophic bacteria, and this complexity will influence the optimal flux conditions and control strategies needed to achieve the desired metabolic

outcomes. Additionally, the possibility of nutrient limitation that was glimpsed in this study warrants further investigation. Many high-strength waste streams have ample nutrients, but application to specialized wastes should take this potential deficiency into consideration. In the many types of high-strength nitrogen wastewater applications, HFMBRs are very likely to find a niche as a preferred technology at full-scale.

REFERENCES

Dahm, K., Hanus, D., and Semmens, M.J. 2000. Membrane technology: an innovative alternative in wastewater treatment. Final Report 97-CTS-10. Water Environ. Res. Found. Alexandria, VA

Semmens, M. J. 2005. Membrane technology: pilot studies of membrane-aerated bioreactors. Final Report 00-CTS-11. Water Environ. Res. Found. Alexandria, VA.

APPENDIX A

TRACER TESTS AND REACTOR HYDRODYNAMICS

Appendix A: Tracer Tests and Reactor Hydrodynamics

A.1 Preliminary Tracer Tests

Preliminary tracer tests were performed at very low recirculation flow rates (40-150 ml/min). These were determined to be too low for subsequent reactor operation, so they are not shown. However, chloride was measured during those tests, and a scatter plot of chloride and concentration data was used to generate a correlation between chloride and conductivity.

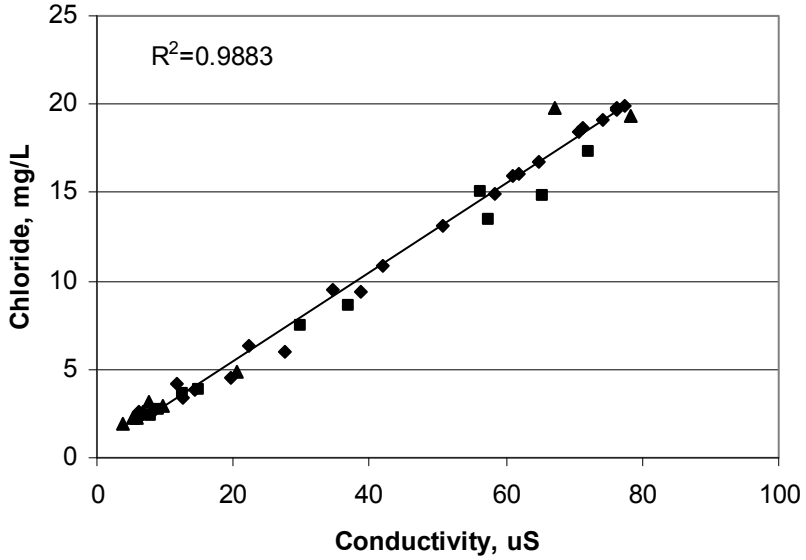

Figure A.1. Chloride-conductivity relationship for tracer tests.

Regression: chloride concentration = 0.2472 * (Conductivity) + 0.5407

In subsequent tracer tests, conductivity was monitored (temperature correction by instrument) in real time, and this regression equation was used to convert to chloride concentration for the purposes of tracking the mass of tracer.

Table A.1. Data for chloride-conductivity correlation.

Conductivity, uS	Chloride, mg/l
5.8	2.22
6.1	2.64
6.3	2.21
8.3	2.63
12.5	3.37
19.6	4.52
27.5	6.01
38.6	9.40
62	16.10
70.7	18.48
76.2	19.66
77.3	19.91
76.1	19.78
74.2	19.16
71.2	18.66
64.8	16.75
61	15.95
58.5	14.93
50.7	13.16
41.8	10.84
34.7	9.45
22.4	6.33
14.3	3.87
11.8	4.17
8	2.37
9.1	2.70
15	3.87
29.8	7.45
56.3	15.10
72	17.31
65.5	14.87
57.6	13.51
36.9	8.61
12.6	3.63
3.7	1.91
7.6	3.21
67.2	19.82
78.2	19.36
20.6	4.89
9.7	2.97
6.8	2.57
5.8	2.32
5.4	2.27

[Data located in spreadsheet file: “Dissertation Appendix A Tracer Tests.xls”]

A.2 Tracer Test No. 1

A detailed analysis is presented and described for test number 1. The same analysis was performed for tests 2 and 3. All the data are shown for tests 2 and 3, but the description is omitted because the methodology is the same.

Test No. 1 was performed with 1 ml spike of 100,000 mg Cl^- / l
Volume of reactor with membrane module installed: 3.452 liters

Flow rates:	Influent:	2 ml/min
	"Recycle":	250 ml/min
	Total:	252 ml/min
	Theoretical HRT:	13.7 min

The "recycle" was not an actual recirculation, but rather was distilled water with no tracer, fed to the system at the flow rate indicated.

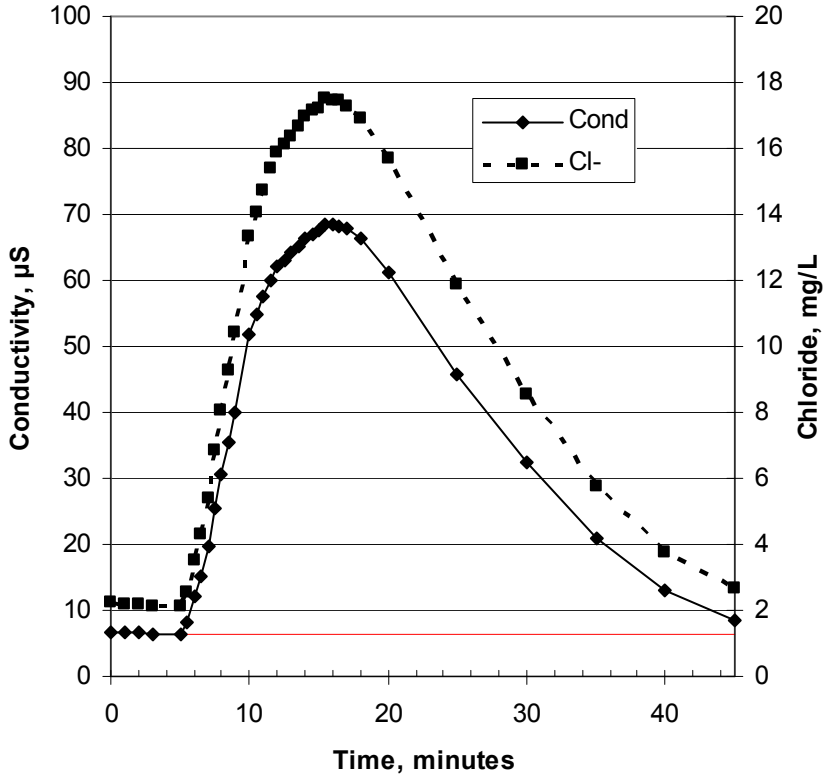

Figure A.2. Tracer test no. 1: 250 ml/min recycle.

Table A.2. Tracer test no. 1 data: 250 ml/min recycle.

Time min	Conductivity µS	Temperature deg. C	Choride mg/l
0.0	6.8	26	2.22
1.0	6.7	26.1	2.20
2.0	6.6	26.1	2.17
3.0	6.5	26.1	2.15
5.0	6.5	26.1	2.15
5.5	8.2	26.1	2.57
6.0	12	26.1	3.51
6.5	15.3	26.1	4.32
7.0	19.7	26.1	5.41
7.5	25.4	26.1	6.82
8.0	30.5	26.1	8.08
8.5	35.4	26.1	9.29
9.0	40	26.1	10.43
10.0	51.7	26.1	13.32
10.5	54.7	26.1	14.06
11.0	57.5	26.1	14.75
11.5	60	26.1	15.37
12.0	62.1	26.1	15.89
12.5	63	26.2	16.11
13.0	64.1	26.2	16.39
13.5	65.3	26.2	16.68
14.0	66.5	26.2	16.98
14.5	67.1	26.2	17.13
15.0	67.5	26.2	17.23
15.5	68.6	26.2	17.50
16.0	68.5	26.2	17.47
16.5	68.3	26.2	17.42
17.0	67.8	26.2	17.30
18.0	66.3	26.2	16.93
20.0	61.2	26.2	15.67
25.0	45.8	26.3	11.86
30.0	32.4	26.3	8.55
35.0	21	26.4	5.73
40.0	13	26.4	3.75
45.0	8.6	26.5	2.67

[Data located in spreadsheet file: “Dissertation Appendix A Tracer Tests.xls”]

The spike input response was converted to an equivalent step input response by integrating the mass of tracer during the test duration. For each time point, the chloride concentration was calculated using the regression equation for chloride vs. conductivity. The duration of each time step was multiplied by the average chloride concentration during that time step to calculate the mass of tracer passing through the effluent during that time step. The cumulative mass and percent recovery were then totalized over the duration of the test to determine the total % recovery. The highest recovery obtained at the end of the test was set equal to 100%.

Mass of spike: 100 mg Cl^-

Table A.3. Tracer mass integration data to determine cumulative residence time distribution function, F(t), tracer test no. 1: 250 ml/min recycle.

Time min	Conductivity µS	Chloride, mg Cl/l	Time step min	Vol passed, L	Avg Conc, mg/L	Mass past mg	Cumul mass past, mg	Percent Recovery	Adjusted % recovery
0.0	6.8	2.22	0	0		0	0	0.0%	0.0%
1.0	6.7	2.20	1.0	0.25	2.18	0.55	0.55	0.6%	0.6%
2.0	6.6	2.17	1.0	0.25	2.16	0.54	1.09	1.1%	1.3%
3.0	6.5	2.15	1.0	0.25	2.15	0.54	1.64	1.6%	1.9%
5.0	6.5	2.15	2.0	0.50	2.36	1.19	2.82	2.8%	3.2%
5.5	8.2	2.57	0.5	0.13	3.04	0.38	3.21	3.2%	3.7%
6.0	12	3.51	0.5	0.13	3.91	0.49	3.70	3.7%	4.2%
6.5	15.3	4.32	0.5	0.13	4.87	0.61	4.31	4.3%	5.0%
7.0	19.7	5.41	0.5	0.13	6.12	0.77	5.08	5.1%	5.8%
7.5	25.4	6.82	0.5	0.13	7.45	0.94	6.02	6.0%	6.9%
8.0	30.5	8.08	0.5	0.13	8.69	1.09	7.12	7.1%	8.2%
8.5	35.4	9.29	0.5	0.13	9.86	1.24	8.36	8.4%	9.6%
9.0	40	10.43	0.5	0.13	11.87	1.50	9.86	9.9%	11.3%
10.0	51.7	13.32	1.0	0.25	13.69	3.45	13.31	13.3%	15.3%
10.5	54.7	14.06	0.5	0.13	14.41	1.82	15.12	15.1%	17.4%
11.0	57.5	14.75	0.5	0.13	15.06	1.90	17.02	17.0%	19.5%
11.5	60	15.37	0.5	0.13	15.63	1.97	18.99	19.0%	21.8%
12.0	62.1	15.89	0.5	0.13	16.00	2.02	21.01	21.0%	24.1%
12.5	63	16.11	0.5	0.13	16.25	2.05	23.05	23.1%	26.5%
13.0	64.1	16.39	0.5	0.13	16.53	2.08	25.14	25.1%	28.9%
13.5	65.3	16.68	0.5	0.13	16.83	2.12	27.26	27.3%	31.3%
14.0	66.5	16.98	0.5	0.13	17.05	2.15	29.41	29.4%	33.8%
14.5	67.1	17.13	0.5	0.13	17.18	2.16	31.57	31.6%	36.2%
15.0	67.5	17.23	0.5	0.13	17.36	2.19	33.76	33.8%	38.8%
15.5	68.6	17.50	0.5	0.13	17.49	2.20	35.96	36.0%	41.3%
16.0	68.5	17.47	0.5	0.13	17.45	2.20	38.16	38.2%	43.8%
16.5	68.3	17.42	0.5	0.13	17.36	2.19	40.35	40.3%	46.3%
17.0	67.8	17.30	0.5	0.13	17.12	2.16	42.50	42.5%	48.8%
18.0	66.3	16.93	1.0	0.25	16.30	4.11	46.61	46.6%	53.5%
20.0	61.2	15.67	2.0	0.50	13.77	6.94	53.55	53.5%	61.5%
25.0	45.8	11.86	5.0	1.26	10.21	12.86	66.41	66.4%	76.2%
30.0	32.4	8.55	5.0	1.26	7.14	9.00	75.41	75.4%	86.6%
35.0	21	5.73	5.0	1.26	4.74	5.98	81.38	81.4%	93.4%
40.0	13	3.75	5.0	1.26	3.21	4.05	85.43	85.4%	98.1%
45.0	8.6	2.67	5.0	1.26	1.33	1.68	87.11	87.1%	100.0%

[Data located in spreadsheet file: "Dissertation Appendix A Tracer Tests.xls"]

The last column is essentially the cumulative residence time distribution function, F(t), of a step input. The values in this column are also equivalent to tracer concentration that would be observed at time t relative to the influent tracer concentration if this were a step input of tracer.

The F(t) curve was then compared to representative F(t) curves for N CSTRs in series, according to the following equation (Grady et al., 1999):

$$\frac{S_{TN}}{S_{To}} = 1 - \left[1 + \frac{1}{\tau} + \frac{(t/\tau)^2}{2!} + \ldots + \frac{(t/\tau)^{N-1}}{(N-1)!}\right] e^{-t/\tau} \qquad \text{eqn. A.1.}$$

Where:

S_{TN}/S_{T0} = F(t) for N CSTRs in series, i.e. concentration (or mass) of tracer relative to input concentration (mass) of tracer in step input

T = time

τ = mean hydraulic residence time of each of the N CSTRs in series

N = number of CSTRs in series

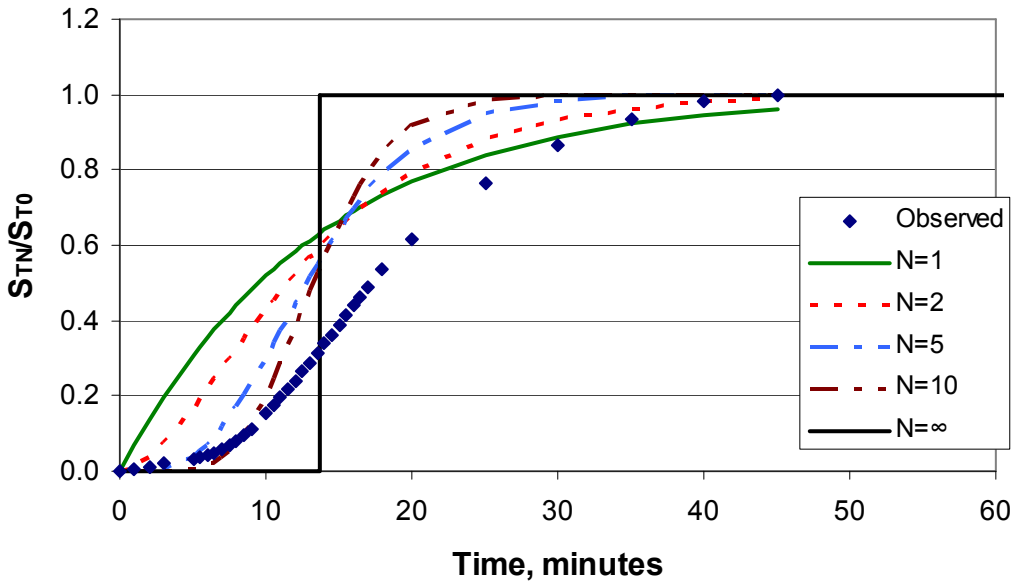

Figure A.3. F(t) for N CSTRs in series and observed data for tracer test no. 1: 250 ml/min recycle.

Table A.4. F(t) data for N CSTRs in series and observed data from tracer test no. 1: 250 ml/min recycle.

N:	1	2	3	4	5	6	7	8	9	10
τ, each CSTR, minutes:	13.70	6.85	4.57	3.42	2.74	2.28	1.96	1.71	1.52	1.37

Time	S_{TN}/S_0	S_{TN}/S_0 for N =									
min	observed	1	2	3	4	5	6	7	8	9	10
0.0	0.00	0.00	0.00	0.00	0.00	0.00	0.00	0.00	0.00	0.00	0.00
1.0	0.01	0.07	0.01	0.00	0.00	0.00	0.00	0.00	0.00	0.00	0.00
2.0	0.01	0.14	0.04	0.01	0.00	0.00	0.00	0.00	0.00	0.00	0.00
3.0	0.02	0.20	0.07	0.03	0.01	0.01	0.00	0.00	0.00	0.00	0.00
5.0	0.03	0.31	0.17	0.10	0.06	0.04	0.02	0.02	0.01	0.01	0.00
5.5	0.04	0.33	0.19	0.12	0.08	0.05	0.04	0.02	0.02	0.01	0.01
6.0	0.04	0.35	0.22	0.15	0.10	0.07	0.05	0.04	0.03	0.02	0.01
6.5	0.05	0.38	0.25	0.17	0.12	0.09	0.07	0.05	0.04	0.03	0.02
7.0	0.06	0.40	0.27	0.20	0.15	0.12	0.09	0.07	0.06	0.05	0.04
7.5	0.07	0.42	0.30	0.23	0.18	0.14	0.12	0.09	0.08	0.06	0.05
8.0	0.08	0.44	0.33	0.26	0.21	0.17	0.14	0.12	0.10	0.09	0.07
8.5	0.10	0.46	0.35	0.29	0.24	0.20	0.17	0.15	0.13	0.11	0.10
9.0	0.11	0.48	0.38	0.32	0.27	0.23	0.21	0.18	0.16	0.14	0.13
10.0	0.15	0.52	0.43	0.37	0.33	0.30	0.28	0.25	0.23	0.22	0.20
10.5	0.17	0.54	0.45	0.40	0.37	0.34	0.31	0.29	0.27	0.26	0.24
11.0	0.20	0.55	0.48	0.43	0.40	0.37	0.35	0.33	0.32	0.30	0.29
11.5	0.22	0.57	0.50	0.46	0.43	0.41	0.39	0.37	0.36	0.35	0.33
12.0	0.24	0.58	0.52	0.49	0.46	0.44	0.43	0.41	0.40	0.39	0.38
12.5	0.26	0.60	0.54	0.52	0.50	0.48	0.47	0.46	0.45	0.44	0.43
13.0	0.29	0.61	0.57	0.54	0.53	0.51	0.50	0.50	0.49	0.48	0.48
13.5	0.31	0.63	0.59	0.57	0.56	0.55	0.54	0.54	0.53	0.53	0.52
14.0	0.34	0.64	0.61	0.59	0.58	0.58	0.58	0.57	0.57	0.57	0.57
14.5	0.36	0.65	0.62	0.61	0.61	0.61	0.61	0.61	0.61	0.61	0.61
15.0	0.39	0.67	0.64	0.64	0.64	0.64	0.64	0.64	0.65	0.65	0.65
15.5	0.41	0.68	0.66	0.66	0.66	0.67	0.67	0.68	0.68	0.69	0.69
16.0	0.44	0.69	0.68	0.68	0.69	0.69	0.70	0.71	0.71	0.72	0.73
16.5	0.46	0.70	0.69	0.70	0.71	0.72	0.73	0.74	0.75	0.75	0.76
17.0	0.49	0.71	0.71	0.72	0.73	0.74	0.75	0.76	0.77	0.78	0.79
18.0	0.54	0.73	0.74	0.75	0.77	0.78	0.80	0.81	0.82	0.83	0.84
20.0	0.61	0.77	0.79	0.81	0.83	0.85	0.87	0.88	0.90	0.91	0.92
25.0	0.76	0.84	0.88	0.91	0.93	0.95	0.96	0.97	0.98	0.98	0.99
30.0	0.87	0.89	0.93	0.96	0.97	0.98	0.99	0.99	1.00	1.00	1.00
35.0	0.93	0.92	0.96	0.98	0.99	1.00	1.00	1.00	1.00	1.00	1.00
40.0	0.98	0.95	0.98	0.99	1.00	1.00	1.00	1.00	1.00	1.00	1.00
45.0	1.00	0.96	0.99	1.00	1.00	1.00	1.00	1.00	1.00	1.00	1.00

[Data located in spreadsheet file: "Dissertation Appendix A Tracer Tests.xls"]

Comparing the observed data with the CSTR models, the reactor appeared to follow a CSTRs-in-series model with a time delay. The observed data was adjusted back by 5 minutes and compared the models.

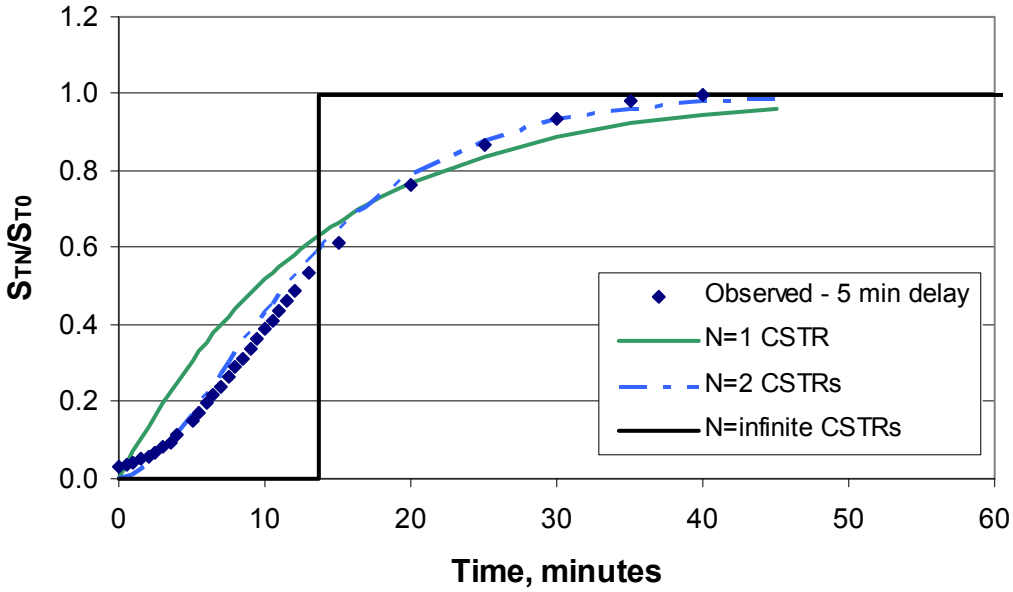

Figure A.4. Non-ideal reactor flow model fit for tracer test no. 1: 250 ml/min recycle.

Table A.5. Data for non-ideal reactor flow model fit for tracer test no. 1: 250 ml/min recycle.

Time minutes	Time minus 5 minutes	S_{TN}/S_{T0} Observed
0.0	-5.0	0.00
1.0	-4.0	0.01
2.0	-3.0	0.01
3.0	-2.0	0.02
5.0	0.0	0.03
5.5	0.5	0.04
6.0	1.0	0.04
6.5	1.5	0.05
7.0	2.0	0.06
7.5	2.5	0.07
8.0	3.0	0.08
8.5	3.5	0.10
9.0	4.0	0.11
10.0	5.0	0.15
10.5	5.5	0.17
11.0	6.0	0.20
11.5	6.5	0.22
12.0	7.0	0.24
12.5	7.5	0.26
13.0	8.0	0.29
13.5	8.5	0.31
14.0	9.0	0.34
14.5	9.5	0.36
15.0	10.0	0.39
15.5	10.5	0.41
16.0	11.0	0.44
16.5	11.5	0.46
17.0	12.0	0.49
18.0	13.0	0.54
20.0	15.0	0.61
25.0	20.0	0.76
30.0	25.0	0.87
35.0	30.0	0.93
40.0	35.0	0.98
45.0	40.0	1.00

[Data located in spreadsheet file: “Dissertation Appendix A Tracer Tests.xls”]

A.3 Tracer Test No. 2

Test No. 2 was performed with 1 ml spike of 100,000 mg Cl^- / l
Volume of reactor with membrane module installed: 3.452 liters

Flow rates:	Influent:	2 ml/min
	"Recycle":	250 ml/min
	Total:	502 ml/min
	Theoretical HRT:	6.9 min

The "recycle" was not an actual recirculation, but rather was distilled water with no tracer, fed to the system at the flow rate indicated.

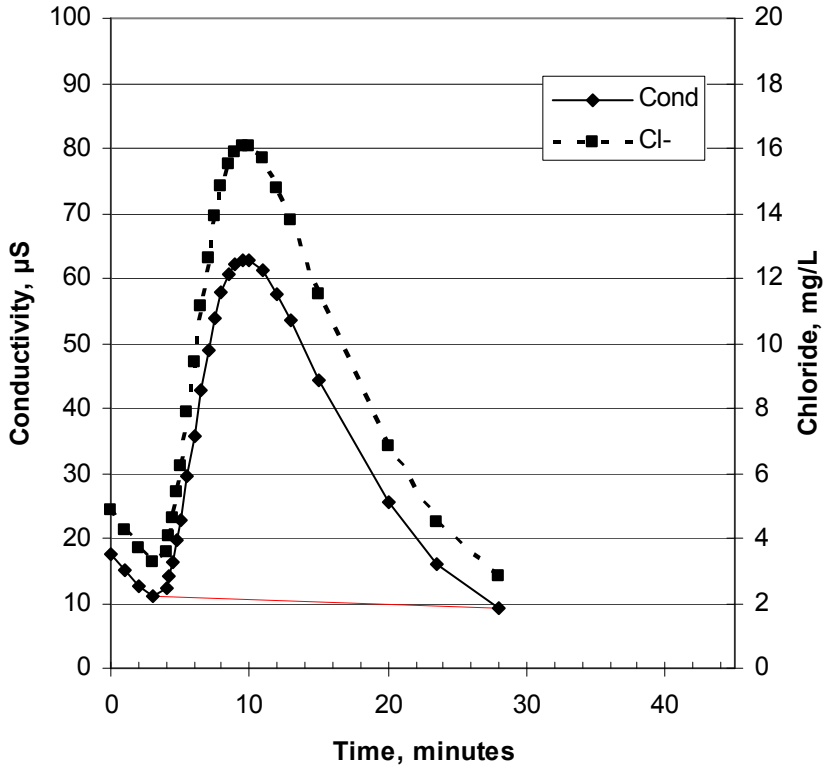

Figure A.5. Tracer test no. 2: 500 ml/min recycle.

Table A.6. Tracer test no. 2 data: 500 ml/min recycle.

Time min	Conductivity µS	Temperature deg. C	Choride mg/l
0.0	17.6	25.4	4.89
1.0	15.1	25.5	4.27
2.0	12.7	25.6	3.68
3.0	11.0	25.7	3.26
4.0	12.3	25.7	3.58
4.25	14.2	25.7	4.05
4.50	16.4	25.8	4.59
4.75	19.7	25.8	5.41
5.0	22.9	25.8	6.20
5.5	29.6	25.8	7.86
6.0	35.8	25.9	9.39
6.5	42.8	25.9	11.12
7.0	48.9	25.9	12.63
7.5	54.0	25.9	13.89
8.0	57.8	26.0	14.83
8.5	60.6	26.0	15.52
9.0	62.1	26.0	15.89
9.5	62.8	26.0	16.06
10.0	62.8	26.0	16.06
11.0	61.2	26.0	15.67
12.0	57.5	26.0	14.75
13.0	53.5	26.1	13.77
15.0	44.4	26.1	11.52
20.0	25.5	26.1	6.84
23.5	16.0	26.1	4.50
28.0	9.2	26.1	2.81

[Data located in spreadsheet file: “Dissertation Appendix A Tracer Tests.xls”]

Table A.7. Tracer mass integration data to determine cumulative residence time distribution function, F(t), tracer test no. 2: 500 ml/min recycle.

Time min	Conductivity µS	Baseline Cond., µS	Corrected Cond., µS	Chloride, mg Cl/l	Time step min	Vol pass. L	Avg Conc, mg/L	Mass pass. mg	Cumul mass past, mg	Percent Recovery	Adjusted % recovery
0.0	17.6	17.60	0.0	0.00	0	0		0	0	0.0%	0.0%
1.0	15.1	15.10	0.0	0.00	1.0	0.50	0.00	0.00	0.00	0.0%	0.0%
2.0	12.7	12.70	0.0	0.00	1.0	0.50	0.00	0.00	0.00	0.0%	0.0%
3.0	11.0	11.00	0.0	0.00	1.0	0.50	1.79	0.90	0.90	0.9%	1.0%
4.0	12.3	10.93	1.4	3.58	1.0	0.50	3.82	1.92	2.81	2.8%	3.0%
4.25	14.2	10.91	3.3	4.05	0.3	0.13	4.32	0.54	3.36	3.4%	3.6%
4.5	16.4	10.89	5.5	4.59	0.3	0.13	5.00	0.63	3.98	4.0%	4.2%
4.75	19.7	10.87	8.8	5.41	0.3	0.13	5.81	0.73	4.71	4.7%	5.0%
5.0	22.9	10.86	12.0	6.20	0.3	0.13	7.03	0.88	5.60	5.6%	5.9%
5.5	29.6	10.82	18.8	7.86	0.5	0.25	8.62	2.16	7.76	7.8%	8.2%
6.0	35.8	10.78	25.0	9.39	0.5	0.25	10.26	2.57	10.33	10.3%	11.0%
6.5	42.8	10.75	32.1	11.12	0.5	0.25	11.87	2.98	13.32	13.3%	14.1%
7.0	48.9	10.71	38.2	12.63	0.5	0.25	13.26	3.33	16.64	16.6%	17.7%
7.5	54.0	10.68	43.3	13.89	0.5	0.25	14.36	3.60	20.25	20.2%	21.5%
8.0	57.8	10.64	47.2	14.83	0.5	0.25	15.17	3.81	24.06	24.1%	25.5%
8.5	60.6	10.60	50.0	15.52	0.5	0.25	15.71	3.94	28.00	28.0%	29.7%
9.0	62.1	10.57	51.5	15.89	0.5	0.25	15.98	4.01	32.01	32.0%	34.0%
9.5	62.8	10.53	52.3	16.06	0.5	0.25	16.06	4.03	36.04	36.0%	38.3%
10.0	62.8	10.50	52.3	16.06	0.5	0.25	15.87	3.98	40.02	40.0%	42.5%
11.0	61.2	10.42	50.8	15.67	1.0	0.50	15.21	7.64	47.66	47.7%	50.6%
12.0	57.5	10.35	47.1	14.75	1.0	0.50	14.26	7.16	54.82	54.8%	58.2%
13.0	53.5	10.28	43.2	13.77	1.0	0.50	12.64	6.35	61.17	61.2%	64.9%
15.0	44.4	10.14	34.3	11.52	2.0	1.00	9.18	9.22	70.38	70.4%	74.7%
20.0	25.5	9.78	15.7	6.84	5.0	2.51	5.67	14.23	84.61	84.6%	89.8%
23.5	16.0	9.52	6.5	4.50	3.5	1.76	3.66	6.42	91.04	91.0%	96.6%
28.0	9.2	9.20	0.0	2.81	4.5	2.26	1.41	3.18	94.22	94.2%	100.0%

[Data located in spreadsheet file: "Dissertation Appendix A Tracer Tests.xls"]

In test 2, the conductivity was corrected for a baseline conductivity defined as a linear function drawn between the starting and ending conductivities.

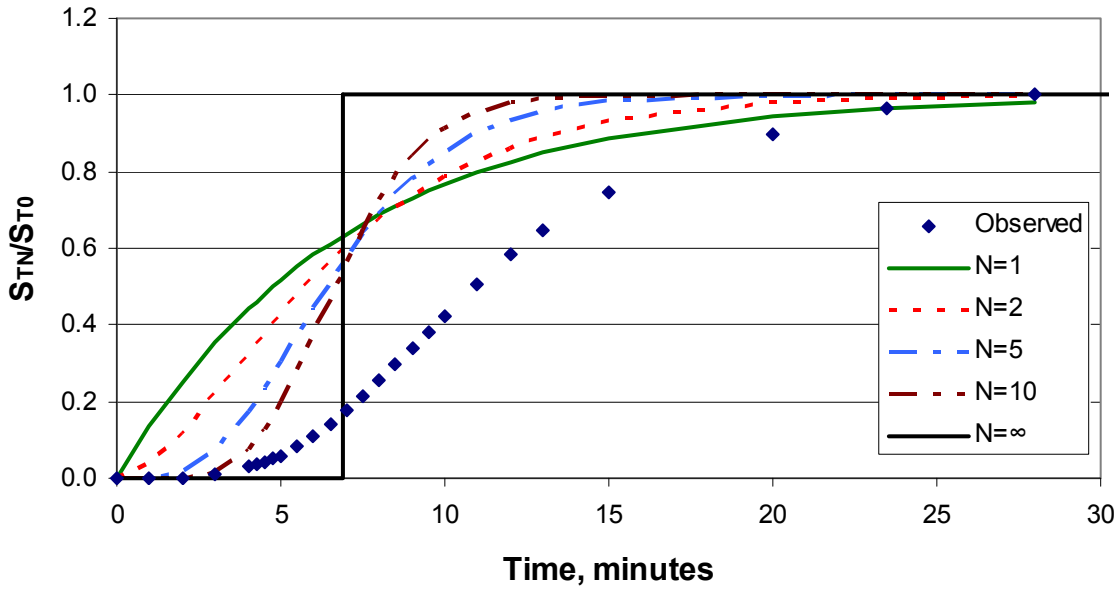

Figure A.6. F(t) for N CSTRs in series and observed data for tracer test no. 2: 500 ml/min recycle.

Table A.8. F(t) data for N CSTRs in series and observed data from tracer test no. 2: 500 ml/min recycle.

N:	1	2	3	4	5	6	7	8	9	10
τ, each CSTR, minutes:	6.88	3.44	2.29	1.72	1.38	1.15	0.98	0.86	0.76	0.69

Time	S_{TN}/S_0	S_{TN}/S_0 for N =									
min	observed	1	2	3	4	5	6	7	8	9	10
0.0	0.00	0.00	0.00	0.00	0.00	0.00	0.00	0.00	0.00	0.00	0.00
1.0	0.00	0.14	0.03	0.01	0.00	0.00	0.00	0.00	0.00	0.00	0.00
2.0	0.00	0.25	0.12	0.06	0.03	0.02	0.01	0.00	0.00	0.00	0.00
3.0	0.01	0.35	0.22	0.14	0.10	0.07	0.05	0.04	0.03	0.02	0.01
4.0	0.03	0.44	0.32	0.25	0.21	0.17	0.14	0.12	0.10	0.08	0.07
4.25	0.04	0.46	0.35	0.28	0.24	0.20	0.17	0.15	0.13	0.11	0.10
4.5	0.04	0.48	0.38	0.31	0.27	0.23	0.20	0.18	0.16	0.14	0.13
4.75	0.05	0.50	0.40	0.34	0.30	0.27	0.24	0.21	0.19	0.18	0.16
5.0	0.06	0.52	0.43	0.37	0.33	0.30	0.27	0.25	0.23	0.21	0.20
5.5	0.08	0.55	0.47	0.43	0.40	0.37	0.35	0.33	0.31	0.30	0.28
6.0	0.11	0.58	0.52	0.49	0.46	0.44	0.43	0.41	0.40	0.39	0.38
6.5	0.14	0.61	0.56	0.54	0.52	0.51	0.50	0.49	0.48	0.48	0.47
7.0	0.18	0.64	0.60	0.59	0.58	0.58	0.57	0.57	0.57	0.57	0.56
7.5	0.21	0.66	0.64	0.63	0.63	0.64	0.64	0.64	0.64	0.65	0.65
8.0	0.26	0.69	0.68	0.68	0.68	0.69	0.70	0.70	0.71	0.72	0.72
8.5	0.30	0.71	0.71	0.72	0.73	0.74	0.75	0.76	0.77	0.78	0.79
9.0	0.34	0.73	0.74	0.75	0.77	0.78	0.79	0.81	0.82	0.83	0.84
9.5	0.38	0.75	0.76	0.78	0.80	0.82	0.83	0.85	0.86	0.87	0.88
10.0	0.42	0.77	0.79	0.81	0.83	0.85	0.87	0.88	0.89	0.90	0.91
11.0	0.51	0.80	0.83	0.86	0.88	0.90	0.92	0.93	0.94	0.95	0.96
12.0	0.58	0.83	0.86	0.89	0.92	0.94	0.95	0.96	0.97	0.97	0.98
13.0	0.65	0.85	0.89	0.92	0.94	0.96	0.97	0.98	0.98	0.99	0.99
15.0	0.75	0.89	0.93	0.96	0.97	0.98	0.99	0.99	1.00	1.00	1.00
20.0	0.90	0.95	0.98	0.99	1.00	1.00	1.00	1.00	1.00	1.00	1.00
23.5	0.97	0.97	0.99	1.00	1.00	1.00	1.00	1.00	1.00	1.00	1.00
28.0	1.00	0.98	1.00	1.00	1.00	1.00	1.00	1.00	1.00	1.00	1.00

[Data located in spreadsheet file: "Dissertation Appendix A Tracer Tests.xls"]

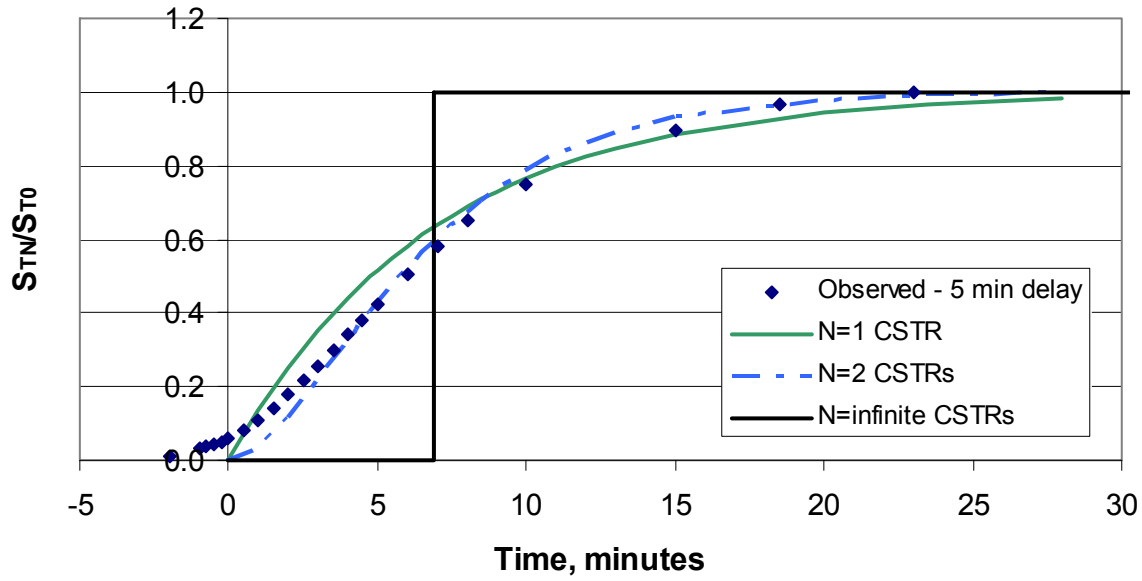

Figure A.7. Non-ideal reactor flow model fit for tracer test no. 2: 500 ml/min recycle.

Table A.9. Data for non-ideal reactor flow model fit for tracer test no. 2: 500 ml/min recycle.

Time minutes	Time minus 5 minutes	S_{TN}/S_{T0} Observed
0.0	-5.0	0.00
1.0	-4.0	0.00
2.0	-3.0	0.00
3.0	-2.0	0.01
4.0	-1.0	0.03
4.25	-0.75	0.04
4.5	-0.5	0.04
4.75	-0.25	0.05
5.0	0.0	0.06
5.5	0.5	0.08
6.0	1.0	0.11
6.5	1.5	0.14
7.0	2.0	0.18
7.5	2.5	0.21
8.0	3.0	0.26
8.5	3.5	0.30
9.0	4.0	0.34
9.5	4.5	0.38
10.0	5.0	0.42
11.0	6.0	0.51
12.0	7.0	0.58
13.0	8.0	0.65
15.0	10.0	0.75
20.0	15.0	0.90
23.5	18.5	0.97
28.0	23.0	1.00

[Data located in spreadsheet file: “Dissertation Appendix A Tracer Tests.xls”]

A.4 Tracer Test No. 3

Test No. 3 was performed with 1 ml spike of 100,000 mg Cl^- / l
Volume of reactor with membrane module installed: 3.452 liters

Flow rates:	Influent:	2 ml/min
	"Recycle":	750 ml/min
	Total:	752 ml/min
	Theoretical HRT:	4.6 min

The "recycle" was not an actual recirculation, but rather was distilled water with no tracer, fed to the system at the flow rate indicated.

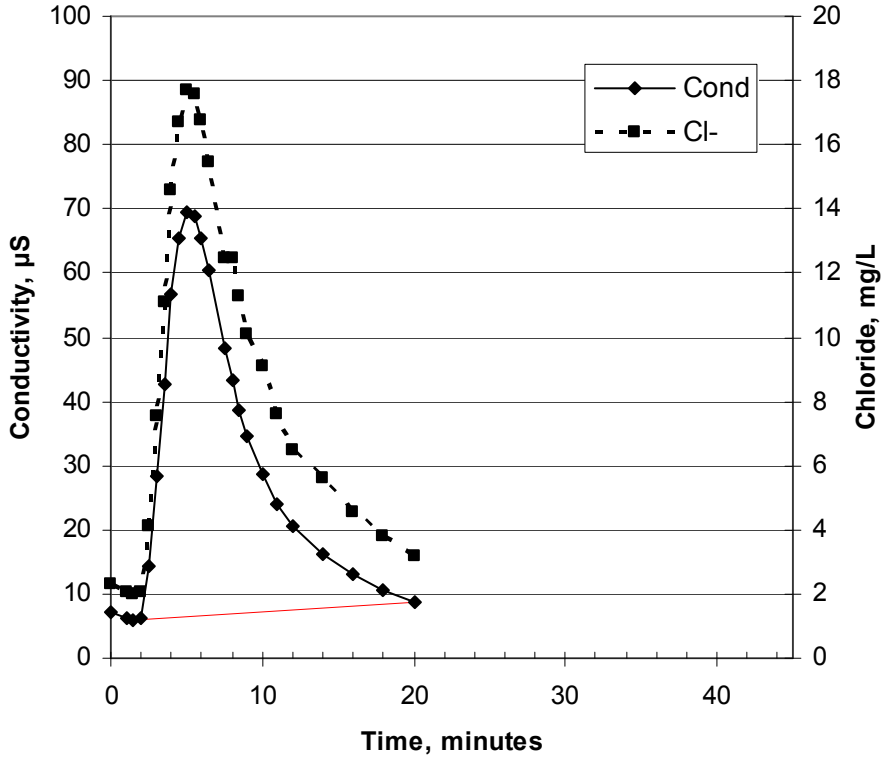

Figure A.8. Tracer test no. 3: 750 ml/min recycle.

Table A.10. Tracer test no. 3 data: 750 ml/min recycle.

Time min	Conductivity µS	Temperature deg. C	Choride mg/l
0.0	7.1	26.6	2.30
1.0	6.2	26.6	2.07
1.5	5.8	26.6	1.97
2.0	6.1	26.6	2.05
2.5	14.4	26.7	4.10
3.0	28.4	26.7	7.56
3.5	42.8	26.8	11.12
4.0	56.7	26.8	14.56
4.5	65.4	26.9	16.71
5.0	69.4	26.9	17.70
5.5	68.8	26.9	17.55
6.0	65.5	27.0	16.73
6.5	60.4	27.0	15.47
7.5	48.2	27.1	12.46
8.0	43.4	27.1	12.46
8.5	38.7	27.2	11.27
9.0	34.7	27.2	10.11
10.0	28.6	27.3	9.12
11.0	23.9	27.3	7.61
12.0	20.6	27.4	6.45
14.0	16.3	27.4	5.63
16.0	13.2	27.4	4.57
18.0	10.6	27.5	3.80
20.0	8.6	27.5	3.16

Table A.11. Tracer mass integration data to determine cumulative residence time distribution function, F(t), tracer test no. 3: 750 ml/min recycle.

Time min	Conductivity µS	Baseline Cond., µS	Corrected Cond., µS	Chloride, mg Cl/l	Time step min	Vol pass. L	Avg Conc, mg/L	Mass pass. mg	Cumul mass past, mg	Percent Recovery	Adjusted % recovery
0.0	7.1	7.1	0.0	0.00	0	0		0	0	0.0%	0.0%
1.0	6.2	6.2	0.0	0.00	1.0	0.75	0.00	0.00	0.00	0.0%	0.0%
1.5	5.8	5.8	0.0	0.00	0.5	0.38	1.02	0.39	0.39	0.4%	0.4%
2.0	6.1	5.9	0.2	2.05	0.5	0.38	3.07	1.16	1.54	1.5%	1.5%
2.5	14.4	6.0	8.4	4.10	0.5	0.38	5.83	2.19	3.73	3.7%	3.7%
3.0	28.4	6.0	22.4	7.56	0.5	0.38	9.34	3.51	7.25	7.2%	7.2%
3.5	42.8	6.1	36.7	11.12	0.5	0.38	12.84	4.83	12.07	12.1%	12.1%
4.0	56.7	6.2	50.5	14.56	0.5	0.38	15.63	5.88	17.95	18.0%	17.9%
4.5	65.4	6.3	59.1	16.71	0.5	0.38	17.20	6.47	24.42	24.4%	24.4%
5.0	69.4	6.3	63.1	17.70	0.5	0.38	17.62	6.63	31.04	31.0%	31.0%
5.5	68.8	6.4	62.4	17.55	0.5	0.38	17.14	6.44	37.49	37.5%	37.5%
6.0	65.5	6.5	59.0	16.73	0.5	0.38	16.10	6.05	43.54	43.5%	43.5%
6.5	60.4	6.6	53.8	15.47	0.5	0.38	13.96	5.25	48.79	48.8%	48.8%
7.5	48.2	6.7	41.5	12.46	1.0	0.75	11.86	8.92	57.71	57.7%	57.7%
8.0	43.4	6.8	36.6	11.27	0.5	0.38	10.69	4.02	61.73	61.7%	61.7%
8.5	38.7	6.9	31.8	10.11	0.5	0.38	9.61	3.61	65.35	65.3%	65.3%
9.0	34.7	6.9	27.8	9.12	0.5	0.38	8.36	3.15	68.49	68.5%	68.4%
10.0	28.6	7.1	21.5	7.61	1.0	0.75	7.03	5.29	73.78	73.8%	73.7%
11.0	23.9	7.2	16.7	6.45	1.0	0.75	6.04	4.54	78.32	78.3%	78.3%
12.0	20.6	7.4	13.2	5.63	1.0	0.75	5.10	3.84	82.16	82.2%	82.1%
14.0	16.3	7.7	8.6	4.57	2.0	1.50	4.19	6.30	88.46	88.5%	88.4%
16.0	13.2	8.0	5.2	3.80	2.0	1.50	3.48	5.24	93.69	93.7%	93.6%
18.0	10.6	8.3	2.3	3.16	2.0	1.50	2.91	4.38	98.08	98.1%	98.0%
20.0	8.6	8.6	0.0	2.67	2.0	1.50	1.33	2.01	100.08	100.1%	100.0%

[Data located in spreadsheet file: "Dissertation Appendix A Tracer Tests.xls"]

In test 3, the conductivity was corrected for a baseline conductivity defined as a linear function drawn between the starting and ending conductivities.

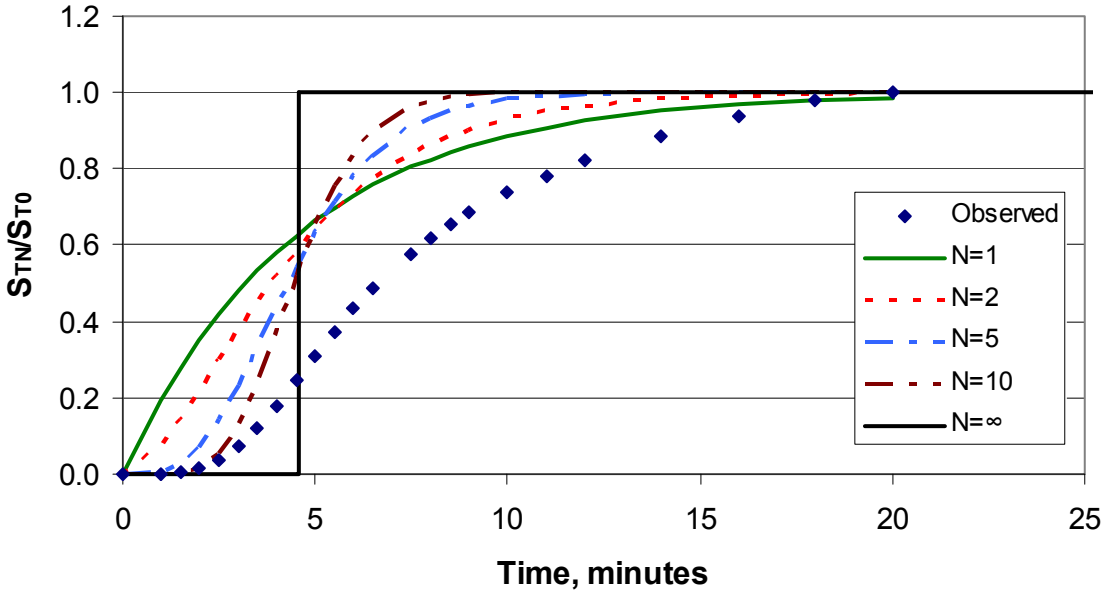

Figure A.9. F(t) for N CSTRs in series and observed data for tracer test no. 3: 750 ml/min recycle.

Table A.12. F(t) data for N CSTRs in series and observed data from tracer test no. 3: 750 ml/min recycle.

N:	1	2	3	4	5	6	7	8	9	10
τ, each CSTR, minutes	4.59	2.30	1.53	1.15	0.92	0.77	0.66	0.57	0.51	0.46

Time	S_{TN}/S_0	S_{TN}/S_0 for N =									
min	observed	1	2	3	4	5	6	7	8	9	10
0.0	0.00	0.00	0.00	0.00	0.00	0.00	0.00	0.00	0.00	0.00	0.00
1.0	0.00	0.20	0.07	0.03	0.01	0.01	0.00	0.00	0.00	0.00	0.00
1.5	0.00	0.28	0.14	0.08	0.04	0.03	0.02	0.01	0.01	0.00	0.00
2.0	0.02	0.35	0.22	0.14	0.10	0.07	0.05	0.04	0.03	0.02	0.01
2.5	0.04	0.42	0.30	0.23	0.18	0.14	0.11	0.09	0.08	0.06	0.05
3.0	0.07	0.48	0.38	0.31	0.27	0.23	0.20	0.18	0.16	0.14	0.13
3.5	0.12	0.53	0.45	0.40	0.36	0.33	0.31	0.29	0.27	0.25	0.24
4.0	0.18	0.58	0.52	0.49	0.46	0.44	0.42	0.41	0.40	0.39	0.37
4.5	0.24	0.62	0.58	0.56	0.55	0.54	0.54	0.53	0.52	0.52	0.52
5.0	0.31	0.66	0.64	0.63	0.63	0.63	0.64	0.64	0.64	0.64	0.65
5.5	0.37	0.70	0.69	0.70	0.70	0.71	0.72	0.73	0.74	0.75	0.76
6.0	0.44	0.73	0.74	0.75	0.77	0.78	0.79	0.81	0.82	0.83	0.84
6.5	0.49	0.76	0.77	0.80	0.82	0.83	0.85	0.86	0.88	0.89	0.90
7.5	0.58	0.80	0.84	0.87	0.89	0.91	0.93	0.94	0.95	0.96	0.96
8.0	0.62	0.82	0.86	0.89	0.92	0.93	0.95	0.96	0.97	0.97	0.98
8.5	0.65	0.84	0.88	0.91	0.94	0.95	0.96	0.97	0.98	0.98	0.99
9.0	0.68	0.86	0.90	0.93	0.95	0.97	0.98	0.98	0.99	0.99	0.99
10.0	0.74	0.89	0.93	0.96	0.97	0.98	0.99	0.99	1.00	1.00	1.00
11.0	0.78	0.91	0.95	0.97	0.99	0.99	1.00	1.00	1.00	1.00	1.00
12.0	0.82	0.93	0.97	0.98	0.99	1.00	1.00	1.00	1.00	1.00	1.00
14.0	0.88	0.95	0.98	0.99	1.00	1.00	1.00	1.00	1.00	1.00	1.00
16.0	0.94	0.97	0.99	1.00	1.00	1.00	1.00	1.00	1.00	1.00	1.00
18.0	0.98	0.98	1.00	1.00	1.00	1.00	1.00	1.00	1.00	1.00	1.00
20.0	1.00	0.99	1.00	1.00	1.00	1.00	1.00	1.00	1.00	1.00	1.00

[Data located in spreadsheet file: "Dissertation Appendix A Tracer Tests.xls"]

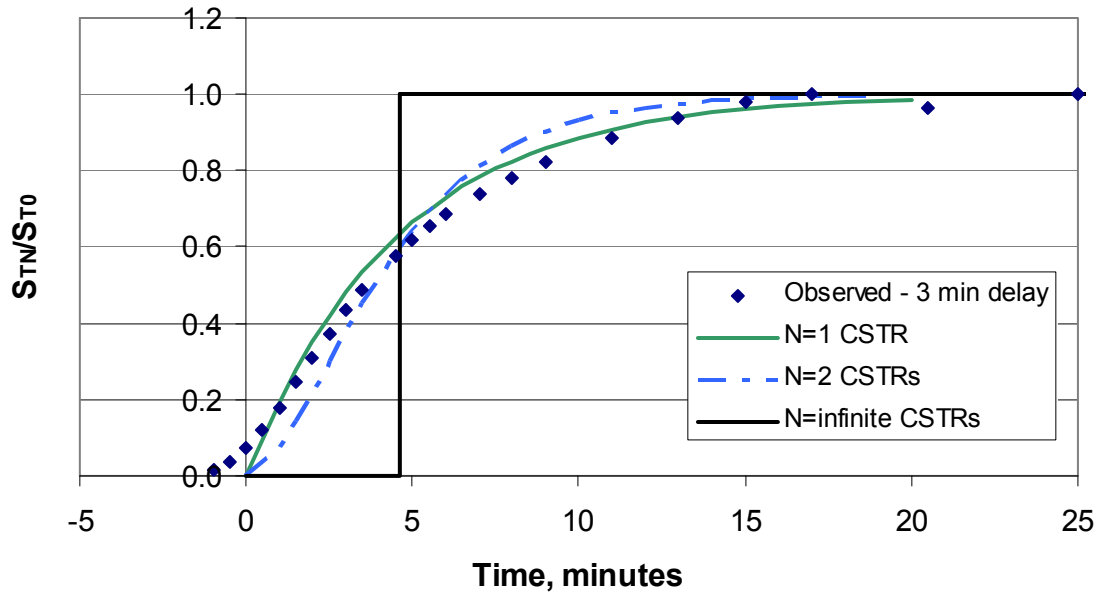

Figure A.10. Non-ideal reactor flow model fit for tracer test no. 3: 750 ml/min recycle.

Table A.13. Data for non-ideal reactor flow model fit for tracer test no. 3: 750 ml/min recycle.

Time minutes	Time minus 5 minutes	S_{TN}/S_{T0} Observed
0.0	-3.0	0.00
1.0	-2.0	0.00
1.5	-1.5	0.00
2.0	-1.0	0.02
2.5	-0.5	0.04
3.0	0.0	0.07
3.5	0.5	0.12
4.0	1.0	0.18
4.5	1.5	0.24
5.0	2.0	0.31
5.5	2.5	0.37
6.0	3.0	0.44
6.5	3.5	0.49
7.5	4.5	0.58
8.0	5.0	0.62
8.5	5.5	0.65
9.0	6.0	0.68
10.0	7.0	0.74
11.0	8.0	0.78
12.0	9.0	0.82
14.0	11.0	0.88
16.0	13.0	0.94
18.0	15.0	0.98
20.0	17.0	1.00
23.5	20.5	0.97
28.0	25.0	1.00

[Data located in spreadsheet file: "Dissertation Appendix A Tracer Tests.xls"]

CONCLUSIONS

The observed tracer test data suggest that the reactor flow regime can be approximated by a non-ideal reactor model with one to two CSTRs in series with a 3 to 5 minute delay.

REFERENCES

Grady, C.P.L., Daigger, G.T., and Lim, H.C. (1999). *Biological Wastewater Treatment*. New York: Marcel Dekker, Inc.

APPENDIX B

CLEAN WATER OXYGEN TRANSFER TESTS WITH BULK LIQUID MEASUREMENTS

Appendix B. Clean Water Oxygen Transfer Tests with Bulk Liquid Measurements

This appendix contains the data and regressions for calculating the mass transfer coefficient under clean water conditions. In these tests, dissolved oxygen (DO) was measured in the bulk liquid.

Table B.1. DO saturation concentrations.

Gauge Pressure psig	Aqueous DO Concentration mg/l
0.0	7.00
1.0	7.47
2.0	7.95
3.0	8.42
4.0	8.90
5.0	9.37
6.0	9.85
7.0	10.33
8.0	10.80
9.0	11.28
10.0	11.75

Parameters:

Membrane inner surface area = 0.177 m^2, or 1,700 cm^2
Volume of system = 4.5 liters, or 4,500 cm^3
(During these tests, the reactor was full and the recirculation tubing and pump were in operation.)
Specific membrane surface area, a = 0.393 cm2/cm^3

Analyses were performed in general accordance with the ASCE standard Measurement of Oxygen Transfer in Clean Water (A-91) (ASCE, 1984), with the following exceptions: total dissolved solids (TDS) and soluble cobalt were not measured between tests, since virgin distilled water was used each time; and the equilibrium DO concentration as time approaches infinity, C^*_∞, was assumed to be equal to C^*_{sat}, the saturation concentration at the measured lumen pressure and temperature, rather than determined from the nonlinear regression of each test condition.

An example is shown, illustrating the regression process for one condition of lumen pressure and gas flow rate.

TableB.2. Example clean water test data: 1 psig and 9 cc/min.

Time, min	Model	DO	Model predict-	Residual,			
min	time,min	mg/l	ion, mg/l	mg/l	Residual^2	Y-Ybar	(Y-Ybar)^2
196.0	0.0	1.386	1.39	0.000	0.0000	-2.248	5.054
196.5	0.5	1.434	1.42	0.015	0.0002	-2.200	4.840
197.0	1.0	1.436	1.45	0.017	0.0003	-2.198	4.831
197.5	1.5	1.484	1.49	0.002	0.0000	-2.150	4.623
198.0	2.0	1.578	1.52	0.060	0.0035	-2.056	4.227
198.5	2.5	1.544	1.55	0.007	0.0001	-2.090	4.368
199.0	3.0	1.536	1.58	0.048	0.0023	-2.098	4.402
199.5	3.5	1.546	1.62	0.070	0.0049	-2.088	4.360
200.0	4.0	1.548	1.65	0.100	0.0100	-2.086	4.352
200.5	4.5	1.518	1.68	0.162	0.0262	-2.116	4.478
201.0	5.0	1.542	1.71	0.170	0.0288	-2.092	4.377
201.5	5.5	1.538	1.74	0.205	0.0422	-2.096	4.393
202.0	6.0	1.628	1.77	0.147	0.0215	-2.006	4.024
202.5	6.5	1.652	1.81	0.154	0.0237	-1.982	3.928
203.0	7.0	1.68	1.84	0.157	0.0247	-1.954	3.818
203.5	7.5	1.702	1.87	0.166	0.0276	-1.932	3.733
204.0	8.0	1.742	1.90	0.157	0.0246	-1.892	3.580
204.5	8.5	1.756	1.93	0.173	0.0300	-1.878	3.527
205.0	9.0	1.802	1.96	0.158	0.0249	-1.832	3.356
205.5	9.5	1.79	1.99	0.200	0.0400	-1.844	3.400
206.0	10.0	1.872	2.02	0.148	0.0219	-1.762	3.105
206.5	10.5	1.896	2.05	0.154	0.0237	-1.738	3.021
207.0	11.0	1.834	2.08	0.246	0.0603	-1.800	3.240
207.5	11.5	1.88	2.11	0.229	0.0525	-1.754	3.077
208.0	12.0	1.95	2.14	0.189	0.0356	-1.684	2.836
208.5	12.5	1.968	2.17	0.200	0.0400	-1.666	2.776
209.0	13.0	2.022	2.20	0.175	0.0306	-1.612	2.599
209.5	13.5	2.086	2.23	0.140	0.0196	-1.548	2.396
210.0	14.0	2.09	2.25	0.165	0.0271	-1.544	2.384
210.5	14.5	2.122	2.28	0.161	0.0260	-1.512	2.286
211.0	15.0	2.178	2.31	0.134	0.0179	-1.456	2.120
211.5	15.5	2.208	2.34	0.132	0.0175	-1.426	2.034
212.0	16.0	2.236	2.37	0.132	0.0175	-1.398	1.955
212.5	16.5	2.256	2.40	0.140	0.0197	-1.378	1.899
213.0	17.0	2.31	2.42	0.114	0.0130	-1.324	1.753
213.5	17.5	2.284	2.45	0.168	0.0281	-1.350	1.823
214.0	18.0	2.34	2.48	0.139	0.0194	-1.294	1.675
214.5	18.5	2.41	2.51	0.097	0.0094	-1.224	1.498
215.0	19.0	2.436	2.53	0.098	0.0096	-1.198	1.435
215.5	19.5	2.39	2.56	0.171	0.0292	-1.244	1.548
216.0	20.0	2.424	2.59	0.164	0.0269	-1.210	1.464
216.5	20.5	2.366	2.61	0.249	0.0619	-1.268	1.608
217.0	21.0	2.374	2.64	0.267	0.0715	-1.260	1.588
217.5	21.5	2.382	2.67	0.286	0.0817	-1.252	1.568
218.0	22.0	2.414	2.69	0.280	0.0785	-1.220	1.489
218.5	22.5	2.458	2.72	0.262	0.0689	-1.176	1.383
219.0	23.0	2.492	2.75	0.255	0.0648	-1.142	1.304
219.5	23.5	2.502	2.77	0.270	0.0731	-1.132	1.282
220.0	24.0	2.554	2.80	0.244	0.0596	-1.080	1.166

Table B.2. Example clean water test data: 1 psig and 9 cc/min, continued.

Time, min min	Model time,min	DO mg/l	Model predict-ion, mg/l	Residual, mg/l	Residual^2	Y-Ybar	(Y-Ybar)^2
220.5	24.5	2.624	2.82	0.200	0.0399	-1.010	1.020
221.0	25.0	2.652	2.85	0.197	0.0389	-0.982	0.964
221.5	25.5	2.726	2.87	0.149	0.0221	-0.908	0.825
222.0	26.0	2.736	2.90	0.164	0.0269	-0.898	0.806
222.5	26.5	2.798	2.93	0.127	0.0161	-0.836	0.699
223.0	27.0	2.832	2.95	0.118	0.0139	-0.802	0.643
223.5	27.5	2.808	2.97	0.167	0.0278	-0.826	0.682
224.0	28.0	2.852	3.00	0.147	0.0217	-0.782	0.612
224.5	28.5	2.934	3.02	0.090	0.0081	-0.700	0.490
225.0	29.0	2.934	3.05	0.114	0.0131	-0.700	0.490
225.5	29.5	2.906	3.07	0.167	0.0278	-0.728	0.530
226.0	30.0	2.932	3.10	0.165	0.0271	-0.702	0.493
226.5	30.5	2.97	3.12	0.151	0.0227	-0.664	0.441
227.0	31.0	2.932	3.14	0.213	0.0452	-0.702	0.493
227.5	31.5	2.948	3.17	0.220	0.0486	-0.686	0.471
228.0	32.0	2.978	3.19	0.214	0.0458	-0.656	0.430
228.5	32.5	3.02	3.22	0.195	0.0382	-0.614	0.377
229.0	33.0	3.03	3.24	0.209	0.0436	-0.604	0.365
229.5	33.5	3.074	3.26	0.188	0.0353	-0.560	0.314
230.0	34.0	3.11	3.29	0.175	0.0307	-0.524	0.275
230.5	34.5	3.156	3.31	0.152	0.0231	-0.478	0.229
231.0	35.0	3.19	3.33	0.141	0.0199	-0.444	0.197
231.5	35.5	3.21	3.35	0.144	0.0206	-0.424	0.180
232.0	36.0	3.254	3.38	0.122	0.0149	-0.380	0.144
232.5	36.5	3.258	3.40	0.141	0.0198	-0.376	0.141
233.0	37.0	3.27	3.42	0.151	0.0228	-0.364	0.133
233.5	37.5	3.286	3.44	0.157	0.0247	-0.348	0.121
234.0	38.0	3.322	3.47	0.143	0.0205	-0.312	0.097
234.5	38.5	3.384	3.49	0.103	0.0107	-0.250	0.063
235.0	39.0	3.416	3.51	0.093	0.0087	-0.218	0.048
235.5	39.5	3.472	3.53	0.059	0.0035	-0.162	0.026
236.0	40.0	3.512	3.55	0.041	0.0016	-0.122	0.015
236.5	40.5	3.524	3.57	0.050	0.0025	-0.110	0.012
237.0	41.0	3.464	3.60	0.131	0.0173	-0.170	0.029
237.5	41.5	3.454	3.62	0.163	0.0265	-0.180	0.032
238.0	42.0	3.502	3.64	0.136	0.0184	-0.132	0.017
238.5	42.5	3.526	3.66	0.133	0.0176	-0.108	0.012
239.0	43.0	3.59	3.68	0.090	0.0081	-0.044	0.002
239.5	43.5	3.65	3.70	0.051	0.0026	0.016	0.000
240.0	44.0	3.778	3.72	0.057	0.0032	0.144	0.021
240.5	44.5	3.734	3.74	0.008	0.0001	0.100	0.010
241.0	45.0	3.756	3.76	0.006	0.0000	0.122	0.015
241.5	45.5	3.734	3.78	0.049	0.0024	0.100	0.010
242.0	46.0	3.756	3.80	0.047	0.0022	0.122	0.015
242.5	46.5	3.7	3.82	0.123	0.0151	0.066	0.004
243.0	47.0	3.752	3.84	0.091	0.0083	0.118	0.014
243.5	47.5	3.768	3.86	0.095	0.0090	0.134	0.018

Table B.2. Example clean water test data: 1 psig and 9 cc/min, continued.

Time, min min	Model time,min	DO mg/l	Model predict-ion, mg/l	Residual, mg/l	Residual^2	Y-Ybar	(Y-Ybar)^2
244.0	48.0	3.828	3.88	0.055	0.0030	0.194	0.038
244.5	48.5	3.87	3.90	0.032	0.0010	0.236	0.056
245.0	49.0	3.942	3.92	0.020	0.0004	0.308	0.095
245.5	49.5	3.958	3.94	0.017	0.0003	0.324	0.105
246.0	50.0	4.022	3.96	0.061	0.0037	0.388	0.151
246.5	50.5	4.01	3.98	0.030	0.0009	0.376	0.141
247.0	51.0	4.048	4.00	0.049	0.0024	0.414	0.171
247.5	51.5	4.07	4.02	0.052	0.0027	0.436	0.190
248.0	52.0	4.102	4.04	0.065	0.0042	0.468	0.219
248.5	52.5	4.076	4.06	0.020	0.0004	0.442	0.195
249.0	53.0	4.054	4.07	0.021	0.0004	0.420	0.176
249.5	53.5	4.02	4.09	0.073	0.0054	0.386	0.149
250.0	54.0	3.96	4.11	0.152	0.0231	0.326	0.106
250.5	54.5	3.956	4.13	0.174	0.0304	0.322	0.104
251.0	55.0	4.068	4.15	0.081	0.0065	0.434	0.188
251.5	55.5	4.11	4.17	0.057	0.0032	0.476	0.227
252.0	56.0	4.148	4.19	0.037	0.0014	0.514	0.264
252.5	56.5	4.28	4.20	0.077	0.0059	0.646	0.417
253.0	57.0	4.3	4.22	0.079	0.0062	0.666	0.443
253.5	57.5	4.206	4.24	0.033	0.0011	0.572	0.327
254.0	58.0	4.236	4.26	0.021	0.0004	0.602	0.362
254.5	58.5	4.2	4.27	0.074	0.0055	0.566	0.320
255.0	59.0	4.174	4.29	0.118	0.0139	0.540	0.292
255.5	59.5	4.182	4.31	0.127	0.0162	0.548	0.300
256.0	60.0	4.182	4.33	0.145	0.0209	0.548	0.300
256.5	60.5	4.272	4.34	0.072	0.0052	0.638	0.407
257.0	61.0	4.354	4.36	0.007	0.0000	0.720	0.518
257.5	61.5	4.354	4.38	0.024	0.0006	0.720	0.518
258.0	62.0	4.46	4.39	0.065	0.0042	0.826	0.682
258.5	62.5	4.538	4.41	0.126	0.0159	0.904	0.817
259.0	63.0	4.444	4.43	0.015	0.0002	0.810	0.656
259.5	63.5	4.528	4.45	0.083	0.0068	0.894	0.799
260.0	64.0	4.606	4.46	0.144	0.0208	0.972	0.945
260.5	64.5	4.564	4.48	0.086	0.0073	0.930	0.865
261.0	65.0	4.582	4.49	0.087	0.0076	0.948	0.899
261.5	65.5	4.726	4.51	0.215	0.0461	1.092	1.192
262.0	66.0	4.692	4.53	0.165	0.0271	1.058	1.119
262.5	66.5	4.646	4.54	0.102	0.0105	1.012	1.024
263.0	67.0	4.672	4.56	0.112	0.0126	1.038	1.077
263.5	67.5	4.686	4.58	0.110	0.0122	1.052	1.107
264.0	68.0	4.698	4.59	0.106	0.0113	1.064	1.132
264.5	68.5	4.696	4.61	0.089	0.0079	1.062	1.128
265.0	69.0	4.728	4.62	0.105	0.0110	1.094	1.197
265.5	69.5	4.792	4.64	0.153	0.0235	1.158	1.341
266.0	70.0	4.816	4.65	0.162	0.0262	1.182	1.397
266.5	70.5	4.782	4.67	0.112	0.0126	1.148	1.318
267.0	71.0	4.806	4.69	0.121	0.0146	1.172	1.373

Table B.2. Example clean water test data: 1 psig and 9 cc/min, continued.

Time, min min	Model time,min	DO mg/l	Model predict-ion, mg/l	Residual, mg/l	Residual^2	Y-Ybar	(Y-Ybar)^2
267.5	71.5	4.816	4.70	0.116	0.0134	1.182	1.397
268.0	72.0	4.824	4.72	0.109	0.0118	1.190	1.416
268.5	72.5	4.84	4.73	0.109	0.0120	1.206	1.454
269.0	73.0	4.908	4.75	0.162	0.0264	1.274	1.623
269.5	73.5	4.918	4.76	0.157	0.0248	1.284	1.649
270.0	74.0	4.906	4.78	0.131	0.0170	1.272	1.618
270.5	74.5	4.854	4.79	0.064	0.0041	1.220	1.488
271.0	75.0	4.838	4.80	0.033	0.0011	1.204	1.450
271.5	75.5	4.74	4.82	0.080	0.0063	1.106	1.223
272.0	76.0	4.764	4.83	0.070	0.0049	1.130	1.277
272.5	76.5	4.794	4.85	0.055	0.0030	1.160	1.346
273.0	77.0	4.836	4.86	0.027	0.0007	1.202	1.445
273.5	77.5	4.868	4.88	0.009	0.0001	1.234	1.523
274.0	78.0	4.932	4.89	0.040	0.0016	1.298	1.685
274.5	78.5	4.91	4.91	0.004	0.0000	1.276	1.628
275.0	79.0	4.992	4.92	0.072	0.0052	1.358	1.844
275.5	79.5	5.036	4.93	0.102	0.0105	1.402	1.965
276.0	80.0	5.058	4.95	0.110	0.0122	1.424	2.028
276.5	80.5	5.016	4.96	0.054	0.0030	1.382	1.910
277.0	81.0	5.052	4.98	0.077	0.0059	1.418	2.011
277.5	81.5	5.07	4.99	0.081	0.0066	1.436	2.062
278.0	82.0	5.066	5.00	0.063	0.0040	1.432	2.051
278.5	82.5	5.104	5.02	0.088	0.0077	1.470	2.161
279.0	83.0	5.242	5.03	0.212	0.0451	1.608	2.586
279.5	83.5	5.252	5.04	0.209	0.0437	1.618	2.618
280.0	84.0	5.218	5.06	0.162	0.0261	1.584	2.509
280.5	84.5	5.28	5.07	0.210	0.0443	1.646	2.709
281.0	85.0	5.252	5.08	0.169	0.0286	1.618	2.618
281.5	85.5	5.192	5.10	0.096	0.0092	1.558	2.427
282.0	86.0	5.288	5.11	0.179	0.0321	1.654	2.736
282.5	86.5	5.286	5.12	0.164	0.0269	1.652	2.729
283.0	87.0	5.196	5.13	0.061	0.0038	1.562	2.440
283.5	87.5	5.334	5.15	0.186	0.0348	1.700	2.890
284.0	88.0	5.372	5.16	0.212	0.0448	1.738	3.020
284.5	88.5	5.332	5.17	0.159	0.0253	1.698	2.883
285.0	89.0	5.396	5.19	0.210	0.0443	1.762	3.104
285.5	89.5	5.468	5.20	0.270	0.0728	1.834	3.363
286.0	90.0	5.382	5.21	0.171	0.0294	1.748	3.055
286.5	90.5	5.32	5.22	0.097	0.0094	1.686	2.842
287.0	91.0	5.418	5.24	0.183	0.0334	1.784	3.183
287.5	91.5	5.484	5.25	0.236	0.0559	1.850	3.422
288.0	92.0	5.494	5.26	0.234	0.0548	1.860	3.459
288.5	92.5	5.53	5.27	0.258	0.0666	1.896	3.595
289.0	93.0	5.57	5.28	0.286	0.0818	1.936	3.748
289.5	93.5	5.518	5.30	0.222	0.0493	1.884	3.549

[Data located in file “Dissertation Appendix B Clean Water O2 Tests-Bulk Liquid.xls”]

Y-bar = 3.63 mg/l (average DO concentration during test period, Y = DO, mg/l)

Sum of squares of residuals = 3.85

Total sum of squares = Sum of squares of (Y-Y-bar) = 285.6

$R^2 = 1\text{-}SS_{res}/SS_{total} = 1 - 3.85/285.6 = 0.987$

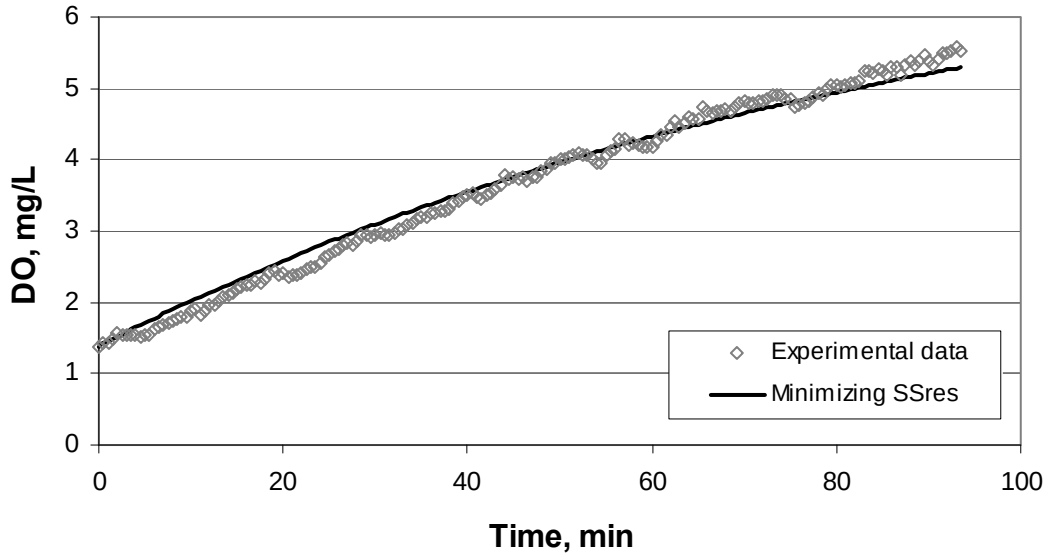

Figure B.1. Solved fit of equation 3.1 to experimental data at 1 psig and 9 cc/min.

Other conditions were analyzed in the same fashion, yielding the results below.

Table B.3. Summary of clean water test results with bulk liquid DO measurements.

Pressure psig	Flow cc/min	C^*_∞, mg/l	Initial DO, C_0, mg/l	K_La sec-1	K_L cm/sec	Residual sum squares	Total sum squares	R^2
1	4.5	7.47	1.04	0.000131	3.33E-04	2.48	333	0.993
	9	7.47	1.386	0.000183	4.66E-04	3.85	285.6	0.987
	18	7.47	0.468	0.000164	4.18E-04	2.48	206.5	0.988
2.5	9	8.18	1.015	0.000150	3.82E-04	0.25	132.4	0.998
	18	8.18	0.5	0.000146	3.72E-04	3.43	425.2	0.992
5	18	9.37	1.055	0.000120	3.05E-04	17.4	230.8	0.925
7	18	10.33	1.3	0.000134	3.40E-04	22.9	267.8	0.914
7.5	9	10.56	0.946	0.000169	4.30E-04	1.05	218.5	0.995
	18	10.56	0.805	0.000167	4.25E-04	5.21	258.0	0.980
10	4.5	11.75	0.77	0.000138	3.51E-04	0.79	71.11	0.989
	9	11.75	0.914	0.000190	4.84E-04	0.12	54.26	0.998
	18	11.75	1.05	0.000218	5.55E-04	1.22	121.1	0.990

Average K_L = 4.05E-04

[Data located in file "Dissertation Appendix B Clean Water O2 Tests-Bulk Liquid.xls"]

The maximum oxygen transfer rate was calculated as discussed in Chapter 3. The mass rate of oxygen applied to the system was calculated for each flow condition (See Appendix D), and the oxygen transfer efficiency was calculated as the ratio of oxygen transfer rate to oxygen supply rate.

Table B.4. Oxygen transfer rates and efficiencies calculated from clean water tests with bulk liquid DO measurements.

Pressure psig	Flow cc/min	C^*_∞, mg/l	K_La min^{-1}	OTR, mg/l-min	System volume, l	OTR g/day	Mass O_2 in, g/day	OTE, %
1	4.5	7.47	0.0079	0.0587	4.5	0.380	1.82	20.9%
	9	7.47	0.0110	0.0822	4.5	0.533	3.64	14.6%
	18	7.47	0.0099	0.0737	4.5	0.477	7.29	6.5%
2.5	9	8.18	0.0090	0.0738	4.5	0.478	3.64	13.1%
	18	8.18	0.0088	0.0718	4.5	0.465	7.29	6.4%
5	18	9.37	0.0072	0.0675	4.5	0.437	7.29	6.0%
7	18	10.33	0.0080	0.0829	4.5	0.537	7.29	7.4%
7.5	9	10.56	0.0101	0.1070	4.5	0.694	3.64	19.1%
	18	10.56	0.0100	0.1059	4.5	0.686	7.29	9.4%
10	4.5	11.75	0.0083	0.0974	4.5	0.631	1.82	34.7%
	9	11.75	0.0114	0.1343	4.5	0.870	3.64	23.9%
	18	11.75	0.0131	0.1539	4.5	0.998	7.29	13.7%

OTR = Oxygen Transfer Rate
OTE = Oxygen Transfer Efficiency
This data is used in Figure 3.3

Table B.5. Other measurements of oxygen transfer efficiency for Figure 3.3.

Air Flow cc/min-m^2	OTE off-gas %	OTE, % from NH_3 removed	OTE, % from OxN produced
31.25	56.4%	40.9%	31.6%
31.25	52.4%	41.1%	31.9%
31.25	47.4%	49.7%	37.0%
31.25	53.4%		
31.25	42.6%		

APPENDIX C

CLEAN WATER OXYGEN TRANSFER TESTS WITH MICROSENSOR MEASUREMENTS AT THE MEMBRANE-LIQUID INTERFACE

Appendix C. Clean water oxygen transfer tests with microsensor DO measurements at the membrane-liquid interface.

This file contains the data and regressions for calculating the mass transfer coefficient under clean water conditions. In these tests, dissolved oxygen (DO) was measured with microsensors positioned at the membrane-liquid interface.

Table C.1. DO saturation concentrations.

Gauge Pressure psig	Aqueous DO Concentration mg/l
0.0	7.00
1.0	7.47
2.0	7.95
3.0	8.42
4.0	8.90
5.0	9.37
6.0	9.85
7.0	10.33
8.0	10.80
9.0	11.28
10.0	11.75

Parameters:

Membrane inner surface area = 0.177 m^2, or 1,700 cm^2
Volume of system = 3.2 liters, or 3,200 cm^3
(During these tests, the reactor had a small headspace, and the recirculation tubing and pump were not in operation. This is the reason the volume is less than for tests performed in bulk liquid, as described in Appendix B.)
Specific membrane surface area, a = 0.553 cm^2/cm^3

Analyses were performed in general accordance with the ASCE standard Measurement of Oxygen Transfer in Clean Water (A-91) (ASCE, 1984), with the following exception: total dissolved solids (TDS) and soluble cobalt were not measured between tests, since virgin distilled water was used each time. In contrast to the tests with bulk liquid DO measurements, the equilibrium DO concentration as time approaches infinity, C^*_∞ was taken as equal to the average of the last 100 data points during each test.

An example is shown, illustrating the regression process for one condition of lumen pressure and gas flow rate. Raw DO data logged by LabView is not shown, because between 550 and 3,700 data point were collected for different ports. Raw data can be found in the spreadsheet file "Dissertation Appendix C Clean Water O2 Tests-Microsensors.xls".

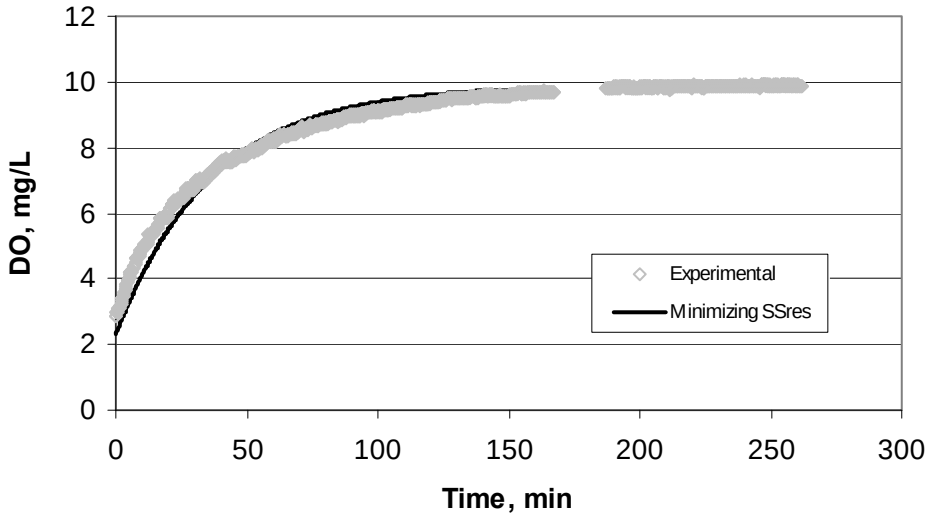

Figure C.1. Solved fit of equation 3.1 to experimental data at 5 psig, 9 cc/min, Port 3.

K_La fit to data = 0.0273 min^{-1}, so $K_L = 8.22 \times 10^{-4}$ cm/sec

Y-bar = 8.722 mg/l (average DO concentration during test period, Y = DO, mg/l)

Sum of squares of residuals = 108.5

Total sum of squares = Sum of squares of (Y - Y-bar) = 3,427

$R^2 = 1\text{-}SS_{res}/SS_{total} = 1 - 108.5/3{,}427 = 0.968$

Other conditions were analyzed in the same fashion, yielding the results below.

Table C.2. Summary of clean water test results with microsensor DO measurements at membrane-liquid interface.

Reactor Port	C^*_∞, mg/l	Initial DO, C_0, mg/l	K_La sec^{-1}	K_L cm/sec	Residual sum squares	Total sum squares	R^2
1	8.27	1.95	0.000719	1.30E-03	128.4	1,568	0.918
2	7.74	2.52	0.001007	1.82E-03	25.0	873	0.971
3	9.89	2.31	0.000455	8.22E-04	108.5	3,427	0.968
4	8.92	2.63	0.001097	1.98E-03	123.0	712	0.827
3-bulk liquid	7.50	0.05	0.000418	6.20E-04	41.7	3,927	0.989
4-bulk liquid	8.37	0.33	0.000343	7.56E-04	158.9	5,593	0.972

So, the average K_L value = 1.48×10^{-3} cm/sec

This value is based on the inner surface area of the fiber (0.177 m^2, a = 0.553 cm^2/cm^3).

To compare with fluxes of aqueous phase nutrients diffusing from the bulk liquid, this value should be converted to an outer surface area-based K_L, as follows:
K_L, outer = K_L, inner × inner specific surface area / outer specific surface area:

K_L, outer = 1.48×10^{-3} cm/sec × 0.553 cm^2-cm^{-3}/ 0.891 cm^2-cm^{-3} = **$\mathbf{9.19 \times 10^{-4}}$ cm/sec**

This is the value that is used in Chapter 4 to calculate oxygen fluxes for the purposes of comparing to ammonia fluxes.

Can also multiply by the ratio of inner surface area to outer surface area (0.177 / 0.285).

APPENDIX D

CALCULATION OF OXYGEN CONCENTRATIONS AND MASS FLOWS

Appendix D. Calculation of Oxygen Concentrations and Mass Flows
[Data located in file "Dissertation Appendix D O2 Concentrations and Masses.xls"]

D.1 Calculations with air as the lumen gas

Mass concentration of oxygen in air:

$$\text{Concentration}, \mu g/m^3 = \frac{\text{ppmv} \times \text{Pressure, Pa} \times \text{Molecular Weight, g/mol}}{8.314\ \text{J/K} - \text{mol} \times \text{Temperature, K}} \qquad \text{(eqn D.1)}$$

Where:
ppmv= parts per million by volume

Oxygen in air is 20.9% by volume, or 209,000 ppmv
Molecular weight of oxygen is 32 g/mol

Therefore, the concentration of oxygen in air can be calculated at the altitude (634 meters, or 2,080 feet), temperature (30°C, or 303 K), and lumen pressures used in this study.

Table D.1. Calculation of gas-phase lumen oxygen concentrations during this study.

Gauge Pressure psig	Absolute Pressure psia	Absolute Pressure Pa	Altitude Corrected Pa	Temper-ature K	Concen-tration ug/m^3	Gas phase conc., 'y' g/cm^3
0	14.7	101,353	93,954	303.15	2.49E+08	0.000249
1	15.7	108,248	100,346	303.15	2.66E+08	0.000266
2	16.7	115,142	106,737	303.15	2.83E+08	0.000283
3	17.7	122,037	113,128	303.15	3.00E+08	0.000300
4	18.7	128,932	119,520	303.15	3.17E+08	0.000317
5	19.7	135,827	125,911	303.15	3.34E+08	0.000334
6	20.7	142,721	132,303	303.15	3.51E+08	0.000351
7	21.7	149,616	138,694	303.15	3.68E+08	0.000368
8	22.7	156,511	145,086	303.15	3.85E+08	0.000385
9	23.7	163,406	151,477	303.15	4.02E+08	0.000402
10	24.7	170,300	157,869	303.15	4.19E+08	0.000419

Altitude correction factor for 634 meters = 0.927.

The aqueous-phase equilibrium dissolved oxygen (DO) concentrations associated with these gas-phase concentrations are governed by Henry's law.

The Henry's constant for oxygen is: 1.23×10^{-3} M/atm

(Average of values reported by Sander (1999)).

Converting this to Henry's constant at 30°C:
Starting temperature, T_1: 25°C
Starting H: 1.26×10^{-3} M/atm
New temperature, T_2: 30°C
Conversion constant, C: 1,700 (same reference as above)

$$H_2 = H_1 e^{\left[C\left(\frac{1}{T2}-\frac{1}{T1}\right)\right]} \qquad \text{(eqn D.2)}$$

So, $H_{30} = 1.15\times10^{-3}$ M/atm

Converting to dimensionless form (C_{gas}/C_{water}): $m_{30} = 35.64$

Table D.2. Tabulation of aqueous-phase equilibrium DO concentrations at lumen pressures used in this study, when air was used as the lumen gas.

Absolute Pressure psia	Gauge Pressure psig	Gas-phase O_2 conc. g/l	Aqueous DO Concentration g/l	Aqueous DO Concentration mg/l
13.63	0.0	0.249	0.00700	7.00
14.52	1.0	0.266	0.00747	7.47
15.52	2.0	0.283	0.00795	7.95
16.52	3.0	0.300	0.00842	8.42
17.52	4.0	0.317	0.00890	8.90
18.52	5.0	0.334	0.00937	9.37
19.52	6.0	0.351	0.00985	9.85
20.52	7.0	0.368	0.0103	10.33
21.52	8.0	0.385	0.0108	10.80
22.52	9.0	0.402	0.0113	11.28
23.52	10.0	0.419	0.0118	11.75

These oxygen concentrations are used in mass transfer calculations when air was used as the lumen gas.

Calculate density of air at mass flow controller calibration temperature (21.1°C):

Density of air at reference point: sea level at 15°C, ρ_0 = 1.225 g/l

Correct density to 21.1°C (this is the calibration temperature for the mass flow controller):

$$\rho_{15} = \frac{m_{air} P}{RT} = 1.225 \text{ g/l} \qquad \text{(eqn D.3)}$$

Where:
P_{15} = density at 15°C
P = pressure, 1 atm at sea level
R = universal gas constant, 0.08206 L-atm/K-mol
K = absolute temperature, Kelvin

So, solving equation D.3 above for m_{air} yields

m_{air} = molecular weight of air = 28.95 g/mol at 15°C

Plugging this molecular weight back into equation D.3 with parameters for 21.1°C yields:

$\rho_{21.1}$ = 1.20 g/l

Calculate mass ratio of oxygen in air:

Volume of oxygen in 1 liter of air: 0.209 liters

0.209 liters × 1mol/22.4 liters × 32 g/mol = 0.299 g O_2/liter air at STP

Volume of nitrogen in 1 liter of air: 0.78 liters

0.8 liters × 1mol/22.4 liters × 39.95 g/mol = 0.975 g N_2/liter air at STP

Sum of oxygen and nitrogen: 0.299 g/l + 0.975 g/l =1.274 g/liter air at STP

Mass fraction of oxygen: 0.299 / 1.274 = 0.234

Assume that this mass ratio is the same at 21.1°C as it is at STP (0°C).

So, the mass concentration of oxygen in the air is 0.234 × 1.20 g/l at 21.1°C

= 0.281 g/liter of air

The mass flow controller was set to 9.0 cc/min during use with air.

9 cc/min × 1 liter/10^3 cc × 1440 min/day = 12.96 liters/day

At calibration temperature, density = 1.20 g/l, so:

12.96 l/day × 1.20 g/l = 15.55 g/day of air

Adjusted for the mass ratio of oxygen in air:

15.55 g/day of air × 0.234 = 3.64 g O_2/day

D.2 Calculations with 80% argon / 20% oxygen as the lumen gas

The argon/oxygen mix is 80% argon by volume, 20% oxygen by volume.

20% O_2 by volume = 200,000 ppmv

Using equation D.1 above, the concentration of oxygen in the mix can be calculated at the altitude (634 meters, or 2,080 feet), temperature (30°C, or 303 K), and lumen pressures used in this study.

Table D.3. Calculation of gas-phase lumen oxygen concentrations during this study when 80% argon/20% oxygen was the lumen gas.

Gauge Pressure psig	Absolute Pressure psia	Absolute Pressure Pa	Altitude Corrected Pa	Temper-ature K	Concen-tration ug/m^3	Gas phase conc., 'y' g/cm^3
0	14.7	101,353	93,954	303.15	2.39E+08	0.000239
1	15.7	108,248	100,346	303.15	2.55E+08	0.000255
2	16.7	115,142	106,737	303.15	2.71E+08	0.000271
3	17.7	122,037	113,128	303.15	2.87E+08	0.000287
4	18.7	128,932	119,520	303.15	3.03E+08	0.000303
5	19.7	135,827	125,911	303.15	3.20E+08	0.000320
6	20.7	142,721	132,303	303.15	3.36E+08	0.000336
7	21.7	149,616	138,694	303.15	3.52E+08	0.000352
8	22.7	156,511	145,086	303.15	3.68E+08	0.000368
9	23.7	163,406	151,477	303.15	3.85E+08	0.000385
10	24.7	170,300	157,869	303.15	4.01E+08	0.000401

Using the temperature-adjusted Henry's constant calculated above, m_{30}:

Table D.4. Tabulation of aqueous-phase equilibrium DO concentrations at lumen pressures used in this study, when air was used as the lumen gas.

Absolute Pressure psia	Gauge Pressure psig	Gas-phase O_2 conc. g/l	Aqueous DO Concentration g/l	Aqueous DO Concentration mg/l
13.63	0.0	0.239	0.00669	6.69
14.52	1.0	0.255	0.00715	7.15
15.52	2.0	0.271	0.00760	7.60
16.52	3.0	0.287	0.00806	8.06
17.52	4.0	0.303	0.00852	8.52
18.52	5.0	0.320	0.00897	8.97
19.52	6.0	0.336	0.00943	9.43
20.52	7.0	0.352	0.0099	9.88
21.52	8.0	0.368	0.0103	10.34
22.52	9.0	0.385	0.0108	10.79
23.52	10.0	0.401	0.0112	11.25

These oxygen concentrations are used in mass transfer calculations when 80% argon/20% oxygen was used as the lumen gas.

Calculate density of argon/oxygen mixture at mass flow controller calibration temperature (21.1°C):

Density of argon at reference point: sea level, 0°C = 1.784 g/l

Correct density to 21.1°C (this is the calibration temperature for the mass flow controller):

$$\rho_0 = \frac{m_{Ar} P}{RT} = 1.784 \text{ g/l} \qquad \text{(eqn D.4)}$$

Where:

ρ_0 =	density at 0°C
m_{Ar} =	molecular weight of argon
P =	pressure, 1 atm at sea level
R =	universal gas constant, 0.08206 L-atm/K-mol
K =	absolute temperature, Kelvin

$\rho_{21.1}$ = 1.66 g/l

Density of oxygen at reference point: sea level, 15°C = 1.354 g/l

Correct density to 21.1°C (this is the calibration temperature for the mass flow controller):

$$\rho_{15} = \frac{m_{O2} P}{RT} = 1.354 \text{ g/l} \qquad \text{(eqn D.5)}$$

Where:

P_{15} =	density at 15°C
m_{O2} =	molecular weight of oxygen
P =	pressure, 1 atm at sea level
R =	universal gas constant, 0.08206 L-atm/K-mol
K =	absolute temperature, Kelvin

$\rho_{21.1}$ = 1.33 g/l

So, combined density of the mixture:

80% × 1.66 g/l + 20% × 1.33 g/l = 1.59 g/l at 21.1°C

Calculate mass ratio of oxygen in argon/oxygen mixture:

Volume of oxygen in 1 liter of gas mixture: 0.2 liters

0.2 liters × 1mol/22.4 liters × 32 g/mol = 0.286 g O_2/liter mixture at STP

Volume of argon in 1 liter of gas mixture: 0.8 liters

0.8 liters × 1mol/22.4 liters × 39.95 g/mol = 1.427 g Ar/liter mixture at STP

Sum of oxygen and argon: 0.286 g/l + 1.427 g/l =1.723 g/liter mixture at STP

Mass fraction of oxygen: 0.286 / 1.723 = 0.167

Assume that this mass ratio is the same at 21.1°C as it is at STP (0°C).

So, the mass concentration of oxygen in the gas is 0.167 × 1.59 g/l at 21.1°C

= 0.266 g/liter of gas mixture

The mass flow controller was set to 6.6 cc/min during use with 80% argon / 20% oxygen.

This is equivalent to a volume of 9 cc/min of air:

(Setpoint 80% Ar/20% O_2) = (Setpoint air) / 1.3549

Where 1.3549 is a manufacturer-determined coefficient based on the relative K-factors of argon and oxygen and the 80/20 ratio of these gases.

9 cc/min × 1 liter/10^3 cc × 1440 min/day = 12.96 liters/day

At calibration temperature, density = 1.59 g/l, so:

12.96 l/day × 1.59 g/l = 20.66 g/day of gas mix

Adjusted for the mass ratio of oxygen in the mix:

20.66 g/day of gas mix × 0.167 = 3.45 g O_2/day

D.3 Calculation of oxygen fluxes

Oxygen fluxes were calculated using the mass transfer coefficient determined by clean water testing with microsensors at the membrane-liquid interface. This coefficient was closer to actual transfer efficiencies than the mechanistic model. The outer membrane surface area is used for these calculations, since ammonia oxidation occurs in the biofilm outside of the membrane.

Parameters common to all conditions:

DO at base of biofilm, average	0.42 mg/l (measured on Day 458)
K_L	9.17×10^{-4} cm/sec (per clean water testing)
Membrane area	0.285 m^2

Formula: $J_{O2} = K_L \times (C^*-C)$

From Day 23 to Day 92:

Aeration Gas: Air
Lumen pressure: 8 psig
C^*, per calculations: 10.8 mg/l

J_{O2} = 0.000571 mg/cm^2-min, or 8.22 g O_2/m^2-day

From Day 93 to Day 108:

Aeration Gas: Air
Lumen pressure: 5 psig
C^*, per calculations: 9.37 mg/l

J_{O2} = 0.000492 mg/cm^2-min, or 7.09 g O_2/m^2-day

From Day 153 to Day 297:

Aeration Gas: 80% argon / 20% oxygen
Lumen pressure: 5 psig
C^*, per calculations: 8.97 mg/l

J_{O2} = 0.000470 mg/cm^2-min, or 6.77 g O_2/m^2-day

From Day 298 to Day 555:

Aeration Gas: 80% argon / 20% oxygen
Lumen pressure: 4 psig
C^*, per calculations: 8.52 mg/l

J_{O2} = 0.000446 mg/cm^2-min, or 6.42 g O_2/m^2-day

Table D.5. Summary of calculated oxygen and ammonia flux conditions.

Period	Aeration Gas	Lumen Pressure psi	J_{O2} g O_2/m^2-d	J_{NH4+} g N/m^2-d	J_{O2} / J_{NH4+}
Day 23-92	Air	8	8.22	1.52	5.41
Day 93-108	Air	5	7.09	1.51	4.70
Day 109-152	Air	5	7.09	1.75	4.05
Day 152-297	Argon/O_2 mix	5	6.77	1.86	3.64
Day 298-555	Argon/O_2 mix	4	6.42	2.12	3.03

REFERENCES

Sander, R. 1999. Compilation of Henry's law constants for inorganic and organic species of potential importance in environmental chemistry (Version 3). http://www.henrys-law.org.

APPENDIX E

OXYGEN TRANSFER MODEL

Appendix E. Oxygen Transfer Model

E.1 Definition of terms

A = cross-sectional area of one membrane fiber, cm^2
a = specific inner surface area of membrane fibers relative to volume, cm^2/cm^3
C = bulk aqueous phase dissolved oxygen (DO) concentration, g/cm^3
C_{int} = membrane/water or membrane/biofilm interface DO concentration, g/cm^3
C^*_{sat} = saturation DO concentration in equilibrium with gas phase, g/cm^3
C^*_{∞} = equilibrium DO concentration as time approaches infinity, g/cm^3
C_0 = bulk aqueous phase DO concentration at beginning (t=0) of clean water test, g/cm^3
d = inside diameter of fibers (lumen diameter), cm
D = diffusion coefficient of oxygen in poly(dimethylsiloxane), cm^2/sec
J = oxygen flux, g O_2/cm^2-sec
K_g = air/membrane partitioning coefficient (concentration of O_2 in membrane / concentration of O_2 in air), dimensionless
K_w = water/membrane partitioning coefficient (concentration of O_2 in membrane / concentration of O_2 in water), dimensionless
K_{OL} = overall mass transfer coefficient, cm/sec
K_L = liquid boundary layer mass transfer coefficient, cm/sec
m = Henry's constant, O_2 equilibrium concentration in gas/O_2 equilibrium concentration in water, dimensionless
n = number of membrane fibers
OTE = Oxygen transfer efficiency, %
OTR = Oxygen transfer rate, g O_2/sec (as derived), also presented as mg O_2/min
P = permeability, cm^2/sec
t = time, sec
U = lumen gas velocity, cm/sec
V = bulk liquid volume, cm^3
x = distance along fiber length, cm
y = gas-phase oxygen concentration in fiber lumens, g/cm^3
y_0 = initial gas-phase oxygen concentration at fiber lumen entrance, g/cm^3
Z = length of fibers, cm
δ = fiber wall thickness, cm

E.2 Derivation of model

Objective: Develop a predictive model for the transfer of oxygen from inside the lumen of a silicone tube to water on the outside.

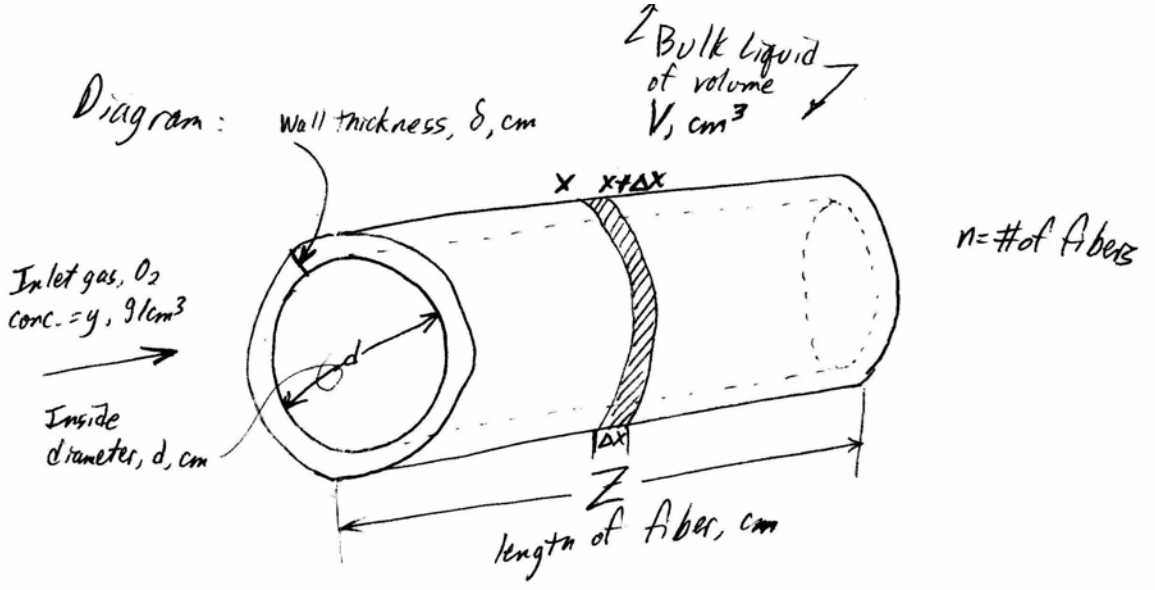

Figure E.1. Diagram of system: silicone tubing in liquid.

First, perform a mass balance of oxygen on a differential fiber element:

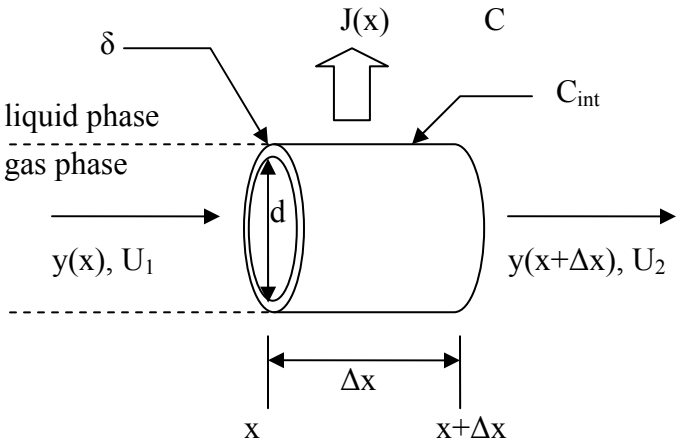

Figure 3.2 and E.2. Diagram of a differential hollow fiber element.

$$U_1 \cdot A \cdot y(x) - \pi d \cdot \Delta x \cdot J(x) = U_2 \cdot A \cdot y(x + \Delta x) \qquad \text{(eqn. E.1)}$$

From this mass balance:

$$\frac{dy}{dx} = \frac{-\pi dJ}{UA} \qquad \text{(eqn. E.2)}$$

The definition of flux is:

$$J(x) = \frac{D \cdot \left(K_g \cdot y(x) - K_w \cdot C_{int}(x)\right)}{\delta} \qquad \text{(eqn. E.3)}$$

Substitute this expression for flux into eqn. E.2:

$$\frac{dy}{dx} = \frac{-\pi d}{UA}\left[\frac{DK_g y}{\delta} - \frac{DK_w C_{int}}{\delta}\right]$$

$$\frac{dy}{dx} = \frac{-\pi dDK_g}{UA\delta} y + \frac{\pi dDK_w C_{int}}{UA\delta} \qquad \text{(eqn. E.4)}$$

This takes the form:

$$\frac{dy}{dx} = by + a$$

where:

$$a = \frac{\pi dDK_w C_{int}}{UA\delta} \qquad b = \frac{-\pi dDK_g}{UA\delta}$$

Separate variables and integrate:

$$\int \frac{dy}{(a + by)} = \int dx$$

$$\frac{1}{b} \ln(a + by) \Big|_{y_0}^{y(x)} = x\Big|_0^x$$

$$\ln(a + by_x) - \ln(a + by_0) = bx$$

$$y(x) = +\frac{a}{b}e^{bx} + y_0 e^{bx} - \frac{a}{b}$$

$$\frac{a}{b} = \frac{\frac{\pi dDK_w C_{int}}{UA\delta}}{\frac{-\pi dDK_g}{UA\delta}} = -\frac{K_w C_{int}}{K_g} \qquad \text{and} \qquad \frac{K_w}{K_g} = m$$

So, $a/b = -mC_{int}$

$$y(x) = y_0 e^{\left(-\frac{\pi dDK_g}{UA\delta}\right)x} - mC_{int} e^{\left(-\frac{\pi dDK_g}{UA\delta}\right)x} + mC_{int}$$

$$y(x) = \left(y_0 - mC_{int}\right) e^{\left(-\frac{\pi dDK_g}{UA\delta}\right)x} + mC_{int} \qquad \text{(eqn. E.5)}$$

Substituting this expression back into the expression for J (eqn. E.3):

$$J(x) = \frac{D}{\delta} K_g \left[\left(y_0 - mC_{int}\right) e^{\left(-\frac{\pi dDK_g}{UA\delta}\right)x} + mC_{int} \right] - \frac{D}{\delta} K_w C_{int}$$

$$J(x) = \frac{D}{\delta} K_g y_0 e^{\left(-\frac{\pi dDK_g}{UA\delta}\right)x} - \frac{D}{\delta} K_g mC_{int} e^{\left(-\frac{\pi dDK_g}{UA\delta}\right)x} + \frac{D}{\delta} K_g mC_{int} - \frac{D}{\delta} K_w C_{int}$$

Since $\frac{K_w}{K_g} = m$, then

$$J(x) = \frac{D}{\delta} K_g y_0 e^{\left(-\frac{\pi dDK_g}{UA\delta}\right)x} - \frac{D}{\delta} \cancel{K_g} \frac{K_w}{\cancel{K_g}} C_{int} e^{\left(-\frac{\pi dDK_g}{UA\delta}\right)x} + \frac{D}{\delta} \cancel{K_g} \frac{K_w}{\cancel{K_g}} C_{int} - \frac{D}{\delta} K_w C_{int}$$

cancels

Simplifying:

$$J(x) = \frac{D(K_g y_0 - K_w C_{int})}{\delta} e^{\left(-\frac{\pi dDK_g}{UA\delta}\right)x} \qquad \text{(eqn. E.6)}$$

Integration over the length of the fiber gives the oxygen transfer rate per unit perimeter:

$$\int J(x) = \int \mathrm{ae}^{\,\mathrm{bx}} = a\int e^{bx} = a\left.\frac{e^{bx}}{b}\right|_{x=0}^{x}$$

$$\mathrm{a} = \frac{\mathrm{D}}{\delta}(\mathrm{K_g y_0} - \mathrm{K_w C_{int}}) \qquad \text{and} \qquad \mathrm{b} = -\frac{\pi \mathrm{dDK_g}}{\mathrm{UA}\delta}$$

$$\int J(x) = \frac{\frac{\cancel{D}}{\cancel{\delta}}(\mathrm{K_g y_0} - \mathrm{K_w C_{int}})}{-\frac{\pi \mathrm{d}\cancel{D}\mathrm{K_g}}{\mathrm{UA}\cancel{\delta}}} e^{\left(-\frac{\pi \mathrm{dDK_g}}{\mathrm{UA}\delta}\right)x}\Bigg|_{0}^{x}$$

$$\int J(x) = UA\left(-\frac{\cancel{\mathrm{K_g}}\mathrm{y_0}}{\pi d\cancel{\mathrm{K_g}}} + \frac{\mathrm{K_w} C_{\mathrm{int}}}{\pi d \mathrm{K_g}}\right) e^{\left(-\frac{\pi dDK_g}{UA\delta}\right)x}\Bigg|_{0}^{x}$$

The resulting oxygen transfer rate is expressed as grams of oxygen per cm of fiber perimeter per second per fiber.

$$\text{Oxygen Transfer R ate} = \frac{UA}{\pi d}\left(mC_{\mathrm{int}} - y_0\right)\mathrm{e}^{\left(-\frac{\pi \mathrm{dDK_g}}{\mathrm{UA}\delta}\right)\mathrm{x}} \qquad \text{(eqn E.7)}$$

Multiplying by the fiber perimeter and number of fibers gives the overall oxygen transfer rate for the entire system.

$$OTR = nUA\left(mC_{\mathrm{int}} - y_0\right)\left[e^{\left(\frac{-\pi dDK_g}{UA\delta}\right)Z} - 1\right] \qquad \text{(eqn E.8)}$$

The HFMBR was operated at a membrane module inlet pressure of 5 psig. During this time, the outlet pressure averaged approximately 3.5 psig. No detail is known about the pressure profile between these two pressure gauges. The model was a better fit at 3.5 psig. Therefore, y(x), J(x), and OTE are shown for 3.5 psig.

Table E.1. Model parameters for y(x).

Parameter	Value	Units
y_0 =	0.000292	g/cm^3
D =	2.22E-05	cm^2/sec
Kg =	2.20E-01	- -
U =	0.15	cm/sec
delta =	0.06	cm
d =	0.198	cm
A =	0.0308	cm^2/sec
m =	35.64	- -
C =	2.00E-07	g/cm^3 (0.2 mg/l)

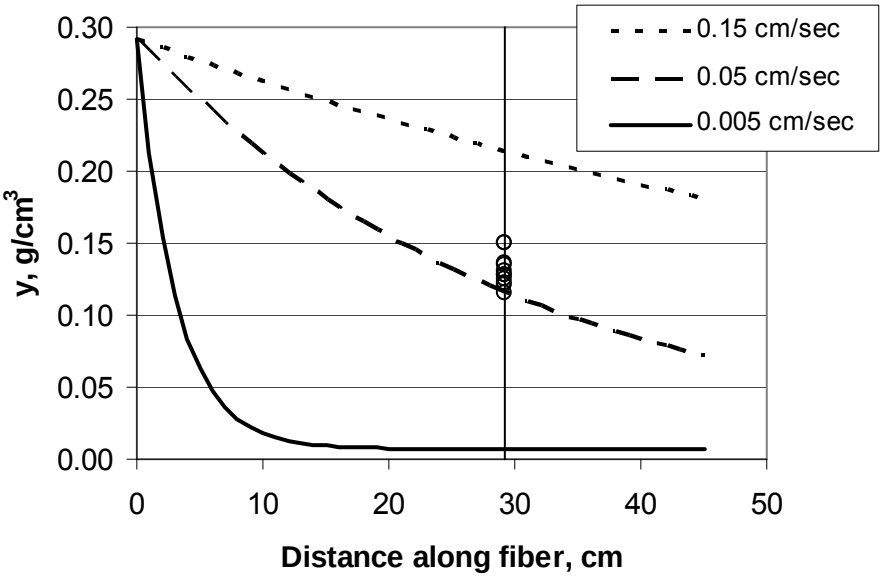

Figure E.3. Gas-phase oxygen concentration (y) as a function of distance at selected gas velocities, 3.5 psig. Vertical line represents the length of fibers used in this study.

Table E.2. Data for (y) as a function of Distance at selected gas velocities, 3.5 psig.

	U, cm/sec		
x, cm	0.15	0.05	0.005
0	2.92E-04	2.92E-04	2.92E-04
1	2.89E-04	2.83E-04	2.12E-04
2	2.86E-04	2.74E-04	1.55E-04
3	2.83E-04	2.65E-04	1.13E-04
4	2.80E-04	2.57E-04	8.36E-05
5	2.77E-04	2.49E-04	6.22E-05
6	2.74E-04	2.41E-04	4.67E-05
7	2.71E-04	2.33E-04	3.56E-05
8	2.68E-04	2.26E-04	2.77E-05
9	2.65E-04	2.19E-04	2.19E-05
10	2.62E-04	2.12E-04	1.78E-05
11	2.60E-04	2.06E-04	1.48E-05
12	2.57E-04	1.99E-04	1.26E-05
13	2.54E-04	1.93E-04	1.11E-05
14	2.51E-04	1.87E-04	9.98E-06
15	2.49E-04	1.81E-04	9.18E-06
16	2.46E-04	1.75E-04	8.61E-06
17	2.44E-04	1.70E-04	8.19E-06
18	2.41E-04	1.65E-04	7.89E-06
19	2.38E-04	1.60E-04	7.68E-06
20	2.36E-04	1.55E-04	7.53E-06
21	2.33E-04	1.50E-04	7.41E-06
22	2.31E-04	1.45E-04	7.33E-06
23	2.29E-04	1.41E-04	7.28E-06
24	2.26E-04	1.37E-04	7.23E-06
25	2.24E-04	1.32E-04	7.20E-06
26	2.21E-04	1.28E-04	7.18E-06
27	2.19E-04	1.24E-04	7.17E-06
28	2.17E-04	1.21E-04	7.16E-06
29	2.14E-04	1.17E-04	7.15E-06
30	2.12E-04	1.13E-04	7.14E-06
31	2.10E-04	1.10E-04	7.14E-06
32	2.08E-04	1.07E-04	7.14E-06
33	2.06E-04	1.03E-04	7.13E-06
34	2.03E-04	1.00E-04	7.13E-06
35	2.01E-04	9.73E-05	7.13E-06
36	1.99E-04	9.43E-05	7.13E-06
37	1.97E-04	9.15E-05	7.13E-06
38	1.95E-04	8.88E-05	7.13E-06
39	1.93E-04	8.62E-05	7.13E-06
40	1.91E-04	8.36E-05	7.13E-06
41	1.89E-04	8.11E-05	7.13E-06
42	1.87E-04	7.87E-05	7.13E-06
43	1.85E-04	7.64E-05	7.13E-06
44	1.83E-04	7.42E-05	7.13E-06
45	1.81E-04	7.20E-05	7.13E-06

Table E.3. Operating outlet gas oxygen concentration data.

Distance	y, mg/cm^3
29.2	0.122
29.2	0.150
29.2	0.115
29.2	0.121
29.2	0.124
29.2	0.127
29.2	0.128
29.2	0.130
29.2	0.136
29.2	0.135
29.2	0.151

Table E.4. Model parameters for J(x).

Parameter	Value	Units
C_{int}	2.0E-07	g/cm3, or 0.2 mg/l
m =	35.64	- -
P =	4.98E-06	cm2/sec various sources --> range from 5.2x10-10 to 8.0 x 10-10 m2/sec, De Bo et al., 2003
K_g =	0.21	from De Bo et al., 2002, J. Membrane Science, other data = 0.20 at 35C, 0.21 at 40C
D =	2.22E-05	cm2/sec, calculated as P/Hg
K_w =	7.601	calculated from Kg*m
n =	98	
d =	0.198	cm
Z =	29	cm
δ =	0.06	cm
V =	4500	cm3
A =	0.0308	cm2
U =	variable	

Table E.5. Gas-phase oxygen concentrations used in flux model.

Pressure psig	y_0 g/cm^3
13	0.000470
12	0.000453
11	0.000436
10	0.000419
9	0.000402
8	0.000385
7	0.000368
6	0.000351
5	0.000334
4	0.000317
3.5	0.000309
3	0.000300
2	0.000283
1	0.000266
0	0.000249

Table E.6. Oxygen transfer rates predicted by model at indicated pressure and velocity.

Velocity	Pressure, psig			
cm/sec	1	3.5	5	10
0.0001	0.00	0.01	0.01	0.01
0.0010	0.05	0.05	0.06	0.07
0.0025	0.12	0.14	0.15	0.19
0.0050	0.23	0.27	0.30	0.37
0.01	0.46	0.54	0.59	0.74
0.02	0.84	0.98	1.06	1.34
0.03	1.10	1.28	1.39	1.75
0.04	1.28	1.48	1.61	2.03
0.05	1.40	1.63	1.77	2.23
0.06	1.50	1.74	1.89	2.38
0.07	1.57	1.83	1.98	2.50
0.08	1.63	1.90	2.06	2.59
0.09	1.68	1.95	2.12	2.66
0.10	1.72	2.00	2.16	2.73
0.15	1.84	2.14	2.32	2.93
0.20	1.91	2.22	2.41	3.04
0.30	1.98	2.31	2.50	3.15

Table E.7. Data for oxygen mass transfer and transfer efficiency versus velocity at 3.5 psig.

Velocity cm/sec	Gas flow rate required cm^3/min	L/day	O_2 applied g/m^2-d	Modeled transfer mg/min	Modeled transfer g/m^2-d	OTE %
0.0001	0.018	0.026	0.041	0.01	0.04	107.2%
0.001	0.181	0.261	0.414	0.05	0.44	107.2%
0.0025	0.453	0.652	1.04	0.14	1.11	107.2%
0.005	0.905	1.304	2.07	0.27	2.22	107.2%
0.01	1.810	2.607	4.14	0.54	4.39	106.1%
0.02	3.621	5.214	8.29	0.98	7.97	96.2%
0.03	5.431	7.821	12.43	1.28	10.40	83.7%
0.04	7.242	10.428	16.57	1.48	12.07	72.9%
0.05	9.052	13.036	20.72	1.63	13.27	64.1%
0.06	10.863	15.643	24.86	1.74	14.17	57.0%
0.07	12.673	18.250	29.00	1.83	14.87	51.3%
0.08	14.484	20.857	33.14	1.90	15.42	46.5%
0.09	16.294	23.464	37.29	1.95	15.87	42.6%
0.10	18.105	26.071	41.43	2.00	16.24	39.2%
0.15	27.157	39.107	62.15	2.14	17.44	28.1%
0.20	36.210	52.142	82.86	2.22	18.08	21.8%
0.30	54.315	78.213	124.29	2.31	18.76	15.1%

O_2 applied is based on a density of 1.20 g/l and an oxygen mass fraction of 0.2344 (see Appendix D).

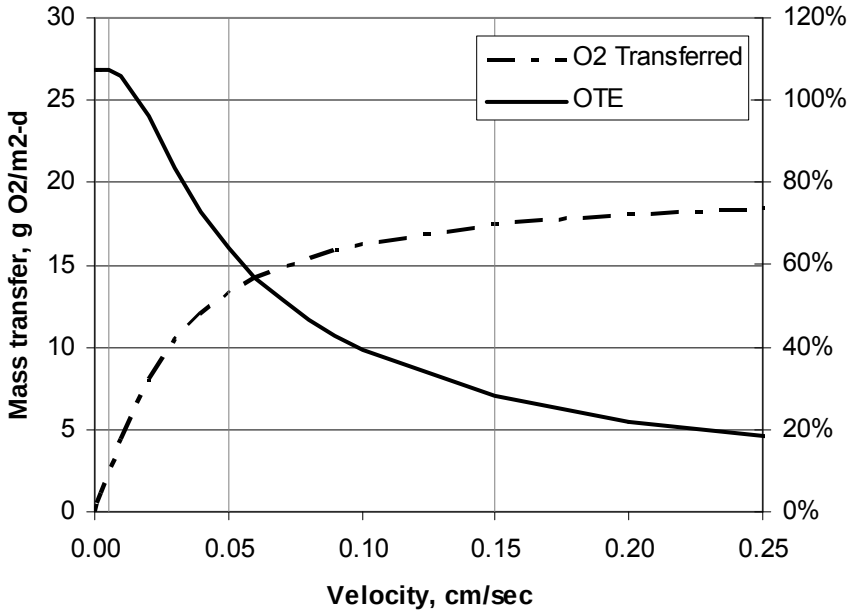

Figure E.4. Model-predicted oxygen transfer and OTE as a function of velocity, 3.5 psig.

APPENDIX F

HFMBR OPERATING DATA

Date	Day of Operation	Room Temp, C	Feed pH	Flow mL/min	Flow L/day	Feed Volume, L	Feed Tank Pressure psi	NH3-N mg/L-N	Stdev mg/L-N	NH3-N Load, gN/d	NH3-N Load, kg/m3-d	NH3-N Load, g/m2-d	NO2-N mg/L-N	Stdev/CI mg/L-N	NO2-N Load gN/d	NO3-N mg/L-N	NO3-N gN/d	COD mg/L
22-Nov-06	1	30	7.8	0.24	0.346	5	10	670	7	0.232	0.067	0.812	0	0	0.000	0.54	0.000	
23-Nov-06	2	30		0.24	0.346	4.2												
24-Nov-06	3	30		0.24	0.346	3.7	8	698	3	0.241	0.070	0.846	0	0	0.000	0.55	0.000	
25-Nov-06	4	30		0.24	0.346	3.1	6.5											
26-Nov-06	5	30		0.24	0.346	2.31	6											
27-Nov-06	6	30	7.9	0.24	0.346	1.5	5	690	4	0.238	0.069	0.836	0	0	0.000	0.52	0.000	
28-Nov-06	7	30		0.24	0.346	9	10											
29-Nov-06	8	30		0.24	0.346	8.7	9.5	731	7	0.253	0.073	0.887				1.6	0.001	
30-Nov-06	9	30		0.24	0.346	8.2	8.5											
1-Dec-06	10	30	7.8	0.24	0.346	7.7	8	601	34	0.208	0.060	0.728	0.3		0.000	0	0.000	
2-Dec-06	11	30		0.24	0.346	7.3	7											
3-Dec-06	12	30		0.24	0.346													
4-Dec-06	13	30		0.24	0.346	2.6	10	719	2	0.249	0.072	0.872	0.01		0.000	1.5	0.001	
5-Dec-06	14	30		0.24	0.346	2.9	9											
6-Dec-06	15	30		0.24	0.346	0.9	8	709	6	0.245	0.071	0.860	0.23		0.000	1	0.000	
7-Dec-06	16	30		0.24	0.346	4.3	8	760	6	0.263	0.076	0.922	0.22		0.000	0.32	0.000	
8-Dec-06	17	30		0.24	0.346	4	8	634	11	0.219	0.063	0.769	0.16		0.000	0.31	0.000	
9-Dec-06	18	30	7.73	0.24	0.346	3.4	7	653	6	0.226	0.065	0.791	0.19		0.000	0.32	0.000	
10-Dec-06	19	30		0.24	0.346	2.9	6.5											
11-Dec-06	20	30		0.24	0.346	2.5	6											
12-Dec-06	21	30	7.9	0.24	0.346	1.9	5.5	659	6	0.228	0.066	0.799	0.73		0.000	0.32	0.000	
13-Dec-06	22	30		0.24	0.346	1.4	5	681	11	0.235	0.068	0.826	0.61	0.01	0.000	0.34	0.000	
14-Dec-06	23	30		0.48	0.691	0.9	5											
15-Dec-06	24	30	7.85	0.48	0.691	4	8	637	18.0	0.441	0.128	1.546	0.64	0.02	0.000	0.33	0.000	
16-Dec-06	25	30		0.48	0.691	2.8	8											
17-Dec-06	26	30		0.48	0.691	1.6	6	628	10.0	0.434	0.126	1.523	0.59		0.000	0	0.000	
18-Dec-06	27	30		0.48	0.691	1	5.5											
19-Dec-06	28	30		0.48	0.691	4	7	669	2.2	0.462	0.134	1.623	0.88		0.001	0.347	0.000	
20-Dec-06	29	30		0.48	0.691	3	7											
21-Dec-06	30	30		0.48	0.691	2.1	6											
22-Dec-06	31	30		0.48	0.691	1.1	5	657	7	0.454	0.132	1.593	2.8	0.39	0.002	0.343	0.000	
23-Dec-06	32	30		0.48	0.691	9	7.8	608	20	0.420	0.122	1.474	3.7	0.25	0.003	0.34	0.000	
24-Dec-06	33	30		0.48	0.691	8.1	6											
25-Dec-06	34	30		0.48	0.691													
26-Dec-06	35	30		0.48	0.691													
27-Dec-06	36	30		0.48	0.691													
28-Dec-06	37	30		0.48	0.691	4.4	4.2	638	2	0.441	0.128	1.548	4.18	0.04	0.003	0	0.000	
29-Dec-06	38	30		0.48	0.691	3.4	6											
30-Dec-06	39	30		0.48	0.691	2.9	6											
31-Dec-06	40	30		0.48	0.691	2	6											
1-Jan-07	41	30		0.48	0.691													
2-Jan-07	42	30	7.8	0.48	0.691	0.3	4	657	18	0.454	0.132	1.593	4.39	0.27	0.003	0	0.000	
3-Jan-07	43	30		0.48	0.691	9.1	8	679	3	0.470	0.136	1.647						
4-Jan-07	44	30		0.48	0.691	8.2	6.5	663	19.45	0.458	0.133	1.608	0.21	0.08	0.000	0.4	0.000	
5-Jan-07	45	30		0.48	0.691	7.5	6											
6-Jan-07	46	30		0.48	0.691	6.5	4.5											

Date	Day of Operation	Room Temp, C	Feed pH	Flow mL/min	Flow L/day	Feed Volume, L	Feed Tank Pressure psi	NH3-N mg/L-N	Stdev mg/L-N	NH3-N Load, gN/d	NH3-N Load, kg/m3-d	NH3-N Load, g/m2-d	NO2-N mg/L-N	Stdev/CI mg/L-N	NO2-N Load gN/d	NO3-N mg/L-N	NO3-N gN/d	COD mg/L
7-Jan-07	47	30		0.48	0.691													
8-Jan-07	48	30	7.9	0.48	0.691	5.4	6	649	9.42	0.448	0.130	1.573	0.55	0.01	0.000			
9-Jan-07	49	30		0.48	0.691	4.8	5											
10-Jan-07	50	30		0.48	0.691	4	4											
11-Jan-07	51	30		0.48	0.691	3.2	4											
12-Jan-07	52	30		0.48	0.691	2.4	7	674	4.84	0.466	0.135	1.635	1.6	0.03	0.001			
13-Jan-07	53	30		0.48	0.691													
14-Jan-07	54	30		0.48	0.691	0.8	6											
15-Jan-07	55	30		0.36	0.518	0.4	5											
16-Jan-07	56	30		0.48	0.691	8.9	7.5	617	10.44	0.426	0.124	1.496	0.83	0.03	0.001			
17-Jan-07	57	30		0.48	0.691													
18-Jan-07	58	30		0.48	0.691	7.5	6	621	0.81	0.429	0.124	1.506	0.66	0.02	0.000			
19-Jan-07	59	30		0.48	0.691	6.8	5.5											
20-Jan-07	60	30		0.48	0.691													
21-Jan-07	61	30		0.48	0.691													
22-Jan-07	62	30		0.48	0.691	4.8	3.5	646	22	0.446	0.129	1.566	1.68	0.03	0.001			
23-Jan-07	63	30		0.48	0.691	3.8	7.5											
24-Jan-07	64	30		0.48	0.691	3	6.5											
25-Jan-07	65	30		0.48	0.691	2.2	6	672	5	0.465	0.135	1.630	2.8	0.076	0.002			
26-Jan-07	66	30		0.48	0.691	1.7	5.5											
27-Jan-07	67	30		0.48	0.691													
28-Jan-07	68	30		0.48	0.691													
29-Jan-07	69	30		0.48	0.691	7.8	6											
30-Jan-07	70	30		0.48	0.691	6.9	5											
31-Jan-07	71	30		0.48	0.691	6.1	8	643	34	0.445	0.129	1.561	1.2	0	0.001			
1-Feb-07	72	30		0.48	0.691	5.5	6.5											
2-Feb-07	73	30		0.48	0.691	4.8	6	678	7	0.469	0.136	1.645	1.61	0.1	0.001			
3-Feb-07	74	30		0.48	0.691													
4-Feb-07	75	30		0.48	0.691													
5-Feb-07	76	30		0.48	0.691	2.7	6	637	10	0.441	0.128	1.546	2.56	0.06	0.002			
6-Feb-07	77	30		0.48	0.691	2.1	5											
7-Feb-07	78	30		0.48	0.691													
8-Feb-07	79	30		0.48	0.691	8.1	8											
9-Feb-07	80	30		0.48	0.691	7.7	8	681	17	0.471	0.136	1.652	0.54	0.01	0.000			
10-Feb-07	81	30		0.48	0.691	7	7.5											
11-Feb-07	82	30		0.48	0.691													
12-Feb-07	83	30		0.48	0.691	6	7.5	707	13	0.489	0.142	1.714	0.65		0.000			
13-Feb-07	84	30		0.48	0.691	5.3	7.8											
14-Feb-07	85	30		0.48	0.691	4.3	6											
15-Feb-07	86	30		0.48	0.691	4	6	683	14	0.472	0.137	1.657	1.87		0.001			
16-Feb-07	87	30		0.48	0.691	3	8											
17-Feb-07	88	30		0.48	0.691	2.2	8											
18-Feb-07	89	30		0.48	0.691													
19-Feb-07	90	30		0.48	0.691	0.8	6	718	33	0.496	0.144	1.742	6.51		0.004			
20-Feb-07	91	30	7.77	0.48	0.691	8.2	8.5											
21-Feb-07	92	30		0.48	0.691	7.8	8.5						0.27		0.000			

Date	Day of Operation	Room Temp, C	Feed pH	Flow mL/min	Flow L/day	Feed Volume, L	Feed Tank Pressure psi	NH3-N mg/L-N	Stdev mg/L-N	NH3-N Load, gN/d	NH3-N Load, kg/m3-d	NH3-N Load, g/m2-d	NO2-N mg/L-N	Stdev/CI mg/L-N	NO2-N Load gN/d	NO3-N mg/L-N	NO3-N gN/d	COD mg/L
22-Feb-07	93	30		0.48	0.691	7.1	8											
23-Feb-07	94	30		0.48	0.691	6.4	6.5	637	11	0.441	0.128	1.546						
24-Feb-07	95	30		0.48	0.691	5.5	8											
25-Feb-07	96	30		0.48	0.691													
26-Feb-07	97	30		0.48	0.691	4.1	6.5	663	12	0.458	0.133	1.608						
27-Feb-07	98	30		0.48	0.691	3.2	9.5	705	12	0.487	0.141	1.709						
28-Feb-07	99	30		0.48	0.691	2.5	8.5											
1-Mar-07	100	30		0.48	0.691	1.6	7.5											
2-Mar-07	101	30		0.48	0.691	10		681	0	0.471	0.136	1.652	3.71	0.03	0.003	1.3	0.001	
3-Mar-07	102	30		0.48	0.691													
4-Mar-07	103	30		0.48	0.691	8.3	10.5											
5-Mar-07	104	30		0.48	0.691													
6-Mar-07	105	30		0.48	0.691													
7-Mar-07	106	30		0.48	0.691													
8-Mar-07	107	30		0.48	0.691	5.2	6.5											
9-Mar-07	108	30		0.48	0.691	4.6	8	679	12.5	0.470	0.136	1.647	0.52	0.4	0.000	0.2	0.000	
10-Mar-07	109	30		0.72	1.037													
11-Mar-07	110	30	7.8	0.72	1.037	1.8	6.5	681	22.6	0.706	0.205	2.478	2.48	0.05	0.003	0	0.000	
12-Mar-07	111	30	7.8	0.72	1.037	10	10											
13-Mar-07	112	30		0.72	1.037	9.1	8											
14-Mar-07	113	30		0.72	1.037													
15-Mar-07	114	30		0.72	1.037	7.1	9											
16-Mar-07	115	30		0.72	1.037	5.8	7	630	5.8	0.654	0.189	2.294	1.2	0.74	0.001	0.02	0.000	
17-Mar-07	116	30		0.72	1.037													
18-Mar-07	117	30		0.72	1.037													
19-Mar-07	118	30		0.72	1.037	2.5	6											
20-Mar-07	119	30		0.72	1.037	1.8	8.5											
21-Mar-07	120	30		0.72	1.037	0.5	7.5	604	11.7	0.626	0.181	2.198	3.76	0.14	0.004	0.2	0.000	
22-Mar-07	121	30		0.72	1.037	8.5	8											
23-Mar-07	122	30		0.72	1.037	7.3	7.5	642	11.9	0.665	0.193	2.334	0.23	0.16	0.000	0	0.000	
24-Mar-07	123	30		0.72	1.037													
25-Mar-07	124	30		0.72	1.037	5	6											
26-Mar-07	125	30		0.72	1.037	4.4	8											
27-Mar-07	126	30		0.72	1.037													
28-Mar-07	127	30		0.72	1.037	1.6	8	639	9.0	0.662	0.192	2.323	1.89	0.04	0.002	0	0.000	
29-Mar-07	128	30		0.72	1.037	0.9	7.5											
30-Mar-07	129	30		0.72	1.037													
31-Mar-07	130	30		0.72	1.037													
1-Apr-07	131	30		0.72	1.037													
2-Apr-07	132	30		0.72	1.037	5.8	6.5											
3-Apr-07	133	30		0.72	1.037								0.71	0.045	0.001			
4-Apr-07	134	30		0.72	1.037	3.2	8											
5-Apr-07	135	30		0.72	1.037	2.2	7.8	656	8.5	0.680	0.197	2.386	1.6	0.013	0.002	0.13	0.000	
6-Apr-07	136	30		0.72	1.037													
7-Apr-07	137	30		0.72	1.037													
8-Apr-07	138	30		0.72	1.037													

Date	Day of Operation	Room Temp, C	Feed pH	Flow mL/min	Flow L/day	Feed Volume, L	Feed Tank Pressure psi	NH3-N mg/L-N	Stdev mg/L-N	NH3-N Load, gN/d	NH3-N Load, kg/m3-d	NH3-N Load, g/m2-d	NO2-N mg/L-N	Stdev/CI mg/L-N	NO2-N Load gN/d	NO3-N mg/L-N	NO3-N gN/d	COD mg/L
9-Apr-07	139	30		0.72	1.037	5.4	6											
10-Apr-07	140	30		0.72	1.037	4.5	8.5	671	10.4	0.696	0.202	2.441	0.7	0.01	0.001	0.1	0.000	
11-Apr-07	141	30		0.72	1.037	3.3	9											
12-Apr-07	142	30		0.72	1.037													
13-Apr-07	143	30		0.72	1.037	1.3	6.5	657	21.2	0.681	0.197	2.389	2.8	0.07	0.003	0.006	0.000	
14-Apr-07	144	30		0.72	1.037													
15-Apr-07	145	30		0.72	1.037													
16-Apr-07	146	30		0.72	1.037													
17-Apr-07	147	30		0.72	1.037	6.1	8											
18-Apr-07	148	30		0.72	1.037	5.1	8.5											
19-Apr-07	149	30		0.72	1.037													
20-Apr-07	150	30		0.72	1.037													
21-Apr-07	151	30		0.72	1.037	2.9	6											
22-Apr-07	152	30		0.72	1.037													
23-Apr-07	153	30		0.72	1.037	0.8	9	681	49.7	0.706	0.205	2.478	3.2	0.04	0.003	0.15	0.000	
24-Apr-07	154	30		0.72	1.037	9	9											
25-Apr-07	155	30		0.72	1.037	7.6	8											
26-Apr-07	156	30		0.72	1.037	6.7	6	675	8	0.700	0.203	2.456	0.3	0.02	0.000	0.16	0.000	
27-Apr-07	157	30		0.72	1.037													
28-Apr-07	158	30		0.72	1.037													
29-Apr-07	159	30		0.72	1.037	2.8	5.5											
30-Apr-07	160	30		0.72	1.037	2.1	9	633	10	0.656	0.190	2.301	1.8	0.01	0.002	0.2	0.000	
1-May-07	161	30		0.72	1.037	0.9	1.9											
2-May-07	162	30		0.72	1.037	8.9	var	627	9	0.651	0.188	2.283	0.16					
3-May-07	163	30		0.72	1.037	7.8	var											
4-May-07	164	30		0.72	1.037	6.9	var											
5-May-07	165	30		0.72	1.037	5.6	8											
6-May-07	166	30		0.72	1.037	4	6.5											
7-May-07	167	30		0.72	1.037													
8-May-07	168	30		0.72	1.037													
9-May-07	169	30		0.72	1.037	0.8	6	640	13	0.663	0.192	2.327						
10-May-07	170	30		0.72	1.037													
11-May-07	171	30		0.72	1.037	8.3	8											
12-May-07	172	30		0.72	1.037													
13-May-07	173	30		0.72	1.037	5.8	10											
14-May-07	174	30		0.72	1.037													
15-May-07	175	30		0.72	1.037	3.7	10											
16-May-07	176	30		0.72	1.037													
17-May-07	177	30		0.72	1.037	1.4	10	657	37	0.681	0.197	2.389	4.1	0.1	0.004	0.6	0.001	
18-May-07	178	30		0.72	1.037													
19-May-07	179	30		0.72	1.037													
20-May-07	180	30		0.72	1.037													
21-May-07	181	30		0.72	1.037	6.9	6.5											
22-May-07	182	30		0.72	1.037	5.3	8											
23-May-07	183	30		0.72	1.037			609	24	0.632	0.183	2.216	0.9	0.03	0.001			
24-May-07	184	30		0.72	1.037	3.4	6											

Date	Day of Operation	Room Temp, C	Feed pH	Flow mL/min	Flow L/day	Feed Volume, L	Feed Tank Pressure psi	NH3-N mg/L-N	Stdev mg/L-N	NH3-N Load, gN/d	NH3-N Load, kg/m3-d	NH3-N Load, g/m2-d	NO2-N mg/L-N	Stdev/CI mg/L-N	NO2-N Load gN/d	NO3-N mg/L-N	NO3-N gN/d	COD mg/L
25-May-07	185	30		0.72	1.037	2.4	9											
26-May-07	186	30		0.72	1.037													
27-May-07	187	30		0.72	1.037													
28-May-07	188	30		0.72	1.037													
29-May-07	189	30		0.72	1.037	3.1	6											
30-May-07	190	30		0.72	1.037	2.3	8.5	633	13	0.656	0.190	2.301	2.2	0.02	0.002			
31-May-07	191	30		0.72	1.037													
1-Jun-07	192	30		0.72	1.037	0.5	8	592	4	0.614	0.178	2.154	5.6	0.1	0.006			
2-Jun-07	193	30		0.72	1.037													
3-Jun-07	194	30		0.72	1.037													
4-Jun-07	195	30		0.72	1.037													
5-Jun-07	196	30		0.72	1.037	5.5	6											
6-Jun-07	197	30		0.72	1.037													
7-Jun-07	198	30		0.72	1.037	4	8	616	11	0.639	0.185	2.242	1.3	0.01	0.001			
8-Jun-07	199	30		0.72	1.037	3.6	9											
9-Jun-07	200	30		0.72	1.037													
10-Jun-07	201	30		0.72	1.037	0.7	6											
11-Jun-07	202	30		0.72	1.037													
12-Jun-07	203	30		0.72	1.037	8.5	8											
13-Jun-07	204	30		0.72	1.037	7.5	7											
14-Jun-07	205	30		0.72	1.037													
15-Jun-07	206	30		0.72	1.037	5.6	8.5	631	25	0.655	0.190	2.297	0.2	0	0.000			
16-Jun-07	207	30		0.72	1.037													
17-Jun-07	208	30		0.72	1.037													
18-Jun-07	209	30		0.72	1.037	2.3	5	665	20	0.689	0.200	2.419	1.6	0.05	0.002	13.7		
19-Jun-07	210	30		0.72	1.037	8.7	8.5	659	6	0.683	0.198	2.397	0.1	0.01	0.000	0.03		
20-Jun-07	211	30		0.72	1.037													
21-Jun-07	212	30		0.72	1.037	6.8	6											
22-Jun-07	213	30		0.72	1.037	5.6	10											
23-Jun-07	214	30		0.72	1.037													
24-Jun-07	215	30		0.72	1.037													
25-Jun-07	216	30		0.72	1.037	2.1	6											
26-Jun-07	217	30		0.72	1.037													
27-Jun-07	218	30		0.72	1.037	0.5	7	636	2	0.659	0.191	2.312	2.9	0.1	0.003			
28-Jun-07	219	30		0.72	1.037	9.1	10											
29-Jun-07	220	30		0.72	1.037	7.8	10											
30-Jun-07	221	30		0.72	1.037													
1-Jul-07	222	30		0.72	1.037													
2-Jul-07	223	30		0.72	1.037	6.3	8.5											
3-Jul-07	224	30		0.72	1.037													
4-Jul-07	225	30		0.72	1.037													
5-Jul-07	226	30		0.72	1.037													
6-Jul-07	227	30		0.72	1.037													
7-Jul-07	228	30		0.72	1.037	1	8.5											
8-Jul-07	229	30	7.68	0.72	1.037	0.5	8.5											
9-Jul-07	230	30		0.72	1.037			615	9	0.638	0.185	2.238						

Date	Day of Operation	Room Temp, C	Feed pH	Flow mL/min	Flow L/day	Feed Volume, L	Feed Tank Pressure psi	NH3-N mg/L-N	Stdev mg/L-N	NH3-N Load, gN/d	NH3-N Load, kg/m3-d	NH3-N Load, g/m2-d	NO2-N mg/L-N	Stdev/CI mg/L-N	NO2-N Load gN/d	NO3-N mg/L-N	NO3-N gN/d	COD mg/L
10-Jul-07	231	30		0.72	1.037	7.8	7											
11-Jul-07	232	30		0.72	1.037	6.6	6											
12-Jul-07	233	30		0.72	1.037	5.4	8	553	28.7	0.573	0.166	2.010	0.2	0.01	0.000			
13-Jul-07	234	30		0.72	1.037	4.5	7											
14-Jul-07	235	30		0.72	1.037													
15-Jul-07	236	30		0.72	1.037													
16-Jul-07	237	30		0.72	1.037	1.4	6.5											
17-Jul-07	238	30		0.72	1.037	0.5	10						5.5	0.1	0.006			
18-Jul-07	239	30		0.72	1.037	8.9	10											
19-Jul-07	240	30		0.72	1.037	8.2	8.5						0.66	0.19	0.001	0		
20-Jul-07	241	30		0.72	1.037	7.1	7.5											
21-Jul-07	242	30		0.72	1.037													
22-Jul-07	243	30		0.72	1.037													
23-Jul-07	244	30		0.72	1.037	4.2	6											
24-Jul-07	245	30		0.72	1.037	3	7						0.61	0.53	0.001	0.11		
25-Jul-07	246	30		0.72	1.037	1.9	8.5											
26-Jul-07	247	30		0.72	1.037	1	7											
27-Jul-07	248	30		0.72	1.037	0.5	6.5											
28-Jul-07	249	30		0.72	1.037													
29-Jul-07	250	30		0.72	1.037													
30-Jul-07	251	30		0.72	1.037													
31-Jul-07	252	30		0.72	1.037	5.8	5											
1-Aug-07	253	30		0.72	1.037	4.9	7.5											
2-Aug-07	254	30		0.72	1.037	3.9	6											
3-Aug-07	255	30		0.72	1.037	2.5	8											
4-Aug-07	256	30		0.72	1.037													
5-Aug-07	257	30		0.72	1.037	0.5	10											
6-Aug-07	258	30		0.72	1.037			602	17.5	0.624	0.181	2.191	0.02		0.000	0		81
7-Aug-07	259	30		0.72	1.037													
8-Aug-07	260	30		0.72	1.037													
9-Aug-07	261	30		0.72	1.037	6.2	7											
10-Aug-07	262	30		0.72	1.037	5	8.5											
11-Aug-07	263	30		0.72	1.037													
12-Aug-07	264	30		0.72	1.037	2.6	8											
13-Aug-07	265	30		0.72	1.037	9.5	7.5	616	17.3	0.639	0.185	2.242	0.01		0.000			
14-Aug-07	266	30		0.72	1.037	8.1	8											
15-Aug-07	267	30		0.72	1.037	7.3	6.5											
16-Aug-07	268	30		0.72	1.037	5.7	8	605	1.6	0.627	0.182	2.202	1.34	0.77	0.001	0		
17-Aug-07	269	30		0.72	1.037	4.9	7											
18-Aug-07	270	30		0.72	1.037													
19-Aug-07	271	30		0.72	1.037													
20-Aug-07	272	30		0.72	1.037	2.1	7.5											
21-Aug-07	273	30		0.72	1.037	1.3	7											
22-Aug-07	274	30	7.71	0.72	1.037	0.5	7						0.8	0.01	0.001			
23-Aug-07	275	30		0.72	1.037													
24-Aug-07	276	30		0.72	1.037	7.9	9											

Date	Day of Operation	Room Temp, C	Feed pH	Flow mL/min	Flow L/day	Feed Volume, L	Feed Tank Pressure psi	NH3-N mg/L-N	Stdev mg/L-N	NH3-N Load, gN/d	NH3-N Load, kg/m3-d	NH3-N Load, g/m2-d	NO2-N mg/L-N	Stdev/CI mg/L-N	NO2-N Load gN/d	NO3-N mg/L-N	NO3-N gN/d	COD mg/L
25-Aug-07	277	30		0.72	1.037													
26-Aug-07	278	30		0.72	1.037	6	6											
27-Aug-07	279	30		0.72	1.037	5.6	9											
28-Aug-07	280	30		0.72	1.037	5.2												
29-Aug-07	281	30		0.72	1.037	3.8												
30-Aug-07	282	30		0.72	1.037			636	8.9	0.659	0.191	2.312	0.7	0.02	0.001	0.88		
31-Aug-07	283	30		0.72	1.037	1.8												
1-Sep-07	284	30		0.72	1.037													
2-Sep-07	285	30		0.72	1.037													
3-Sep-07	286	30		0.72	1.037	6.1												
4-Sep-07	287	30		0.72	1.037	5.4		735	7	0.762	0.221	2.673	0.44	0.01	0.000	0.04		63
5-Sep-07	288	30		0.72	1.037	4												
6-Sep-07	289	30		0.72	1.037	3.2												
7-Sep-07	290	30		0.72	1.037	1.9												
8-Sep-07	291	30		0.72	1.037													
9-Sep-07	292	30		0.72	1.037	0.5												
10-Sep-07	293	30		0.72	1.037	8.9												
11-Sep-07	294	30		0.72	1.037	8		663	42	0.687	0.199	2.411	0.16	0	0.000	0.04		
12-Sep-07	295	30		0.72	1.037	6.6												
13-Sep-07	296	30		0.72	1.037	5.8		746	15.3	0.773	0.224	2.713	0.43	0.01	0.000	0.03		
14-Sep-07	297	30		0.72	1.037	4.5												
15-Sep-07	298	30		0.72	1.037													
16-Sep-07	299	30		0.72	1.037	2												
17-Sep-07	300	30		0.72	1.037			716	37	0.743	0.215	2.607	0.17	0.01	0.000	0.03		
18-Sep-07	301	30		0.72	1.037	7.9												
19-Sep-07	302	30		0.72	1.037	7.1												
20-Sep-07	303	30		0.72	1.037	6		714	32	0.741	0.215	2.599	0.6	0.005	0.001	0.05		81
21-Sep-07	304	30		0.72	1.037													
22-Sep-07	305	30		0.72	1.037													
23-Sep-07	306	30		0.72	1.037	2.8												
24-Sep-07	307	30		0.72	1.037													
25-Sep-07	308	30		0.72	1.037													
26-Sep-07	309	30		0.72	1.037													
27-Sep-07	310	30		0.72	1.037	5.8		623	22	0.646	0.187	2.268	0.23	0.01	0.000			
28-Sep-07	311	30		0.72	1.037	4.5												
29-Sep-07	312	30		0.72	1.037													
30-Sep-07	313	30		0.72	1.037													
1-Oct-07	314	30		0.72	1.037													
2-Oct-07	315	30		0.72	1.037	0.5	5.5											
3-Oct-07	316	30		0.72	1.037	8.8	8											
4-Oct-07	317	30		0.72	1.037	7.7	8	602	4.2	0.624	0.181	2.191	0.11		0.000			45
5-Oct-07	318	30		0.72	1.037													
6-Oct-07	319	30		0.72	1.037													
7-Oct-07	320	30		0.72	1.037													
8-Oct-07	321	30		0.72	1.037	3.9	5.5	606	4.5	0.628	0.182	2.205	0.59		0.001			
9-Oct-07	322	30		0.72	1.037													

Date	Day of Operation	Room Temp, C	Feed pH	Flow mL/min	Flow L/day	Feed Volume, L	Feed Tank Pressure psi	NH3-N mg/L-N	Stdev mg/L-N	NH3-N Load, gN/d	NH3-N Load, kg/m3-d	NH3-N Load, g/m2-d	NO2-N mg/L-N	Stdev/CI mg/L-N	NO2-N Load gN/d	NO3-N mg/L-N	NO3-N gN/d	COD mg/L
10-Oct-07	323	30		0.72	1.037													
11-Oct-07	324	30		0.72	1.037			624	4.72	0.647	0.188	2.272	2.28		0.002			
12-Oct-07	325	30		0.72	1.037	0.6	6											
13-Oct-07	326	30		0.72	1.037													
14-Oct-07	327	30		0.72	1.037													
15-Oct-07	328	30		0.72	1.037													
16-Oct-07	329	30		0.72	1.037													
17-Oct-07	330	30		0.72	1.037													
18-Oct-07	331	30		0.72	1.037													
19-Oct-07	332	30		0.72	1.037	2.2	3	606	3.39	0.628	0.182	2.205	0.89		0.001			47
20-Oct-07	333	30		0.72	1.037													
21-Oct-07	334	30		0.72	1.037													
22-Oct-07	335	30		0.72	1.037	4.2	7.5											
23-Oct-07	336	30		0.72	1.037													
24-Oct-07	337	30		0.72	1.037													
25-Oct-07	338	30		0.72	1.037	1.1	6	651	8.04	0.675	0.195	2.367	1.3		0.001			
26-Oct-07	339	30		0.72	1.037													
27-Oct-07	340	30		0.72	1.037													
28-Oct-07	341	30		0.72	1.037													
29-Oct-07	342	30		0.72	1.037													
30-Oct-07	343	30		0.72	1.037	4.8	9	614	7.56	0.637	0.184	2.235	0.28		0.000			
31-Oct-07	344	30		0.72	1.037	3.6	7.5											
1-Nov-07	345	30		0.72	1.037													
2-Nov-07	346	30		0.72	1.037	1.8	6	625	2.45	0.648	0.188	2.275	0.96		0.001			
3-Nov-07	347	30		0.72	1.037													
4-Nov-07	348	30		0.72	1.037													
5-Nov-07	349	30		0.72	1.037	6.5	6											
6-Nov-07	350	30		0.72	1.037													
7-Nov-07	351	30		0.72	1.037	4.8	6											
8-Nov-07	352	30		0.72	1.037													
9-Nov-07	353	30		0.72	1.037													
10-Nov-07	354	30		0.72	1.037													
11-Nov-07	355	30		0.72	1.037	0.5	4	676	21.5	0.701	0.203	2.459						
12-Nov-07	356	30		0.72	1.037	9.1	8											
13-Nov-07	357	30		0.72	1.037													
14-Nov-07	358	30		0.72	1.037	7.5	6	644	4	0.667	0.193	2.341	0.21		0.000			11
15-Nov-07	359	30		0.72	1.037													
16-Nov-07	360	30		0.72	1.037	5.2	8											
17-Nov-07	361	30		0.72	1.037													
18-Nov-07	362	30		0.72	1.037													
19-Nov-07	363	30		0.72	1.037	2.3	5											
20-Nov-07	364	30		0.72	1.037	1.2	8	719	12.9	0.745	0.216	2.614	2.23		0.002			
21-Nov-07	365	30		0.72	1.037													
22-Nov-07	366	30		0.72	1.037													
23-Nov-07	367	30		0.72	1.037													
24-Nov-07	368	30		0.72	1.037													

Date	Day of Operation	Room Temp, C	Feed pH	Flow mL/min	Flow L/day	Feed Volume, L	Feed Tank Pressure psi	NH3-N mg/L-N	Stdev mg/L-N	NH3-N Load, gN/d	NH3-N Load, kg/m3-d	NH3-N Load, g/m2-d	NO2-N mg/L-N	Stdev/CI mg/L-N	NO2-N Load gN/d	NO3-N mg/L-N	NO3-N gN/d	COD mg/L
25-Nov-07	369	30		0.72	1.037													
26-Nov-07	370	30		0.72	1.037													
27-Nov-07	371	30		0.72	1.037	2.7	6	593	28.7	0.615	0.178	2.157	1.77		0.002			
28-Nov-07	372	30		0.72	1.037													
29-Nov-07	373	30		0.72	1.037	0.5	4.5											
30-Nov-07	374	30		0.72	1.037	8.7	8											
1-Dec-07	375	30		0.72	1.037													
2-Dec-07	376	30		0.72	1.037													
3-Dec-07	377	30		0.72	1.037													
4-Dec-07	378	30		0.72	1.037	4.5	4.5	562	2.64	0.582	0.169	2.043	0.74		0.001			35
5-Dec-07	379	30		0.72	1.037													
6-Dec-07	380	30		0.72	1.037	2.2	6.5											
7-Dec-07	381	30		0.72	1.037	0.9		552	2.77	0.572	0.166	2.006	2.34		0.002			
8-Dec-07	382	30		0.72	1.037													
9-Dec-07	383	30		0.72	1.037													
10-Dec-07	384	30		0.72	1.037	7	6											
11-Dec-07	385	30		0.72	1.037													
12-Dec-07	386	30		0.72	1.037	4.9	7	593	9.86	0.615	0.178	2.157	0.69		0.001			
13-Dec-07	387	30		0.72	1.037	3.9	6											
14-Dec-07	388	30		0.72	1.037	2.3	7	598	3.72	0.620	0.180	2.176	1.62		0.002			18
15-Dec-07	389	30		0.72	1.037	1.5	6											
16-Dec-07	390	30		0.72	1.037													
17-Dec-07	391	30		0.72	1.037	7.8	7											
18-Dec-07	392	30		0.72	1.037			578	4.94	0.599	0.174	2.102	0.42		0.000			
19-Dec-07	393	30		0.72	1.037	5.3	7											
20-Dec-07	394	30		0.72	1.037	4.5	6	580	22.3	0.601	0.174	2.110	0.97		0.001			
21-Dec-07	395	30		0.72	1.037													
22-Dec-07	396	30		0.72	1.037													
23-Dec-07	397	30		0.72	1.037													
24-Dec-07	398	30		0.72	1.037	0.5	6	563	12.3	0.583	0.169	2.047						49
25-Dec-07	399	30		0.72	1.037													
26-Dec-07	400	30		0.72	1.037													
27-Dec-07	401	30		0.72	1.037													
28-Dec-07	402	30		0.72	1.037													
29-Dec-07	403	30		0.72	1.037													
30-Dec-07	404	30		0.72	1.037													
31-Dec-07	405	30		0.72	1.037	3.1	2											
1-Jan-08	406	30		0.72	1.037	1.4	7	566	3.59	0.587	0.170	2.058	2.44		0.003			
2-Jan-08	407	30		0.72	1.037	0.8	6											
3-Jan-08	408	30		0.72	1.037	8.9	9	605	19	0.627	0.182	2.202	0.48		0.000			
4-Jan-08	409	30		0.72	1.037	7.9	8.9											
5-Jan-08	410	30		0.72	1.037													
6-Jan-08	411	30		0.72	1.037													
7-Jan-08	412	30		0.72	1.037	5.1	4.5											
8-Jan-08	413	30		0.72	1.037	4	8	622	19	0.645	0.187	2.264	1.18		0.001			
9-Jan-08	414	30		0.72	1.037	3	7											

Date	Day of Operation	Room Temp, C	Feed pH	Flow mL/min	Flow L/day	Feed Volume, L	Feed Tank Pressure psi	NH3-N mg/L-N	Stdev mg/L-N	NH3-N Load, gN/d	NH3-N Load, kg/m3-d	NH3-N Load, g/m2-d	NO2-N mg/L-N	Stdev/CI mg/L-N	NO2-N Load gN/d	NO3-N mg/L-N	NO3-N gN/d	COD mg/L
10-Jan-08	415	30		0.72	1.037	1.8	6											
11-Jan-08	416	30		0.72	1.037	0.9	7	607	13.5	0.630	0.182	2.209	3.06		0.003			
12-Jan-08	417	30		0.72	1.037													
13-Jan-08	418	30		0.72	1.037													
14-Jan-08	419	30		0.72	1.037													
15-Jan-08	420	30		0.72	1.037	5.2	4											
16-Jan-08	421	30		0.72	1.037													
17-Jan-08	422	30		0.72	1.037													
18-Jan-08	423	30		0.72	1.037	2.3	6	619	9.28	0.642	0.186	2.253	1.38		0.001			68
19-Jan-08	424	30		0.72	1.037													
20-Jan-08	425	30		0.72	1.037	0.5	2											
21-Jan-08	426	30		0.72	1.037													
22-Jan-08	427	30		0.72	1.037	7.6	7											
23-Jan-08	428	30		0.72	1.037													
24-Jan-08	429	30		0.72	1.037													
25-Jan-08	430	30		0.72	1.037	4.6	6	670	10	0.695	0.201	2.437	0.81		0.001			
26-Jan-08	431	30		0.72	1.037													
27-Jan-08	432	30		0.72	1.037													
28-Jan-08	433	30		0.72	1.037													
29-Jan-08	434	30		0.72	1.037													
30-Jan-08	435	30		0.72	1.037													
31-Jan-08	436	30		0.72	1.037	3.4	4											
1-Feb-08	437	30		0.72	1.037													
2-Feb-08	438	30		0.72	1.037													
3-Feb-08	439	30		0.72	1.037	~0												
4-Feb-08	440	30		0.72	1.037	10	5											
5-Feb-08	441	30		0.72	1.037	8.9	8	612	7.63	0.635	0.184	2.227	0.19		0.000			
6-Feb-08	442	30		0.72	1.037	7.8	7											
7-Feb-08	443	30		0.72	1.037	5.8	5											
8-Feb-08	444	30		0.72	1.037													
9-Feb-08	445	30		0.72	1.037													
10-Feb-08	446	30		0.72	1.037													
11-Feb-08	447	30		0.72	1.037													
12-Feb-08	448	30		0.72	1.037													
13-Feb-08	449	30		0.72	1.037	0.5	8	545	3.66	0.566	0.164	1.984	2.08		0.002			47
14-Feb-08	450	30		0.72	1.037													
15-Feb-08	451	30		0.72	1.037	8.3	7.5											
16-Feb-08	452	30		0.72	1.037													
17-Feb-08	453	30		0.72	1.037													
18-Feb-08	454	30		0.72	1.037	5.4	6	667	5.15	0.691	0.200	2.426	0.63		0.001			
19-Feb-08	455	30		0.72	1.037													
20-Feb-08	456	30		0.72	1.037	3												
21-Feb-08	457	30		0.72	1.037													
22-Feb-08	458	30		0.72	1.037	1.2												
23-Feb-08	459	30		0.72	1.037													
24-Feb-08	460	30		0.72	1.037	8.2												

Date	Day of Operation	Room Temp, C	Feed pH	Flow mL/min	Flow L/day	Feed Volume, L	Feed Tank Pressure psi	NH3-N mg/L-N	Stdev mg/L-N	NH3-N Load, gN/d	NH3-N Load, kg/m3-d	NH3-N Load, g/m2-d	NO2-N mg/L-N	Stdev/CI mg/L-N	NO2-N Load gN/d	NO3-N mg/L-N	NO3-N gN/d	COD mg/L
25-Feb-08	461	30		0.72	1.037	7.1		660	3	0.684	0.198	2.400	0.36			0.09		54
26-Feb-08	462	30		0.72	1.037	6.4												
27-Feb-08	463	30		0.72	1.037													
28-Feb-08	464	30		0.72	1.037													
29-Feb-08	465	30		0.72	1.037	3.3												
1-Mar-08	466	30		0.72	1.037													
2-Mar-08	467	30		0.72	1.037													
3-Mar-08	468	30		0.72	1.037	0.5												
4-Mar-08	469	30		0.72	1.037	9												
5-Mar-08	470	30		0.72	1.037			627	31.1	0.651	0.188	2.283	0.22			0.19		82
6-Mar-08	471	30		0.72	1.037	6.6												
7-Mar-08	472	30		0.72	1.037													
8-Mar-08	473	30		0.72	1.037													
9-Mar-08	474	30		0.72	1.037	3.4												
10-Mar-08	475	30		0.72	1.037	2.5												
11-Mar-08	476	30		0.72	1.037	1.8		677	4	0.702	0.203	2.463	2.02			0.11		61
12-Mar-08	477	30		0.72	1.037	0.8												
13-Mar-08	478	30		0.72	1.037													
14-Mar-08	479	30		0.72	1.037	7.8												
15-Mar-08	480	30		0.72	1.037													
16-Mar-08	481	30		0.72	1.037													
17-Mar-08	482	30		0.72	1.037	5.1												
18-Mar-08	483	30		0.72	1.037	4												
19-Mar-08	484	30		0.72	1.037													
20-Mar-08	485	30		0.72	1.037													
21-Mar-08	486	30		0.72	1.037													
22-Mar-08	487	30		0.72	1.037	0												
23-Mar-08	488	30		0.72	1.037													
24-Mar-08	489	30		0.72	1.037													
25-Mar-08	490	30		0.72	1.037													
26-Mar-08	491	30		0.72	1.037													
27-Mar-08	492	30		0.72	1.037	6.2												
28-Mar-08	493	30		0.72	1.037													
29-Mar-08	494	30		0.72	1.037	4.2												
30-Mar-08	495	30		0.72	1.037													
31-Mar-08	496	30		0.72	1.037													
1-Apr-08	497	30		0.72	1.037	1.5												
2-Apr-08	498	30		0.72	1.037													
3-Apr-08	499	30		0.72	1.037													
4-Apr-08	500	30		0.72	1.037	0.5												
5-Apr-08	501	30		0.72	1.037													
6-Apr-08	502	30		0.72	1.037													
7-Apr-08	503	30		0.72	1.037			595	9.7	0.617	0.179	2.165	0.58					32
8-Apr-08	504	30		0.72	1.037													
9-Apr-08	505	30		0.72	1.037													
10-Apr-08	506	30		0.72	1.037	3.1												

Date	Day of Operation	Room Temp, C	Feed pH	Flow mL/min	Flow L/day	Feed Volume, L	Feed Tank Pressure psi	NH3-N mg/L-N	Stdev mg/L-N	NH3-N Load, gN/d	NH3-N Load, kg/m3-d	NH3-N Load, g/m2-d	NO2-N mg/L-N	Stdev/CI mg/L-N	NO2-N Load gN/d	NO3-N mg/L-N	NO3-N gN/d	COD mg/L
11-Apr-08	507	30		0.72	1.037													
12-Apr-08	508	30		0.72	1.037													
13-Apr-08	509	30		0.72	1.037													
14-Apr-08	510	30		0.72	1.037	9.5		553	12.6	0.573	0.166	2.010	7.5					
15-Apr-08	511	30		0.72	1.037													
16-Apr-08	512	30		0.72	1.037													
17-Apr-08	513	30		0.72	1.037													
18-Apr-08	514	30		0.72	1.037	5.8												
19-Apr-08	515	30		0.72	1.037													
20-Apr-08	516	30		0.72	1.037													
21-Apr-08	517	30		0.72	1.037	2.4		662	33.6	0.686	0.199	2.408	1.62					11
22-Apr-08	518	30		0.72	1.037													
23-Apr-08	519	30		0.72	1.037	0.5												
24-Apr-08	520	30		0.72	1.037	9.1												
25-Apr-08	521	30		0.72	1.037	8												
26-Apr-08	522	30		0.72	1.037													
27-Apr-08	523	30		0.72	1.037													
28-Apr-08	524	30		0.72	1.037													
29-Apr-08	525	30		0.72	1.037	4												
30-Apr-08	526	30		0.72	1.037													
1-May-08	527	30		0.72	1.037													
2-May-08	528	30		0.72	1.037	0.9												
3-May-08	529	30		0.72	1.037													
4-May-08	530	30		0.72	1.037													
5-May-08	531	30		0.72	1.037													
6-May-08	532	30		0.72	1.037													
7-May-08	533	30		0.72	1.037	5.5		639	12	0.662	0.192	2.323	0.65			0.83	0.03	32
8-May-08	534	30		0.72	1.037													
9-May-08	535	30		0.72	1.037													
10-May-08	536	30		0.72	1.037													
11-May-08	537	30		0.72	1.037													
12-May-08	538	30		0.72	1.037													
13-May-08	539	30		0.72	1.037								0.14					
14-May-08	540	30		0.72	1.037													18
15-May-08	541	30		0.72	1.037													
16-May-08	542	30		0.72	1.037													
17-May-08	543	30		0.72	1.037													
18-May-08	544	30		0.72	1.037													
19-May-08	545	30		0.72	1.037													
20-May-08	546	30		0.72	1.037													
21-May-08	547	30		0.72	1.037													
22-May-08	548	30		0.72	1.037													
23-May-08	549	30		0.72	1.037													
24-May-08	550	30		0.72	1.037													
25-May-08	551	30		0.72	1.037													
26-May-08	552	30		0.72	1.037													

Date	Day of Operation	Room Temp, C	Feed pH	Flow mL/min	Flow L/day	Feed Volume, L	Feed Tank Pressure psi	NH3-N mg/L-N	Stdev mg/L-N	NH3-N Load, gN/d	NH3-N Load, kg/m3-d	NH3-N Load, g/m2-d	NO2-N mg/L-N	Stdev/CI mg/L-N	NO2-N Load gN/d	NO3-N mg/L-N	NO3-N gN/d	COD mg/L
27-May-08	553	30		0.72	1.037													
28-May-08	554	30		0.72	1.037													
29-May-08	555	30		0.72	1.037													
Reactor shut down on day 555																		

Date	Day of Operation	Reactor								5-day Running avg of base used
		DO mg/L	pH setpoint	Mass Flow cc/min	Inlet Press psi	Outlet Press psi	Air Tank psi	Base Level, mL	Consumed mL	
22-Nov-06	1			9	9	8	1100	250		
23-Nov-06	2	5	7.2	9	8.25	7.1	1100	234	16	
24-Nov-06	3	1.38	7.2	9	8.1	7.2	1100	234	0	
25-Nov-06	4	0.52	7.2	9	9.2	8.2	1100	234	0	
26-Nov-06	5	0.26	7.2	9	9.1	8	1100	228	6	5.5
27-Nov-06	6	0.34	7	9	9.2	8.2	1100	228	0	4.4
28-Nov-06	7	0.36	6.8	9	9.5	8.5	1100	154	74	16
29-Nov-06	8	0.3	6.8	9	6.2	5.1	1100	70	84	32.8
30-Nov-06	9	0.17	7.1	4.5	5	3.9	1100	254	0	32.8
1-Dec-06	10	0.22	7.1	9	9	9.1	1100	254	0	31.6
2-Dec-06	11	0.19	7.1	9	9.5	8.4	1100	72	182	68
3-Dec-06	12									66.5
4-Dec-06	13	0.15	7.1	9	9	7.6	1100	250	0	45.5
5-Dec-06	14	0.17	7.1	9	9.2	8.2	1090	6	244	106.5
6-Dec-06	15	0.21	7.1	9	9.2	8	1090		320	186.5
7-Dec-06	16	0.24	7.1	9	9.3	8.2	1090		180	186
8-Dec-06	17	0.15	7.1	9	9.2	8.2	1090		125	173.8
9-Dec-06	18	0.17	7.1	9	9.2	8.2	1090		0	173.8
10-Dec-06	19		7.1	9	9.6	8.6	1080		352	195.4
11-Dec-06	20	0.27	7.1	9	9.6	8.6	1080		0	131.4
12-Dec-06	21	1.16	7.1	9	9.7	8.7	1080		0	95.4
13-Dec-06	22	2.31	7.1	9	9.8	8.8	1080		0	70.4
14-Dec-06	23	3.2	7.1	9	8	7.1	1070		70	84.4
15-Dec-06	24	0.36	7.1	9	7	6	1070		64	26.8
16-Dec-06	25	0.15	7.1	9	7.9	7	1060		43	35.4
17-Dec-06	26	0.25	7.1	9	8	7	1060		102	55.8
18-Dec-06	27	0.16	7.1	9	8	7	1060		78	71.4
19-Dec-06	28	0.54	7.1	9	8	7	1040		197	96.8
20-Dec-06	29	0.15	7.1	9	8	7	1030		130	110
21-Dec-06	30	0.14	7.1	9	8	7	1010		88	119
22-Dec-06	31	0.14	7.1	9	8	7	1010		104	119.4
23-Dec-06	32	0.25	7.1	9	8	7	1010		88	121.4
24-Dec-06	33	0.19	7.1	9	8	7	1010		118	105.6
25-Dec-06	34		7.1	9	8	7				99.5
26-Dec-06	35		7.1	9	8	7				103.3
27-Dec-06	36		7.1	9	8	7				103
28-Dec-06	37	0.12	7.1	9	8	7	1000			118
29-Dec-06	38		7.1	9	8	7	1000		136	136
30-Dec-06	39		7.1	9	8	7	1000		112	124
31-Dec-06	40		7.1	9	8	7	1000		92	113.3
1-Jan-07	41		7.1	9	8	7			87.5	106.9
2-Jan-07	42	0.2	7.1	9	8	7	1000		87.5	103
3-Jan-07	43	0.22	7.1	9	8	7	990		184	112.6
4-Jan-07	44	0.3	7.1	9	8	7	990		0	90.2
5-Jan-07	45	0.34	7.1	9	8	7	990		98	91.4
6-Jan-07	46	0.36	7.1	9	8	7	980		183	110.5

Date	Day of Operation	Reactor								5-day Running avg of base used
		DO mg/L	pH setpoint	Mass Flow cc/min	Inlet Press psi	Outlet Press psi	Air Tank psi	Base Level, mL	Consumed mL	
7-Jan-07	47		7.1	9	8	7				116.3
8-Jan-07	48	0.38	7.1	9	8	7	970		114	98.75
9-Jan-07	49	0.37	7.1	9	8	7	970		126	130.3
10-Jan-07	50		7.1	9	8	7	970		90	128.3
11-Jan-07	51		7.1	9	8	7	970		103	108.3
12-Jan-07	52	0.23	7.1	9	8	7	970		76	101.8
13-Jan-07	53		7.1	9						98.8
14-Jan-07	54		7.1	9	8	7	970		107	94
15-Jan-07	55	0.87	7.1	9	8	7	970		250	134
16-Jan-07	56	0.36	7.1	9	7.6	6.9	960		0	108.3
17-Jan-07	57		7.1	9						119
18-Jan-07	58	0.21	7.1	9	8	7	950			119
19-Jan-07	59		7.1	9	8	7	950		88	112.7
20-Jan-07	60		7.1	9						44
21-Jan-07	61		7.1	9						88
22-Jan-07	62	0.24	7.1	9	8	7	940			88
23-Jan-07	63	0.27	7.1	9	8	7	920		120	104
24-Jan-07	64	0.34	7.1	9	8	7	910		96	108
25-Jan-07	65		7.1	9	8	7	910			108
26-Jan-07	66		7.1	9	8	7	910			108
27-Jan-07	67		7.1	9						108
28-Jan-07	68		7.1	9						96
29-Jan-07	69		7.1	9	8	7	910	810		
30-Jan-07	70		7.1	9	8	7	900	710	100	100
31-Jan-07	71	0.18	7.1	9	8	7	900	620	90	95
1-Feb-07	72	0.16	7.1	9	8	7	900	510	110	100
2-Feb-07	73	0.17	7.1	9	8	7	900	410	100	100
3-Feb-07	74		7.1	9					99.3	99.9
4-Feb-07	75		7.1	9					99.3	99.7
5-Feb-07	76	0.14	7.1	9	8	7	900	112	99.3	101.6
6-Feb-07	77		7.1	9	8	7	890	590	270	133.6
7-Feb-07	78		7.1	9					163	146.2
8-Feb-07	79		7.1	9	8	7	890	264	163	158.9
9-Feb-07	80	0.18	7.1	9	8	7	870	160	104	159.9
10-Feb-07	81		7.1	9	9	8	880	355	155	171
11-Feb-07	82		7.1	9					47.5	126.5
12-Feb-07	83	2.35	7.1	9	8.2	7.5	880	260	47.5	103.4
13-Feb-07	84	0.14	7.1	9	7.1	6.8	860	180	80	86.8
14-Feb-07	85		7.1	9	7.4	6.4	860	0	180	102
15-Feb-07	86	0.18	7.1	9	7.5	6.4	860	0	0	71
16-Feb-07	87	0.2	7.1	9	7.5	6.5	860	750	250	111.5
17-Feb-07	88	0.35	7.1	9	7.5	6.5	860	640	110	124
18-Feb-07	89		7.1	9					140	136
19-Feb-07	90		7.1	9	7.4	6.4	850	360	140	128
20-Feb-07	91	0.17	7.1	9	7.5	6.5	840	215	145	157
21-Feb-07	92		7.1	9	5.2	4.6	820	215	0	107

Date	Day of Operation	Reactor								5-day Running avg of base used
		DO mg/L	pH setpoint	Mass Flow cc/min	Inlet Press psi	Outlet Press psi	Air Tank psi	Base Level, mL	Consumed mL	
22-Feb-07	93	0.9	7.1	9	5.2	4.7	820	20	195	124
23-Feb-07	94	0.15	7.1	9	4.8	3.9	820	820	180	132
24-Feb-07	95		7.1	9	4.9	3.9	820	820	0	104
25-Feb-07	96		7.1	9					125	100
26-Feb-07	97	0.15	7.1	9	4.9	3.9	820	570	125	125
27-Feb-07	98	0.18	7.1	9	4.9	3.9	810	480	90	104
28-Feb-07	99	0.14	7.1	9	4.9	3.9	810	400	80	84
1-Mar-07	100		7.1	9	4.9	3.9	810	240	160	116
2-Mar-07	101		7.1	9	4.9	3.9	810	90	150	121
3-Mar-07	102		7.1	9	4.9	3.9			67.5	109.5
4-Mar-07	103		7.1	9	4.9	3.9	800	865	67.5	105
5-Mar-07	104		7.1	9	4.9	3.9			120	113
6-Mar-07	105		7.1	9	4.9	3.9			120	105
7-Mar-07	106		7.1	9	4.9	3.9			120	99
8-Mar-07	107	0.11	7.1	9	4.9	3.9	790	385	120	109.5
9-Mar-07	108	0.17	7.1	9	4.9	3.9	790	290	95	115
10-Mar-07	109		7.1	9	4.9	3.9			145	120
11-Mar-07	110	0.1	7.1	9	4.9	3.9	790	0	145	125
12-Mar-07	111		7.3	9	4.9	3.9	770	1000	0	101
13-Mar-07	112		7.3	9	4.9	3.9	770	1000	0	77
14-Mar-07	113		7.1	9	4.9	3.9			135	85
15-Mar-07	114	0.15	7.1	9	4.9	3.9	770	730	135	83
16-Mar-07	115	0.2	7.1	9	4.9	3.9	730	700	30	60
17-Mar-07	116		7.1	9	4.9	3.9			120	84
18-Mar-07	117		7.1	9	4.9	3.9			120	108
19-Mar-07	118	0.15	7.1	9	5.1	4.0	730	340	120	105
20-Mar-07	119	0.13	7.1	9	5.2	4.0	720	340	0	78
21-Mar-07	120	0.13	7.1	9	5.2	4.0	720	165	175	107
22-Mar-07	121		7.1	9	5.2	4.0	720	910	90	101
23-Mar-07	122		7.1	9	5.2	4.0	710	820	90	95
24-Mar-07	123		7.1	9	5.2	4.0			150	101
25-Mar-07	124		7.1	9	5.2	4.0	710	520	150	131
26-Mar-07	125	0.16	7.1	9	5.2	4.0	710	520	0	96
27-Mar-07	126		7.1	9					192.5	116.5
28-Mar-07	127	0.17	7.1	9	5		710	135	192.5	137
29-Mar-07	128		7.1	9	5	4.6	700	375	0	107
30-Mar-07	129		7.1	9					63.75	89.8
31-Mar-07	130		7.1	9					63.75	102.5
1-Apr-07	131		7.1	9					63.75	76.8
2-Apr-07	132	0.22	7.1	9	5	4.5	700	745	63.75	51
3-Apr-07	133		7.1	9					122.5	75.5
4-Apr-07	134		7.1	9	5	4.5	700	500	122.5	87.3
5-Apr-07	135	0.18	7.1	9	5	4.5	700	410	90	92.5
6-Apr-07	136		7.1	9	5	4.5			140	107.8
7-Apr-07	137		7.1	9	5	4.5			140	123
8-Apr-07	138		7.1	9	5	4.5			140	126.5

Date	Day of Operation	Reactor								5-day Running avg of base used
		DO mg/L	pH setpoint	Mass Flow cc/min	Inlet Press psi	Outlet Press psi	Air Tank psi	Base Level, mL	Consumed mL	
9-Apr-07	139	0.17	7.1	9	5	4.5	700	650	140	130
10-Apr-07	140	0.16	7.1	9	5	4.5	690	576	74	126.8
11-Apr-07	141		7.1	9	5	4.5	690	510	66	112
12-Apr-07	142		7.1	9	5	4.5			42	92.4
13-Apr-07	143		7.1	9	5	4.5	670	426	42	72.8
14-Apr-07	144		7.1	9	5	4.5			75.3	59.9
15-Apr-07	145		7.1	9	5	4.5			75.3	60.1
16-Apr-07	146		7.1	9	5	4.5		200	75.3	62
17-Apr-07	147	0.17	7.1	9	5	3	640	425	75	68.6
18-Apr-07	148		7.1	9	5	3.1	640	350	75	75.2
19-Apr-07	149		7.1	9	5	3.1			66.7	73.5
20-Apr-07	150		7.1	9	5	3.1			66.7	71.7
21-Apr-07	151	0.3	7.1	9	5	3.2	630	150	66.7	70
22-Apr-07	152		7.1	9	5	3.2			55	66
23-Apr-07	153	0.18	7.1	9	5	3.2	620	890	55	62
24-Apr-07	154		7.1	6.6	5.8	4.5	2010	830	60	60.7
25-Apr-07	155		7.1	6.6	5.8	4.5	2010	760	70	61.3
26-Apr-07	156	0.19	7.1	6.6	5.5	4.6	2010	760	0	48
27-Apr-07	157		7.1	6.6					63.3	49.7
28-Apr-07	158		7.1	6.6					63.3	51.3
29-Apr-07	159	0.19	7.1	6.6	5.5	4.6	2000	570	63.3	52
30-Apr-07	160	0.17	7.1	6.6	5.5	4.6	1990	510	60	50
1-May-07	161	0.19	7.05	6.6	5.5	4.5	1980	445	65	63
2-May-07	162		7.05	6.6	var	var	1960	380	65	63.3
3-May-07	163	0.16	7.05	6.6	var	var	1960	315	65	63.7
4-May-07	164	0.19	7.05	6.6	5	3.9	1950	245	70	65
5-May-07	165	0.17	7.05	6.6	5	3.9	1940	185	60	65
6-May-07	166		7.05	6.6	5	3.9	1930	275	65	65
7-May-07	167		7.05	6.6					43	60.7
8-May-07	168		7.05	6.6					43	56.3
9-May-07	169	0.16	7.05	6.6	5.5	4.2	1910	870	43	51
10-May-07	170		7.05	6.6					75	54
11-May-07	171		7.05	6.6	5	4	1900	720	75	56
12-May-07	172		7.05	6.6					65	60.3
13-May-07	173		7.05	6.6	5.1	3.3	1900	590	65	64.7
14-May-07	174		7.05	6.6					70	70
15-May-07	175		7.05	6.6	5	3.3	1900	450	70	69
16-May-07	176		7.05	6.6					65	67
17-May-07	177	0.12	7.05	6.6	5	3.8	1880	320	65	67
18-May-07	178		7.05	6.6					74	68.75
19-May-07	179		7.05	6.6					74	69.5
20-May-07	180		7.05	6.6					74	70.25
21-May-07	181		7.05	6.6	5	3.9	1820	305	74	72
22-May-07	182		7.05	6.6	5	3.9	1800	240	65	72
23-May-07	183		7.05	6.6					65	70.25
24-May-07	184		7.05	6.6	5	3.9	1800	110	65	68.5

Date	Day of Operation	Reactor								5-day Running avg of base used
		DO mg/L	pH setpoint	Mass Flow cc/min	Inlet Press psi	Outlet Press psi	Air Tank psi	Base Level, mL	Consumed mL	
25-May-07	185		7.05	6.6	5	3.9	1790	915	85	70.75
26-May-07	186		7.05	6.6					65	69
27-May-07	187		7.05	6.6					65	69
28-May-07	188		7.05	6.6					65	69
29-May-07	189	0.2	7.05	6.6	5	3.9	1760	655	65	69
30-May-07	190		7.05	6.6	5	3.9	1750	595	60	64
31-May-07	191		7.05	6.6					27.5	56.5
1-Jun-07	192		7.05	6.6	5	3.9	1730	540	27.5	49
2-Jun-07	193		7.05	6.6					77.5	51.5
3-Jun-07	194		7.05	6.6					77.5	54
4-Jun-07	195		7.05	6.6					77.5	57.5
5-Jun-07	196		7.05	6.6	5	3	1700	230	77.5	67.5
6-Jun-07	197		7.05	6.6					60	74
7-Jun-07	198		7.05	6.6	5	3	1690	110	60	70.5
8-Jun-07	199		7.05	6.6	5	3		190	60	67
9-Jun-07	200		7.05	6.6					120	75.5
10-Jun-07	201		7.05	6.6	5	3	1680	760	120	84
11-Jun-07	202		7.05	6.6					90	90
12-Jun-07	203		7.05	6.6	5	3	1630	580	90	96
13-Jun-07	204		7.05	6.6	5	3	1620	510	70	98
14-Jun-07	205		7.05	6.6					80	90
15-Jun-07	206		7.05	6.6	5	3	1610	350	80	82
16-Jun-07	207		7.05	6.6					76.67	79.3
17-Jun-07	208		7.05	6.6					76.67	76.7
18-Jun-07	209	0.14	7.05	6.6	5	3.2	1600	120	76.67	78
19-Jun-07	210		7.05	6.6	5	3.2	1590		100	82
20-Jun-07	211		7.05	6.6					100	86
21-Jun-07	212	0.11	7.05	6.6	5	3.2	1570	1000	100	90.7
22-Jun-07	213		7.05	6.6	5	3	1560	1000	100	95.3
23-Jun-07	214		7.05	6.6					53.33	90.7
24-Jun-07	215		7.05	6.6					53.33	81.3
25-Jun-07	216		7.05	6.6	5	3	1540	840	53.33	72
26-Jun-07	217		7.05	6.6					42.5	60.5
27-Jun-07	218	0.12	7.05	6.6	5	3	1520	755	42.5	49
28-Jun-07	219		7.05	6.6	5	3.1	1500	600	155	69.3
29-Jun-07	220		7.05	6.6	5	3.1	1500	540	60	70.7
30-Jun-07	221		7.05	6.6					76.67	75.3
1-Jul-07	222		7.05	6.6					76.67	82.2
2-Jul-07	223		7.05	6.6	5	3.1	1500	770	76.67	89
3-Jul-07	224		7.05	6.6					76	73.2
4-Jul-07	225		7.05	6.6					76	76.4
5-Jul-07	226		7.05	6.6					76	76.3
6-Jul-07	227		7.05	6.6					76	76.1
7-Jul-07	228		7.05	6.6	5	3.1	1450	390	76	76
8-Jul-07	229	0.14	7.05	6.6	5	3.1	1450	315	75	75.8
9-Jul-07	230		7.05	6.6					70	74.6

Date	Day of Operation	Reactor								5-day Running avg of base used
		DO mg/L	pH setpoint	Mass Flow cc/min	Inlet Press psi	Outlet Press psi	Air Tank psi	Base Level, mL	Consumed mL	
10-Jul-07	231		7.05	6.6	5	3.1	1420		70	73.4
11-Jul-07	232		7.05	6.6	5	3.1	1410	790	70	72.2
12-Jul-07	233		7.05	6.6	5	3.1	1410	720	70	71
13-Jul-07	234		7.05	6.6	5	3.1	1400	650	70	70
14-Jul-07	235		7.05	6.6					70	70
15-Jul-07	236		7.05	6.6					70	70
16-Jul-07	237		7.05	6.6	5	3.2	1390	440	70	70
17-Jul-07	238		7.05	6.6	5	3.1	1320	r	70	70
18-Jul-07	239		7.05	6.6					35	63
19-Jul-07	240		7.05	6.6	5	3.1	1310	930	35	56
20-Jul-07	241		7.05	6.6	5	3.1	1310	790	140	70
21-Jul-07	242		7.05	6.6					105	77
22-Jul-07	243		7.05	6.6					105	84
23-Jul-07	244		7.05	6.6	5	3.1	1300	580	105	98
24-Jul-07	245		7.05	6.6	5	3.1	1300	505	75	106
25-Jul-07	246		7.05	6.6	5	3.1	1300	440	65	91
26-Jul-07	247		7.05	6.6	5	3.1	1290	370	70	84
27-Jul-07	248		7.05	6.6	5	3.1	1270	300	70	77
28-Jul-07	249	0.22	7.05	6.6					66.25	69.25
29-Jul-07	250		7.05	6.6					66.25	67.5
30-Jul-07	251		7.05	6.6					66.25	67.75
31-Jul-07	252		7.05	6.6	5.1	3.2	1220	540	66.25	67
1-Aug-07	253		7.05	6.6	5	3.2	1220	470	70	67
2-Aug-07	254		7.05	6.6	5	3.2	1220	390	80	69.75
3-Aug-07	255		7.05	6.6	5	3.2	1210	275	115	79.5
4-Aug-07	256	0.17	7.05	6.6					65	79.25
5-Aug-07	257		7.05	6.6	5	3.2	1200	870	65	79
6-Aug-07	258		7.05	6.6					66.25	78.25
7-Aug-07	259		7.05	6.6					66.25	75.5
8-Aug-07	260		7.05	6.6					66.25	65.75
9-Aug-07	261		7.05	6.6	5	3.1	1170	605	66.25	66
10-Aug-07	262		7.05	6.6	5	3.1	1160	540	65	66
11-Aug-07	263	0.16	7.05	6.6					27.5	58.25
12-Aug-07	264		7.05	6.6	5	3.1	1130	485	27.5	50.5
13-Aug-07	265		7.05	6.6	5	3.1	1130	400	85	54.25
14-Aug-07	266		7.05	6.6	5	3.1	1120	470	140	69
15-Aug-07	267		7.05	6.6	5	3.1	1120	375	95	75
16-Aug-07	268		7.15	6.6	5	3.1	1120	230	145	98.5
17-Aug-07	269		7.15	6.6	5	3.1	1110	940	60	105
18-Aug-07	270		7.15	6.6					156.67	119.3
19-Aug-07	271		7.15	6.6					156.67	122.7
20-Aug-07	272		7.15	6.6	5	3.1	1110	470	156.67	135
21-Aug-07	273		7.15	6.6	5	3.1	1100	370	100	126
22-Aug-07	274		7.15	6.6	5	3.1	1090	825	175	149
23-Aug-07	275	0.15	7.15	6.6					125	142.7
24-Aug-07	276		7.15	6.6	5	3.1	1090	575	125	136.3

Date	Day of Operation	Reactor								5-day
		DO mg/L	pH setpoint	Mass Flow cc/min	Inlet Press psi	Outlet Press psi	Air Tank psi	Base Level, mL	Consumed mL	Running avg of base used
25-Aug-07	277		7.15	6.6					120	129
26-Aug-07	278		7.15	6.6	5	3.1	1070	335	120	133
27-Aug-07	279		7.15	6.6	5	3.1	1020	255	80	114
28-Aug-07	280	0.22	7.15	6.6	5	3.1	1020	185	70	103
29-Aug-07	281		7.15	6.6	5	3.1	1020	510	235	125
30-Aug-07	282		7.25	6.6					160	133
31-Aug-07	283		7.25	6.6	5	3.1	1020	190	160	141
1-Sep-07	284		7.15	6.6					113.3	147.7
2-Sep-07	285		7.15	6.6					113.3	156.3
3-Sep-07	286		7.15	6.6	5	3.1	1000	660	113.3	132.0
4-Sep-07	287	0.17	7.15	6.6	5	3.1	1000	575	85	117
5-Sep-07	288		7.15	6.6	5	3.1	980	415	160	117
6-Sep-07	289		7.15	6.6	5	3.1	980	335	80	110.3
7-Sep-07	290		7.15	6.6	5	3.1	970	180	155	118.7
8-Sep-07	291		7.15	6.6					112.5	118.5
9-Sep-07	292		7.15	6.6	5	3.1	940	160	112.5	124
10-Sep-07	293		7.15	6.6	5	3.1	920	940	60	104
11-Sep-07	294	0.16	7.15	6.6	5	3.1	920	850	90	106
12-Sep-07	295		7.15	6.6	5	3.1	920	730	120	99
13-Sep-07	296		7.15	6.6	5	3.1	920	730	0	76.5
14-Sep-07	297		7.15	6.6	5	3.1	910	575	155	85
15-Sep-07	298		7.15	6.6					72.5	87.5
16-Sep-07	299		7.15	6.6	4	2.2	900	430	72.5	84
17-Sep-07	300		7.15	6.6					145	89
18-Sep-07	301		7.15	6.6	4.1	2.2	890	710	145	118
19-Sep-07	302		7.15	6.6	4.1	2.2	880	710	0	87
20-Sep-07	303		7.15	6.6	4.1	2.2	880	710	0	72.5
21-Sep-07	304		7.15	6.6					76.7	73.3
22-Sep-07	305		7.15	6.6					76.7	59.7
23-Sep-07	306	0.15	7.15	6.6	4.1	2.2	850	480	76.7	46
24-Sep-07	307		7.15	6.6					77.5	61.5
25-Sep-07	308		7.15	6.6					77.5	77.0
26-Sep-07	309		7.15	6.6					77.5	77.2
27-Sep-07	310		7.15	6.6	4.1	2.2	800	690	77.5	77.3
28-Sep-07	311		7.15	6.6	4.1	2.2	800	540	150	92
29-Sep-07	312		7.15	6.6					56.25	87.8
30-Sep-07	313		7.15	6.6					56.25	83.5
1-Oct-07	314		7.15	6.6					56.25	79.25
2-Oct-07	315		7.15	6.6	4.1	2.2	790	315	56.25	75.0
3-Oct-07	316		7.15	6.6	4.1	2.2	780	245	70	59.0
4-Oct-07	317	0.12	7.15	6.6	4.1	2.2	760	105	140	75.75
5-Oct-07	318		7.15	6.6					73.75	79.3
6-Oct-07	319		7.15	6.6					73.75	82.8
7-Oct-07	320		7.15	6.6					73.75	86.25
8-Oct-07	321	0.14	7.15	6.6	4.1	2.2	720	705	73.75	87.0
9-Oct-07	322		7.15	6.6					48.75	68.8

Date	Day of Operation	Reactor								5-day
		DO mg/L	pH setpoint	Mass Flow cc/min	Inlet Press psi	Outlet Press psi	Air Tank psi	Base Level, mL	Consumed mL	Running avg of base used
10-Oct-07	323		7.15	6.6					48.75	63.75
11-Oct-07	324		7.15	6.6					48.75	58.8
12-Oct-07	325		7.15	6.6	4	2.2	690	510	48.75	53.8
13-Oct-07	326		7.15	6.6					70	53
14-Oct-07	327		7.15	6.6					70	57.3
15-Oct-07	328		7.15	6.6					70	61.5
16-Oct-07	329		7.15	6.6					70	65.75
17-Oct-07	330		7.15	6.6					70	70.0
18-Oct-07	331		7.15	6.6					70	70.0
19-Oct-07	332		7.15	6.6	4	2.2	620	510	70	70
20-Oct-07	333		7.15	6.6					45	65.0
21-Oct-07	334		7.15	6.6					45	60.0
22-Oct-07	335		7.15	6.6	4	2.2	600	375	45	55
23-Oct-07	336		7.15	6.6					68.33	54.7
24-Oct-07	337		7.15	6.6					68.33	54.3
25-Oct-07	338		7.15	6.6	4	2.2	600	170	68.33	59
26-Oct-07	339		7.15	6.6					58	61.6
27-Oct-07	340		7.15	6.6					58	64.2
28-Oct-07	341		7.15	6.6					58	62.13
29-Oct-07	342		7.15	6.6					58	60.1
30-Oct-07	343	0.1	7.15	6.6	4	2.2	550	530	58	58.0
31-Oct-07	344		7.15	6.6	4.1	2.2	540	460	70	60.4
1-Nov-07	345		7.15	6.6					35	55.8
2-Nov-07	346		7.15	6.6	4.2	2.2	520	390	35	51.2
3-Nov-07	347		7.15	6.6					68.33	53.27
4-Nov-07	348		7.15	6.6					68.33	55.3
5-Nov-07	349		7.15	6.6	4.2	2.3	500	795	68.33	55.0
6-Nov-07	350		7.15	6.6					37.5	55.5
7-Nov-07	351		7.15	6.6	4.2	2.2	490	720	37.5	56.0
8-Nov-07	352		7.15	6.6					70	56.3
9-Nov-07	353		7.15	6.6					70	56.67
10-Nov-07	354		7.15	6.6					70	57.0
11-Nov-07	355	0.13	7.15	6.6	4	2	450	440	70	63.5
12-Nov-07	356		7.15	6.6	4.1	2.1	440	440	0	56
13-Nov-07	357		7.15	6.6					35	49.0
14-Nov-07	358		7.15	6.6	4.1	2.1	420	370	35	42.0
15-Nov-07	359		7.15	6.6					65	41
16-Nov-07	360		7.15	6.6	4.1	2.1	410	240	65	40.0
17-Nov-07	361		7.15	6.6					43.33	48.7
18-Nov-07	362		7.15	6.6					43.33	50.33
19-Nov-07	363		7.15	6.6	4.1	2.1	400	530	43.33	52.0
20-Nov-07	364		7.15	6.6	4.1	2.1	380	460	70	53.0
21-Nov-07	365		7.15	6.6					49.29	49.86
22-Nov-07	366		7.15	6.6					49.29	51.0
23-Nov-07	367		7.15	6.6					49.29	52.2
24-Nov-07	368		7.15	6.6					49.29	53.43

Date	Day of Operation	Reactor								5-day Running avg of base used
		DO mg/L	pH setpoint	Mass Flow cc/min	Inlet Press psi	Outlet Press psi	Air Tank psi	Base Level, mL	Consumed mL	
25-Nov-07	369		7.15	6.6					49.29	49.3
26-Nov-07	370		7.15	6.6					49.29	49.3
27-Nov-07	371		7.15	6.6	4.1	2.1	320	655	49.29	49.29
28-Nov-07	372		7.15	6.6					35	46.4
29-Nov-07	373		7.15	6.6	4.1	2.1	300	585	35	43.6
30-Nov-07	374	0.15	7.15	6.6	4.1	2.1	300	490	95	52.71
1-Dec-07	375		7.15	6.6					35	49.9
2-Dec-07	376		7.15	6.6					35	47.0
3-Dec-07	377		7.15	6.6					35	47.00
4-Dec-07	378		7.15	6.6	4.1	2.1	290	770	35	47.0
5-Dec-07	379		7.15	6.6					35	35.0
6-Dec-07	380		7.15	6.6	4.1	2.2	260	700	35	35.00
7-Dec-07	381		7.15	6.6	4.1	2.2	240	620	80	44.0
8-Dec-07	382		7.15	6.6					48.33	46.7
9-Dec-07	383		7.15	6.6					48.33	49.33
10-Dec-07	384		7.15	6.6	4.1	2.2	200	475	48.33	52.0
11-Dec-07	385		7.15	6.6					35	52.0
12-Dec-07	386	0.11	7.15	6.6	4.1	2.2	200	405	35	43.00
13-Dec-07	387		7.15	6.6	4.2	2.2	200	405	0	33.3
14-Dec-07	388		7.15	6.6	4.2	2.2	190	370	35	30.7
15-Dec-07	389		7.15	6.6	4.2	2.2	180	275	95	40.00
16-Dec-07	390		7.15	6.6					25	38.00
17-Dec-07	391		7.15	6.6	4.2	2.2	180	950	25	36.00
18-Dec-07	392		7.15	6.6					30	42.00
19-Dec-07	393		7.15	6.6	4.2	2.2	150	890	30	41.00
20-Dec-07	394		7.15	6.6	4.2	2.3	150	830	60	34.00
21-Dec-07	395		7.15	6.6					26.25	34.25
22-Dec-07	396		7.15	6.6					26.25	34.50
23-Dec-07	397		7.15	6.6					26.25	33.75
24-Dec-07	398		7.15	6.6	4.2	2.3	100	725	26.25	33.00
25-Dec-07	399		7.15	6.6					40.71	29.14
26-Dec-07	400		7.15	6.6					40.71	32.04
27-Dec-07	401		7.15	6.6					40.71	34.93
28-Dec-07	402		7.15	6.6					40.71	37.82
29-Dec-07	403		7.15	0					40.71	40.71
30-Dec-07	404		7.15	0					40.71	40.71
31-Dec-07	405		7.15	0	2	0	0	440	40.71	40.71
1-Jan-08	406		7.15	0	2	0	0	440	0	32.57
2-Jan-08	407		7.15	6.6	2	0	0	440	0	24.43
3-Jan-08	408		7.15	6.6	4.1	2.2	2000	440	0	16.29
4-Jan-08	409		7.15	6.6	4.1	2.3	1990	440	0	8.14
5-Jan-08	410		7.15	6.6					60	12.00
6-Jan-08	411		7.15	6.6					60	24.00
7-Jan-08	412		7.15	6.6	4.1	2.4	1990	560	60	36.00
8-Jan-08	413		7.15	6.6	4.1	2.4	1980	500	60	48.00
9-Jan-08	414		7.15	6.6	4.1	2.4	1980	500	0	48.00

Date	Day of Operation	Reactor								5-day Running avg of base used
		DO mg/L	pH setpoint	Mass Flow cc/min	Inlet Press psi	Outlet Press psi	Air Tank psi	Base Level, mL	Consumed mL	
10-Jan-08	415		7.15	6.6	4.1	2.4	1950	445	55	47.00
11-Jan-08	416		7.15	6.6	4.1	2.5	1930	395	50	45.00
12-Jan-08	417		7.15	6.6					28.75	38.75
13-Jan-08	418		7.15	6.6					28.75	32.50
14-Jan-08	419		7.15	6.6					28.75	38.25
15-Jan-08	420		7.15	6.6	4.1	2.6	1900	280	28.75	33.00
16-Jan-08	421		7.15	6.6					36.67	30.33
17-Jan-08	422		7.15	6.6					36.67	31.92
18-Jan-08	423		7.15	6.6	4.1	2.8	1900	170	36.67	33.50
19-Jan-08	424		7.15	6.6					55	38.75
20-Jan-08	425		7.15	6.6	4.1	2.8	1880	60	55	44.00
21-Jan-08	426		7.15	6.6					25	41.67
22-Jan-08	427		7.15	6.6	4.2	2.8	1830	950	25	39.33
23-Jan-08	428		7.15	6.6					40	40.00
24-Jan-08	429		7.15	6.6					40	37.00
25-Jan-08	430		7.15	6.6	4.2	2.8	1820	830	40	34.00
26-Jan-08	431		7.15	6.6					40	37.00
27-Jan-08	432		7.15	6.6					40	40.00
28-Jan-08	433		7.15	6.6					40	40.00
29-Jan-08	434		7.15	6.6					40	40.00
30-Jan-08	435		7.15	6.6					40	40.00
31-Jan-08	436		7.15	6.6	4.1	2.8	1780	590	40	40.00
1-Feb-08	437		7.15	6.6					43.8	40.75
2-Feb-08	438		7.15	6.6					43.8	41.50
3-Feb-08	439		7.15	6.6					43.8	42.25
4-Feb-08	440	6.6	7.15	6.6	4.1	2.8	1740	415	43.8	43.00
5-Feb-08	441	0.11	7.15	6.6	4.3	2.8	1740	415	0.0	35.00
6-Feb-08	442		7.15	6.6	4.3	2.8	1720	370	45.0	35.25
7-Feb-08	443		7.15	6.6	4.2	2.8	1710	310	60.0	38.50
8-Feb-08	444		7.15	6.6					28.3	35.42
9-Feb-08	445		7.15	6.6					28.3	32.33
10-Feb-08	446		7.15	6.6					28.3	38.00
11-Feb-08	447		7.15	6.6					28.3	34.67
12-Feb-08	448		7.15	6.6					28.3	28.33
13-Feb-08	449		7.15	6.6	4.2	2.8	1690	830	28.3	28.33
14-Feb-08	450		7.15	6.6					30.0	28.67
15-Feb-08	451		7.15	6.6	4.2	2.5	1690	770	30.0	29.00
16-Feb-08	452		7.15	6.6					40.0	31.33
17-Feb-08	453		7.15	6.6					40.0	33.67
18-Feb-08	454	0.24	7.15	6.6	4.2	2.6	1650	650	40.0	36.00
19-Feb-08	455		7.15	6.6					60.0	42.00
20-Feb-08	456		7.15	6.6	4.2	2.7	1620	530	60.0	48.00
21-Feb-08	457		7.15	6.6					25.0	45.00
22-Feb-08	458		7.15	6.6	4.1	2.6	1610	480	25.0	42.00
23-Feb-08	459		7.15	6.6					55.0	45.00
24-Feb-08	460		7.15	6.6	4.1	2.8	1600	370	55.0	44.00

Date	Day of Operation	Reactor								5-day
		DO mg/L	pH setpoint	Mass Flow cc/min	Inlet Press psi	Outlet Press psi	Air Tank psi	Base Level, mL	Consumed mL	Running avg of base used
25-Feb-08	461		7.15	6.6	4.1	2.8	1600	310	60.0	44.00
26-Feb-08	462		7.15	6.6	4.1	2.8	1600	310	0.0	39.00
27-Feb-08	463		7.15	6.6					53.3	44.67
28-Feb-08	464		7.15	6.6					53.3	44.33
29-Feb-08	465		7.15	6.6	4.1	2.8	1570	150	53.3	44.00
1-Mar-08	466		7.15	6.6					35.0	39.00
2-Mar-08	467		7.15	6.6					35.0	46.00
3-Mar-08	468		7.15	6.6	4.1	2.8	1530	370	35.0	42.33
4-Mar-08	469		7.15	6.6	4.1	2.8	1520	370	55.0	42.67
5-Mar-08	470		7.15	6.6					55.0	43.00
6-Mar-08	471		7.15	6.6	4.1	2.8	1510	260	55.0	47.00
7-Mar-08	472		7.15	6.6					38.3	47.67
8-Mar-08	473		7.15	6.6					38.3	48.33
9-Mar-08	474		7.15	6.6	4.1	2.8	1500	145	38.3	45.00
10-Mar-08	475		7.15	6.6	4	2.8	1490	90	55.0	45.00
11-Mar-08	476		7.15	6.6	4	2.8	1490	1000	0.0	34.00
12-Mar-08	477		7.15	6.6	4.1	2.8	1490	950	50.0	36.33
13-Mar-08	478		7.15	6.6					62.5	41.17
14-Mar-08	479		7.15	6.6	4.1	2.8	1470	825	62.5	46.00
15-Mar-08	480		7.15	6.6					18.3	38.67
16-Mar-08	481		7.15	6.6					18.3	42.33
17-Mar-08	482		7.15	6.6	4	2.8	1450	770	18.3	36.00
18-Mar-08	483		7.15	6.6	4	2.8	1430	710	60.0	35.50
19-Mar-08	484		7.15	6.6					42.5	31.50
20-Mar-08	485		7.15	6.6					42.5	36.33
21-Mar-08	486		7.15	6.6					42.5	41.17
22-Mar-08	487		7.15	6.6	3.9	2.6	1400	540	42.5	46.00
23-Mar-08	488		7.15	6.6					13.0	36.60
24-Mar-08	489		7.15	6.6					13.0	30.70
25-Mar-08	490		7.15	6.6					13.0	24.80
26-Mar-08	491		7.15	6.6					13.0	18.90
27-Mar-08	492		7.15	6.6	4	2.7	1390	475	13.0	13.00
28-Mar-08	493		7.15	6.6					57.5	21.90
29-Mar-08	494		7.15	6.6	4	2.7	1360	360	57.5	30.80
30-Mar-08	495		7.15	6.6					40.0	36.20
31-Mar-08	496		7.15	6.6					40.0	41.60
1-Apr-08	497		7.15	6.6	4	2.7	1330	240	40.0	47.00
2-Apr-08	498		7.15	6.6					20.0	39.50
3-Apr-08	499		7.15	6.6					20.0	32.00
4-Apr-08	500		7.15	6.6	4	2.7	1320	180	20.0	28.00
5-Apr-08	501		7.15	6.6					36.0	27.20
6-Apr-08	502		7.15	6.6					36.0	26.40
7-Apr-08	503		7.15	6.6					36.0	29.60
8-Apr-08	504		7.15	6.6					36.0	32.80
9-Apr-08	505		7.15	6.6					36.0	36.00
10-Apr-08	506		7.15	6.6	4	2.6	1280	820	36.0	36.00

Date	Day of Operation	Reactor								5-day
		DO mg/L	pH setpoint	Mass Flow cc/min	Inlet Press psi	Outlet Press psi	Air Tank psi	Base Level, mL	Consumed mL	Running avg of base used
11-Apr-08	507		7.15	6.6					30.0	34.80
12-Apr-08	508		7.15	6.6					30.0	33.60
13-Apr-08	509		7.15	6.6					30.0	32.40
14-Apr-08	510		7.15	6.6	4.1	2.6	1250	700	30.0	31.20
15-Apr-08	511		7.15	6.6					42.5	32.50
16-Apr-08	512		7.15	6.6					42.5	35.00
17-Apr-08	513		7.15	6.6					42.5	37.50
18-Apr-08	514		7.15	6.6	4	2.7	1210	530	42.5	40.00
19-Apr-08	515		7.15	6.6					41.7	42.33
20-Apr-08	516		7.15	6.6					41.7	42.17
21-Apr-08	517		7.15	6.6	4	2.7	1200	405	41.7	42.00
22-Apr-08	518		7.15	6.6	4	2.7	1190	370	35.0	40.50
23-Apr-08	519		7.15	6.6					60.0	44.00
24-Apr-08	520		7.15	6.6	4	2.7	1190	250	60.0	47.67
25-Apr-08	521		7.15	6.6	4.1	2.7	1180	190	60.0	51.33
26-Apr-08	522		7.15	6.6					27.5	48.50
27-Apr-08	523		7.15	6.6					27.5	47.00
28-Apr-08	524		7.15	6.6					27.5	40.50
29-Apr-08	525		7.15	6.6	4.1	2.7	1140	290	27.5	34.00
30-Apr-08	526		7.15	6.6					56.7	33.33
1-May-08	527		7.15	6.6					56.7	39.17
2-May-08	528		7.15	6.6	4.1	2.7	1110	120	56.7	45.00
3-May-08	529		7.15	6.6					36.0	46.70
4-May-08	530		7.15	6.6					36.0	48.40
5-May-08	531		7.15	6.6					36.0	44.27
6-May-08	532		7.15	6.6					36.0	40.13
7-May-08	533		7.15	6.6	4.1	2.8	1090	820	36.0	36.00
8-May-08	534		7.15	6.6						
9-May-08	535		7.15	6.6						
10-May-08	536		7.15	6.6						
11-May-08	537		7.15	6.6						
12-May-08	538		7.15	6.6						
13-May-08	539		7.15	6.6						
14-May-08	540		7.15	6.6						
15-May-08	541		7.15	6.6						
16-May-08	542		7.15	6.6						
17-May-08	543		7.15	6.6						
18-May-08	544		7.15	6.6						
19-May-08	545		7.15	6.6						
20-May-08	546		7.15	6.6						
21-May-08	547		7.15	6.6						
22-May-08	548		7.15	6.6						
23-May-08	549		7.15	6.6						
24-May-08	550		7.15	6.6						
25-May-08	551		7.15	6.6						
26-May-08	552		7.15	6.6						

Date	Day of Operation	Reactor								5-day Running avg of base used
		DO mg/L	pH setpoint	Mass Flow cc/min	Inlet Press psi	Outlet Press psi	Air Tank psi	Base Level, mL	Consumed mL	
27-May-08	553		7.15	6.6						
28-May-08	554		7.15	6.6						
29-May-08	555		7.15	6.6						
Reactor shut down on day 555										

Date	Day of Operation	**Effluent** Volume L	Flow L/day	NH3-N mg/L-N	Stdev mg/L-N	NH3-N Load gN/day	NH3-N Load g N/m2-d	NO2-N mg/L-N	Cl or Stdev mg/L-N	NO2-N Load gN/d	NO2-N by IC	stdev of IC NO2	NO3-N mg/L-N	stdev of IC NO3	NO3-N Load gN/d	COD mg/L
22-Nov-06	1	0	0.3456													
23-Nov-06	2	0.8	0.3616													
24-Nov-06	3	1.3	0.3456	561	4	0.194	0.680	0	0	0.000			1.2		0.0004	
25-Nov-06	4	0.5	0.3456													
26-Nov-06	5	1.7	0.3516													
27-Nov-06	6	2.5	0.3456	520	2	0.180	0.630	66.8	0.7	0.023			0.57		0.0002	
28-Nov-06	7	0.8	0.4196													
29-Nov-06	8	1.3	0.4296	408	7	0.175	0.615						1.7		0.0007	
30-Nov-06	9	1.7	0.3456					176	8	0.061						
1-Dec-06	10	0.7	0.3456	259	9	0.089	0.314	237		0.082			2.0		0.0007	
2-Dec-06	11	1.6	0.5276					253		0.133			2.0		0.0011	
3-Dec-06	12		0.3456													
4-Dec-06	13	0.0	0.3456	560	18	0.193	0.679	86		0.030			1.8		0.0006	
5-Dec-06	14	0.9	0.5896					149		0.088			1.6		0.0009	
6-Dec-06	15	0.8	0.6656	482	6	0.321	1.125	174		0.116			1.3		0.0009	
7-Dec-06	16	1.4	0.5256	301	16	0.158	0.555	285		0.150			0		0.0000	
8-Dec-06	17	0.6	0.4706	132	3	0.062	0.218	370		0.174			1.4		0.0007	
9-Dec-06	18	1.3	0.3456	73	0.7	0.025	0.088	383		0.132			0		0.0000	
10-Dec-06	19	2.1						437		0.000						
11-Dec-06	20	0.7	0.3456													
12-Dec-06	21	1.3	0.3456	20	1	0.007	0.025	415	1.93	0.143			1.9		0.0007	
13-Dec-06	22	0.6	0.3456	18	0.5	0.006	0.022	449	2.47	0.155			4.4		0.0015	
14-Dec-06	23	0.8	0.7612													
15-Dec-06	24	1.3	0.7552	11	0.34	0.008	0.030	446	4.9	0.337			3.8		0.0029	
16-Dec-06	25	1.3	0.7342													
17-Dec-06	26	1.4	0.7932	39	0.85	0.031	0.108	427		0.339			3.7		0.0029	
18-Dec-06	27	0.7	0.7692													
19-Dec-06	28	1.6	0.8882	49	0.99	0.044	0.153	440		0.391			2		0.0018	
20-Dec-06	29	1	0.8212													
21-Dec-06	30	1	0.7792													
22-Dec-06	31	1	0.7952	39	1.8	0.031	0.108	442	21.1	0.351			1.3		0.0010	
23-Dec-06	32	1	0.7792	36	1.6	0.028	0.098	447	0	0.348			1.1		0.0009	
24-Dec-06	33	1	0.8092					475		0.384						
25-Dec-06	34		0.6912													
26-Dec-06	35		0.6912													
27-Dec-06	36		0.6912													
28-Dec-06	37	4.6	0.6912	50	2.5	0.035	0.122	467	3.6	0.323			1.1		0.0008	
29-Dec-06	38	1	0.8272													
30-Dec-06	39	1	0.8032													
31-Dec-06	40	1.8	0.7832													
1-Jan-07	41		0.7787													
2-Jan-07	42	3.5	0.7787	47	1.4	0.037	0.129	487	8.1	0.379			2.3		0.0018	
3-Jan-07	43	0.9	0.8752													
4-Jan-07	44	0.9	0.6912	17	0.24	0.012	0.042	514	4.3	0.355			3.1		0.0021	
5-Jan-07	45	0.9	0.7892													
6-Jan-07	46	1.3	0.8742													

Date	Day of Operation	**Effluent** Volume L	Flow L/day	NH3-N mg/L-N	Stdev mg/L-N	NH3-N Load gN/day	NH3-N Load g N/m2-d	NO2-N mg/L-N	CI or Stdev mg/L-N	NO2-N Load gN/d	NO2-N by IC	stdev of IC NO2	NO3-N mg/L-N	stdev of IC NO3	NO3-N Load gN/d	COD mg/L
7-Jan-07	47		0.6912													
8-Jan-07	48	2.6	0.8052	28	0.59	0.022	0.078	510	19.4	0.411	256	24	3	1	0.0024	
9-Jan-07	49	0.9	0.8172													
10-Jan-07	50	0.8	0.7812													
11-Jan-07	51	0.8	0.7942													
12-Jan-07	52	0.7	0.7672	28	1.18	0.021	0.074	515	9	0.395	158	68	3	1	0.0023	
13-Jan-07	53		0.6912													
14-Jan-07	54	2.2	0.7982													
15-Jan-07	55	2.8	0.7684													
16-Jan-07	56	0.8	0.6912	26	0.56	0.018	0.062	499	6.3	0.345	240	33	4	1	0.0028	
17-Jan-07	57		0.6912													
18-Jan-07	58	2.4	0.6912	11	0.9	0.008	0.027	520	18.45	0.359	216	77	3	3	0.0021	
19-Jan-07	59	3.1	0.7792													
20-Jan-07	60		0.6912													
21-Jan-07	61		0.6912													
22-Jan-07	62	5.7	0.6912	27	1	0.018	0.065	508	2.44	0.351	211	21	4	1	0.0028	
23-Jan-07	63	0.8	0.8112													
24-Jan-07	64	1.6	0.7872													
25-Jan-07	65		0.6912	24	0.3	0.016	0.057	484	10.2	0.335	415	5	11	2	0.0076	
26-Jan-07	66	0.8	0.6912													
27-Jan-07	67		0.6912													
28-Jan-07	68		0.6912													
29-Jan-07	69	3.3	0.6912													
30-Jan-07	70	4.4	0.7912													
31-Jan-07	71	0.9	0.7812	27	0.3	0.021	0.073	468	7.6	0.366						
1-Feb-07	72	1.5	0.8012													
2-Feb-07	73	2.3	0.7912	27	0.5	0.021	0.074	448	11.6	0.354						
3-Feb-07	74		0.790533													
4-Feb-07	75		0.790533													
5-Feb-07	76	4.8	0.790533	30	3	0.023	0.082	442	2.15	0.349	130	65	9	4	0.0071	
6-Feb-07	77	0.8	0.9612													
7-Feb-07	78		0.8542													
8-Feb-07	79		0.8542													
9-Feb-07	80	0.9	0.7952	28	2	0.022	0.077	388	3	0.309	178	86	71	4	0.0565	
10-Feb-07	81	1.8	0.8462													
11-Feb-07	82		0.7387													
12-Feb-07	83	2.8	0.7387	6	0.5	0.005	0.016	358		0.264	140	10	118	3	0.0872	
13-Feb-07	84	0.8	0.7712													
14-Feb-07	85	1.1	0.8712													
15-Feb-07	86	1.7	0.6912	27	5.4	0.018	0.065	333	9.07	0.230	116	5	157	1	0.1085	
16-Feb-07	87	2.6	0.9412													
17-Feb-07	88	3.4	0.8012													
18-Feb-07	89		0.8312													
19-Feb-07	90	5.1	0.8312	20	1	0.017	0.060	338	12.1	0.281	136	7				
20-Feb-07	91	1.4	0.8362													
21-Feb-07	92	0	0.6912					299		0.207						

Date	Day of Operation	**Effluent** Volume L	Flow L/day	NH3-N mg/L-N	Stdev mg/L-N	NH3-N Load gN/day	NH3-N Load g N/m2-d	NO2-N mg/L-N	Cl or Stdev mg/L-N	NO2-N Load gN/d	NO2-N by IC	stdev of IC NO2	NO3-N mg/L-N	stdev of IC NO3	NO3-N Load gN/d	COD mg/L
22-Feb-07	93	0.8	0.8862													
23-Feb-07	94	1.9	0.8712	20	1	0.018	0.063	359								
24-Feb-07	95	2.8	0.6912													
25-Feb-07	96		0.8162													
26-Feb-07	97	4.5	0.8162	24	2	0.019	0.067	356		0.291						
27-Feb-07	98	0.7	0.7812	25	0.5	0.019	0.067	381	5.44	0.298						
28-Feb-07	99	1.7	0.7712													
1-Mar-07	100	2.8	0.8512													
2-Mar-07	101	0	0.8412	131	3	0.110	0.386	364	2.9	0.306	365	0.28	101	5.55	0.0850	
3-Mar-07	102		0.7587													
4-Mar-07	103	1.7	0.7587													
5-Mar-07	104		0.8112													
6-Mar-07	105		0.8112													
7-Mar-07	106		0.8112													
8-Mar-07	107	3.9	0.8112													
9-Mar-07	108	0.8	0.7862	14	0.5	0.011	0.040	346	9.2	0.272	309	5.76	104	6.7	0.0818	
10-Mar-07	109		1.1818													
11-Mar-07	110		1.1818	48	2	0.056	0.197	345	18.7	0.408	302	6.4	89	5.06	0.1052	
12-Mar-07	111	0	1.0368													
13-Mar-07	112	0.9	1.0368													
14-Mar-07	113		1.1718													
15-Mar-07	114	2.7	1.1718					308	14.9							
16-Mar-07	115	1.1	1.0668	171	2.8	0.182	0.640	284	5.9	0.303	268	11.7	47.5	3.4	0.0507	
17-Mar-07	116		1.1568													
18-Mar-07	117		1.1568													
19-Mar-07	118	1.6	1.1568					232	1.15	0.268						
20-Mar-07	119	0.8	1.0368					242								
21-Mar-07	120	2.4	1.2118	163	7.3	0.197	0.693	254	3.06	0.308	236	2.4	52.3	5	0.0634	
22-Mar-07	121	1.6	1.1268													
23-Mar-07	122	1.4	1.1268	148	5.5	0.166	0.584	261	3.7	0.294	250	4.8	56	4.7	0.0631	
24-Mar-07	123		1.1868													
25-Mar-07	124	4	1.1868													
26-Mar-07	125	0.7	1.0368													
27-Mar-07	126		1.2293													
28-Mar-07	127		1.2293	156	4.5	0.192	0.672	276	9.5	0.339	279	1.17	66.8	0.3	0.0821	
29-Mar-07	128	0.9	1.0368								295	0.62	71.4	0.4	0.0740	
30-Mar-07	129		1.10055													
31-Mar-07	130		1.10055													
1-Apr-07	131		1.10055													
2-Apr-07	132	5.2	1.10055					304	0	0.335						
3-Apr-07	133		1.1593	164	1.8	0.190	0.667	293	1.68	0.340	300	2.12	66.8	4.83	0.0774	
4-Apr-07	134	2.9	1.1593													
5-Apr-07	135	4	1.1268	158	3.4	0.178	0.624	290	2.9	0.327	302	1.07	63.4	0.72	0.0714	
6-Apr-07	136		1.1768													
7-Apr-07	137		1.1768													
8-Apr-07	138		1.1768													

Date	Day of Operation	**Effluent** Volume L	Flow L/day	NH3-N mg/L-N	Stdev mg/L-N	NH3-N Load gN/day	NH3-N Load g N/m2-d	NO2-N mg/L-N	CI or Stdev mg/L-N	NO2-N Load gN/d	NO2-N by IC	stdev of IC NO2	NO3-N mg/L-N	stdev of IC NO3	NO3-N Load gN/d	COD mg/L
9-Apr-07	139	5	1.1768													
10-Apr-07	140		1.1108	182	1.1	0.202	0.710	283	5.5	0.314	279	0.82	77	0.2	0.0855	
11-Apr-07	141	1.4	1.1028													
12-Apr-07	142		1.0788													
13-Apr-07	143	1	1.0788	186	1.6	0.201	0.705	291	2.9	0.314	310	0.01	66	0.5	0.0712	
14-Apr-07	144		1.112133													
15-Apr-07	145		1.112133													
16-Apr-07	146		1.112133													
17-Apr-07	147	1	1.1118													
18-Apr-07	148	2	1.1118													
19-Apr-07	149		1.103467													
20-Apr-07	150		1.103467													
21-Apr-07	151	4.8	1.103467													
22-Apr-07	152		1.0918													
23-Apr-07	153	6.9	1.0918	72	2.6	0.078	0.275	353	2.6	0.385	358	2.7	77.4	0.19	0.0845	
24-Apr-07	154	1	1.0968													
25-Apr-07	155	2.5	1.1068													
26-Apr-07	156	3.5	1.0368	131	1.6	0.135	0.475	346	6.6	0.359	342	2.65	68.3	0.28	0.0708	30
27-Apr-07	157		1.100133													
28-Apr-07	158		1.100133													
29-Apr-07	159		1.100133													
30-Apr-07	160	0.7	1.0968	162	13	0.178	0.623	322	2.1	0.353	322	3.4	51.7	0.65	0.0567	
1-May-07	161	1.9	1.1018													
2-May-07	162	var	1.1018	160	3	0.176	0.618	333	4.5	0.367	339.1	4.46	55.8	0.6	0.0615	81
3-May-07	163	var	1.1018	177	14	0.195		339	8.1	0.374	345.1	0.18	68.4	0.01	0.0754	
4-May-07	164	var	1.1068	153	3	0.169		344	7.3	0.381	352.8	0.77	63.7	0.68	0.0705	
5-May-07	165	3.7	1.0968	163	1	0.179		321	3.6	0.352	341.6	3.4	70.5	1.61	0.0773	
6-May-07	166	5.3	1.1018	172	1	0.190		316	5.3	0.348	334.1	0.24	69.1	0.06	0.0761	
7-May-07	167		1.080133													
8-May-07	168		1.080133													
9-May-07	169	3.3	1.080133	158	2	0.171	0.598	332	2.2	0.359	379	0.3	85	0.06	0.0918	
10-May-07	170		1.1118													
11-May-07	171	2	1.1118													
12-May-07	172		1.1018													
13-May-07	173	2.5	1.1018													
14-May-07	174		1.1068													
15-May-07	175	5	1.1068													
16-May-07	176		1.1018													
17-May-07	177		1.1018	149	6	0.164	0.575	343	10.7	0.378	351	1.6	71.9	0.7	0.0792	101
18-May-07	178		1.11055													
19-May-07	179		1.11055													
20-May-07	180		1.11055													
21-May-07	181	4.7	1.11055													
22-May-07	182	1.6	1.1018													
23-May-07	183		1.1018	125	6	0.138	0.485	338	1.8	0.372	347	1.9	69	0.4	0.0760	
24-May-07	184	2.1	1.1018													

Date	Day of Operation	**Effluent** Volume L	Flow L/day	NH3-N mg/L-N	Stdev mg/L-N	NH3-N Load gN/day	NH3-N Load g N/m2-d	NO2-N mg/L-N	Cl or Stdev mg/L-N	NO2-N Load gN/d	NO2-N by IC	stdev of IC NO2	NO3-N mg/L-N	stdev of IC NO3	NO3-N Load gN/d	COD mg/L
25-May-07	185	1	1.1218	138	2	0.154	0.542	346	9.3	0.388	358	0.5	60	0.1	0.0673	
26-May-07	186		1.1018			0.000										
27-May-07	187		1.1018													
28-May-07	188		1.1018													
29-May-07	189	1.6	1.1018													
30-May-07	190	2.5	1.0968	134	4	0.147	0.514	373	2.2	0.409	371	0.2	51	0.1	0.0559	
31-May-07	191		1.0643													
1-Jun-07	192	0.8	1.0643	125	2	0.134	0.469	371	5	0.395						
2-Jun-07	193		1.1143													
3-Jun-07	194		1.1143													
4-Jun-07	195		1.1143													
5-Jun-07	196		1.1143	123	2	0.138	0.483	392	3.4	0.437	399	1.8	55	0.4	0.0613	
6-Jun-07	197		1.0968													
7-Jun-07	198	2.5	1.0968	109	2	0.120	0.421	405	16.7	0.444	403	0.1	55	0.1	0.0603	
8-Jun-07	199	3	1.0968													
9-Jun-07	200		1.1568								358	0.04	68.7	0	0.0795	
10-Jun-07	201	5.8	1.1568													
11-Jun-07	202		1.1268													
12-Jun-07	203	1.6	1.1268													
13-Jun-07	204	1	1.1068													
14-Jun-07	205		1.1168													
15-Jun-07	206	1	1.1168	128	7	0.142	0.500	353	2.6	0.394	357.6	0.04	68.7	0.0002	0.0767	
16-Jun-07	207		1.1135													
17-Jun-07	208		1.1135													
18-Jun-07	209	4.6	1.1135	154	17	0.171	0.601	319	2	0.355	336	0.07	74.9	0	0.0834	
19-Jun-07	210		1.1368	137	3	0.155	0.545	303	5.4	0.344	313.9	0.6	77.8	0.03	0.0884	98
20-Jun-07	211		1.1368	151	1.6	0.171		257	2.3	0.292	266	0.15	49.5	0.05	0.0563	
21-Jun-07	212	2.5	1.1368	145	3	0.165		282	1.6	0.321	271	0.06	54.2	0.05	0.0616	
22-Jun-07	213		1.1368	161	7	0.183		295	3	0.335	287	0.19	51.5	0.02	0.0585	
23-Jun-07	214		1.0901													
24-Jun-07	215		1.0901													
25-Jun-07	216	4	1.0901													
26-Jun-07	217		1.0793													
27-Jun-07	218	5.8	1.0793	146	3	0.157	0.552	318	2	0.343	313	0.54	79.6	0.2	0.0859	57
28-Jun-07	219	1	1.1918													
29-Jun-07	220	2.6	1.0968													
30-Jun-07	221		1.1135													
1-Jul-07	222		1.1135													
2-Jul-07	223	3.5	1.1135													
3-Jul-07	224		1.1128													
4-Jul-07	225		1.1128													
5-Jul-07	226		1.1128													
6-Jul-07	227		1.1128													
7-Jul-07	228	9.2	1.1128													
8-Jul-07	229	10.3	1.1118					292	1.7	0.325						
9-Jul-07	230		1.1068	158	3	0.175	0.613	319	3.5	0.353	312	4	43.9	0.82	0.0486	

Date	Day of Operation	**Effluent** Volume L	Flow L/day	NH3-N mg/L-N	Stdev mg/L-N	NH3-N Load gN/day	NH3-N Load g N/m2-d	NO2-N mg/L-N	Cl or Stdev mg/L-N	NO2-N Load gN/d	NO2-N by IC	stdev of IC NO2	NO3-N mg/L-N	stdev of IC NO3	NO3-N Load gN/d	COD mg/L
10-Jul-07	231	2.2	1.1068													
11-Jul-07	232	3.6	1.1068													
12-Jul-07	233	1.4	1.1068	141	6.4	0.156	0.548	319	4.1	0.353	330	0.3	51	0.26	0.0564	
13-Jul-07	234	2	1.1068													
14-Jul-07	235		1.1068													
15-Jul-07	236		1.1068													
16-Jul-07	237	5.5	1.1068													
17-Jul-07	238	1.2	1.1068					333	2.2	0.369	337	0.56	64.1	0.62	0.0709	
18-Jul-07	239	2	1.0718													
19-Jul-07	240	2.8	1.0718								330	1.83	58.7	1.65	0.0629	
20-Jul-07	241	1.5	1.1768													
21-Jul-07	242		1.1418													
22-Jul-07	243		1.1418													
23-Jul-07	244	4.8	1.1418													
24-Jul-07	245	1.5	1.1118								336	0.39	66.1	0.02	0.0735	
25-Jul-07	246	2.6	1.1018													
26-Jul-07	247	3.6	1.1068													
27-Jul-07	248		1.1068													
28-Jul-07	249		1.1031													
29-Jul-07	250		1.1031													
30-Jul-07	251		1.1031													
31-Jul-07	252		1.1031													
1-Aug-07	253		1.1068													
2-Aug-07	254		1.1168													
3-Aug-07	255		1.1518													
4-Aug-07	256		1.1018													
5-Aug-07	257		1.1018													
6-Aug-07	258		1.1031	105	1.2	0.116	0.406	267	1.35	0.295	274.7	0.25	133.4	0.42	0.1471	73
7-Aug-07	259		1.1031													
8-Aug-07	260		1.1031													
9-Aug-07	261		1.1031													
10-Aug-07	262		1.1018	121	1.7	0.133	0.468	252.8		0.279	252.4	0.59	151.8	0.26	0.1673	
11-Aug-07	263		1.0643													
12-Aug-07	264		1.0643					249		0.265						
13-Aug-07	265		1.1218	113	4.8	0.127	0.445	247.6	1.18	0.278	252.6	0.30	168.6	0.24	0.1891	64
14-Aug-07	266		1.1768	105	0.95	0.124		265.7	2.32	0.313	272.5	1.63	150.5	0.92	0.1771	
15-Aug-07	267		1.1318	101	0	0.114		230.9	2.76	0.261	236.5	0.19	172.7	0.31	0.1955	
16-Aug-07	268		1.1818	116	4.1	0.137	0.481	232.9	1.06	0.275	243.9	0.55	159.5	0.24	0.1885	
17-Aug-07	269		1.0968													
18-Aug-07	270		1.1935													
19-Aug-07	271		1.1935													
20-Aug-07	272		1.1935													
21-Aug-07	273		1.1368													
22-Aug-07	274		1.2118	107		0.130	0.455	238.6	0.758	0.289						
23-Aug-07	275		1.1618													
24-Aug-07	276		1.1618													

Date	Day of Operation	**Effluent** Volume L	Flow L/day	NH3-N mg/L-N	Stdev mg/L-N	NH3-N Load gN/day	NH3-N Load g N/m2-d	NO2-N mg/L-N	CI or Stdev mg/L-N	NO2-N Load gN/d	NO2-N by IC	stdev of IC NO2	NO3-N mg/L-N	stdev of IC NO3	NO3-N Load gN/d	COD mg/L
25-Aug-07	277		1.1568													
26-Aug-07	278		1.1568													
27-Aug-07	279		1.1168													
28-Aug-07	280		1.1068					256.2	1.47	0.284						
29-Aug-07	281		1.2718													
30-Aug-07	282		1.1968	49	1.7	0.059	0.206	238.6	0.758	0.286	251.4	1.55	218.5	1.7	0.2615	
31-Aug-07	283		1.1968													
1-Sep-07	284		1.1501													
2-Sep-07	285		1.1501													
3-Sep-07	286		1.1501													
4-Sep-07	287		1.1218	131	4.6	0.147	0.516	246.1	7.29	0.276	217.5	3	98.1	1.57	0.1100	49
5-Sep-07	288		1.1968													
6-Sep-07	289		1.1168													
7-Sep-07	290		1.1918													
8-Sep-07	291		1.1493													
9-Sep-07	292		1.1493													
10-Sep-07	293		1.0968													
11-Sep-07	294		1.1268	36	0.6	0.041	0.142	144	0	0.162	142.3	0	149.3	0.01	0.1682	
12-Sep-07	295		1.1568													
13-Sep-07	296		1.0368	34	0.6	0.035	0.124	97.1	1.87	0.101	95.5	0.44	161.4	0.08	0.1673	
14-Sep-07	297		1.1918													
15-Sep-07	298		1.1093													
16-Sep-07	299		1.1093													
17-Sep-07	300		1.1818	22	0.48	0.026	0.091	7.6	0.03	0.009	6.8	0	107.6	0.01	0.1272	81
18-Sep-07	301		1.1818	26	0.2	0.031	0.108	7.27	0.05	0.009	7.11	0.03	106.5	0.03	0.1259	
19-Sep-07	302		1.0368	38				7.55	0	0.008	7.1	0.3	105.9	3	0.1098	
20-Sep-07	303		1.0368	24	0.8	0.025	0.087	5.43	0.06	0.006	4.42	0.04	112.2	0.09	0.1163	
21-Sep-07	304		1.1135													
22-Sep-07	305		1.1135													
23-Sep-07	306		1.1135													
24-Sep-07	307		1.1143													
25-Sep-07	308		1.1143													
26-Sep-07	309		1.1143													
27-Sep-07	310		1.1143	32.4	4.58	0.036	0.127	4.6	0.11	0.005			107.8		0.1201	
28-Sep-07	311		1.1868													
29-Sep-07	312		1.0931													
30-Sep-07	313		1.0931													
1-Oct-07	314		1.0931													
2-Oct-07	315	4.3	1.0931													
3-Oct-07	316	5.5	1.1068													
4-Oct-07	317		1.1768	26.3	0.89	0.031	0.109	4.8	0.06	0.006			121		0.1424	77
5-Oct-07	318		1.1106													
6-Oct-07	319		1.1106													
7-Oct-07	320		1.1106													
8-Oct-07	321	4.5	1.1106	18.2	0.37	0.020	0.071	7.5	0.21	0.008						
9-Oct-07	322		1.0856													

Date	Day of Operation	**Effluent** Volume L	Flow L/day	NH3-N mg/L-N	Stdev mg/L-N	NH3-N Load gN/day	NH3-N Load g N/m2-d	NO2-N mg/L-N	Cl or Stdev mg/L-N	NO2-N Load gN/d	NO2-N by IC	stdev of IC NO2	NO3-N mg/L-N	stdev of IC NO3	NO3-N Load gN/d	COD mg/L
10-Oct-07	323		1.0856					6.4								
11-Oct-07	324		1.0856	21.3	0.25	0.023	0.081	6.6	0.31	0.007			127.5	1.04	0.1384	
12-Oct-07	325	3.8	1.0856													
13-Oct-07	326		1.1068													
14-Oct-07	327		1.1068													
15-Oct-07	328		1.1068													
16-Oct-07	329		1.1068													
17-Oct-07	330		1.1068													
18-Oct-07	331		1.1068													
19-Oct-07	332	8.3	1.1068	24.3	1.62	0.027	0.094	9.6	0.21	0.011			117.8	1.13	0.1304	25
20-Oct-07	333		1.0818													
21-Oct-07	334		1.0818													
22-Oct-07	335	3.2	1.0818													
23-Oct-07	336		1.1051													
24-Oct-07	337		1.1051													
25-Oct-07	338	6	1.1051	16.2	1.01	0.018	0.063	6.3	0.18	0.007			115.7	0.64	0.1279	
26-Oct-07	339		1.0948													
27-Oct-07	340		1.0948													
28-Oct-07	341		1.0948													
29-Oct-07	342		1.0948													
30-Oct-07	343		1.0948	22.3	1.27	0.024	0.086	9.8	0.11	0.011			104.6	0.015	0.1145	47
31-Oct-07	344	1.5	1.1068													
1-Nov-07	345		1.0718													
2-Nov-07	346	3.3	1.0718	25.3	0.73	0.027	0.095	7.5	0.07	0.008			91.3	1.27	0.0979	
3-Nov-07	347		1.1051													
4-Nov-07	348		1.1051													
5-Nov-07	349	3.8	1.1051													
6-Nov-07	350		1.0743													
7-Nov-07	351	5.6	1.0743													
8-Nov-07	352		1.1068													
9-Nov-07	353		1.1068													
10-Nov-07	354		1.1068													
11-Nov-07	355		1.1068	17.2	14	0.019	0.067									
12-Nov-07	356	0.8	1.0368													
13-Nov-07	357		1.0718													
14-Nov-07	358	2.7	1.0718	42.5	2.08	0.046	0.160	2.4	0.09	0.003			86.9	0.2	0.0931	18
15-Nov-07	359		1.1018													
16-Nov-07	360	2.1	1.1018													
17-Nov-07	361		1.0801													
18-Nov-07	362		1.0801													
19-Nov-07	363	5.4	1.0801													
20-Nov-07	364	6.4	1.1068	40.5	1.05	0.045	0.157	4.8	0.04	0.005			99.3	0.96	0.1099	61
21-Nov-07	365		1.0861													
22-Nov-07	366		1.0861													
23-Nov-07	367		1.0861													
24-Nov-07	368		1.0861													

Date	Day of Operation	**Effluent** Volume L	Flow L/day	NH3-N mg/L-N	Stdev mg/L-N	NH3-N Load gN/day	NH3-N Load g N/m2-d	NO2-N mg/L-N	CI or Stdev mg/L-N	NO2-N Load gN/d	NO2-N by IC	stdev of IC NO2	NO3-N mg/L-N	stdev of IC NO3	NO3-N Load gN/d	COD mg/L
25-Nov-07	369		1.0861													
26-Nov-07	370		1.0861													
27-Nov-07	371	7.8	1.0861	36.4	2.7	0.040	0.139	7.96	0.07	0.009			peaks splitting			
28-Nov-07	372		1.0718													
29-Nov-07	373		1.0718													
30-Nov-07	374	1.3	1.1318													
1-Dec-07	375		1.0718													
2-Dec-07	376		1.0718													
3-Dec-07	377		1.0718													
4-Dec-07	378	5.8	1.0718	25.3	0.66	0.027	0.095	14.52	0.137	0.016			98.4	2.79	0.1055	35
5-Dec-07	379		1.0718													
6-Dec-07	380	2.5	1.0718													
7-Dec-07	381	3.8	1.1168	22.3	1.03	0.025	0.087	9.79	0.041	0.011			94.54	0.45	0.1056	
8-Dec-07	382		1.0851													
9-Dec-07	383		1.0851													
10-Dec-07	384	6.9	1.0851													
11-Dec-07	385		1.0718													
12-Dec-07	386	2.1	1.0718	38.5	2.4	0.041	0.145	7.37	0.145	0.008			97.54	0.28	0.1045	54
13-Dec-07	387	3.3	1.0368													
14-Dec-07	388	1.4	1.0718	31.4	0.87	0.034	0.118	4.03	0.036	0.004			100	0.38	0.1072	39
15-Dec-07	389	2.3	1.1318													
16-Dec-07	390		1.0618													
17-Dec-07	391	4.4	1.0618													
18-Dec-07	392		1.0668	32.4	0.58	0.035	0.121	5.96	0.154	0.006			73.2	0.3	0.0781	
19-Dec-07	393	1.4	1.0668													
20-Dec-07	394	2.2	1.0968	39.5	1.14	0.043	0.152	4.8	0.091	0.005			102.2	0.33	0.1121	32
21-Dec-07	395		1.0631													
22-Dec-07	396		1.0631													
23-Dec-07	397		1.0631													
24-Dec-07	398	6.7	1.0631	41.5	2.29	0.044	0.155	6.84	0.162	0.007			103.1	0.08	0.1096	49
25-Dec-07	399		1.0775													
26-Dec-07	400		1.0775													
27-Dec-07	401		1.0775													
28-Dec-07	402		1.0775													
29-Dec-07	403		1.0775													
30-Dec-07	404		1.0775													
31-Dec-07	405	7.7	1.0775													
1-Jan-08	406	1.5	1.0368	110.3	8.57	0.114	0.401	21.05	1.68	0.022			66.4	5.2	0.0688	
2-Jan-08	407	2	1.0368													
3-Jan-08	408	1	1.0368	190.3	4.24	0.197	0.692	25.94	0.682	0.027			43.9	0.06	0.0455	
4-Jan-08	409	2	1.0368													
5-Jan-08	410		1.0968													
6-Jan-08	411		1.0968													
7-Jan-08	412	5.1	1.0968													
8-Jan-08	413	1.2	1.0968	18.2	1.77	0.020	0.070	23.54	0.388	0.026			100.9	0.06	0.1107	
9-Jan-08	414	2.2	1.0368													

Date	Day of Operation	**Effluent** Volume L	Flow L/day	NH3-N mg/L-N	Stdev mg/L-N	NH3-N Load gN/day	NH3-N Load g N/m2-d	NO2-N mg/L-N	CI or Stdev mg/L-N	NO2-N Load gN/d	NO2-N by IC	stdev of IC NO2	NO3-N mg/L-N	stdev of IC NO3	NO3-N Load gN/d	COD mg/L
10-Jan-08	415	3.5	1.0918													
11-Jan-08	416	0.9	1.0868	7.1	0.09	0.008	0.027	20.38	0.626	0.022			76.8	0.13	0.0835	27
12-Jan-08	417		1.0656													
13-Jan-08	418		1.0656													
14-Jan-08	419		1.0656													
15-Jan-08	420	5.2	1.0656													
16-Jan-08	421		1.0735													
17-Jan-08	422		1.0735													
18-Jan-08	423	8.8	1.0735	19.2	1.02	0.021	0.072	18.48	0.076	0.020			117.1	0.07	0.1257	39
19-Jan-08	424		1.0918													
20-Jan-08	425	2.4	1.0918													
21-Jan-08	426		1.0618													
22-Jan-08	427		1.0618													
23-Jan-08	428		1.0768													
24-Jan-08	429		1.0768													
25-Jan-08	430		1.0768	22.3	2.56	0.024	0.084	14.6	0.28	0.016			130.95	0.57	0.1410	
26-Jan-08	431		1.0768													
27-Jan-08	432		1.0768													
28-Jan-08	433		1.0768													
29-Jan-08	434		1.0768													
30-Jan-08	435		1.0768													
31-Jan-08	436		1.0768													
1-Feb-08	437		1.0806													
2-Feb-08	438		1.0806													
3-Feb-08	439		1.0806													
4-Feb-08	440		1.0806													
5-Feb-08	441		1.0368	9.1	0.92	0.009	0.033	12.9	0.25	0.013			126.825	0.53	0.1315	47
6-Feb-08	442		1.0818													
7-Feb-08	443		1.0968													
8-Feb-08	444		1.0651													
9-Feb-08	445		1.0651													
10-Feb-08	446		1.0651													
11-Feb-08	447		1.0651													
12-Feb-08	448		1.0651													
13-Feb-08	449		1.0651	33.4	6.1	0.036	0.125	20		0.021			103.575	0.57	0.1103	25
14-Feb-08	450		1.0668													
15-Feb-08	451		1.0668													
16-Feb-08	452		1.0768													
17-Feb-08	453		1.0768													
18-Feb-08	454		1.0768	30.4	1.2	0.033	0.115	18.8	0.25	0.020			104.225	0.04	0.1122	
19-Feb-08	455		1.0968													
20-Feb-08	456		1.0968													
21-Feb-08	457		1.0618													
22-Feb-08	458		1.0618													
23-Feb-08	459		1.0918													
24-Feb-08	460		1.0918													

Date	Day of Operation	**Effluent** Volume L	Flow L/day	NH3-N mg/L-N	Stdev mg/L-N	NH3-N Load gN/day	NH3-N Load g N/m2-d	NO2-N mg/L-N	CI or Stdev mg/L-N	NO2-N Load gN/d	NO2-N by IC	stdev of IC NO2	NO3-N mg/L-N	stdev of IC NO3	NO3-N Load gN/d	COD mg/L
25-Feb-08	461		1.0968	15.2	3.2	0.017	0.058	18.9	0	0.021	24.36	0.15	115.28	0.062	0.1264	18
26-Feb-08	462		1.0368													
27-Feb-08	463		1.0901													
28-Feb-08	464		1.0901													
29-Feb-08	465		1.0901													
1-Mar-08	466		1.0718													
2-Mar-08	467		1.0718													
3-Mar-08	468		1.0718													
4-Mar-08	469		1.0918													
5-Mar-08	470		1.0918	24.3	1.1	0.027	0.093	15.2	0.23	0.017	20.2	0.014	101.63	0.004	0.1110	47
6-Mar-08	471		1.0918													
7-Mar-08	472		1.0751													
8-Mar-08	473		1.0751													
9-Mar-08	474		1.0751													
10-Mar-08	475		1.0918													
11-Mar-08	476		1.0368	29.3	1.2	0.030	0.107	14.4	0.078	0.015	19.29	0.054	100.44	0.69	0.1041	25
12-Mar-08	477		1.0868													
13-Mar-08	478		1.0993													
14-Mar-08	479		1.0993													
15-Mar-08	480		1.0551													
16-Mar-08	481		1.0551													
17-Mar-08	482		1.0551													
18-Mar-08	483		1.0968													
19-Mar-08	484		1.0793													
20-Mar-08	485		1.0793													
21-Mar-08	486		1.0793													
22-Mar-08	487		1.0793													
23-Mar-08	488		1.0498													
24-Mar-08	489		1.0498													
25-Mar-08	490		1.0498													
26-Mar-08	491		1.0498													
27-Mar-08	492		1.0498													
28-Mar-08	493		1.0943													
29-Mar-08	494		1.0943													
30-Mar-08	495		1.0768													
31-Mar-08	496		1.0768													
1-Apr-08	497		1.0768													
2-Apr-08	498		1.0568													
3-Apr-08	499		1.0568													
4-Apr-08	500		1.0568													
5-Apr-08	501		1.0728													
6-Apr-08	502		1.0728													
7-Apr-08	503		1.0728	58.7	1	0.063	0.221	7.6	0.11	0.008			143.1	1.5	0.1535	18
8-Apr-08	504		1.0728													
9-Apr-08	505		1.0728													
10-Apr-08	506		1.0728													

Date	Day of Operation	**Effluent** Volume L	Flow L/day	NH3-N mg/L-N	Stdev mg/L-N	NH3-N Load gN/day	NH3-N Load g N/m2-d	NO2-N mg/L-N	CI or Stdev mg/L-N	NO2-N Load gN/d	NO2-N by IC	stdev of IC NO2	NO3-N mg/L-N	stdev of IC NO3	NO3-N Load gN/d	COD mg/L
11-Apr-08	507		1.0668													
12-Apr-08	508		1.0668													
13-Apr-08	509		1.0668													
14-Apr-08	510		1.0668	56.7	2.1	0.060	0.212	16.2	0.1	0.017			146.4	1.2	0.1562	
15-Apr-08	511		1.0793													
16-Apr-08	512		1.0793													
17-Apr-08	513		1.0793													
18-Apr-08	514		1.0793													
19-Apr-08	515		1.0785													
20-Apr-08	516		1.0785													
21-Apr-08	517		1.0785	53.6	2.1	0.058	0.203	20	0.17	0.022			165.4	0.7	0.1784	18
22-Apr-08	518		1.0718													
23-Apr-08	519		1.0968													
24-Apr-08	520		1.0968													
25-Apr-08	521		1.0968													
26-Apr-08	522		1.0643													
27-Apr-08	523		1.0643													
28-Apr-08	524		1.0643													
29-Apr-08	525		1.0643													
30-Apr-08	526		1.0935													
1-May-08	527		1.0935													
2-May-08	528		1.0935													
3-May-08	529		1.0728													
4-May-08	530		1.0728													
5-May-08	531		1.0728													
6-May-08	532		1.0728													
7-May-08	533		1.0728	38.5	2.7	0.041	0.145	27.5	0.844	0.030			161.6	0.5	0.1734	11
8-May-08	534															
9-May-08	535															
10-May-08	536															
11-May-08	537															
12-May-08	538															
13-May-08	539							0					180.25			
14-May-08	540															11
15-May-08	541															
16-May-08	542															
17-May-08	543															
18-May-08	544															
19-May-08	545															
20-May-08	546															
21-May-08	547															
22-May-08	548															
23-May-08	549															
24-May-08	550															
25-May-08	551															
26-May-08	552															

Date	Day of Operation	**Effluent** Volume L	Flow L/day	NH3-N mg/L-N	Stdev mg/L-N	NH3-N Load gN/day	NH3-N Load g N/m2-d	NO2-N mg/L-N	CI or Stdev mg/L-N	NO2-N Load gN/d	NO2-N by IC	stdev of IC NO2	NO3-N mg/L-N	stdev of IC NO3	NO3-N Load gN/d	COD mg/L
27-May-08	553															
28-May-08	554															
29-May-08	555															
Reactor shut down on day 555																

In the table of operating data, horizontal lines indicate significant events or observations, which are described in the table below along with other less significant changes not marked in the tables above.

Table F.4. HFMBR Events.

Day	Event/Observation/Comments
12	Siphon event nearly emptied reactor into effluent bottle. Returned to HFMBR.
19	Modifications to recirc. line so that it slopes to reactor and will not siphon. Air break installed.
83	Feed tube clogged. Replaced.
92	Reduced lumen pressure from ~8 to ~5 psig.
108	Increased feed flow from 0.48 ml/min to 0.72 ml/min.
111	First feed batch sparged with Ar/CO_2.
114-115	Changed most of external reactor tubing.
151	Feed tube clogged. Replaced.
153	Began use of Ar/O_2 mix for aeration.
196	Sloughing observed on right side of module.
203	Recirculation pump burned out; replaced. Changed out sample ports.
274	New feed batch prepared using trace element solutions 1 and 2.
280	Feed tube clogged. Replaced.
283	New feed batch prepared using trace element solutions 1 and 2.
292	New feed batch prepared using trace element solutions 1 and 2.
297	Reduced lumen pressure to ~4 psig.
299	New feed batch prepared, used original feed recipe w/out add'l trace element solutions.
365	Feed tube clogged. Replaced.
405	Found aeration gas tank empty. Based on pH log data, probably not empty for more than 1-2 days.
407	Replaced with new aeration gas tank.
439	Feed turned off ~ 11am.
440	Made new feed batch and restarted.
454	New Ar/CO_2 sparge tank installed.
468	Leak in recirculation tubing. Replaced.
518	Recirculation tubing bound up on one pump head. Replaced.

Phases defined in Chapter 4 are as follows:
1-23: Startup
24-92: Nitritation
93-297: Nitritation and Partial Nitrite Oxidation
298-555: Nitritation and Anaerobic Ammonium Oxidation

APPENDIX G

MICROSENSOR PROFILES IN BIOFILM

Appendix G. Microsensor Profiles in Biofilm

An entire data set is shown for Port 1, illustrating the data collection and processing procedure. For subsequent ports, only summary tables are shown.

Table G.1. Port 1 oxygen microsensor profile, Day 204.

**********	**********	**********	**********					
Profix	(c) by	Pyro	Imagination					
**********	**********	**********	**********					
6/13/2007	Time:	1:36 PM	Data Set:	1	Sample	Time [s]:	2	
Range:	+/- 10V	Description:	Channel A	Cal. units:	uM			
Range:	+/- 10V	Description:	Channel B	Cal. units:	uM			
Profile Time	**Depth [µm]**	**Dist. [µm]**	**Ch.A [µm]**	**Stdev [µm]**	**Ch. A [mg/L]**	**Dist. [µm]**	**mg/L**	**Stdev**
	0	710	0.471	7.66E-01	0.02	710	0.01	0.0036
0:00:06	0	710	0.252	7.26E-01	0.01			
0:00:11	0	710	0.262	7.05E-01	0.01			
0:00:15	0	710	0.431	7.24E-01	0.01			
0:00:21	0	710	0.491	7.05E-01	0.02			
0:00:25	0	710	0.481	7.14E-01	0.02			
0:00:31	0	710	0.332	7.22E-01	0.01			
0:00:35	100	610	0.342	8.33E-01	0.01	610	0.01	0.0035
0:00:41	100	610	0.193	8.59E-01	0.01			
0:00:45	100	610	0.063	8.00E-01	0.00			
0:00:51	100	610	0.123	7.04E-01	0.00			
0:00:56	100	610	0.252	7.45E-01	0.01			
0:01:01	100	610	0.073	6.71E-01	0.00			
0:01:06	200	510	0.212	7.61E-01	0.01	510	0.00	0.0027
0:01:10	200	510	0.053	7.31E-01	0.00			
0:01:16	200	510	-0.026	7.18E-01	0.00			
0:01:20	200	510	0.033	8.30E-01	0.00			
0:01:26	200	510	0.004	7.94E-01	0.00			
0:01:30	200	510	0.044	7.31E-01	0.00			
0:01:36	250	460	-0.086	7.64E-01	0.00	460	0.00	0.0038
0:01:40	250	460	-0.136	6.84E-01	0.00			
0:01:46	250	460	0.033	6.87E-01	0.00			
0:01:51	250	460	-0.026	7.14E-01	0.00			
0:01:55	250	460	-0.205	7.65E-01	-0.01			
0:02:01	250	460	0.123	8.02E-01	0.00			
0:02:05	300	410	-0.116	7.60E-01	0.00	410	0.00	0.0034
0:02:11	300	410	-0.145	7.36E-01	0.00			
0:02:16	300	410	0.044	7.45E-01	0.00			
0:02:20	300	410	-0.235	6.90E-01	-0.01			
0:02:26	300	410	0.004	7.54E-01	0.00			
0:02:30	300	410	-0.006	7.05E-01	0.00			
0:02:36	320	390	-0.026	7.61E-01	0.00	390	0.00	0.0028
0:02:40	320	390	-0.136	6.99E-01	0.00			
0:02:46	320	390	-0.076	8.19E-01	0.00			
0:02:51	320	390	-0.225	7.56E-01	-0.01			
0:02:55	320	390	-0.145	7.73E-01	0.00			
0:03:01	320	390	0.014	7.86E-01	0.00			

Table G.1. Port 1 oxygen microsensor profile, Day 204, continued.

Profile Time	Depth [µm]	Dist. [µm]	Ch.A [µm]	Stdev [µm]	Ch. A [mg/L]	Dist. [µm]	mg/L	Stdev
0:03:05	340	370	-0.046	7.12E-01	0.00	370	0.00	0.0040
0:03:11	340	370	-0.225	7.13E-01	-0.01			
0:03:16	340	370	-0.295	7.11E-01	-0.01			
0:03:21	340	370	0.014	8.17E-01	0.00			
0:03:26	340	370	-0.016	8.28E-01	0.00			
0:03:30	340	370	-0.066	7.15E-01	0.00			
0:03:36	360	350	-0.086	7.82E-01	0.00	350	0.00	0.0033
0:03:40	360	350	-0.116	7.41E-01	0.00			
0:03:46	360	350	-0.116	7.32E-01	0.00			
0:03:51	360	350	-0.036	7.22E-01	0.00			
0:03:55	360	350	-0.215	7.49E-01	-0.01			
0:04:01	360	350	-0.325	6.84E-01	-0.01			
0:04:05	380	330	-0.086	7.46E-01	0.00	330	0.00	0.0038
0:04:11	380	330	-0.205	7.03E-01	-0.01			
0:04:16	380	330	0.044	8.95E-01	0.00			
0:04:21	380	330	-0.165	7.27E-01	-0.01			
0:04:26	380	330	-0.275	6.82E-01	-0.01			
0:04:30	380	330	-0.245	7.22E-01	-0.01			
0:04:36	400	310	0.004	7.86E-01	0.00	310	0.00	0.0039
0:04:41	400	310	-0.245	6.45E-01	-0.01			
0:04:46	400	310	-0.066	6.69E-01	0.00			
0:04:51	400	310	-0.325	6.48E-01	-0.01			
0:04:55	400	310	-0.165	7.13E-01	-0.01			
0:05:01	400	310	-0.096	7.58E-01	0.00			
0:05:05	420	290	-0.175	7.10E-01	-0.01	290	0.00	0.0038
0:05:11	420	290	-0.195	7.35E-01	-0.01			
0:05:15	420	290	0.093	7.40E-01	0.00			
0:05:21	420	290	-0.195	6.91E-01	-0.01			
0:05:26	420	290	-0.235	7.58E-01	-0.01			
0:05:30	420	290	-0.145	7.12E-01	0.00			
0:05:36	440	270	0.014	7.86E-01	0.00	270	-0.01	0.0038
0:05:40	440	270	-0.265	8.16E-01	-0.01			
0:05:46	440	270	-0.275	7.51E-01	-0.01			
0:05:51	440	270	-0.315	8.31E-01	-0.01			
0:05:56	440	270	-0.155	8.33E-01	0.00			
0:06:01	440	270	-0.215	7.53E-01	-0.01			
0:06:05	460	250	-0.006	8.20E-01	0.00	250	0.00	0.0048
0:06:11	460	250	-0.195	7.58E-01	-0.01			
0:06:15	460	250	-0.354	7.37E-01	-0.01			
0:06:21	460	250	0.044	8.13E-01	0.00			
0:06:26	460	250	-0.245	6.76E-01	-0.01			
0:06:30	460	250	-0.136	7.61E-01	0.00			
0:06:36	480	230	0.053	6.87E-01	0.00	230	0.00	0.0032
0:06:40	480	230	-0.175	7.20E-01	-0.01			
0:06:46	480	230	-0.205	7.47E-01	-0.01			
0:06:51	480	230	-0.185	7.18E-01	-0.01			
0:06:56	480	230	-0.126	7.86E-01	0.00			
0:07:01	480	230	-0.215	7.58E-01	-0.01			

Table G.1. Port 1 oxygen microsensor profile, Day 204, continued.

Profile Time	Depth [µm]	Dist. [µm]	Ch.A [µm]	Stdev [µm]	Ch. A [mg/L]	Dist. [µm]	mg/L	Stdev
0:07:05	500	210	-0.096	7.49E-01	0.00	210	-0.01	0.0039
0:07:11	500	210	-0.344	6.92E-01	-0.01			
0:07:15	500	210	-0.424	6.44E-01	-0.01			
0:07:21	500	210	-0.215	6.90E-01	-0.01			
0:07:26	500	210	-0.315	8.27E-01	-0.01			
0:07:30	500	210	-0.175	7.99E-01	-0.01			
0:07:36	520	190	-0.126	7.86E-01	0.00	190	0.00	0.0018
0:07:40	520	190	-0.036	7.88E-01	0.00			
0:07:46	520	190	-0.076	7.52E-01	0.00			
0:07:50	520	190	-0.116	8.00E-01	0.00			
0:07:56	520	190	-0.126	7.81E-01	0.00			
0:08:01	520	190	-0.205	8.35E-01	-0.01			
0:08:05	540	170	-0.155	7.00E-01	0.00	170	-0.01	0.0021
0:08:11	540	170	-0.265	7.40E-01	-0.01			
0:08:15	540	170	-0.225	7.08E-01	-0.01			
0:08:21	540	170	-0.225	7.69E-01	-0.01			
0:08:26	540	170	-0.275	8.00E-01	-0.01			
0:08:31	540	170	-0.354	7.18E-01	-0.01			
0:08:36	560	150	-0.255	7.70E-01	-0.01	150	-0.01	0.0055
0:08:40	560	150	-0.225	7.51E-01	-0.01			
0:08:46	560	150	-0.205	6.67E-01	-0.01			
0:08:50	560	150	0.083	7.16E-01	0.00			
0:08:56	560	150	-0.404	6.81E-01	-0.01			
0:09:00	560	150	-0.046	7.31E-01	0.00			
0:09:06	580	130	-0.235	7.05E-01	-0.01	130	-0.01	0.0043
0:09:11	580	130	-0.245	7.41E-01	-0.01			
0:09:15	580	130	-0.275	8.00E-01	-0.01			
0:09:21	580	130	0.033	7.31E-01	0.00			
0:09:25	580	130	-0.275	8.00E-01	-0.01			
0:09:31	580	130	-0.354	5.64E-01	-0.01			
0:09:35	600	110	-0.334	7.21E-01	-0.01	110	-0.01	0.0043
0:09:41	600	110	-0.175	7.10E-01	-0.01			
0:09:46	600	110	-0.145	7.73E-01	0.00			
0:09:50	600	110	-0.185	7.28E-01	-0.01			
0:09:56	600	110	-0.265	7.44E-01	-0.01			
0:10:00	600	110	-0.503	6.09E-01	-0.02			
0:10:06	620	90	0.023	7.86E-01	0.00	90	-0.01	0.0039
0:10:11	620	90	-0.305	7.60E-01	-0.01			
0:10:16	620	90	-0.225	7.65E-01	-0.01			
0:10:21	620	90	-0.295	7.35E-01	-0.01			
0:10:25	620	90	-0.195	6.91E-01	-0.01			
0:10:31	620	90	-0.126	7.68E-01	0.00			
0:10:35	640	70	-0.036	7.08E-01	0.00	70	-0.01	0.0033
0:10:41	640	70	-0.305	7.46E-01	-0.01			
0:10:46	640	70	-0.096	7.11E-01	0.00			
0:10:50	640	70	-0.225	7.65E-01	-0.01			
0:10:56	640	70	-0.245	6.87E-01	-0.01			
0:11:00	640	70	-0.255	6.94E-01	-0.01			

Table G.1. Port 1 oxygen microsensor profile, Day 204, continued.

Profile Time	Depth [µm]	Dist. [µm]	Ch.A [µm]	Stdev [µm]	Ch. A [mg/L]	Dist. [µm]	mg/L	Stdev
0:11:06	660	50	-0.275	7.22E-01	-0.01	50	0.00	0.0033
0:11:10	660	50	-0.026	8.01E-01	0.00			
0:11:16	660	50	-0.126	7.49E-01	0.00			
0:11:21	660	50	-0.145	7.78E-01	0.00			
0:11:26	660	50	-0.215	7.10E-01	-0.01			
0:11:31	660	50	-0.016	6.94E-01	0.00			
0:11:35	680	30	0.133	7.23E-01	0.00	30	0.01	0.0021
0:11:41	680	30	0.193	8.59E-01	0.01			
0:11:45	680	30	0.173	6.95E-01	0.01			
0:11:51	680	30	0.262	7.15E-01	0.01			
0:11:56	680	30	0.073	6.71E-01	0.00			
0:12:00	680	30	0.222	7.83E-01	0.01			
0:12:06	700	10	3.962	7.89E-01	0.13			
0:12:10	700	10	2.699	8.40E-01	0.09			
0:12:16	690	20	1.485	4.80E-01	0.05	20	0.05	0.0062
0:12:21	690	20	1.446	7.02E-01	0.05			
0:12:26	690	20	1.416	5.95E-01	0.05			
0:12:31	690	20	1.833	5.48E-01	0.06			
0:12:35	700	10	3.136	7.22E-01	0.10	10	0.10	0.0134
0:12:41	700	10	2.977	6.53E-01	0.10			
0:12:45	700	10	3.027	5.57E-01	0.10			
0:12:51	700	10	3.037	7.73E-01	0.10			
0:12:56	700	10	3.415	6.79E-01	0.11			
0:13:00	700	10	3.703	6.97E-01	0.12			
0:13:35	710	0	10.048	6.85E-01	0.32	0	0.33	0.0083
0:13:41	710	0	10.286	8.57E-01	0.33			
0:13:45	710	0	10.227	8.20E-01	0.33			
0:13:51	710	0	10.674	6.96E-01	0.34			
0:13:56	710	0	10.475	6.92E-01	0.34			
0:14:01	710	0	10.694	7.50E-01	0.34			

Table G.2. Port 2 oxygen microsensor profile, Day 204.

Distance µm	DO mg/L	Standard Deviation
710	0.03	0.0021
660	0.03	0.0023
610	0.03	0.0025
560	0.02	0.0038
510	0.02	0.0022
460	0.02	0.0027
410	0.02	0.0031
360	0.01	0.0036
310	0.01	0.0018
260	0.01	0.0053
210	0.01	0.0020
160	0.01	0.0017
110	0.01	0.0030
60	0.02	0.0046
50	0.03	0.0036
30	0.12	0.0102
20	0.15	0.0024
10	0.17	0.0025
0	0.19	0.0047

Table G.3. Port 2 clean fiber oxygen microsensor profile, Day 204.

Distance µm	DO mg/L	Standard Deviation
820	0.01	0.0058
720	0.02	0.0056
620	0.01	0.0036
520	0.05	0.0205
470	0.13	0.0289
460	0.18	0.0044
450	0.17	0.0079
440	0.17	0.0058
430	0.18	0.0053
420	0.19	0.0052
410	0.19	0.0052
400	0.19	0.0052
390	0.20	0.0044
380	0.21	0.0019
370	0.24	0.0032
360	0.24	0.0064
350	0.23	0.0124
340	0.25	0.0122
330	0.28	0.0053
320	0.31	0.0040
300	0.33	0.0078
280	0.34	0.0106
260	0.36	0.0039
240	0.37	0.0072
220	0.39	0.0023
200	0.41	0.0023
180	0.44	0.0059
160	0.46	0.0056
140	0.49	0.0060
120	0.51	0.0077
100	0.53	0.0077
80	0.55	0.0034
60	0.58	0.0117
40	0.68	0.0256
20	0.76	0.0116
0	0.90	0.0288

Table G.4. Port 3 oxygen microsensor profile, Day 204.

Distance µm	DO mg/L	Standard Deviation
1,180	0.08	0.0038
1,130	0.05	0.0067
1,080	0.04	0.0040
1,030	0.04	0.0030
980	0.03	0.0044
930	0.04	0.0025
880	0.03	0.0044
830	0.02	0.0027
780	0.02	0.0042
730	0.01	0.0049
680	0.01	0.0072
630	0.00	0.0035
580	0.00	0.0044
530	0.00	0.0058
480	0.00	0.0053
460	0.00	0.0034
440	0.01	0.0019
420	0.01	0.0043
400	0.01	0.0032
380	0.00	0.0043
360	0.00	0.0032
340	0.00	0.0031
320	0.00	0.0018
300	0.00	0.0033
280	0.00	0.0019
260	0.00	0.0047
240	0.00	0.0033
220	0.00	0.0059
200	0.00	0.0045
180	0.00	0.0063
130	0.01	0.0050
80	0.01	0.0026
30	0.04	0.0189
10	0.15	0.0149
0	0.20	0.0100

Table G.5. Port 4 oxygen microsensor profile, Day 204.

Distance µm	DO mg/L	Standard Deviation
300	0.00	0.006
200	0.00	0.001
100	-0.01	0.003
50	0.00	0.005
40	0.00	0.005
30	0.01	0.026
20	0.04	0.011
10	0.11	0.018
0	0.25	0.004

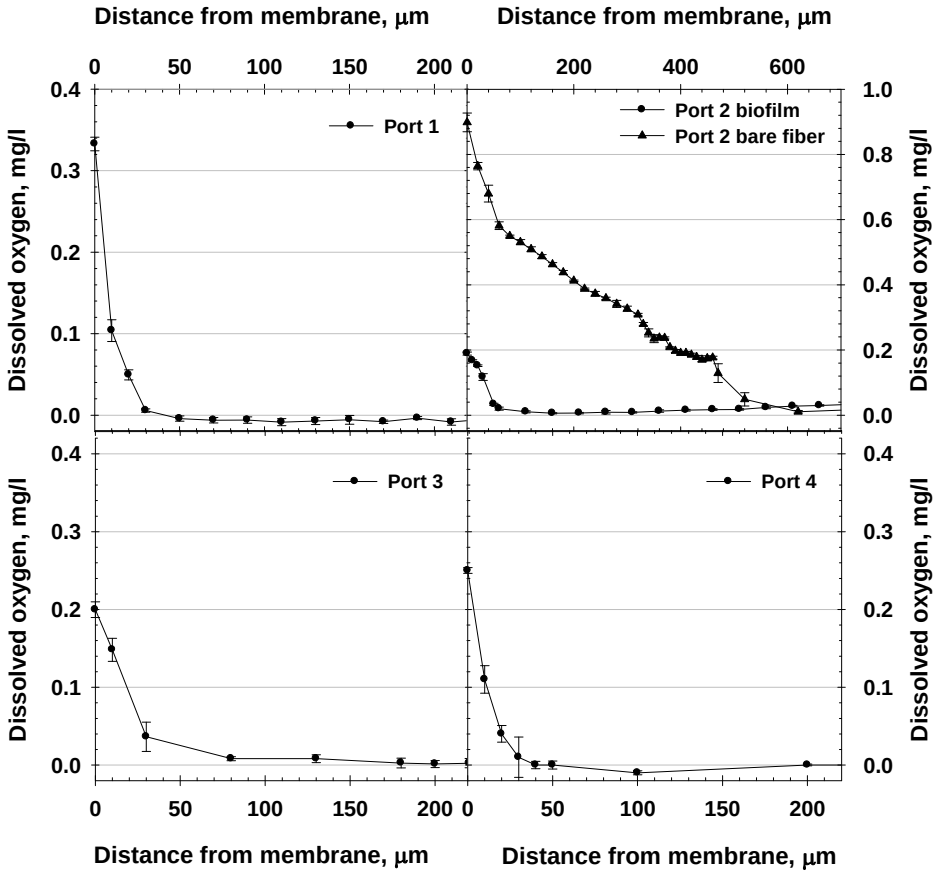

Figure 3.5 and G.1. Oxygen microsensor profiles, Day 204.

Table G.6. Port 1 oxygen microsensor profile, Day 458.

Distance µm	DO mg/L	Standard Deviation
440	0.01	0.0028
390	0.01	0.0041
340	0.01	0.0064
290	0.01	0.0038
280	0.01	0.0077
270	0.01	0.0034
260	0.01	0.0043
250	0.01	0.0043
240	0.01	0.0049
230	0.01	0.0037
220	0.01	0.0036
210	0.00	0.0026
200	0.00	0.0049
190	0.01	0.0046
180	0.01	0.0047
170	0.01	0.0038
160	0.01	0.0022
150	0.01	0.0026
140	0.01	0.0059
130	0.01	0.0042
120	0.00	0.0031
110	0.00	0.0030
100	0.01	0.0048
90	0.00	0.0032
80	0.00	0.0045
70	0.01	0.0036
60	0.03	0.0093
50	0.07	0.0193
40	0.16	0.0284
30	0.22	0.0296
20	0.26	0.0388
10	0.53	0.0558
0	0.79	0.0171

Table G.7. Port 2 oxygen microsensor profile, Day 458.

Distance µm	DO mg/L	Standard Deviation
470	0.02	0.0041
445	0.02	0.0044
420	0.01	0.0068
395	0.01	0.0047
370	0.01	0.0029
350	0.02	0.0036
330	0.01	0.0034
310	0.01	0.0040
290	0.02	0.0029
270	0.01	0.0040
250	0.01	0.0055
230	0.01	0.0032
210	0.01	0.0070
190	0.01	0.0039
170	0.01	0.0024
150	0.01	0.0044
130	0.02	0.0036
110	0.01	0.0037
90	0.01	0.0050
70	0.01	0.0028
50	0.03	0.0086
40	0.05	0.0067
30	0.09	0.0053
20	0.12	0.0179
10	0.23	0.0144
0	0.26	0.0039

Table G.8. Port 3 oxygen microsensor profile, Day 458.

Distance µm	DO mg/L	Standard Deviation
410	0.018	0.0043
310	0.016	0.0044
210	0.012	0.0048
110	0.009	0.0068
60	0.011	0.0069
10	0.166	0.0575
0	0.242	0.0059

Table G.9. Port 3 clean fiber oxygen microsensor profile, Day 458.

Distance µm	DO mg/L	Standard Deviation
1,250	-0.01	0.0018
1,150	-0.01	0.0054
1,050	-0.01	0.0068
1,000	0.00	0.0056
950	0.10	0.0837
925	0.20	0.0049
900	0.21	0.0051
875	0.23	0.0059
850	0.24	0.0061
825	0.25	0.0082
800	0.27	0.0064
775	0.28	0.0061
750	0.29	0.0037
725	0.30	0.0037
700	0.31	0.0058
675	0.32	0.0049
650	0.34	0.0099
625	0.39	0.0069
600	0.40	0.0044
575	0.40	0.0022
550	0.42	0.0084
525	0.46	0.0092
500	0.49	0.0041
475	0.50	0.0030
450	0.52	0.0088
425	0.53	0.0029
400	0.54	0.0029
375	0.55	0.0071
350	0.56	0.0039
325	0.57	0.0112
300	0.58	0.0053
275	0.60	0.0034
250	0.63	0.0035
225	0.65	0.0169
200	0.67	0.0047
175	0.67	0.0077
150	0.70	0.0067
125	0.71	0.0049
100	0.72	0.0026
75	0.75	0.0132
50	0.76	0.0055
25	0.76	0.0052
0	0.78	0.0103

Table G.10. Port 4 oxygen microsensor profile, Day 458.

Distance µm	DO mg/L	Standard Deviation
800	0.01	0.0036
700	0.01	0.0094
600	0.01	0.0020
550	0.00	0.0010
500	0.01	0.0087
450	0.01	0.0067
400	0.00	0.0020
350	0.01	0.0030
300	0.01	0.0040
250	0.01	0.0081
200	0.01	0.0042
150	0.01	0.0046
100	0.00	0.0023
50	0.01	0.0054
0	0.38	0.0149

Table G.11. Port 4 clean fiber oxygen microsensor profile, Day 458.

Distance µm	DO mg/L	Standard Deviation	Distance µm	DO mg/L	Standard Deviation
2,140	0.08	0.0036	420	0.75	0.0013
1,890	0.07	0.0016	410	0.76	0.0067
1,640	0.07	0.0054	400	0.75	0.0065
1,540	0.07	0.0023	390	0.75	0.0080
1,440	0.07	0.0040	380	0.77	0.0212
1,340	0.07	0.0045	370	0.79	0.0032
1,240	0.06	0.0013	360	0.80	0.0043
1,140	0.06	0.0015	350	0.79	0.0084
1,040	0.06	0.0051	340	0.81	0.0152
940	0.06	0.0027	330	0.81	0.0020
840	0.07	0.0178	320	0.83	0.0071
740	0.31	0.0600	310	0.83	0.0037
740	0.36	0.0010	300	0.83	0.0006
730	0.38	0.0077	290	0.85	0.0121
720	0.40	0.0043	280	0.85	0.0043
710	0.41	0.0032	270	0.86	0.0023
700	0.48	0.0484	260	0.86	0.0090
690	0.52	0.0017	250	0.88	0.0023
680	0.52	0.0063	240	0.90	0.0231
670	0.52	0.0004	230	0.93	0.0075
651	0.52	0.0019	220	0.93	0.0053
650	0.53	0.0105	210	0.94	0.0013
640	0.53	0.0081	200	0.96	0.0250
630	0.54	0.0070	190	0.99	0.0065
620	0.55	0.0034	180	1.00	0.0033
610	0.56	0.0019	170	1.00	0.0060
600	0.55	0.0027	160	1.01	0.0075
590	0.56	0.0088	150	1.01	0.0042
580	0.58	0.0081	140	1.01	0.0049
570	0.57	0.0016	130	1.02	0.0030
560	0.58	0.0043	120	1.03	0.0068
550	0.59	0.0036	110	1.02	0.0016
540	0.60	0.0081	100	1.03	0.0007
530	0.61	0.0072	90	1.07	0.0264
520	0.63	0.0088	80	1.08	0.0039
510	0.64	0.0114	70	1.09	0.0088
500	0.65	0.0039	60	1.09	0.0054
490	0.65	0.0040	50	1.10	0.0048
480	0.65	0.0079	40	1.12	0.0137
470	0.67	0.0189	30	1.13	0.0049
460	0.68	0.0084	20	1.14	0.0023
450	0.70	0.0049	10	1.17	0.0271
440	0.72	0.0250	0	1.18	0.0028
430	0.75	0.0060			

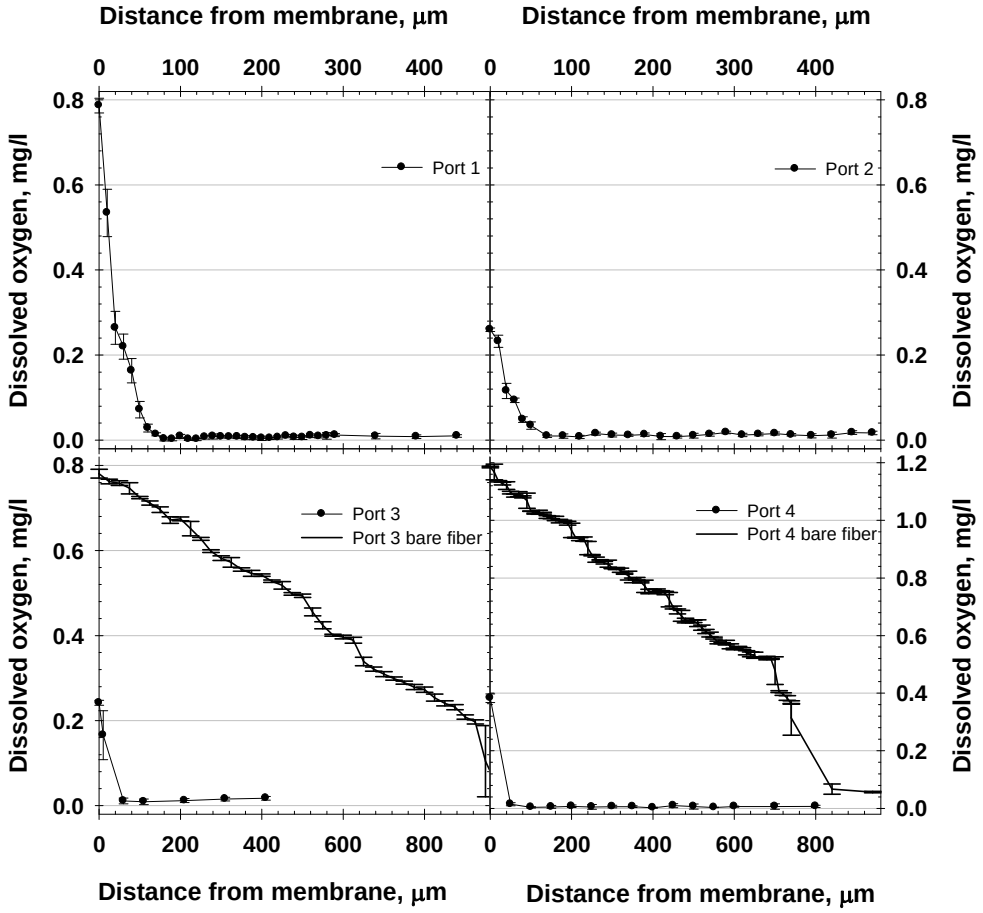

Figure G.2. Oxygen microsensor profiles, Day 458.

All data for this appendix can be found in the spreadsheet files:

"Dissertation Appendix G Part a Day 204 Sensor Profiles.xls" and
"Dissertation Appendix G Part b Day 458 Sensor Profiles.xls"

APPENDIX H

NITROGEN MASS BALANCES AND NITROGEN OXIDE EMISSIONS

Appendix H: Nitrogen mass balances and nitrogen oxide emissions.

Example calculations are provided for each component of the mass balance.

H.1. Soluble N species

N load, g N/day = Concentration, mg/l-N × 1 g / 1,000 mg × Flow, l / day

Example, for day 127:

Effluent NH_4^+-N = 156 mg/l-N × 1 g / 1,000 mg × 1.23 l / day

Effluent NH_4^+-N = 0.662 g N/day

Calculation of dissolved nitrogen oxide species (NO, NO_2, N_2O):

First, concentrations were converted from ppm to g/m3 (see below).

Second, Henry's constants were tabulated and converted to dimensionless constants ($C_{(aq)}$ / $C_{(g)}$).

Table H.1. Henry's constants for nitrogen oxide species.

N-oxide species	K_H^{cp} M/atm	K_H^{cc} dimensionless
$NO_{(g)}$	0.0019	0.0468
$NO_{2(g)}$	0.0120	0.2940
$N_2O_{(g)}$	0.00061	0.0149

Next, aqueous phase concentrations were calculated from K_H^{cc} and gas phase concentrations.

$C_{(aq)}$, g/m^3 = $C_{(g)}$, g/m^3 × K_H^{cc} × Mass of N / Mass of Molecule

Example, for N_2O on Day 127:

$N_2O_{(aq)}$-N Load = 4.11 g-N/m^3 × 0.0149 × 28 g N/44 g N_2O = 0.0612 g/m^3 = 0.06 mg/l

Mass load is then calculated using effluent flow rate as described above.

H.2. Gaseous N species

Concentration, g / m^3 = Concentration, ppm × molec. Weight, g/mol / (1,000 × R × T, K)

Where R = 0.08206 L-atm/K-mol
T = Temperature, Kelvin

N Load, g N/day = Concentration, g/m^3 × Gas flow, m^3/day × Mass of N / Mass of Molecule

Example, for day 127:

Outlet $N_2O_{(g)}$ = (3,651 ppm × 44 g/mol) / (1,000 × 0.08206 L-atm/K-mol × 303.15 K)

Outlet $N_2O_{(g)}$ = 6.46 g/m^3

$N_2O_{(g)}$-N Load = 6.46 g/m^3 × 0.013 m^3/day × 28 mg N / 44 mg N_2O

$N_2O_{(g)}$-N Load = 0.053 g N/day

Table H.2. Summary of example N balance, Day 127.

Nitrogen Component	Conc. mg/l-N (aq) or ppm (g)	Conc. g N/m^3 (g)	Flow[a,b] l/d (aq) or m^3/d (g)	Mass N g N/day	% of Total N
Influent					
NH_4^+	639		1.04	0.663	99.7%
NO_2^-	2		1.04	0.002	0.3%
NO_3^-	0		1.04	0.0	0.0%
Total Mass In				0.665	100%
Effluent aqueous species (aq)					
NH_4^+	156		1.23	0.192	28.7%
NO_2^-	276		1.23	0.339	50.8%
NO_3^-	67		1.23	0.082	12.3%
Org. N	neg.		1.23	0.0	0.0%
$NO_{(aq)}$	0.001		1.23	0.0	0.0%
$NO_{2(aq)}$	0.02		1.23	0.0	0.0%
$N_2O_{(aq)}$	0.06		1.23	0.0	0.0%
Outlet gaseous species (g)					
$NO_{(g)}$	27.3	0.03	0.013	0.0002	0.0%
$NO_{2(g)}$	49	0.06	0.013	0.0004	0.1%
$N_2O_{(g)}$	3,650	4.11	0.013	0.0534	8.0%
Total Mass Out				0.667	100%
Percent recovery		100.7%			

[a] Liquid effluent flow includes flow of base ($NaHCO_3$) from the pH control system.
[b] Outlet gas flow was measured using a flow tube rotameter. Outlet flows were not significantly different from inlet flow; therefore, inlet flow was used to calculate outlet load of N gases.

Table H.3. Data for N mass balances: Influent N.

Day of operation	Total N Influent g N/day	Day of operation	Total N Influent g N/day	Day of operation	Total N Influent g N/day
1	0.232	135	0.680	392	0.599
3	0.241	140	0.696	394	0.601
6	0.238	143	0.681	398	0.583
8	0.253	153	0.706	406	0.587
10	0.208	156	0.700	408	0.627
13	0.249	160	0.656	413	0.645
15	0.245	162	0.651	416	0.630
16	0.263	169	0.663	423	0.642
17	0.219	177	0.681	430	0.695
18	0.226	183	0.632	441	0.635
21	0.228	190	0.656	449	0.566
22	0.235	192	0.614	454	0.691
24	0.441	198	0.639	461	0.684
26	0.434	206	0.655	470	0.651
28	0.462	209	0.689	476	0.702
31	0.454	210	0.683	503	0.617
32	0.420	218	0.659	510	0.573
37	0.441	230	0.638	517	0.686
42	0.454	233	0.573	533	0.662
43	0.470	258	0.624		
44	0.458	265	0.639		
48	0.448	268	0.627		
52	0.466	282	0.659		
56	0.426	289	0.762		
58	0.429	294	0.687		
62	0.446	296	0.773		
65	0.465	300	0.743		
71	0.445	303	0.741		
73	0.469	310	0.646		
76	0.441	317	0.624		
80	0.471	321	0.628		
83	0.489	324	0.647		
86	0.472	332	0.628		
90	0.496	338	0.675		
94	0.441	343	0.637		
97	0.458	346	0.648		
98	0.487	355	0.701		
101	0.471	358	0.667		
108	0.470	364	0.745		
110	0.706	371	0.615		
115	0.654	378	0.582		
120	0.626	381	0.572		
122	0.665	386	0.615		
127	0.662	388	0.620		

Table H.4. Data for N mass balances: Effluent NH_4^+-N.

Day of operation	Effluent NH_4^+ g N/day	Day of operation	Effluent NH_4^+ g N/day	Day of operation	Effluent NH_4^+ g N/day
3	0.194	156	0.135	343	0.024
6	0.180	160	0.178	346	0.027
8	0.175	162	0.176	355	0.019
10	0.089	163	0.195	358	0.046
13	0.193	164	0.169	364	0.045
16	0.158	165	0.179	371	0.040
17	0.062	166	0.190	378	0.027
18	0.025	169	0.171	381	0.025
21	0.007	177	0.164	386	0.041
22	0.006	183	0.138	388	0.034
24	0.008	185	0.154	392	0.035
26	0.031	190	0.147	394	0.043
28	0.044	192	0.134	398	0.044
31	0.031	196	0.138	406	0.114
32	0.028	198	0.120	408	0.197
42	0.037	206	0.142	413	0.020
44	0.012	209	0.171	416	0.008
48	0.022	210	0.155	423	0.021
52	0.021	211	0.171	430	0.024
56	0.018	212	0.165	441	0.009
58	0.008	213	0.183	449	0.036
62	0.018	218	0.157	454	0.033
71	0.021	230	0.175	461	0.017
73	0.021	233	0.156	470	0.027
76	0.023	258	0.116	476	0.030
80	0.022	262	0.133	503	0.063
83	0.005	265	0.127	510	0.060
86	0.018	266	0.124	517	0.058
90	0.017	267	0.114	533	0.041
94	0.018	268	0.137		
97	0.019	274	0.130		
98	0.019	282	0.059		
101	0.110	287	0.147		
108	0.011	294	0.041		
110	0.056	296	0.035		
115	0.182	300	0.026		
120	0.197	301	0.031		
122	0.166	303	0.025		
127	0.192	310	0.036		
133	0.190	317	0.031		
135	0.178	321	0.020		
140	0.202	324	0.023		
143	0.201	332	0.027		
153	0.078	338	0.018		

Table H.5. Data for N mass balances: Effluent NO_2^--N and NO_2^--N + NH_4^+-N.

Day of operation	Effluent NO_2^- g N/day	NH_4^+ + NO_2^- g N/day	Day of operation	Effluent NO_2^- g N/day	NH_4^+ + NO_2^- g N/day	Day of operation	Effluent NO_2^- g N/day	NH_4^+ + NO_2^- g N/day
6	0.023	0.203	133	0.340	0.530	300	0.009	0.035
9	0.061	0.171	135	0.327	0.505	301	0.009	0.039
10	0.082		140	0.314	0.517	302	0.008	
11	0.133		143	0.314	0.515	303	0.006	0.031
13	0.030	0.223	153	0.385	0.464	310	0.005	0.041
14	0.088		156	0.359	0.494	317	0.006	0.037
15	0.116		160	0.353	0.531	321	0.008	0.029
16	0.150		162	0.367	0.543	324	0.007	0.030
17	0.174	0.236	163	0.374	0.569	332	0.011	0.038
18	0.132	0.157	164	0.381	0.550	338	0.007	0.025
21	0.143	0.150	165	0.352	0.531	343	0.011	0.035
22	0.155	0.162	166	0.348	0.538	346	0.008	0.035
24	0.337	0.345	169	0.359	0.529	358	0.003	0.048
26	0.339	0.370	177	0.378	0.542	364	0.005	0.050
28	0.391	0.434	183	0.372	0.511	371	0.009	0.048
31	0.351	0.382	185	0.388	0.543	378	0.016	0.043
32	0.348	0.376	190	0.409	0.556	381	0.011	0.036
33	0.384		192	0.395	0.528	386	0.008	0.049
42	0.379	0.416	196	0.437	0.574	388	0.004	0.038
44	0.355	0.367	198	0.444	0.564	392	0.006	0.041
48	0.411	0.433	206	0.394	0.537	394	0.005	0.049
52	0.395	0.416	209	0.355	0.526	398	0.007	0.051
56	0.345	0.363	210	0.344	0.500	406	0.022	0.136
58	0.359	0.367	211	0.292	0.464	408	0.027	0.224
62	0.351	0.370	212	0.321	0.485	413	0.026	0.046
71	0.366	0.386	213	0.335	0.518	416	0.022	0.030
73	0.354	0.376	218	0.343	0.501	423	0.020	0.040
76	0.349	0.373	229	0.325		430	0.016	0.040
80	0.309	0.331	230	0.353	0.528	441	0.013	0.023
83	0.264	0.269	233	0.353	0.509	449	0.021	0.057
86	0.230	0.249	238	0.369		454	0.020	0.053
90	0.281	0.298	258	0.295	0.410	461	0.021	0.037
92	0.207		262	0.279	0.412	470	0.017	0.043
97	0.291	0.310	264	0.265		476	0.015	0.045
98	0.298	0.317	265	0.278	0.405	503	0.008	0.071
101	0.306	0.416	266	0.313	0.436	510	0.017	0.078
108	0.272	0.283	267	0.261	0.376	517	0.022	0.079
110	0.408	0.464	268	0.275	0.412	533	0.030	0.071
115	0.303	0.485	274	0.289	0.419			
118	0.268		280	0.284				
120	0.308	0.505	282	0.286	0.344			
122	0.294	0.461	287	0.276	0.423			
127	0.339	0.531	294	0.162	0.203			
132	0.335		296	0.101	0.136			

Table H.6. Data for N mass balances: Effluent NO_3^--N and NO_3^--N + NO_2^--N + NH_4^+-N.

Day of operation	Effluent NO_3^- g N/day	NH_4^++NO_2^- + NO_3^- g N/day	Day of operation	Effluent NO_3^- g N/day	NH_4^++NO_2^- + NO_3^- g N/day	Day of operation	Effluent NO_3^- g N/day	NH_4^++NO_2^- + NO_3^- g N/day
8	0.0007		183	0.076	0.587	388	0.107	0.145
10	0.0007	0.172	185	0.067	0.610	392	0.078	0.119
11	0.0011		190	0.056	0.612	394	0.112	0.161
13	0.0006	0.224	196	0.061	0.636	398	0.110	0.161
14	0.0009		198	0.060	0.624	406	0.069	0.205
21	0.0007	0.151	200	0.079		408	0.046	0.270
22	0.0015	0.163	206	0.077	0.613	413	0.111	0.156
24	0.0029	0.348	209	0.083	0.610	416	0.083	0.113
26	0.0029	0.372	210	0.088	0.588	423	0.126	0.166
28	0.0018	0.436	211	0.056	0.520	430	0.141	0.181
31	0.0010	0.383	212	0.062	0.547	441	0.131	0.154
32	0.0009	0.377	213	0.059	0.577	449	0.110	0.167
42	0.0018	0.418	218	0.086	0.586	454	0.112	0.165
44	0.0021	0.369	230	0.049	0.576	461	0.126	0.164
48	0.0024	0.435	233	0.056	0.566	470	0.111	0.154
52	0.0023	0.419	238	0.071		476	0.104	0.149
56	0.0028	0.365	240	0.063		503	0.154	0.225
58	0.0021	0.369	245	0.073		510	0.156	0.234
62	0.0028	0.372	258	0.147	0.557	517	0.178	0.258
76	0.0071	0.380	262	0.167	0.579	533	0.173	0.244
80	0.0565	0.387	265	0.189	0.594			
83	0.087	0.356	266	0.177	0.613			
86	0.109	0.357	267	0.195	0.571			
101	0.085	0.501	268	0.188	0.601			
108	0.082	0.365	282	0.262	0.606			
110	0.105	0.569	287	0.110	0.533			
120	0.063	0.569	294	0.168	0.371			
122	0.063	0.524	296	0.167	0.303			
127	0.082	0.613	300	0.127	0.162			
128	0.074		301	0.126	0.165			
133	0.077	0.607	302	0.110				
135	0.071	0.576	303	0.116	0.147			
140	0.086	0.602	310	0.120	0.161			
143	0.071	0.586	317	0.142	0.179			
153	0.085	0.548	324	0.138	0.169			
156	0.071	0.565	332	0.130	0.168			
160	0.057	0.587	338	0.128	0.153			
162	0.061	0.605	343	0.115	0.150			
163	0.075	0.644	346	0.098	0.133			
164	0.071	0.620	358	0.093	0.141			
165	0.077	0.608	364	0.110	0.160			
166	0.076	0.614	378	0.105	0.148			
169	0.092	0.621	381	0.106	0.141			
177	0.079	0.621	386	0.105	0.154			

Table H.7. Data for N mass balances: Outlet N oxides and N oxides + sum of soluble N.

Day of operation	Outlet NO g N/day	Soluble N + NO g N/day	Outlet NO_2 g N/day	Soluble N +NO+NO_2 g N/day	Outlet + N2O g N/day	Sol. N+NO +NO_2+N_2O g N/day
56	0.00010	0.366	0.00098	0.367		
77	0.00015	0.381	0.00025	0.381		
86	0.00010	0.358	0.00016	0.358	0.042	0.400
87	0.00019	0.357	0.00038	0.358	0.037	0.394
127	0.00020	0.613	0.00036	0.614	0.053	0.667
162	0.00019	0.605	0.00028	0.605	0.038	0.643
210	0.00018	0.588	0.00004	0.588	0.041	0.629
265	0.00017	0.594	7.6E-05	0.594	0.012	0.605
300	0.00004	0.162	1.1E-05	0.162	0	0.162
317		0.179		0.179	0	0.179
338	0.00003	0.153	5.0E-05	0.153	0	0.153
406		0.205		0.205	0	0.205

For Day 87, used gas data measured on Day 93.

For gaseous compounds, outlet gas was collected in gas bags and analyzed for the gases indicated. Gas phase concentrations were converted to mass rates in the outlet gas. Soluble partition of the gaseous compounds NO, NO_2, and N_2O were negligible and are not included in the mass balance.

H.3. Nitrogen oxide emissions.

The table below shows routine outlet gas monitoring data. Outlet gas was collected in gas bags and analyzed for the gases indicated. All concentrations are in the gas phase.

Table H.8. Nitrogen oxide monitoring data.

Day of Operation	Gas flow cc/min	gas flow m^3/day	NO ppm	NO g/m^3	NO-N, g N/day	NO_x ppm	NO_2 ppm	NO_2 g/m^3	NO_2-N, g N/day	N_2O ppm	N_2O g/m^3	N_2O Mass g N/day
56	9	0.0130	13.80	0.017	0.00010	148.00	134.20	0.25	0.00098			
77	9	0.0130	20.45	0.025	0.00015	54.04	33.58	0.06	0.00024			
86	9	0.0130	15.96	0.019	0.00012	38.38	22.42	0.04	0.00016			
93	9	0.0130	25.76	0.031	0.00019	77.77	52.02	0.10	0.00038	2902	5.13	0.042
94	9	0.0130								2523	4.46	0.037
127	9	0.0130	27.27	0.033	0.00020	76.26	48.99	0.09	0.00036	3651	6.46	0.053
162	9	0.0130	26.01	0.031	0.00019	64.64	38.63	0.07	0.00028	2577	4.56	0.038
210	9	0.0130	24.75	0.030	0.00018	29.80	5.05	0.01	0.00004	2808	4.97	0.041
265	9	0.0130	23.12	0.028	0.00017	33.58	10.46	0.02	0.00008	791	1.40	0.012
300	9	0.0130	5.10	0.006	0.00004		1.48	0.0027	0.00001	0	0.0	0.0
317	9	0.0130								0	0.0	0.0
338	9	0.0130								0	0.0	0.0
407	9	0.0130								0	0.0	0.0

APPENDIX I

BIOFILM STRUCTURE/THICKNESS ANALYSIS

Appendix I. Biofilm Structure/Thickness Analysis

Images and data for this appendix can be found in the image directories and in the spreadsheet file "Dissertation Appendix I Thickness Measurements.xls"

I.1 Port 1 Thickness Measurement Images

100X:

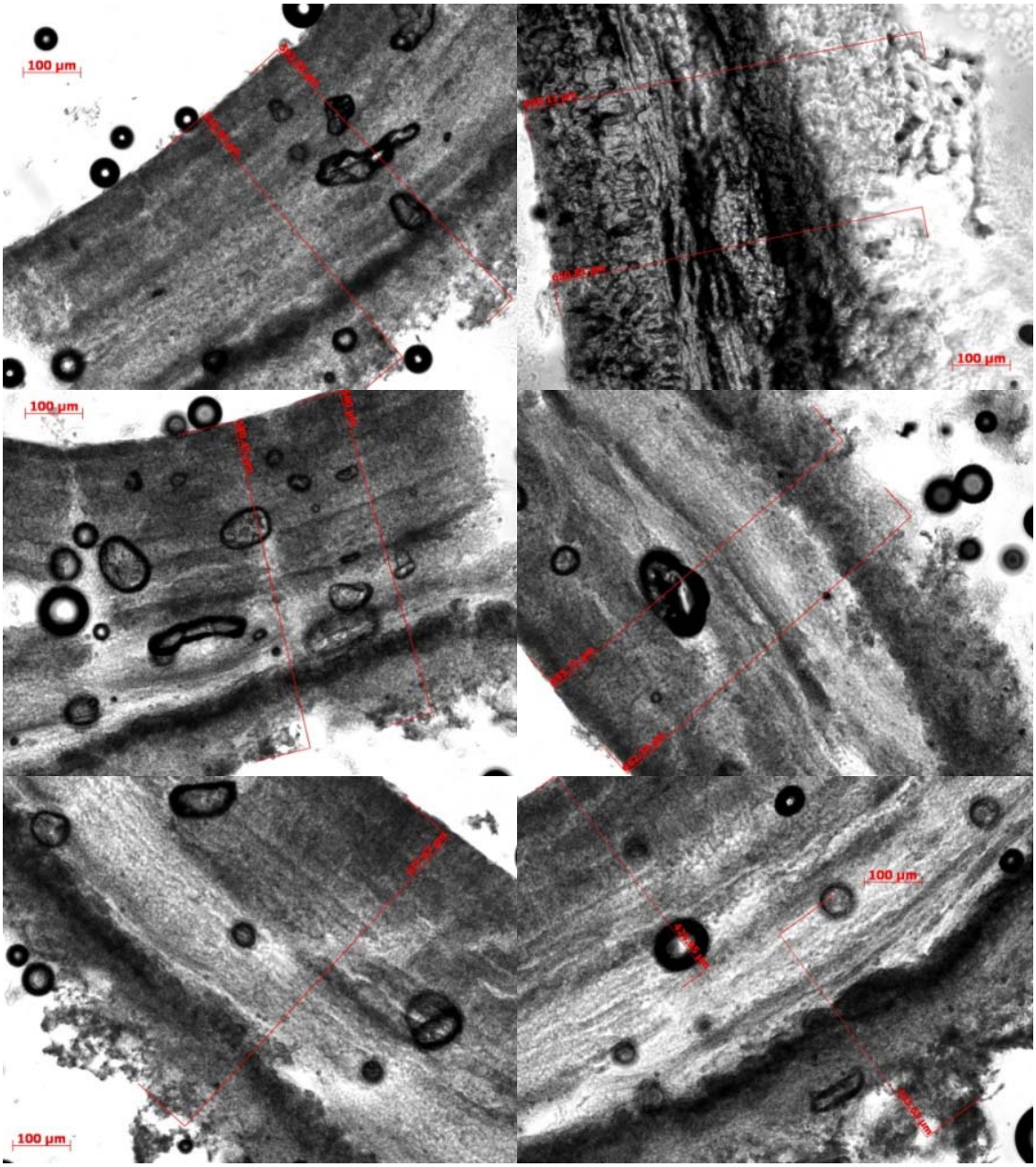

Port 1 Thickness Measurement Images
100X (continued):

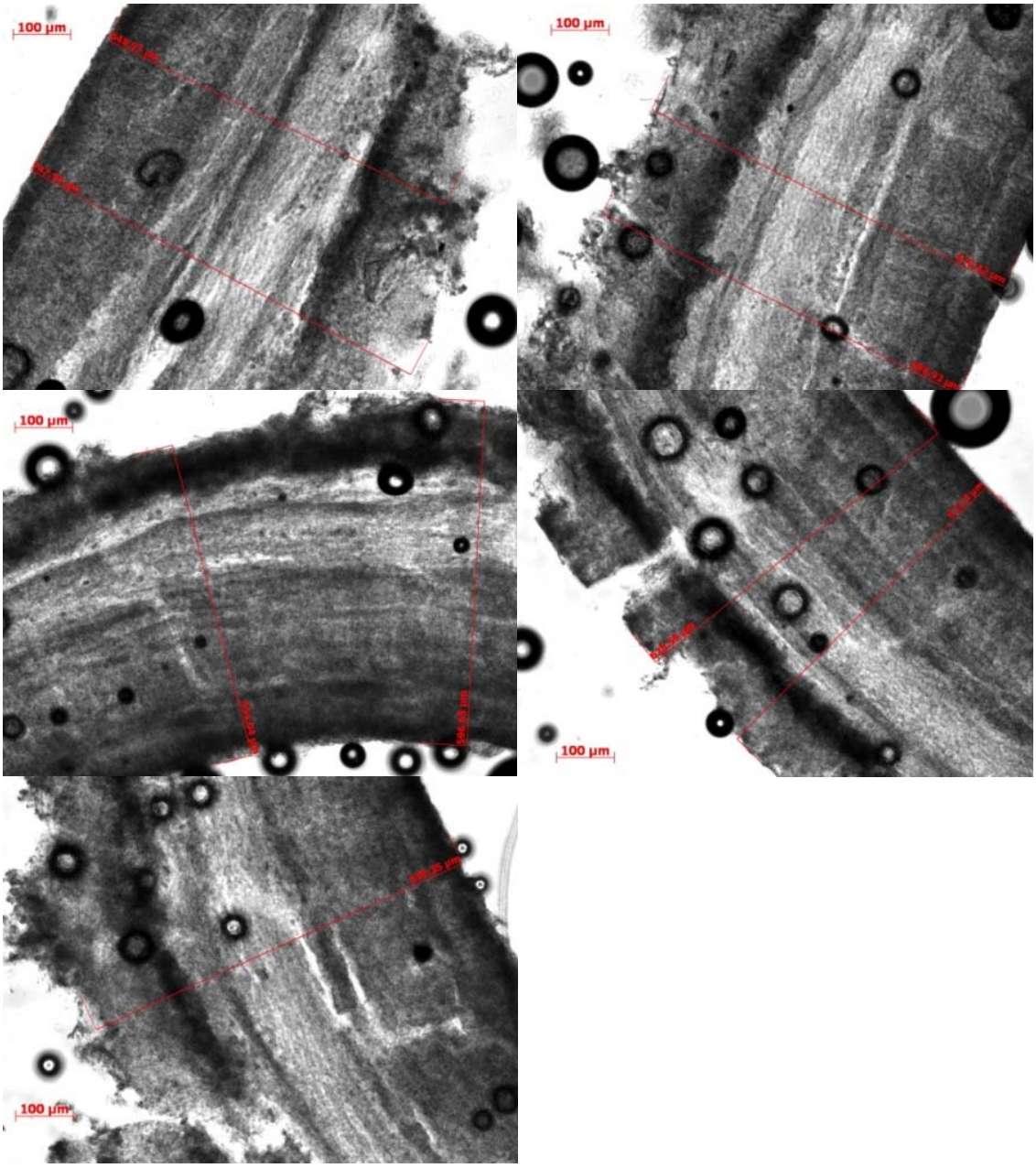

Port 1 Thickness Measurement Images
40X:

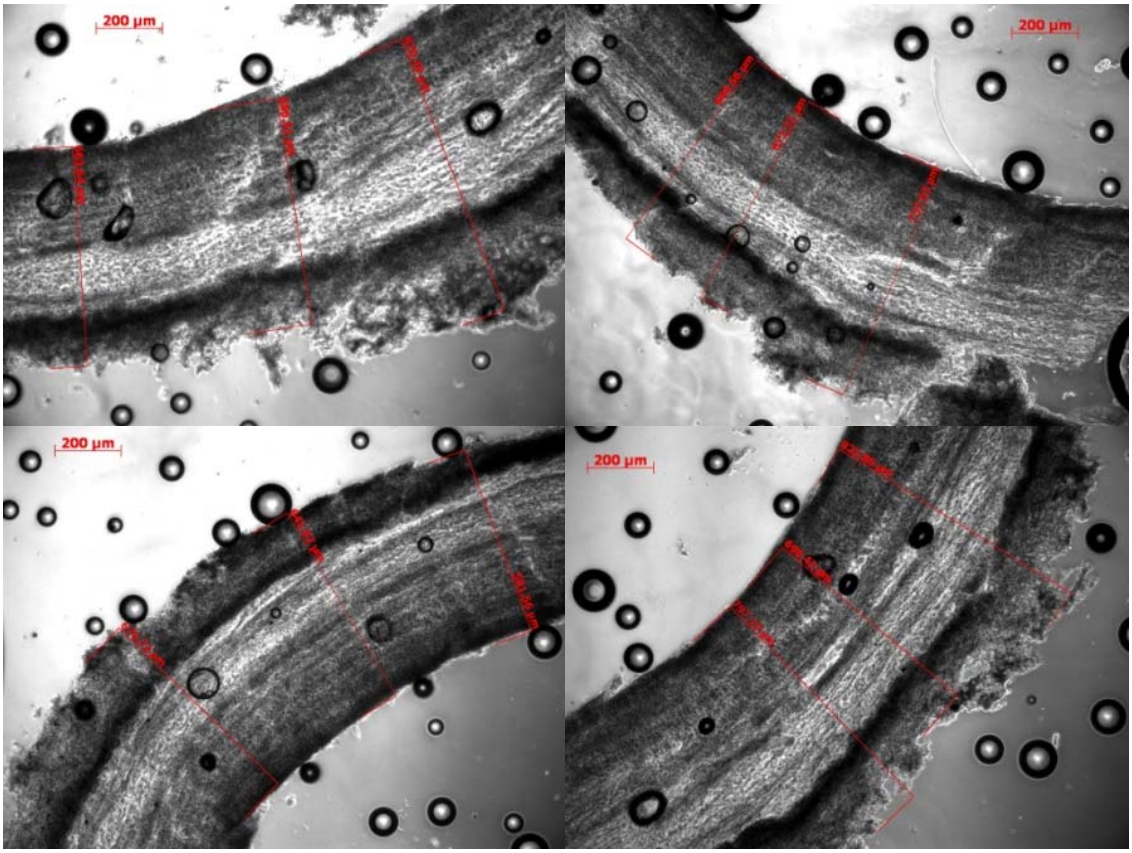

I.2 Port 2 Thickness Measurement Images

100X:

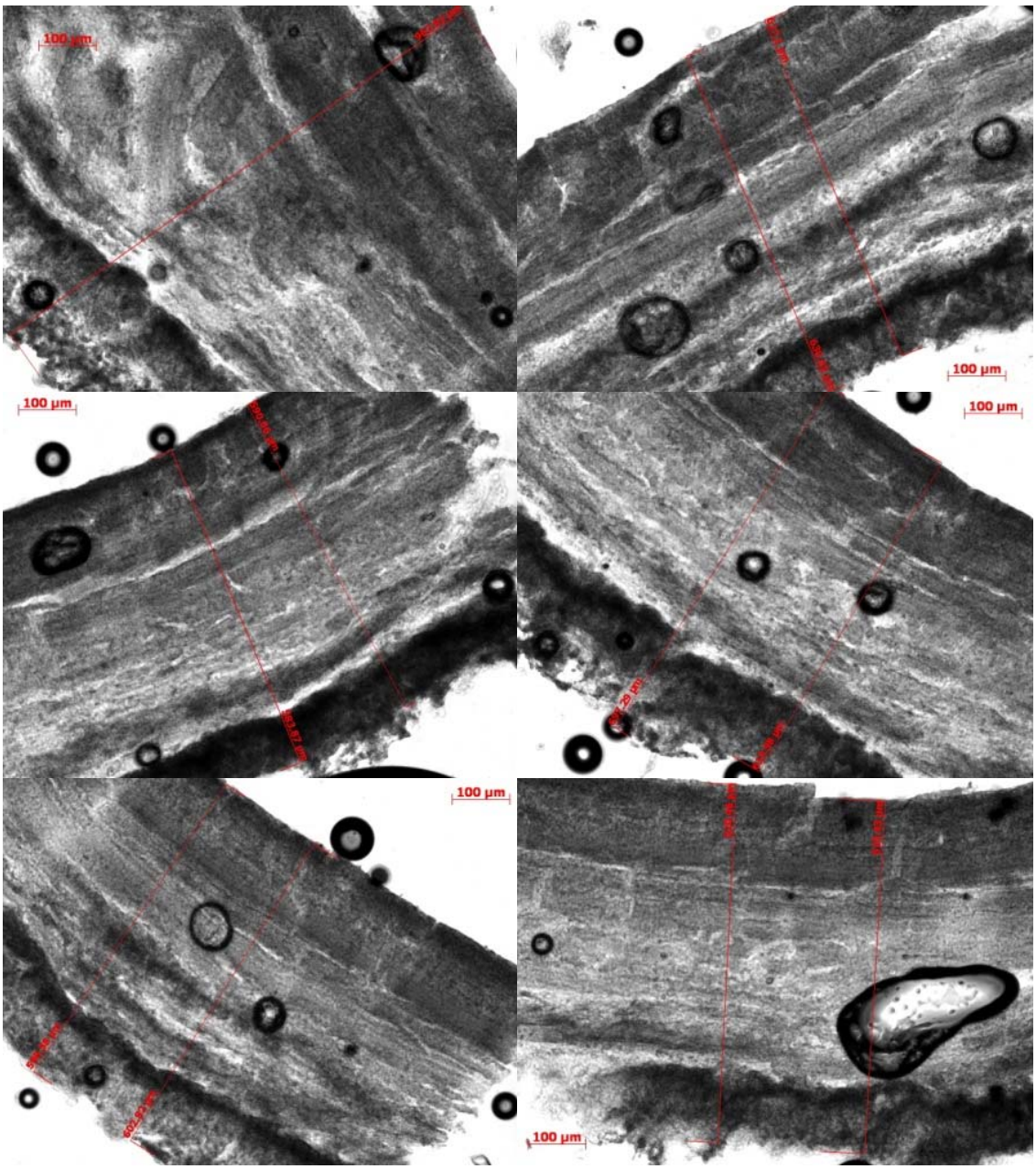

Port 2 Thickness Measurement Images
100X (continued):

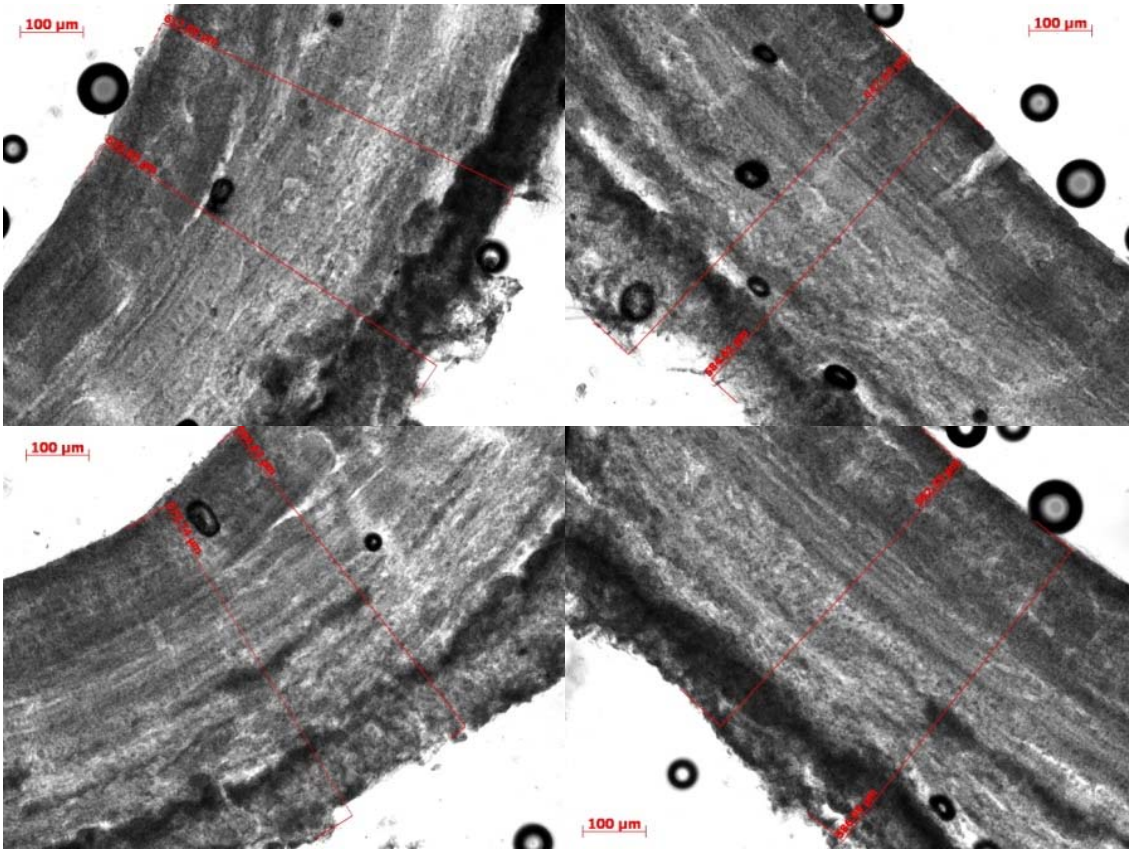

Port 2 Thickness Measurement Images
40X

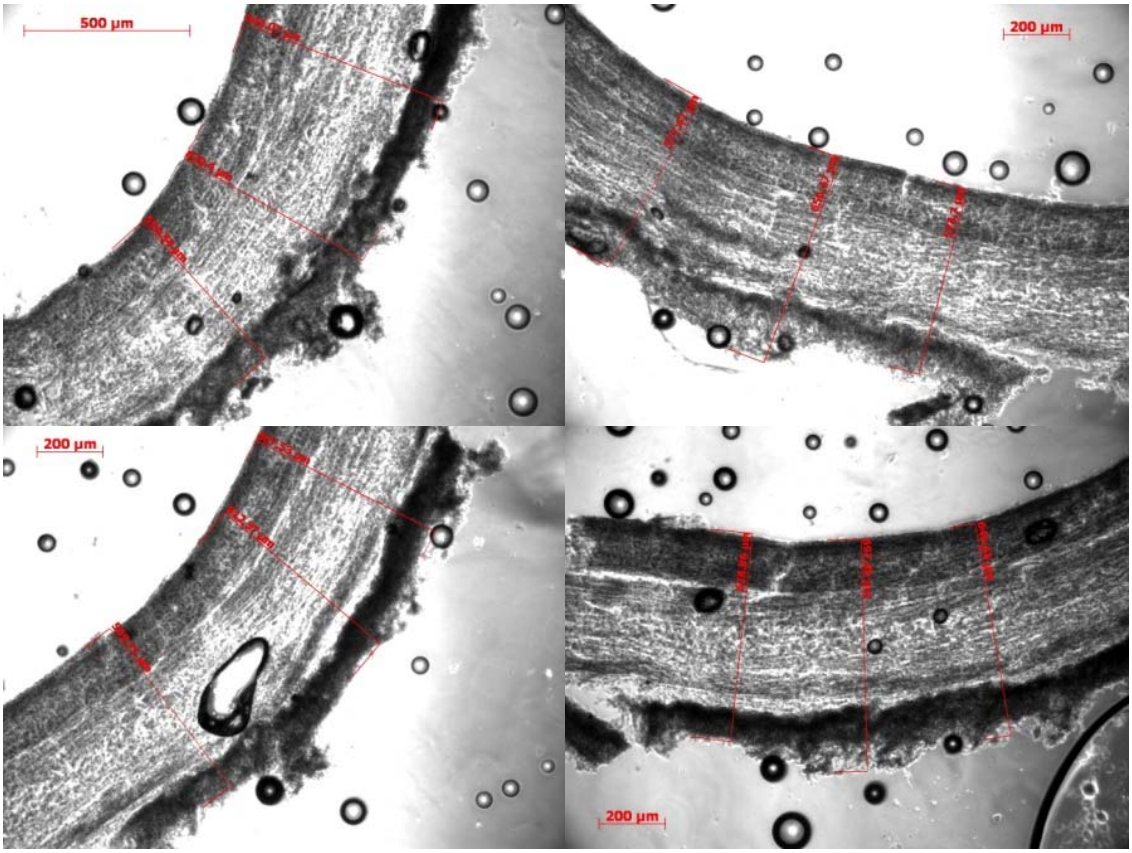

I.3 Port 3 Thickness Measurement Images

100X:

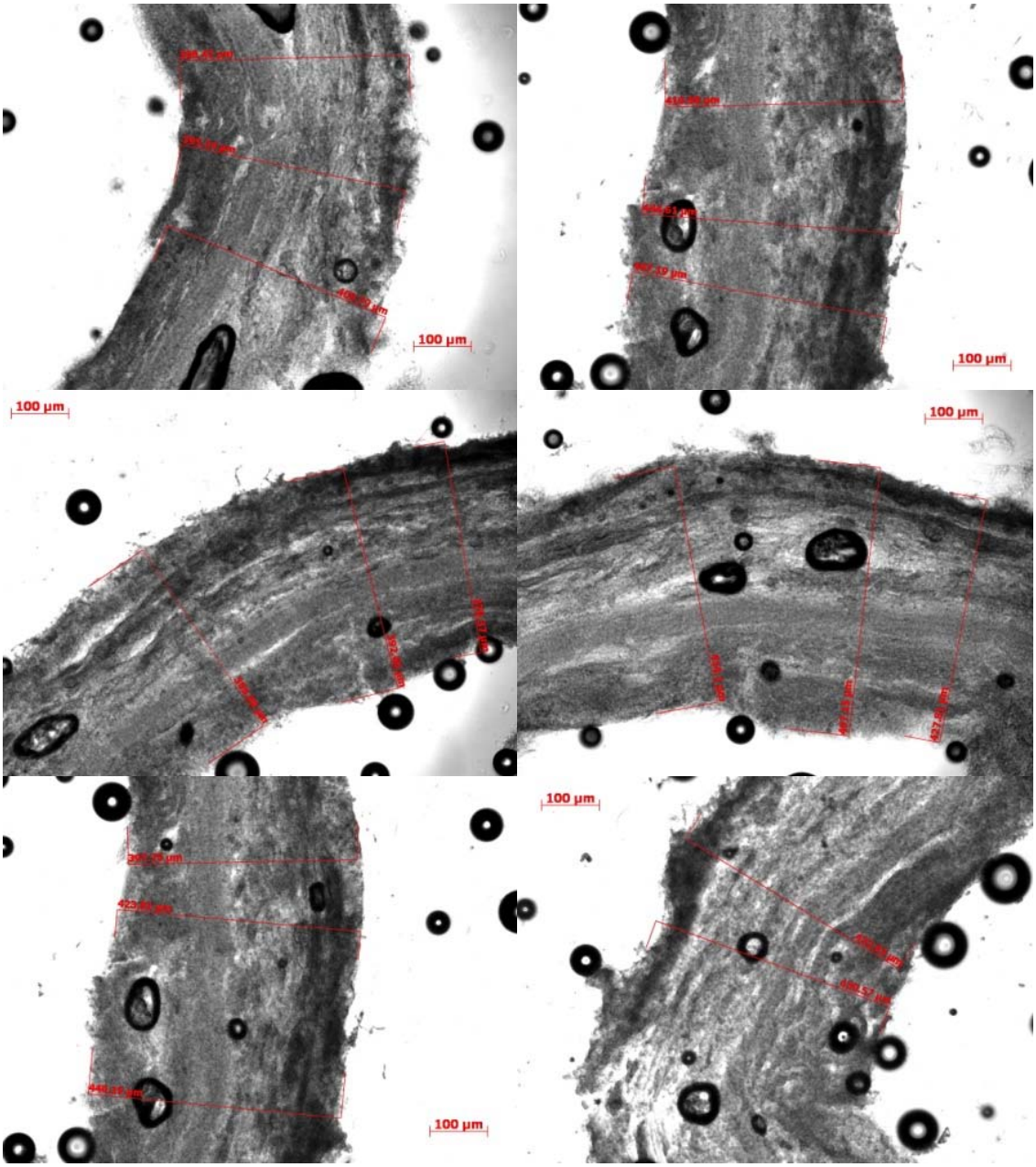

Port 3 Thickness Measurement Images 100X (continued):

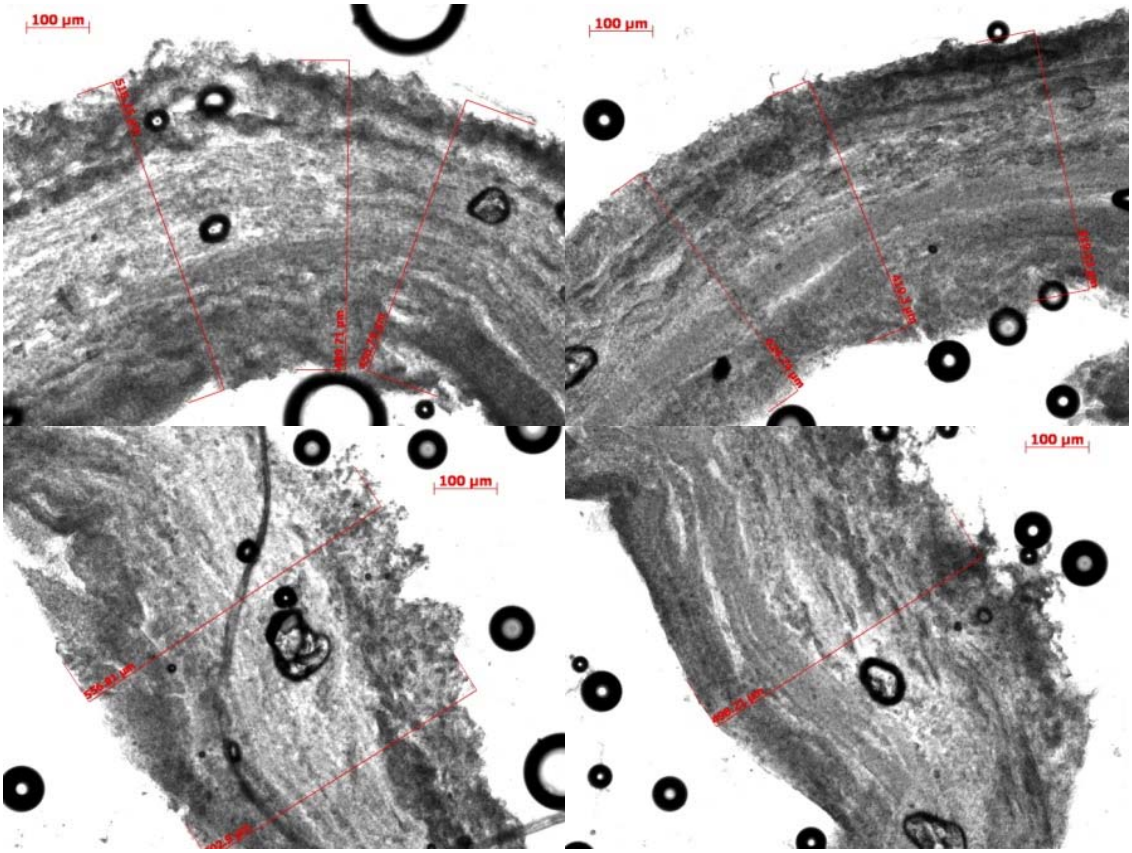

Port 3 Thickness Measurement Images
40X:

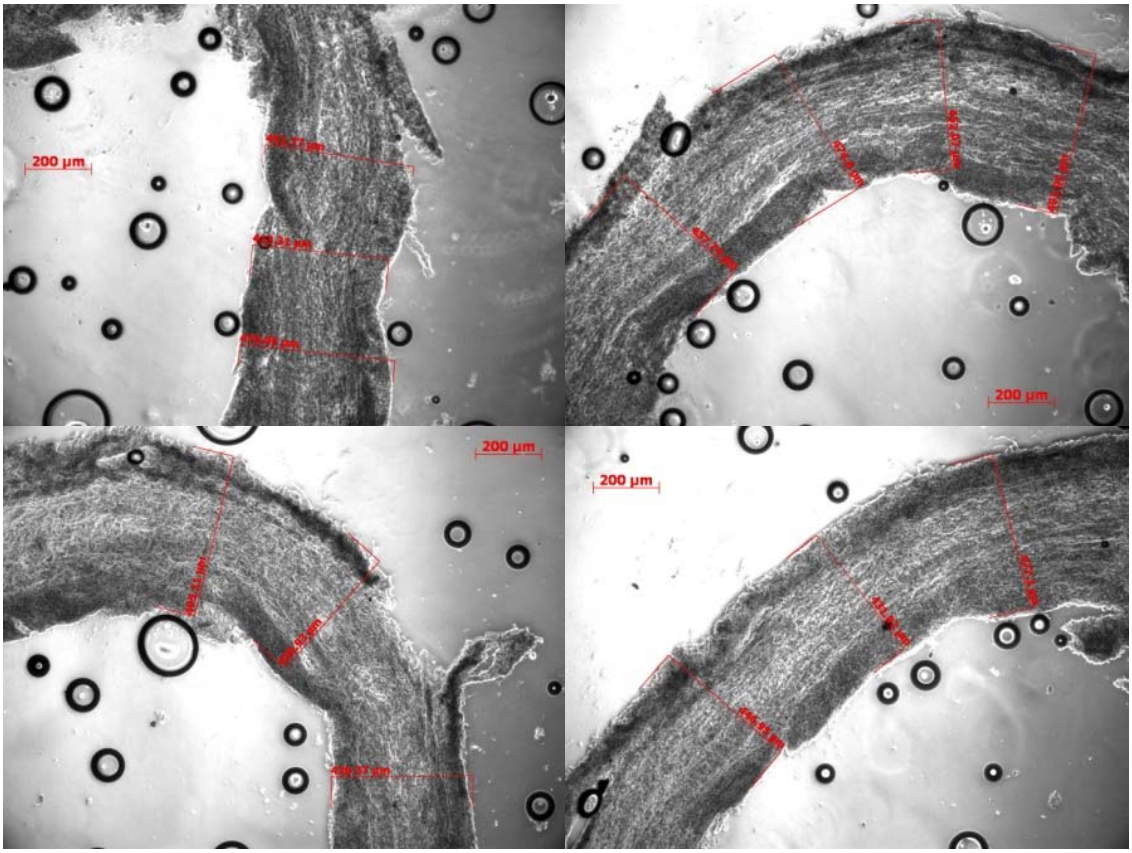

I.4 Port 4 Thickness Measurement Images

100X:

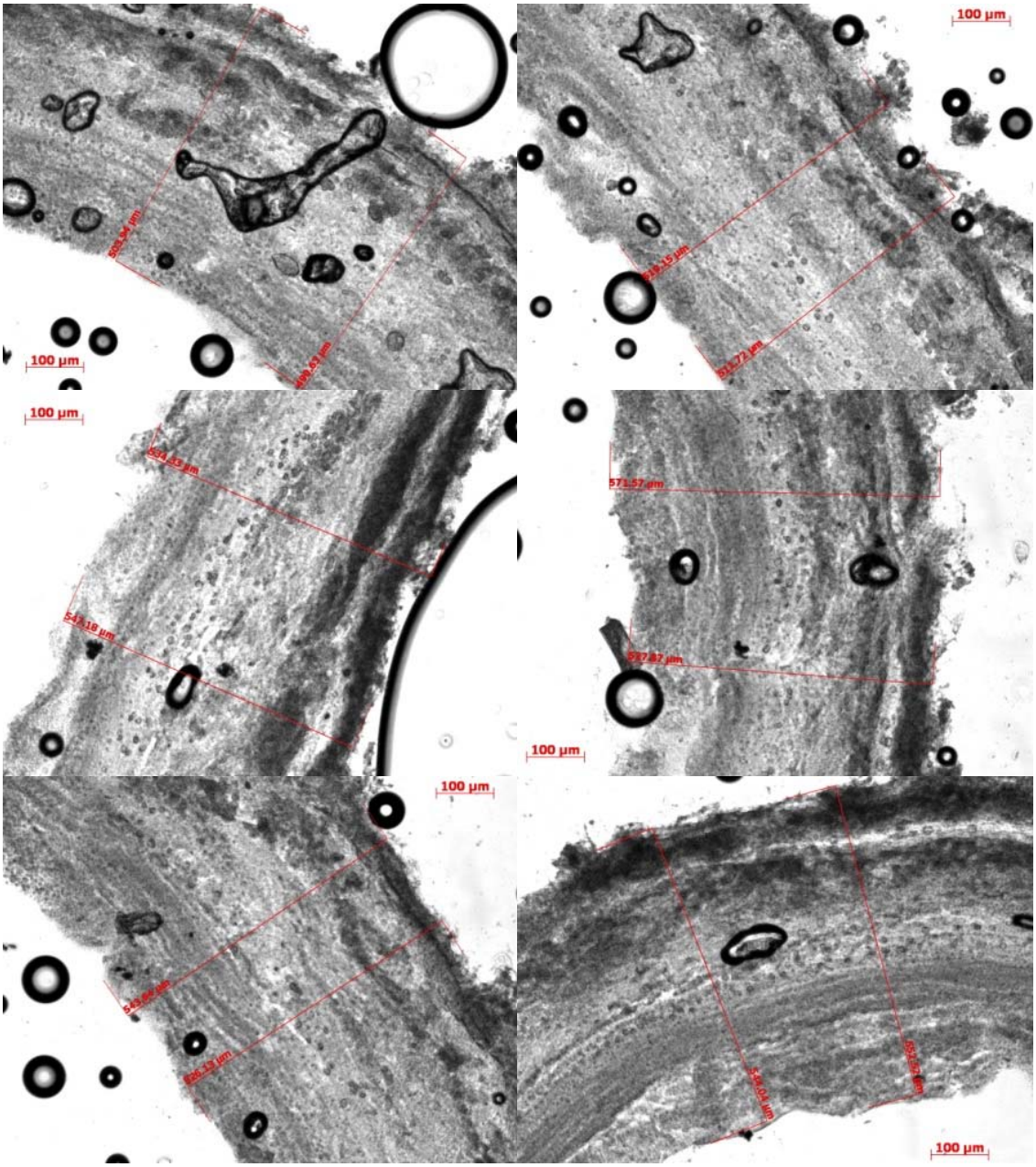

Port 4 Thickness Measurement Images
100X (continued):

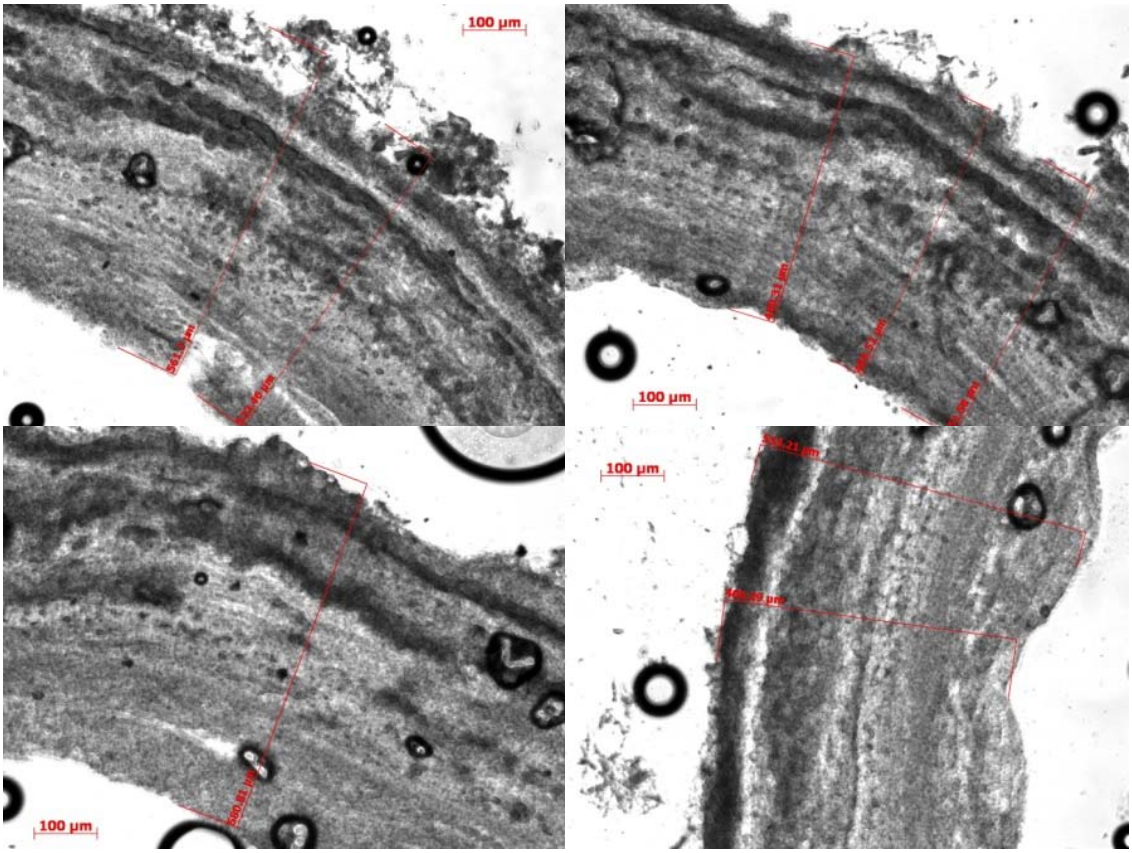

Port 4 Thickness Measurement Images
40X:

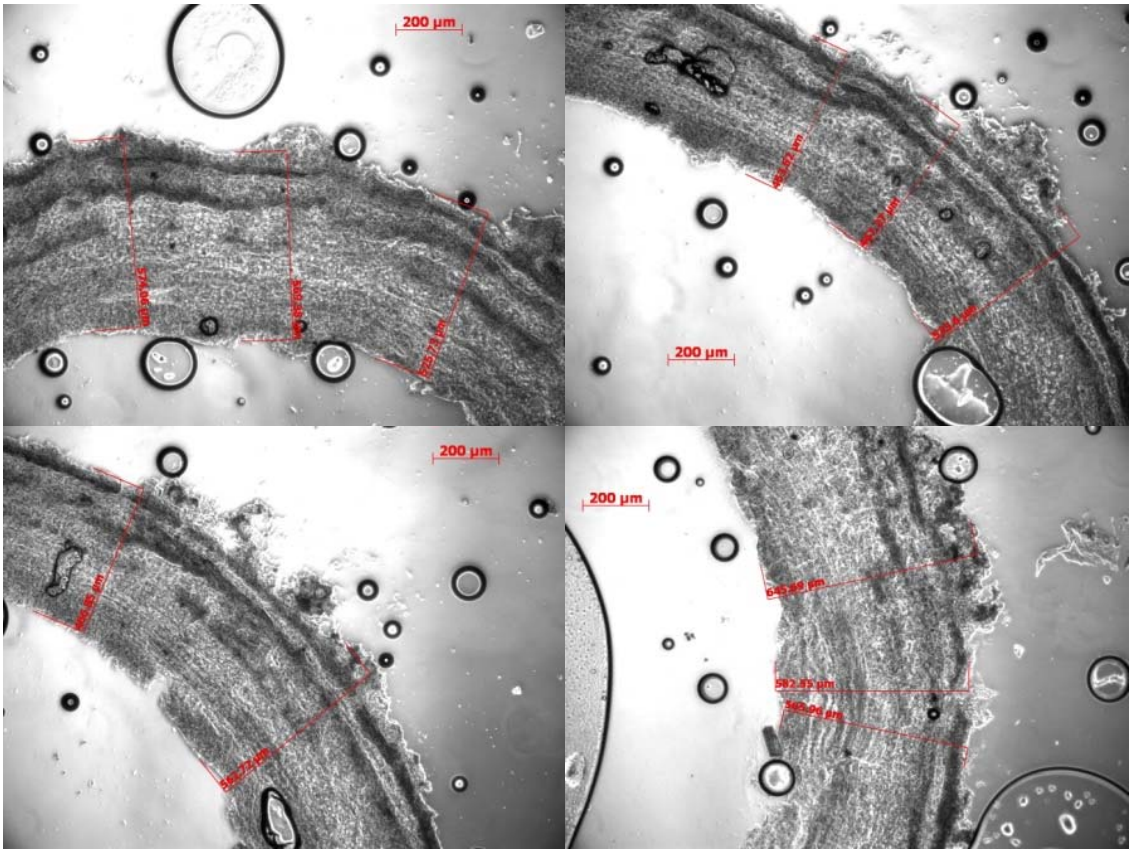

Comments:

All images were taken with Axiovision on an Axioskip 2 (Zeiss MicroImaging, Inc.).

All images were analyzed at either 40X (4X objective) or 100X (10X objective).

Microscope scaling was re-calibrated prior to measurements.

Table I.1. Biofilm thickness measurements.

Port	Image No.	Biofilm Thickness, μm	Average for the Port, μm	Port Std. Deviation, μm	Port 95% Conf. Interval, μm
1	1	542.06	674.4	81.5	28.7
	1	593.55			
	2	650.81			
	2	698.11			
	3	580.00			
	3	580.45			
	4	655.71			
	4	662.34			
	5	677.67			
	6	858.58			
	7	648.97			
	7	747.94			
	8	679.42			
	8	688.93			
	9	554.04			
	9	596.65			
	10	628.59			
	10	613.80			
	11	696.35			
	12	666.56			
	12	672.21			
	12	737.63			
	13	670.72			
	13	691.62			
	13	581.56			
	14	822.86			
	14	690.42			
	14	797.15			
	15	870.49			
	15	686.51			
	15	663.64			

Table I.1. Biofilm thickness measurements, continued.

Port	Image No.	Biofilm Thickness, µm	Average for the Port, µm	Port Std. Deviation, µm	Port 95% Conf. Interval, µm
2	1	963.02	624.7	71.5	25.2
	2	627.10			
	2	630.65			
	3	583.87			
	3	590.06			
	4	697.29			
	4	619.98			
	5	598.58			
	5	602.82			
	6	620.46			
	6	610.43			
	7	617.09			
	7	633.55			
	8	584.61			
	8	647.64			
	9	594.63			
	9	573.74			
	10	562.33			
	10	586.09			
	11	554.54			
	11	620.40			
	11	644.07			
	12	574.70			
	12	577.47			
	12	656.47			
	13	599.71			
	13	612.37			
	13	607.53			
	14	628.86			
	14	697.86			
	14	646.65			

Table I.1. Biofilm thickness measurements, continued.

Port	Image No.	Biofilm Thickness, µm	Average for the Port, µm	Port Std. Deviation, µm	Port 95% Conf. Interval, µm
3	1	398.42	442.9	40.2	12.5
	1	395.24			
	1	409.79			
	2	369.09			
	2	392.66			
	2	370.37			
	3	414.10			
	3	467.15			
	3	427.81			
	4	440.19			
	4	423.82			
	4	397.75			
	5	430.57			
	5	432.93			
	6	456.79			
	6	489.71			
	6	518.25			
	7	419.13			
	7	419.30			
	7	424.74			
	8	502.90			
	8	556.81			
	9	498.21			
	10	410.68			
	10	444.61			
	10	447.19			
	11	452.77			
	11	413.31			
	11	470.05			
	12	437.74			
	12	474.80			
	12	452.07			
	12	493.92			
	13	430.93			
	13	428.37			
	13	495.40			
	14	446.95			
	14	431.82			
	14	477.30			
	15	453.02			

Table I.1. Biofilm thickness measurements, continued.

Port	Image No.	Biofilm Thickness, μm	Average for the Port, μm	Port Std. Deviation, μm	Port 95% Conf. Interval, μm
4	1	503.94	526.3	48.1	16.9
	1	460.63			
	2	511.72			
	2	519.15			
	3	534.33			
	3	547.18			
	4	571.57			
	4	527.87			
	5	526.13			
	5	543.64			
	6	552.52			
	6	544.04			
	7	522.46			
	7	561.30			
	8	440.31			
	8	460.52			
	8	451.58			
	9	580.81			
	10	466.29			
	10	533.21			
	11	525.73			
	11	569.38			
	11	574.06			
	12	533.60			
	12	463.62			
	12	467.27			
	14	466.85			
	14	562.72			
	15	565.96			
	15	582.55			
	15	645.69			

Table I.2. Summary of biofilm thickness measurements.

Port	Thickness, μm	95% Conf. Interv.
1	674.4	28.7
2	624.7	25.2
3	442.9	12.46
4	526.3	16.9

I.5 Biofilm volume calculations

Using the biofilm thickness measurements, a calculation was performed to determine the biofilm volume.

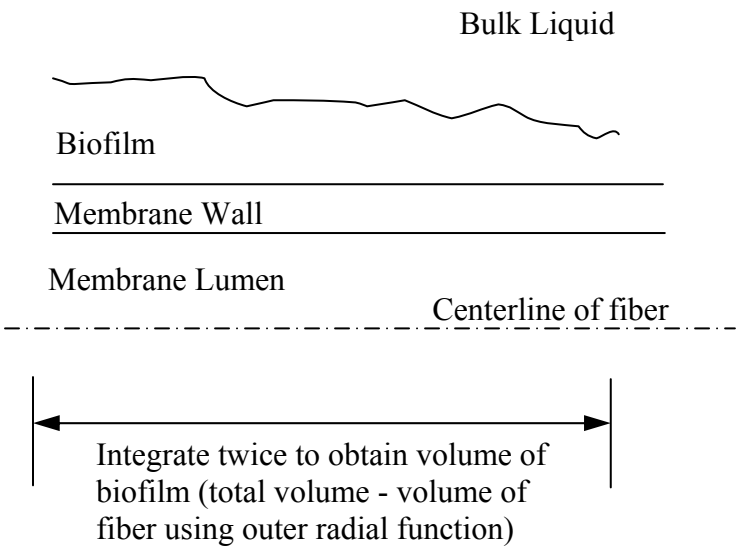

Figure I.1. Schematic of membrane fiber and biofilm

Normalize the thickness so that it is relative to a new datum: the center of the hollow fiber:

Fiber inner diameter: 1.98 mm
Fiber outer diameter: 3.18 mm
Fiber inner radius: 0.99 mm, or 990 μm
Fiber outer radius: 1.59 mm, or 1,590 μm

Table I.3. Biofilm thickness relative to centerline of hollow fiber.

Port	Distance along fiber		Distance of surface from center of fiber		
	inches	mm	um	mm	95% C.I., mm
P1	1	25.40	2264.4	2.26	0.011
P2	4	101.60	2214.7	2.21	0.066
P3	7	177.80	2032.9	2.03	0.028
P4	10	254.00	2116.3	2.12	0.009

C.I. = confidence interval

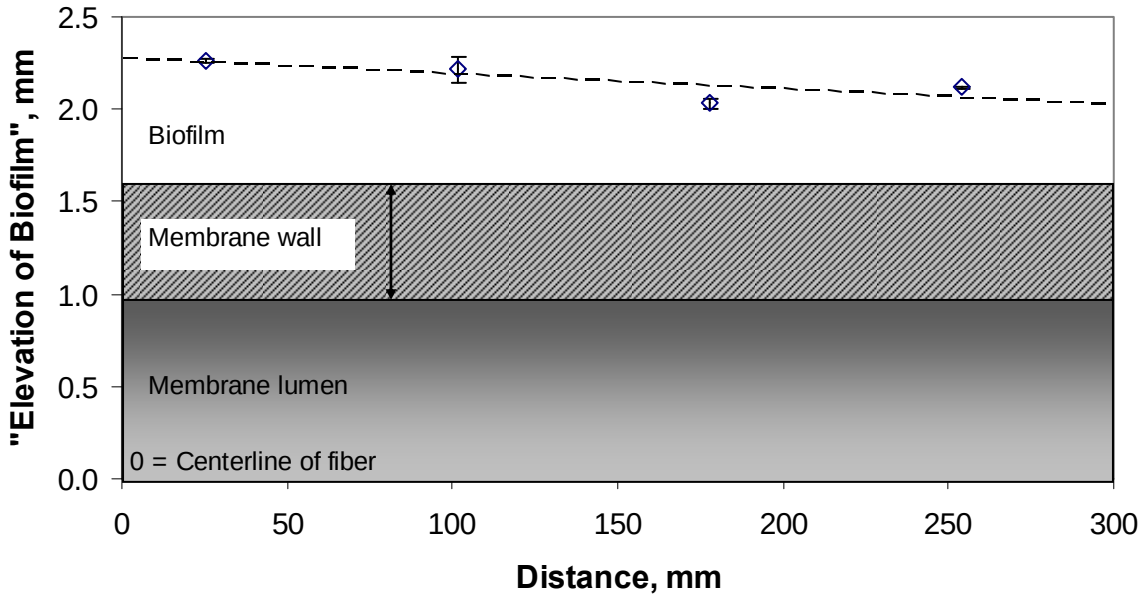

Figure I.2. Biofilm 'elevation' versus distance along hollow fiber.

Results of regression: Elevation, mm = -0.0008213 × (Distance, mm) + 2.272

This is the mathematical function that represents the surface of the biofilm versus distance, relative to the fiber centerline.

The function of the fiber is: Fiber surface, mm = 1.59

By rotating these fibers around the x-axis, a solid of revolution is obtained, giving the volume of each function. The volume of the biofilm is calculated as the volume of revolution for the fiber+biofilm minus the volume of revolution for the fiber alone.

Fiber alone:

Volume = π $(f(x))^2$ x evaluated from 0 to 292 mm, where f(x) = 1.59

$$V_f = \pi \int_0^{292} (1.590)^2 \, dx$$

Volume of 1 hollow fiber = 2,319 mm^3

Fiber plus biofilm:

Volume = π (f(x))^2 x evaluated from 0 to 292 mm, where f(x) = -0.0008213 (x) + 2.272

$$V_{b+f} = \pi \int_0^{292} \left(-8.213x10^{-4}x + 2.272\right)^2 dx$$

$$V_{b+f} = \pi \int_0^{292} \left(6.745^{-7}x^2 - 0.00373x + 5.161\right) dx$$

$$V_{b+f} = \pi \left(\frac{6.754^{-7}x^3}{3} - \frac{0.00373x^2}{2} + 5.161x \right) \Big|_0^{292}$$

$$V_{b+f} = \pi (2.248^{-7}x^3 - 1.866x10^{-3}x^2 + 5.161x) \Big|_0^{292}$$

Volume of fiber plus biofilm for one fiber = 4,252 mm^3

Subtract fiber from fiber plus biofilm:

4,252 mm^3 – 2,319 mm^3 = 1,933 mm^3 of biofilm per fiber

Multiply by the number of fibers:

1,922 mm^3 per fiber × 98 fibers = 189,436 mm^3 of biofilm volume in reactor

Or,

189,436 mm^3 × 1 cm^3/1,000 mm^3 = 189.4 cm^3 of biofilm volume in reactor

From solids analysis:

Total biomass = 7.36 g 'TSS'
6.84 g 'VSS'

Normalized to biofilm volume:

0.0389 g TSS / cm^3, or 38.9 mg TSS / cm^3
0.0361 g VSS / cm^3, or 3.61 mg TSS / cm^3

This equates to a little less than 4% solids.

I.6 Calculation of aerobic region

Minimum O_2 penetration: 50 μm
Maximum O_2 penetration: 90 μm
Mean biofilm thickness: 567 μm
Range of depth that O_2 penetrates = 8.8% to 15.9% of biofilm depth

On a volume basis, for O_2 penetration of 50 μm, the function of the aerobic biofilm is

$$f(x) = 1.59 + 0.05 = 1.64$$

Volume of function rotated about x-axis is

$$V_f = \pi \int_0^{292} (1.640)^2 \, dx$$

Volume of aerobic region + fiber = 2,467 mm^3

Minus volume of fiber

2,467 mm^3 – 2,319 mm^3 = 148 mm^3 per fiber, or 14.52 cm^3 total in reactor

Divided by total biofilm volume in reactor

14.52 cm^3 aerobic / 189.4 cm^3 total = 7.7% of the biofilm volume is aerobic

On a volume basis, for O_2 penetration of 90 μm, the function of the aerobic biofilm is

$$f(x) = 1.59 + 0.09 = 1.68$$

Volume of function rotated about x-axis is

$$V_f = \pi \int_0^{292} (1.680)^2 \, dx$$

Volume of aerobic region + fiber = 2,589 mm^3

Minus volume of fiber

2,589 mm^3 – 2,319 mm^3 = 270 mm^3 per fiber, or 26.46 cm^3 total in reactor

Divided by total biofilm volume in reactor

26.46 cm^3 aerobic / 189.4 cm^3 total = 14.0% of the biofilm volume is aerobic

Therefore, if oxygen penetration ranges from 50 to 90 μm into the biofilm (from the membrane surface), 7.7-14.0% of the biofilm is aerobic or microaerobic.

APPENDIX J

MICROBIAL POPULATION ANALYSES

Appendix J. Microbial population analyses.

J.1. Image analysis approach and procedure.

An example is given to illustrate the method of image processing and relative population determination. See Chapter 4, Methods, for additional details describing the method.

Step 1. After hybridization and mounting, images are captured on the confocal scanning laser microscope (CSLM), using different channels for Cy3, Cy5, and DAPI fluorochromes.

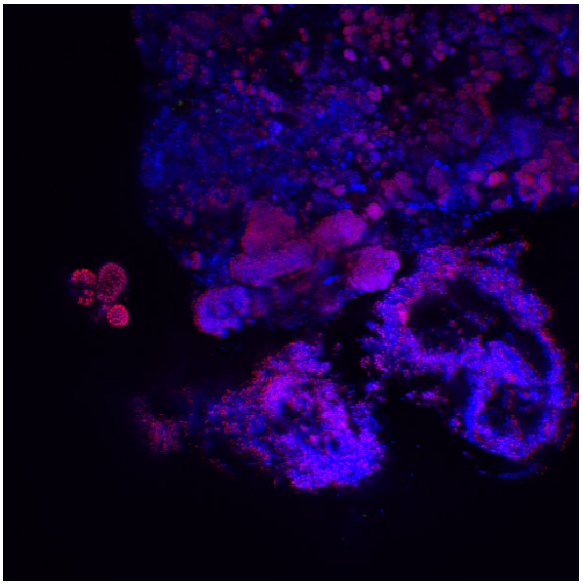

Figure J.1. Example FISH image captured from CSLM.

Step 2. Image files are opened in LSM Image Browser (v. 4.2.0.121, Carl Zeiss MicroImaging, Inc., Thornwood, NY), and each channel images is exported as a .tif file, one image per channel (fluorophore).

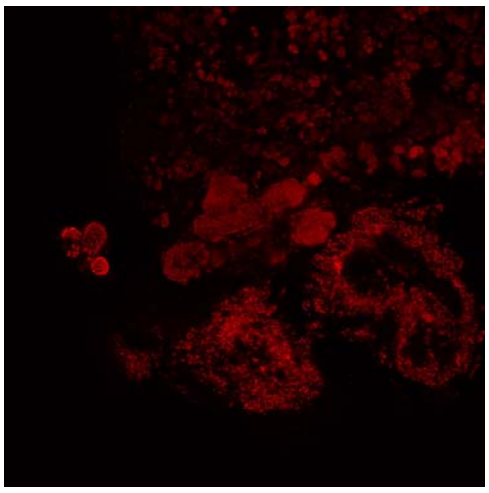

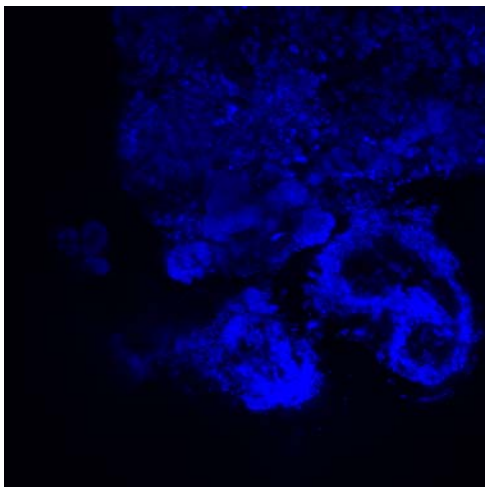

Figure J.2. Example Cy3 channel image. **Figure J.3. Example DAPI channel image.**

Step 3. Images are imported into ImageJ software (v 1.40, NIH, USA), and the background is subtracted with a rolling ball radius of 50 pixels.

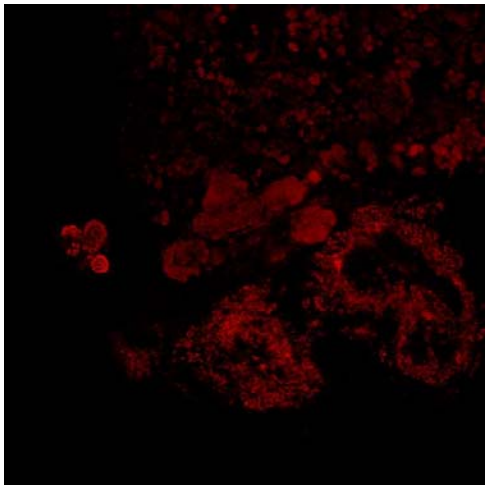

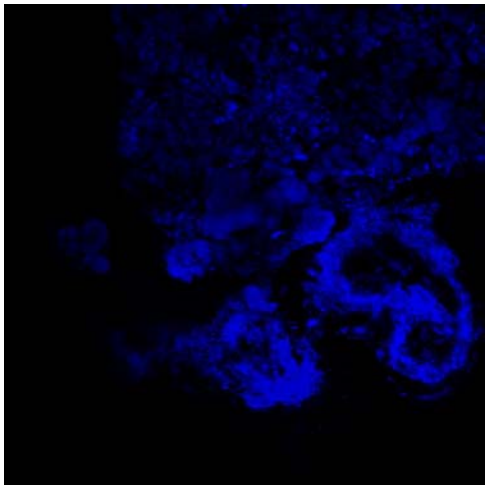

Figure J.4. Background subtracted Cy3. **Figure J.5. Background subtracted DAPI.**

Step 4. Images are converted to 8-bit grayscale images.

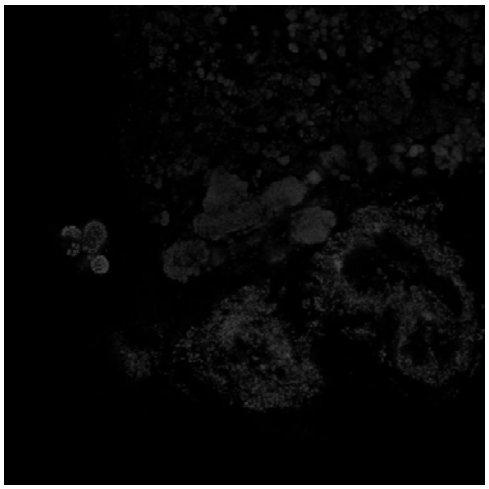

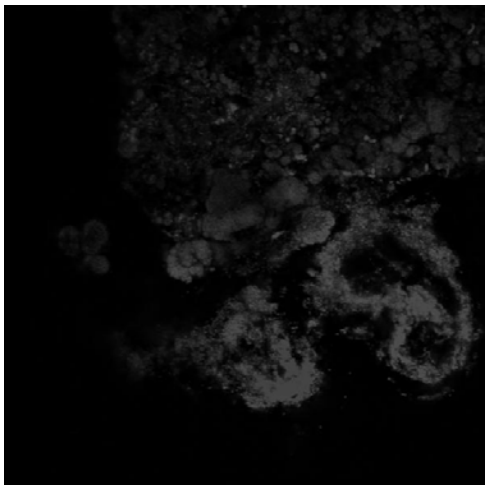

Figure J.6. Cy3 converted to 8-bit. **Figure J.7. DAPI converted to 8-bit.**

Step 5. Images are thresholded based on no-probe controls. Typical thresholds are 15-30 out of 255.

Figure J.8. Thresholded Cy3 image.

Figure J.9. Thresholded DAPI image.

Step 6. Using the software, a measurement is performed, calculating the amount of filled area relative to the total image area:

Cy3 image: 6.61% of total image area DAPI image: 16.14% of total image area

6.61% / 16.14% = 41.0% of DAPI-positive signal area is also Cy3-positive

J.2. Microbial populations along the length of the fibers.

Populations were investigated at three time points during operation and at each of the four ports along the length of the reactor.

Table J.1. Image analysis data for Day 192, Pla46.

Port	Image #	Distance in rctr, cm	DAPI Threshold	DAPI Area %	Pla46 Threshold	Pla46 Area %	Image J max area	DAPI abs area	Pla abs area	Pla area, % of DAPI	Mean	Stdev, in %	95% CI
Port 1	1	2.5	23	3.107	15	0.129	389376	12097.9	502.3	4.2%	0.53%	1.280	0.7934
	2	2.5	23	8.457	15	0.003		32929.5	11.7	0.0%			
	3	2.5	23	5.311	15	0.003		20679.8	11.7	0.1%			
	4	2.5	23	20.824	15	0.104		81083.7	405.0	0.5%			
	5	2.5	23	20.77	15	0.041		80873.4	159.6	0.2%			
	6	2.5	23	4.453	15	0		17338.9	0.0	0.0%			
	7	2.5	23	15.547	15	0.004		60536.3	15.6	0.0%			
	8	2.5	23	4.353	15	0.003		16949.5	11.7	0.1%			
	9	2.5	23	5.492	15	0.013		21384.5	50.6	0.2%			
	10	2.5	23	7.659	15	0.005		29822.3	19.5	0.1%			
Port 2	1	10.2	23	11.542	15	0.028		44941.8	109.0	0.2%	0.24%	0.286	0.1771
	2	10.2	23	13.085	15	0.117		50949.8	455.6	0.9%			
	3	10.2	23	9.732	15	0.009		37894.1	35.0	0.1%			
	4	10.2	23	4.165	15	0.005		16217.5	19.5	0.1%			
	5	10.2	23	17.747	15	0.017		69102.6	66.2	0.1%			
	6	10.2	23	24	15	5.73E-04		93450.2	2.2	0.0%			
	7	10.2	23	11.743	15	0.006		45724.4	23.4	0.1%			
	8	10.2	23	16.661	15	0.006		64873.9	23.4	0.0%			
	9	10.2	23	7.311	15	0.023		28467.3	89.6	0.3%			
	10	10.2	23	8.384	15	0.048		32645.3	186.9	0.6%			
Port 3	1	17.8	23	13.973	15	0.005		54407.5	19.5	0.0%	0.57%	0.644	0.3988
	2	17.8	23	10.35	15	0.132		40300.4	514.0	1.3%			
	3	17.8	23	7.31	15	0.005		28463.4	19.5	0.1%			
	4	17.8	23	28.74	15	0.026		111906.7	101.2	0.1%			
	5	17.8	23	10.016	15	0.084		38999.9	327.1	0.8%			
	6	17.8	23	8.387	15	6.00E-03		32657.0	23.4	0.1%			
	7	17.8	23	4.535	15	0.047		17658.2	183.0	1.0%			
	8	17.8	23	7.226	15	0.132		28136.3	514.0	1.8%			
	9	17.8	23	3.864	15	0.016		15045.5	62.3	0.4%			
	10	17.8	23	8.078	15	2.86E-04		31453.8	1.1	0.0%			
Port 4	1	25.4	23	7.557	15	0.041		29425.1	159.6	0.5%	0.27%	0.257	0.1594
	2	25.4	23	4.396	15	0.001		17117.0	3.9	0.0%			
	3	25.4	23	1.166	15	0		4540.1	0.0	0.0%			
	4	25.4	23	8.451	15	0.026		32906.2	101.2	0.3%			
	5	25.4	23	4.329	15	0.035		16856.1	136.3	0.8%			
	6	25.4	23	6.037	15	2.30E-02		23506.6	89.6	0.4%			
	7	25.4	23	7.417	15	0.008		28880.0	31.2	0.1%			
	8	25.4	23	10.711	15	0.004		41706.1	15.6	0.0%			
	9	25.4	23	8.201	15	0.02		31932.7	77.9	0.2%			
	10	25.4	23	8.369	15	0.019		32586.9	74.0	0.2%			

Table J.2. Image analysis data for Day 192, Nso190.

Port	Image #		DAPI Ch. Threshold	DAPI Ch. Area %	Nso190 Threshold	Nso190 Area %	Image J max area	DAPI abs area	Nso abs area	Nso area % of DAPI	Mean	Stdev, in %	95% CI
Port 1	1	2.5	25	19.082	20	7.246	389376	74300.7	28214.2	38.0%	22.7%	18.114	11.2271
	2	2.5	25	19.827	20	3.418		77201.6	13308.9	17.2%			
	3	2.5	25	12.989	20	0.542		50576.0	2110.4	4.2%			
	4	2.5	25	11.957	20	1.294		46557.7	5038.5	10.8%			
	5	2.5	25	19.876	20	2.846		77392.4	11081.6	14.3%			
	6	2.5	25	11.829	20	2.178		46059.3	8480.6	18.4%			
	7	2.5	25	5.986	20	1.068		23308.0	4158.5	17.8%			
	8	2.5	25	4.854	20	3.13		18900.3	12187.5	64.5%			
	9	2.5	25	16.764	20	1.288		65275.0	5015.2	7.7%			
	10	2.5	25	7.653	20	2.583		29798.9	10057.6	33.8%			
Port 2	1	10.2	25	4.474	20	0.847		17420.7	3298.0	18.9%	30.9%	24.474	14.4628
	2	10.2	25	9.67	20	4.285		37652.7	16684.8	44.3%			
	3	10.2	25	3.703	20	0.701		14418.6	2729.5	18.9%			
	4	10.2	25	14.482	20	1.482		56389.4	5770.6	10.2%			
	5	10.2	25	12.314	20	2.221		47947.8	8648.0	18.0%			
	6	10.2	25	8.035	20	7.186		31286.4	27980.6	89.4%			
	7	10.2	25	5.762	20	2.012		22435.8	7834.2	34.9%			
	8	10.2	25	18.642	20	1.448		72587.5	5638.2	7.8%			
	9	10.2	25	13.244	20	2.851		51569.0	11101.1	21.5%			
	10	10.2	25	3.09	20	0.562		12031.7	2188.3	18.2%			
	11	10.2	25	16.14	20	9.269		62845.3	36091.3	57.4%			
Port 3	1	17.8	25	5.453	20	1.707		21232.7	6646.6	31.3%	33.2%	20.985	13.0063
	2	17.8	25	1.981	20	0.086		7713.5	334.9	4.3%			
	3	17.8	25	6.178	20	0.734		24055.6	2858.0	11.9%			
	4	17.8	25	1.462	20	0.495		5692.7	1927.4	33.9%			
	5	17.8	25	1.288	20	0.525		5015.2	2044.2	40.8%			
	6	17.8	25	6.103	20	1.326		23763.6	5163.1	21.7%			
	7	17.8	25	2.552	20	1.026		9936.9	3995.0	40.2%			
	8	17.8	25	10.777	20	8.726		41963.1	33976.9	81.0%			
	9	17.8	25	16.755	20	7.103		65239.9	27657.4	42.4%			
	10	17.8	25	6.367	20	1.59		24791.6	6191.1	25.0%			
Port 4	1	25.4	25	9.086	20	5.997		35378.7	23350.9	66.0%	37.1%	18.302	11.3437
	2	25.4	25	12.576	20	4.509		48967.9	17557.0	35.9%			
	3	25.4	25	8.293	20	4.777		32291.0	18600.5	57.6%			
	4	25.4	25	5.5	20	0.403		21415.7	1569.2	7.3%			
	5	25.4	25	3.694	20	0.72		14383.5	2803.5	19.5%			
	6	25.4	25	8.478	20	3.295		33011.3	12829.9	38.9%			
	7	25.4	25	7.706	20	4.066		30005.3	15832.0	52.8%			
	8	25.4	25	4.577	20	1.123		17821.7	4372.7	24.5%			
	9	25.4	25	4.561	20	1.189		17759.4	4629.7	26.1%			
	10	25.4	25	4.605	20	1.973		17930.8	7682.4	42.8%			

Table J.3. Image analysis data for Day 192, NIT3.

Port	Image #		DAPI Ch. Threshold	DAPI Ch. Area %	NIT3 Threshold	NIT3 Area %	Image J max area	DAPI abs area	NIT3 abs area	NIT3 area, % of DAPI	Mean	Stdev, in %	95% CI
Port 1	1	2.5	25	2.423	10	0.253	389376	9434.6	985.1	10.4%	4.1%	2.724	1.6885
	2	2.5	25	6.484	10	0.204		38976.5	794.3	2.0%			
	3	2.5	25	6.079	10	0.344		31009.9	1339.5	4.3%			
	4	2.5	25	7.964	10	0.249		23670.2	969.5	4.1%			
	5	2.5	25	10.01	10	0.358		25247.1	1394.0	5.5%			
	6	2.5	20	12.997	20	0.699		50607.2	2721.7	5.4%			
	7	2.5	20	12.055	20	0.537		46939.3	2090.9	4.5%			
	8	2.5	20	17.209	20	0.178		67007.7	693.1	1.0%			
	9	2.5	20	7.949	20	0.226		30951.5	880.0	2.8%			
	10	2.5	20	7.314	20	0.099		28479.0	385.5	1.4%			
Port 2	1	10.2	25	5.93	10	0.38		23097.8	1479.6	6.4%	1.9%	2.211	1.3702
	2	10.2	25	13.88	10	0.67		54025.9	2608.8	4.8%			
	3	10.2	25	10.00	10	0.12		38941.5	467.3	1.2%			
	4	10.2	25	7.84	10	0.28		30527.1	1070.8	3.5%			
	5	10.2	25	12.83	10	0.15		49972.5	564.6	1.1%			
	6	10.2	20	11.492	20	0.012		44747.1	46.7	0.1%			
	7	10.2	20	20.408	20	0.028		79463.9	109.0	0.1%			
	8	10.2	20	15.739	20	0.062		61283.9	241.4	0.4%			
	9	10.2	20	18.976	20	0.14		73888.0	545.1	0.7%			
	10	10.2	20	10.888	20	0.074		42395.3	288.1	0.7%			
Port 3	1	17.8	25	7.35	10	0.21		28615.2	825.5	2.9%	6.5%	8.245	5.1100
	2	17.8	25	10.74	10	0.27		41826.8	1047.4	2.5%			
	3	17.8	20	3.44	10	0.81		13390.6	3138.4	23.4%			
	4	17.8	25	5.23	10	0.02		20344.9	70.1	0.3%			
	5	17.8	25	7.80	10	0.71		30383.0	2760.7	9.1%			
	6	17.8	20	3.44	10	0.66		13379.0	2550.4	19.1%			
	7	17.8	20	11.046	20	0.062		43010.5	241.4	0.6%			
	8	17.8	20	4.78	20	0.206		18612.2	802.1	4.3%			
	9	17.8	20	15.238	20	0.417		59333.1	1623.7	2.7%			
	10	17.8	20	22.546	20	0.053		87788.7	206.4	0.2%			
Port 4	1	25.4	25	5.04	10	0.75		19605.1	2908.6	14.8%	14.9%	16.363	10.1419
	2	25.4	20	9.42	10	3.33		36683.1	12974.0	35.4%			
	3	25.4	20	1.61	10	0.63		6261.2	2445.3	39.1%			
	4	25.4	25	2.91	10	1.12		11319.2	4372.7	38.6%			
	5	25.4	25	4.05	10	0.0003		15769.7	1.1	0.0%			
	6	25.4	20	19.162	20	0.761		74612.2	2963.2	4.0%			
	7	25.4	20	9.265	20	0.515		36075.7	2005.3	5.6%			
	8	25.4	20	5.547	20	0.571		21598.7	2223.3	10.3%			
	9	25.4	20	23.296	20	0.306		90709.0	1191.5	1.3%			
	10	25.4	20	7.59	20	0.031		29553.6	120.7	0.4%			

Table J.4. Image analysis data for Day 192, Ntspa662.

Port	Image #		DAPI Ch. Threshold	DAPI Ch. Area %	Ntspa Threshold	Ntspa Area %	Image J max area	DAPI abs area	Ntspa abs area	Ntspa area, % of DAPI	Mean	Stdev, in %	95% CI
Port 1	1	2.5	25	4.69	10	0.14	389376	18250.1	537.3	2.9%	9.1%	11.683	7.2411
	2	2.5	25	21.61	10	0.07		84132.5	280.4	0.3%			
	3	2.5	25	3.63	10	0.07		14122.7	284.2	2.0%			
	4	2.5	25	17.76	10	0.51		69145.4	1989.7	2.9%			
	5	2.5	25	8.31	10	0.47		32341.6	1826.2	5.6%			
	6	2.5	25	5.10	10	0.15		19854.3	599.6	3.0%			
	7	2.5	25	8.98	10	0.53		34954.3	2067.6	5.9%			
	8	2.5	20	12.44	10	4.54		48426.7	17693.2	36.5%			
	9	2.5	25	10.66	10	2.52		41499.7	9827.9	23.7%			
	10	2.5	25	9.59	10	0.82		37356.7	3177.3	8.5%			
Port 2	1	10.2	25	5.37	15	0.165		20890.0	642.5	3.1%	19.0%	20.169	12.5008
	2	10.2	25	1.04	30	0.46		4065.1	1787.2	44.0%			
	3	10.2	25	2.24	15	0.06		8722.0	241.4	2.8%			
	4	10.2	25	3.87	15	0.06		15065.0	245.3	1.6%			
	5	10.2	25	7.22	15	0.27		28093.5	1059.1	3.8%			
	6	10.2	25	9.59	15	0.14		37337.3	525.7	1.4%			
	7	10.2	25	3.73	15	1.57		14508.1	6124.9	42.2%			
	8	10.2	15	15.60	35	5.64		60750.4	21968.6	36.2%			
	9	10.2	25	9.39	15	0.85		36570.2	3305.8	9.0%			
	10	10.2	20	6.88	30	3.18		26781.3	12397.7	46.3%			
Port 3	1	17.8	20	15.03	15	0.337		58523.2	1312.2	2.2%	4.4%	4.251	2.6345
	2	17.8	20	13.59	15	0.294		52900.6	1144.8	2.2%			
	3	17.8	20	2.99	15	0.366		11638.4	1425.1	12.2%			
	4	17.8	20	12.63	15	0.488		49166.5	1900.2	3.9%			
	5	17.8	20	13.30	15	1.300		51794.8	5061.9	9.8%			
	6	17.8	20	12.04	15	0.100		46888.7	389.4	0.8%			
	7	17.8	20	6.54	15	0.173		25453.5	673.6	2.6%			
	8	17.8	20	11.52	15	0.076		44836.6	295.9	0.7%			
	9	17.8	20	6.04	15	0.526		23530.0	2048.1	8.7%			
	10	17.8	20	7.48	15	0.050		29129.2	194.7	0.7%			
Port 4	1	25.4	20	6.156	15	0.214		23970.0	833.3	3.5%	11.4%	15.845	9.8204
	2	25.4	20	5.857	15	1.323		22805.8	5151.4	22.6%			
	3	25.4	20	6.409	15	0.569		24955.1	2215.5	8.9%			
	4	25.4	20	6.907	15	1.422		26894.2	5536.9	20.6%			
	5	25.4	20	18.953	15	0.377		73798.4	1467.9	2.0%			
	6	25.4	20	2.71	15	1.359		10552.1	5291.6	50.1%			
	7	25.4	20	5.935	15	0.07		23109.5	272.6	1.2%			
	8	25.4	20	17.131	15	0.089		66704.0	346.5	0.5%			
	9	25.4	20	4.978	15	0.032		19383.1	124.6	0.6%			
	10	25.4	20	14.616	15	0.61		56911.2	2375.2	4.2%			

Table J.5. Image analysis data for Day 325, Pla46.

Port	Image #	DAPI Ch. Threshold	DAPI Ch. Area %	Pla46 Threshold	Pla46 Area %	Image J max area	DAPI abs area	Pla abs area	Pla area, % of DAPI	Mean	Stdev, in %	95% CI
Port 1	1	25	12.743	15	5.73E-04	389376	49618.2	2.2	0.0%	0.4%	0.521	0.3232
	2	25	3.172	15	0.054		12351.0	210.3	1.7%			
	3	25	3.966	15	0.027		15442.7	105.1	0.7%			
	4	25	10.283	15	0.008		40039.5	31.2	0.1%			
	5	25	8.326	15	0.001		32419.4	3.9	0.0%			
	6	25	15.477	15	0.011		60263.7	42.8	0.1%			
	7	25	12.703	15	0.006		49462.4	23.4	0.0%			
	8	25	6.837	15	0.025		26621.6	97.3	0.4%			
	9	25	7.530	15	0.019		29320.0	74.0	0.3%			
	10	25	8.963	15	0.046		34899.8	179.1	0.5%			
Port 2	1	25	6.354	15	2.86E-04		24741.0	1.1	0.0%	0.11%	0.176	0.1093
	2	25	9.061	15	8.59E-04		35281.4	3.3	0.0%			
	3	25	9.412	15	0.003		36648.1	11.7	0.0%			
	4	25	12.380	15	0		48204.7	0.0	0.0%			
	5	25	8.165	15	0		31792.6	0.0	0.0%			
	6	25	6.855	15	0.001		26691.7	3.9	0.0%			
	7	25	9.282	15	0.032		36141.9	124.6	0.3%			
	8	25	10.594	15	0.002		41250.5	7.8	0.0%			
	9	25	2.975	15	0.015		11583.9	58.4	0.5%			
	10	25	18.521	15	0.025		72116.3	97.3	0.1%			
Port 3	1	25	6.144	15	3.40E-02		23923.3	132.4	0.6%	0.30%	0.317	0.1962
	2	25	12.525	15	6.00E-03		48769.3	23.4	0.0%			
	3	25	10.894	15	0.076		42418.6	295.9	0.7%			
	4	25	3.770	15	0.01		14679.5	38.9	0.3%			
	5	25	8.306	15	0.004		32341.6	15.6	0.0%			
	6	25	3.991	15	0.016		15540.0	62.3	0.4%			
	7	25	4.765	15	0.042		18553.8	163.5	0.9%			
	8	25	11.625	15	0.005		45265.0	19.5	0.0%			
	9	25	10.343	15	0.008		40273.2	31.2	0.1%			
	10	25	8.374	15	2.86E-04		32606.3	1.1	0.0%			

Table J.5. Image analysis data for Day 325, Pla46., continued.

Port	Image #	DAPI Ch. Threshold	DAPI Ch. Area %	Pla46 Threshold	Pla46 Area %	Image J max area	DAPI abs area	Pla abs area	Pla area, % of DAPI	Mean	Stdev, in %	95% CI
Port 4	1	25	3.461	15	0.06		13476.3	233.6	1.7%	0.57%	0.682	0.4224
	2	25	6.476	15	0.122		25216.0	475.0	1.9%			
	3	25	3.302	15	0.005		12857.2	19.5	0.2%			
	4	25	8.231	15	0.019		32049.5	74.0	0.2%			
	5	25	4.579	15	0.028		17829.5	109.0	0.6%			
	6	25	7.162	15	0.023		27887.1	89.6	0.3%			
	7	25	2.657	15	0.015		10345.7	58.4	0.6%			
	8	25	3.667	15	0		14278.4	0.0	0.0%			
	9	25	8.802	15	0.011		34272.9	42.8	0.1%			
	10	25	8.272	15	0.008		32209.2	31.2	0.1%			
P2 regrowt	1	25	7.277	15	0.028		28334.9	109.0	0.4%	2.3%	3.197	2.5581
	2	25	16.255	15	0.492		63293.1	1915.7	3.0%			
	3	25	15.648	15	0.194		60929.6	755.4	1.2%			
	4	25	10.762	15	0.037		41904.6	144.1	0.3%			
	5	25	3.580	15	0.305		13939.7	1187.6	8.5%			
	6	25	11.259	15	0.055		43839.8	214.2	0.5%			

Table J.6. Image analysis data for Day 325, Nso190.

Port	Image #	DAPI Ch. Threshold	DAPI Ch. Area %	Nso190 Threshold	Nso190 Area %	Image J max area	DAPI abs area	Nso abs area	Nso area % of DAPI	Mean	Stdev, in %	95% CI
Port 1	1	25	10.263	25	0.322	389376	39961.7	1253.8	3.1%	26.7%	32.694	20.26
	2	25	9.458	25	0.159		36827.2	619.1	1.7%			
	3	25	6.726	25	2.455		26189.4	9559.2	36.5%			
	4	25	9.853	25	7.984		38365.2	31087.8	81.0%			
	5	25	10.076	25	0.114		39233.5	443.9	1.1%			
	6	25	5.671	25	0.21		22081.5	817.7	3.7%			
	7	25	10.065	25	0.453		39190.7	1763.9	4.5%			
	8	25	7.058	25	0.347		27482.2	1351.1	4.9%			
	9	25	5.703	25	3.069		22206.1	11949.9	53.8%			
	10	25	3.52	25	2.702		13706.0	10520.9	76.8%			
Port 2	1	25	7.001	25	1.19		27260.2	4633.6	17.0%	7.0%	8.732	5.41
	2	25	11.755	25	0.184		45771.1	716.5	1.6%			
	3	25	13.55	25	0.167		52760.4	650.3	1.2%			
	4	25	10.448	25	0.03		40682.0	116.8	0.3%			
	5	25	3.505	25	0.708		13647.6	2756.8	20.2%			
	6	25	4.831	25	0.027		18810.8	105.1	0.6%			
	7	25	11.654	25	0.218		45377.9	848.8	1.9%			
	8	25	3.946	25	0.839		15364.8	3266.9	21.3%			
	9	25	3.027	25	0.072		11786.4	280.4	2.4%			
	10	25	1.283	25	0.046		4995.7	179.1	3.6%			
Port 3	1	25	6.185	25	0.191		24082.9	743.7	3.1%	15.1%	22.211	13.77
	2	25	5.368	25	4.043		20901.7	15742.5	75.3%			
	3	25	5.806	25	1.028		22607.2	4002.8	17.7%			
	4	25	12.001	25	0.77		46729.0	2998.2	6.4%			
	5	25	14.485	25	1.177		56401.1	4583.0	8.1%			
	6	25	9.125	25	2.044		35530.6	7958.8	22.4%			
	7	25	6.427	25	0.57		25025.2	2219.4	8.9%			
	8	25	10.646	25	0.353		41453.0	1374.5	3.3%			
	9	25	7.835	25	0.484		30507.6	1884.6	6.2%			
	10	25	4.985	25	0		19410.4	0.0	0.0%			

Table J.6. Image analysis data for Day 325, Nso190, continued.

Port	Image #	DAPI Ch. Threshold	DAPI Ch. Area %	Nso190 Threshold	Nso190 Area %	Image J max area	DAPI abs area	Nso abs area	Nso area % of DAPI	Mean	Stdev, in %	95% CI
Port 4	1	25	5.085	25	0.349		19799.8	1358.9	6.9%	7.0%	8.315	5.15
	2	25	3.596	25	0.857		14002.0	3337.0	23.8%			
	3	25	9.651	25	0.031		37578.7	120.7	0.3%			
	4	25	6.69	25	0.029		26049.3	112.9	0.4%			
	5	25	6.896	25	0.062		26851.4	241.4	0.9%			
	6	25	13.065	25	1.559		50872.0	6070.4	11.9%			
	7	25	7.717	25	0.155		30048.1	603.5	2.0%			
	8	25	4.713	25	0.26		18351.3	1012.4	5.5%			
	9	25	5.407	25	0.02		21053.6	77.9	0.4%			
	10	25	5.579	25	0.998		21723.3	3886.0	17.9%			
P2 Regrow	1	25	7.895	25	0.074		30741.2	288.1	0.9%	4.4%	3.228	2.00
	2	25	9.163	25	0.705		35678.5	2745.1	7.7%			
	3	25	9.432	25	0.636		36725.9	2476.4	6.7%			
	4	25	16.078	25	0.393		62603.9	1530.2	2.4%			
	5	25	6.776	25	0.177		26384.1	689.2	2.6%			
	6	25	6.84	25	0.124		26633.3	482.8	1.8%			
	7	25	3.381	25	0.216		13164.8	841.1	6.4%			
	8	25	9.113	25	0.951		35483.8	3703.0	10.4%			
	9	25	8.171	25	0.302		31815.9	1175.9	3.7%			
	10	25	13.193	25	0.146		51370.4	568.5	1.1%			

Table J.7. Image analysis data for Day 325, NIT3.

Port	Image #	DAPI Ch. Threshold	DAPI Ch. Area %	NIT3 Threshold	NIT3 Area %	Image J max area	DAPI abs area	NIT3 abs area	NIT3 area, % of DAPI	Mean	Stdev, in %	95% CI
Port 1	1	25	10.178	20	0.013	389376	39630.7	50.6	0.1%	0.3%	0.258	0.1598
	2	25	12.701	20	0.036		49454.6	140.2	0.3%			
	3	25	20.008	20	0.068		77906.4	264.8	0.3%			
	4	25	5.359	20	0.026		20866.7	101.2	0.5%			
	5	25	11.221	20	0.094		43691.9	366.0	0.8%			
	6	25	3.431	20	0.003		13359.5	11.7	0.1%			
	7	25	13.272	20	0.082		51678.0	319.3	0.6%			
	8	25	6.171	20	0.019		24028.4	74.0	0.3%			
	9	25	7.2	20	0.008		28035.1	31.2	0.1%			
	10	25	4.873	20	0.002		18974.3	7.8	0.0%			
Port 2	1	25	15.815		0.002		61579.8	7.8	0.0%	1.3%	3.521	2.1824
	2	25	12.062		0.056		46966.5	218.1	0.5%			
	3	25	9.158		0.024		35659.1	93.5	0.3%			
	4	25	15.72		3.81E-04		61209.9	1.5	0.0%			
	5	25	5.913		0.669		23023.8	2604.9	11.3%			
	6	25	3.599		0		14013.6	0.0	0.0%			
	7	25	7.093		0.02		27618.4	77.9	0.3%			
	8	25	6.453		0.031		25126.4	120.7	0.5%			
	9	25	6.779		0.017		26395.8	66.2	0.3%			
	10	25	14.193		0		55264.1	0.0	0.0%			
Port 3	1	25	6.363		0.309		24776.0	1203.2	4.9%	7.1%	5.779	3.5815
	2	25	7.179		1.219		27953.3	4746.5	17.0%			
	3	25	7.644		0.216		29763.9	841.1	2.8%			
	4	25	5.905		0.419		22992.7	1631.5	7.1%			
	5	25	6.263		0.11		24386.6	428.3	1.8%			
	6	25	4.301		0.275		16747.1	1070.8	6.4%			
	7	25	3.637		0.07		14161.6	272.6	1.9%			
	8	25	7.889		0.723		30717.9	2815.2	9.2%			
	9	25	15.35		2.65		59769.2	10318.5	17.3%			
	10	25	12.301		0.378		47897.1	1471.8	3.1%			

Table J.7. Image analysis data for Day 325, NIT3, continued.

Port	Image #	DAPI Ch. Threshold	DAPI Ch. Area %	NIT3 Threshold	NIT3 Area %	Image J max area	DAPI abs area	NIT3 abs area	NIT3 area, % of DAPI	Mean	Stdev, in %	95% CI
Port 4	1	25	4.313	0.593		16793.8	2309.0	13.7%	4.8%	4.311	2.6721	
	2	25	4.64	0.006		18067.0	23.4	0.1%				
	3	25	10.153	0.259		39533.3	1008.5	2.6%				
	4	25	6.256	0.319		24359.4	1242.1	5.1%				
	5	25	14.829	0.109		57740.6	424.4	0.7%				
	6	25	8.94	0.652		34810.2	2538.7	7.3%				
	7	25	8.774	0.705		34163.9	2745.1	8.0%				
	8	25	10.194	0.686		39693.0	2671.1	6.7%				
	9	25	9.741	0.404		37929.1	1573.1	4.1%				
	10	25	14.575	0.002		56751.6	7.8	0.0%				
P2 Regrow	1	25	7.635	1.82		29728.9	7086.6	23.8%	9.2%	7.903	4.8984	
	2	25	10.712	0.366		41710.0	1425.1	3.4%				
	3	25	18.156	0.005		70695.1	19.5	0.0%				
	4	25	22.602	1.267		88006.8	4933.4	5.6%				
	5	25	13.868	0.792		53998.7	3083.9	5.7%				
	6	25	8.922	1.811		34740.1	7051.6	20.3%				
	7	25	5.633	0.864		21933.6	3364.2	15.3%				
	8	25	6.047	0.284		23545.6	1105.8	4.7%				
	9	25	6.672	0.608		25979.2	2367.4	9.1%				
	10	25	2.773	0.119		10797.4	463.4	4.3%				

Table J.8. Image analysis data for Day 325, Ntspa662.

Port	Image #	DAPI Ch. Threshold	DAPI Ch. Area %	Ntspa Threshold	Ntspa Area %	Image J max area	DAPI abs area	Ntspa abs area	Ntspa area, % of DAPI	Mean	Stdev, in %	95% CI
Port 1	1	25	4.736	20	0.023	389376	18440.8	89.6	0.5%	1.6%	3.619	2.2427
	2	25	7.526	20	0.003		29304.4	11.7	0.0%			
	3	25	9.929	20	0.002		38661.1	7.8	0.0%			
	4	25	5.502	20	0.202		21423.5	786.5	3.7%			
	5	25	10.296	20	0		40090.2	0.0	0.0%			
	6	25	4.42	20	0.007		17210.4	27.3	0.2%			
	7	25	2.211	20	0.008		8609.1	31.2	0.4%			
	8	25	3.74E+00	20	7.63E-04		14554.9	3.0	0.0%			
	9	25	11.806	20	1.347		45969.7	5244.9	11.4%			
	10	25	3.63E+00	20	7.63E-04		14142.1	3.0	0.0%			
Port 2	1	25	4.018	20	0.002		15645.1	7.8	0.0%	2.1%	2.842	1.7612
	2	25	14.269	20	0.039		55560.1	151.9	0.3%			
	3	25	9.991	20	0.002		38902.6	7.8	0.0%			
	4	25	8.588	20	0.732		33439.6	2850.2	8.5%			
	5	25	15.042	20	0.529		58569.9	2059.8	3.5%			
	6	25	2.266	20	0		8823.3	0.0	0.0%			
	7	25	4.694	20	0.003		18277.3	11.7	0.1%			
	8	25	6.288	20	0.059		24484.0	229.7	0.9%			
	9	25	5.611	20	0.164		21847.9	638.6	2.9%			
	10	25	10.807	20	0.512		42079.9	1993.6	4.7%			
Port 3	1	25	13.972	20	0.872		54403.6	3395.4	6.2%	10.1%	7.399	4.5858
	2	25	15.376	20	2.342		59870.5	9119.2	15.2%			
	3	25	3.034	20	0.413		11813.7	1608.1	13.6%			
	4	25	9.42	20	0.298		36679.2	1160.3	3.2%			
	5	25	8.477	20	0.336		33007.4	1308.3	4.0%			
	6	25	7.639	20	0.949		29744.4	3695.2	12.4%			
	7	25	10.79	20	0.494		42013.7	1923.5	4.6%			
	8	25	1.47	20	0.398		5723.8	1549.7	27.1%			
	9	25	8.956	20	0.421		34872.5	1639.3	4.7%			
	10	25	6.441	20	0.623		25079.7	2425.8	9.7%			

Table J.8. Image analysis data for Day 325, Ntspa662, continued.

Port	Image #	DAPI Ch. Threshold	DAPI Ch. Area %	Ntspa Threshold	Ntspa Area %	Image J max area	DAPI abs area	Ntspa abs area	Ntspa area, % of DAPI	Mean	Stdev, in %	95% CI
Port 4	1	25	4.746	20	1.428		18479.8	5560.3	30.1%	12.9%	10.186	6.3132
	2	25	18.943	20	2.17		73759.5	8449.5	11.5%			
	3	25	10.815	20	1.743		42111.0	6786.8	16.1%			
	4	25	9.78	20	0.658		38081.0	2562.1	6.7%			
	5	25	11.593	20	0.888		45140.4	3457.7	7.7%			
	6	25	5.613	20	0.081		21855.7	315.4	1.4%			
	7	25	7.825	20	0.704		30468.7	2741.2	9.0%			
	8	25	7.516	20	2.379		29265.5	9263.3	31.7%			
	9	25	5.993	20	0.353		23335.3	1374.5	5.9%			
	10	25	7.734	20	0.718		30114.3	2795.7	9.3%			
P2 Regrow	1	25	6.21	20	0.466		24180.2	1814.5	7.5%	17.1%	15.080	9.3468
	2	25	8.179	20	2.008		31847.1	7818.7	24.6%			
	3	25	1.129	20	0.438		4396.1	1705.5	38.8%			
	4	25	6.845	20	0.351		26652.8	1366.7	5.1%			
	5	25	4.885	25	2.253		19021.0	8772.6	46.1%			
	6	25	6.445	20	1.306		25095.3	5085.3	20.3%			
	7	25	4.707	20	0.159		18327.9	619.1	3.4%			
	8	25	7.788	20	0.52		30324.6	2024.8	6.7%			
	9	25	5.146	20	0.352		20037.3	1370.6	6.8%			
	10	25	3.228	20	0.373		12569.1	1452.4	11.6%			

Table J.9. Image analysis data for Day 325, EUBMix (Mix of EUB I, II, and III) vs. DAPI.

Port	Image #	DAPI Ch. Threshold	DAPI Ch. Area %	Eub Threshold	Eub Area %	Image J max area	DAPI abs area	Eub abs area	Eub area, % of DAPI	Mean	Stdev, in %	95% CI
Port 1	1	20	7.182	15	2.539	389376	27965.0	9886.3	35.4%	88.7%	53.558	19.17
	2		19.714		24.41		76761.6	95046.7	123.8%			
	3		7.233		12.45		28163.6	48477.3	172.1%			
	4		16.673		7.503		64920.7	29214.9	45.0%			
	5		20.398		6.305		79424.9	24550.2	30.9%			
	6		10.699		4.649		41659.3	18102.1	43.5%			
	7		17.57		2.901		68413.4	11295.8	16.5%			
	8		13.732		11.552		53469.1	44980.7	84.1%			
	9		21.831		21.31		85004.7	82976.0	97.6%			
	10		15.486		18.74		60298.8	72969.1	121.0%			
	11		16.052		9.007		62502.6	35071.1	56.1%			
	12		19.275		11.591		75052.2	45132.6	60.1%			
	13		14.981		14.062		58332.4	54754.1	93.9%			
	14		13.374		19.176		52075.1	74666.7	143.4%			
	15		6.291		5.158		24495.6	20084.0	82.0%			
	16		7.163		1.528		27891.0	5949.7	21.3%			
	17		26.761		28.859		104200.9	112370.0	107.8%			
	18		24.014		18.619		93504.8	72497.9	77.5%			
	19		22.358		5.294		87056.7	20613.6	23.7%			
	20		11.371		2.909		44275.9	11326.9	25.6%			
	21		14.81		15.105		57666.6	58815.2	102.0%			
	22		14.96		11.439		58250.6	44540.7	76.5%			
	23		12.007		11.579		46752.4	45085.8	96.4%			
	24		1		2.251		3893.8	8764.9	225.1%			
	25		2.466		1.61		9602.0	6269.0	65.3%			
	26		18.478		24.545		71948.9	95572.3	132.8%			
	27		14.179		11.419		55209.6	44462.8	80.5%			
	28		7.953		4.554		30967.1	17732.2	57.3%			
	29		6.862		13.271		26719.0	51674.1	193.4%			
	30		19.919		34.103		77559.8	132788.9	171.2%			

Table J.10. Image analysis data for Day 538, Pla46.

Port	Image #	DAPI Ch. Threshold	DAPI Ch. Area %	Pla46 Threshold	Pla46 Area %	Image J max area	DAPI abs area	Pla abs area	Pla area, % of DAPI	Mean	Stdev, in %	95% CI
Port 1	1	26	8.485	33	0.774	389376	33038.6	3013.8	9.1%	3.7%	3.865	1.9560
	2	26	5.346	33	0.421		20816.0	1639.3	7.9%			
	3	26	13.263	33	0.119		51642.9	463.4	0.9%			
	4	26	27.324	33	1.849		106393.1	7199.6	6.8%			
	5	26	10.324	33	0.838		40199.2	3263.0	8.1%			
	6	26	8.509	33	0.436		33132.0	1697.7	5.1%			
	7	26	15.202	33	0.769		59192.9	2994.3	5.1%			
	8	26	15.784	33	0.147		61459.1	572.4	0.9%			
	9	26	18.922	33	0.008		73677.7	31.2	0.0%			
	10	26	8.714	33	0.029		33930.2	112.9	0.3%			
	11	26	23.01	33	0.062		89595.4	241.4	0.3%			
	12	26	9.403	33	0.944		36613.0	3675.7	10.0%			
	13	26	11.663	33	0.032		45412.9	124.6	0.3%			
	14	26	34.582	33	0.045		134654.0	175.2	0.1%			
	15	26	13.464	33	0.015		52425.6	58.4	0.1%			
Port 2	1	25	4.839	33	0.445		18841.9	1732.7	9.2%	16.4%	28.536	14.4409
	2	25	17.24	33	1.13		67128.4	4399.9	6.6%			
	3	25	9.771	33	2.263		38045.9	8811.6	23.2%			
	4	25	5.832	33	4.04		22708.4	15730.8	69.3%			
	5	25	5.683	33	5.528		22128.2	21524.7	97.3%			
	6	25	16.498	33	2.833		64239.3	11031.0	17.2%			
	7	25	16.266	33	1.67		63335.9	6502.6	10.3%			
	8	25	12.038	33	0.215		46873.1	837.2	1.8%			
	9	25	17.886	33	0.119		69643.8	463.4	0.7%			
	10	25	10.219	33	1.042		39790.3	4057.3	10.2%			
	11	25	7.465	33	0.017		29066.9	66.2	0.2%			
	12	25	7.051	33	0.007		27454.9	27.3	0.1%			
	13	25	11.157	33	0.002		43442.7	7.8	0.0%			
	14	25	10.002	33	0.003		38945.4	11.7	0.0%			
	15	25	9.338	33	0.002		36359.9	7.8	0.0%			
	16	25	5.88	33	0.021		22895.3	81.8	0.4%			

Table J.10. Image analysis data for Day 538, Pla46, continued.

Port	Image #	DAPI Ch. Threshold	DAPI Ch. Area %	Pla46 Threshold	Pla46 Area %	Image J max area	DAPI abs area	Pla abs area	Pla area, % of DAPI	Mean	Stdev, in %	95% CI
Port 3	1	26	8.94	30	0.407		34810.2	1584.8	4.6%	5.6%	5.545	2.8061
	2	26	9.389	30	0.082		36558.5	319.3	0.9%			
	3	26	9.492	30	0.047		36959.6	183.0	0.5%			
	4	26	10.134	30	0.022		39459.4	85.7	0.2%			
	5	26	13.217	30	0.375		51463.8	1460.2	2.8%			
	6	26	8.196	30	0.372		31913.3	1448.5	4.5%			
	7	26	8.705	30	1.132		33895.2	4407.7	13.0%			
	8	26	9.209	30	1.095		35857.6	4263.7	11.9%			
	9	26	30.209	30	1.906		117626.6	7421.5	6.3%			
	10	26	22.388	30	3.33		87173.5	12966.2	14.9%			
	11	26	17.279	30	0		67280.3	0.0	0.0%			
	12	26	24.174	30	0.001		94127.8	3.9	0.0%			
	13	26	15.69	30	0.166		61093.1	646.4	1.1%			
	14	26	14.968	30	1.606		58281.8	6253.4	10.7%			
	15	26	14.991	30	1.928		58371.4	7507.2	12.9%			
Port 4	1	27	10.479	26	0.155		40802.7	603.5	1.5%	10.3%	24.749	12.5246
	2	27	9.251	26	0.019		36021.2	74.0	0.2%			
	3	27	8.438	26	0.121		32855.5	471.1	1.4%			
	4	27	9.507	26	0.059		37018.0	229.7	0.6%			
	5	27	16.414	26	1.036		63912.2	4033.9	6.3%			
	6	27	13.065	26	12.584		50872.0	48999.1	96.3%			
	7	27	5.808	26	0.011		22615.0	42.8	0.2%			
	8	27	10.905	26	1.382		42461.5	5381.2	12.7%			
	9	27	16.75	26	4.251		65220.5	16552.4	25.4%			
	10	27	9.189	26	0.007		35779.8	27.3	0.1%			
	11	27	22.706	26	0.874		88411.7	3403.1	3.8%			
	12	27	33.808	26	0.142		131640.2	552.9	0.4%			
	13	27	9.21	26	0.085		35861.5	331.0	0.9%			
	14	27	16.853	26	0.596		65621.5	2320.7	3.5%			
	15	27	18.781	26	0.098		73128.7	381.6	0.5%			

Table J.11. Image analysis data for Day 538, Nso190.

Port	Image #	DAPI Ch. Threshold	DAPI Ch. Area %	Nso190 Threshold	Nso190 Area %	Image J max area	DAPI abs area	Nso abs area	Nso area % of DAPI	Mean	Stdev, in %	95% CI
Port 1	1	20	6.499	29	3.551		25305.5	13826.7	54.6%	18.3%	15.812	8.0019
	2	27	11.208	29	5.546		43641.3	21594.8	49.5%			
	3	27	11.244	29	1.183		43781.4	4606.3	10.5%			
	4	27	8.293	29	1.141		32291.0	4442.8	13.8%			
	5	27	15.318	29	2.098		59644.6	8169.1	13.7%			
	6	27	7.99	29	0.568		31111.1	2211.7	7.1%			
	7	27	10.276	29	1.693		40012.3	6592.1	16.5%			
	8	27	25.09	29	4.128		97694.4	16073.4	16.5%			
	9	27	14.394	29	1.97		56046.8	7670.7	13.7%			
	10	27	37.548	29	0.461		146202.9	1795.0	1.2%			
	11	27	3.785	29	1.368		14737.9	5326.7	36.1%			
	12	27	7.129	29	0.28		27758.6	1090.3	3.9%			
	13	27	10.681	29	1.404		41589.3	5466.8	13.1%			
	14	27	7.505	29	0.614		29222.7	2390.8	8.2%			
	15	27	13.426	29	2.114		52277.6	8231.4	15.7%			
Port 2	1	28	10.36	30	0.073		40339.4	284.2	0.7%	4.9%	6.759	3.4206
	2	28	18.766	30	2.018		73070.3	7857.6	10.8%			
	3	28	11.397	30	0.388		44377.2	1510.8	3.4%			
	4	28	12.028	30	3.083		46834.1	12004.5	25.6%			
	5	28	13.364	30	0.282		52036.2	1098.0	2.1%			
	6	28	9.428	30	0.043		36710.4	167.4	0.5%			
	7	28	10.914	30	0.272		42496.5	1059.1	2.5%			
	8	28	11.347	30	1.002		44182.5	3901.5	8.8%			
	9	28	7.233	30	0.02		28163.6	77.9	0.3%			
	10	28	9.705	30	0.388		37788.9	1510.8	4.0%			
	11	28	6.26	30	0.275		24374.9	1070.8	4.4%			
	12	28	6.076	30	0.033		23658.5	128.5	0.5%			
	13	28	13.846	30	6.612							
	14	28	5.441	30	0.269		21185.9	1047.4	4.9%			
	15	28	10.309	30	0.046		40140.8	179.1	0.4%			

Table J.11. Image analysis data for Day 538, Nso190, continued.

Port	Image #	DAPI Ch. Threshold	DAPI Ch. Area %	Nso190 Threshold	Nso190 Area %	Image J max area	DAPI abs area	Nso abs area	Nso area % of DAPI	Mean	Stdev, in %	95% CI
Port 3	1	27	16.809	30	0.73		65450.2	2842.4	4.3%	5.9%	3.666	1.8554
	2	27	12.903	30	0.943		50241.2	3671.8	7.3%			
	3	27	10.802	30	1.056		42060.4	4111.8	9.8%			
	4	27	13.86	30	1.123		53967.5	4372.7	8.1%			
	5	27	12.283	30	1.163		47827.1	4528.4	9.5%			
	6	27	16.021	30	0.948		62381.9	3691.3	5.9%			
	7	27	8.434	30	0.002		32840.0	7.8	0.0%			
	8	27	5.673	30	0.538		22089.3	2094.8	9.5%			
	9	27	17.921	30	0.603		69780.1	2347.9	3.4%			
	10	27	11.371	30	0.372		44275.9	1448.5	3.3%			
	11	27	5.195	30	0.106		20228.1	412.7	2.0%			
	12	27	5.676	30	0.695		22101.0	2706.2	12.2%			
	13	27	14.025	30	0.797		54610.0	3103.3	5.7%			
	14	27	5.495	30	0.379		21396.2	1475.7	6.9%			
	15	27	4.577	30	0.002		17821.7	7.8	0.0%			
Port 4	1	29	8.454	28	2.866		32917.8	11159.5	33.9%	21.8%	16.232	8.2146
	2	29	15.997	28	2.215		62288.5	8624.7	13.8%			
	3	29	23.666	28	2.013		92149.7	7838.1	8.5%			
	4	29	12.083	28	6.167		47048.3	24012.8	51.0%			
	5	29	12.628	28	4.353		49170.4	16949.5	34.5%			
	6	29	3.123	28	0.029		12160.2	112.9	0.9%			
	7	29	9.063	28	3.556		35289.1	13846.2	39.2%			
	8	29	7.139	28	1.738		27797.6	6767.4	24.3%			
	9	29	16.389	28	6.964		63814.8	27116.1	42.5%			
	10	29	5.016	28	1.116		19531.1	4345.4	22.2%			
	11	29	6.411	28	0.155		24962.9	603.5	2.4%			
	12	29	10.682	28	1.474		41593.1	5739.4	13.8%			
	13	29	15.103	28	0.608		58807.5	2367.4	4.0%			
	14	29	14.335	28	0.741		55817.0	2885.3	5.2%			
	15	29	8.868	28	2.728		34529.9	10622.2	30.8%			

Table J.12. Image analysis data for Day 538, NIT3.

Port	Image #	DAPI Ch. Threshold	DAPI Ch. Area %	NIT3 Threshold	NIT3 Area %	Image J max area	DAPI abs area	NIT3 abs area	NIT3 area, % of DAPI	Mean	Stdev, in %	95% CI
Port 1	1	23	9.064	18	1.028	389376	35293.0	4002.8	11.3%	12.8%	18.943	9.5862
	2	23	10.225	18	0.216		39813.7	841.1	2.1%			
	3	23	8.571	18	0.594		33373.4	2312.9	6.9%			
	4	23	14.376	18	0.567		55976.7	2207.8	3.9%			
	5	23	4.89	18	0.132		19040.5	514.0	2.7%			
	6	23	5.54	18	3.219		21571.4	12534.0	58.1%			
	7	23	7.266	18	0.752		28292.1	2928.1	10.3%			
	8	23	10.543	18	0.541		41051.9	2106.5	5.1%			
	9	23	19.689	18	1.266		76664.2	4929.5	6.4%			
	10	23	21.048	18	1.582		81955.9	6159.9	7.5%			
	11	23	25.111	18	1.546		97776.2	6019.8	6.2%			
	12	23	23.091	18	0.287		89910.8	1117.5	1.2%			
	13	23	9.5	18	5.661		36990.7	22042.6	59.6%			
	14	23	20.719	18	0.429		80674.8	1670.4	2.1%			
	15	23	9.582	18	0.752		37310.0	2928.1	7.8%			
Port 2	1	25	19.183	24	0.009		74694.0	35.0	0.0%	12.5%	18.220	9.2203
	2	25	7.811	24	0.198		30414.2	771.0	2.5%			
	3	25	18.397	24	1.949		71633.5	7588.9	10.6%			
	4	25	11.572	24	6.972		45058.6	27147.3	60.2%			
	5	25	11.877	24	0.583		46246.2	2270.1	4.9%			
	6	15	3.347	24	1.041		13032.4	4053.4	31.1%			
	7	25	0.722	24	0.32		2811.3	1246.0	44.3%			
	8	25	2.69	24	0.353		10474.2	1374.5	13.1%			
	9	25	6.766	24	0.547		26345.2	2129.9	8.1%			
	10	25	3.897	24	0.059		15174.0	229.7	1.5%			
	11	25	11.711	24	0.688		45599.8	2678.9	5.9%			
	12	25	10.905	24	0.251		42461.5	977.3	2.3%			
	13	25	3.951	24	0.021		15384.2	81.8	0.5%			
	14	25	4.779	24	0.007		18608.3	27.3	0.1%			
	15	25	7.604	24	0.157		29608.2	611.3	2.1%			

Table J.12. Image analysis data for Day 538, NIT3, continued.

Port	Image #	DAPI Ch. Threshold	DAPI Ch. Area %	NIT3 Threshold	NIT3 Area %	Image J max area	DAPI abs area	NIT3 abs area	NIT3 area, % of DAPI	Mean	Stdev, in %	95% CI
Port 3	1	25	2.142	20	0.177		8340.4	689.2	8.3%	3.3%	4.804	2.4310
	2	25	15.988	20	1.301		62253.4	5065.8	8.1%			
	3	25	3.301	20	0.058		12853.3	225.8	1.8%			
	4	25	14.646	20	0.202		57028.0	786.5	1.4%			
	5	25	17.288	20	0.492		67315.3	1915.7	2.8%			
	6	25	3.518	20	0.046		13698.2	179.1	1.3%			
	7	25	6.711	20	0.125		26131.0	486.7	1.9%			
	8	25	9.891	20	1.785		38513.2	6950.4	18.0%			
	9	25	6.931	20	0.029		26987.7	112.9	0.4%			
	10	25	2.945	20	0.012		11467.1	46.7	0.4%			
	11	25	12.543	20	0.01		48839.4	38.9	0.1%			
	12	25	8.613	20	0.146		33537.0	568.5	1.7%			
	13	25	14.409	20	0.158		56105.2	615.2	1.1%			
	14	25	17.846	20	0.176		69488.0	685.3	1.0%			
	15	25	12.075	20	0.117		47017.2	455.6	1.0%			
Port 4	1	25	28.058	20	0.17		109251.1	661.9	0.6%	1.9%	1.946	0.9846
	2	25	4.876	20	0.098		18986.0	381.6	2.0%			
	3	25	5.141	20	0.007		20017.8	27.3	0.1%			
	4	25	18.585	20	0.521		72365.5	2028.6	2.8%			
	5	25	12.321	20	0.078		47975.0	303.7	0.6%			
	6	25	2.296	20	0.128		8940.1	498.4	5.6%			
	7	25	7.613	20	0.18		29643.2	700.9	2.4%			
	8	25	4.995	20	0.098		19449.3	381.6	2.0%			
	9	25	12.254	20	0.065		47714.1	253.1	0.5%			
	10	25	5.634	20	0.03		21937.4	116.8	0.5%			
	11	25	10.336	20	0.127		40245.9	494.5	1.2%			
	12	25	10.787	20	0.08		42002.0	311.5	0.7%			
	13	25	10.222	20	0.205		39802.0	798.2	2.0%			
	14	25	4.704	20	0.322		18316.2	1253.8	6.8%			
	15	25	2.341	20	0.011		9115.3	42.8	0.5%			

Table J.13. Image analysis data for Day 538, Ntspa662.

Port	Image #	DAPI Ch. Threshold	DAPI Ch. Area %	Ntspa Threshold	Ntspa Area %	Image J max area	DAPI abs area	Ntspa abs area	Ntspa area, % of DAPI	Mean	Stdev, in %	95% CI
Port 1	1	27	4.893	20	0.04	389376	19052.2	155.8	0.8%	3.5%	6.952	3.5180
	2	27	12.011	20	0.129		46768.0	502.3	1.1%			
	3	27	14.448	20	0.166		56257.0	646.4	1.1%			
	4	27	24.738	20	1.449		96323.8	5642.1	5.9%			
	5	27	15.303	20	4.163		59586.2	16209.7	27.2%			
	6	27	6.452	20	0.007		25122.5	27.3	0.1%			
	7	27	10.764	20	0.005		41912.4	19.5	0.0%			
	8	27	9.794	20	0.782		38135.5	3044.9	8.0%			
	9	27	15.612	20	0.529		60789.4	2059.8	3.4%			
	10	27	9.231	20	0.122		35943.3	475.0	1.3%			
	11	27	21.125	20	0.076		82255.7	295.9	0.4%			
	12	27	6.643	20	0.046		25866.2	179.1	0.7%			
	13	27	7.123	20	0.018		27735.3	70.1	0.3%			
	14	27	10.315	20	0.153		40164.1	595.7	1.5%			
	15	27	10.665	20	0.038		41527.0	148.0	0.4%			
Port 2	1	30	10.313	19	0.058		40156.3	225.8	0.6%	6.9%	7.165	6.2803
	2	30	5.966	19	0.785		23230.2	3056.6	13.2%			
	3	30	2.396	19	0.396		9329.4	1541.9	16.5%			
	4	30	8.275	19	1.564		32220.9	6089.8	18.9%			
	5	30	13.489	19	0.581		52522.9	2262.3	4.3%			
	6	30	9.629	19	0.13		37493.0	506.2	1.4%			
	7	30	6.229	19	0.144		24254.2	560.7	2.3%			
	8	30	8.529	19	0.888		33209.9	3457.7	10.4%			
	9	30	10.728	19	0.153		41772.3	595.7	1.4%			
	10	30	2.757	19	0.005		10735.1	19.5	0.2%			
	11	30	5.902	19	0.086		22981.0	334.9	1.5%			
	12	30	4.569	19	0.121		17790.6	471.1	2.6%			
	13	30	3.102	19	0.187		12078.4	728.1	6.0%			
	14	30	7.323	19	0.179		28514.0	697.0	2.4%			
	15	30	10.023	19	0.313		39027.2	1218.7	3.1%			

Table J.13. Image analysis data for Day 538, NIT3, continued.

Port	Image #	DAPI Ch. Threshold	DAPI Ch. Area %	Ntspa Threshold	Ntspa Area %	Image J max area	DAPI abs area	Ntspa abs area	Ntspa area, % of DAPI	Mean	Stdev, in %	95% CI
Port 3	1	30	13.844	20	2.032		53905.2	7912.1	14.7%	5.2%	5.253	2.6581
	2	30	9.892	20	1.181		38517.1	4598.5	11.9%			
	3	30	13.891	20	0.093		54088.2	362.1	0.7%			
	4	30	9.184	20	0.023		35760.3	89.6	0.3%			
	5	30	10.073	20	0.365		39221.8	1421.2	3.6%			
	6	30	1.958	20	0.043		7624.0	167.4	2.2%			
	7	30	6.37	20	0.064		24803.3	249.2	1.0%			
	8	30	5.609	20	0.505		21840.1	1966.3	9.0%			
	9	30	14.456	20	1.346		56288.2	5241.0	9.3%			
	10	30	7.407	20	0.218		28841.1	848.8	2.9%			
	11	30	5.752	20	0.824		22396.9	3208.5	14.3%			
	12	30	5.141	20	0.039		20017.8	151.9	0.8%			
	13	30	11.671	20	0		45444.1	0.0	0.0%			
	14	30	6.542	20	0.318		25473.0	1238.2	4.9%			
	15	30	3.509	20	0.07		13663.2	272.6	2.0%			
Port 4	1	30	5.908	17	0.514		23004.3	2001.4	8.7%	7.2%	7.797	3.9457
	2	30	12.901	17	0.686		50233.4	2671.1	5.3%			
	3	30	6.541	17	0.393		25469.1	1530.2	6.0%			
	4	30	3.203	17	0.325		12471.7	1265.5	10.1%			
	5	30	17.219	17	0.778		67046.7	3029.3	4.5%			
	6	30	1.894	17	0.613		7374.8	2386.9	32.4%			
	7	30	8.778	17	0.178		34179.4	693.1	2.0%			
	8	30	5.019	17	0.254		19542.8	989.0	5.1%			
	9	30	3.235	17	0.094		12596.3	366.0	2.9%			
	10	30	4.225	17	0.188		16451.1	732.0	4.4%			
	11	30	6.316	17	0.011		24593.0	42.8	0.2%			
	12	30	7.511	17	1.068		29246.0	4158.5	14.2%			
	13	30	5.059	17	0.245		19698.5	954.0	4.8%			
	14	30	9.608	17	0.199		37411.2	774.9	2.1%			
	15	30	3.694	17	0.169		14383.549	658.0	4.6%			

J.3. Radial distribution of microbial populations

Selected representative images are shown.

Planctomycetes, with Pla46 (magenta) and AerAOB with Nso1225 (green):

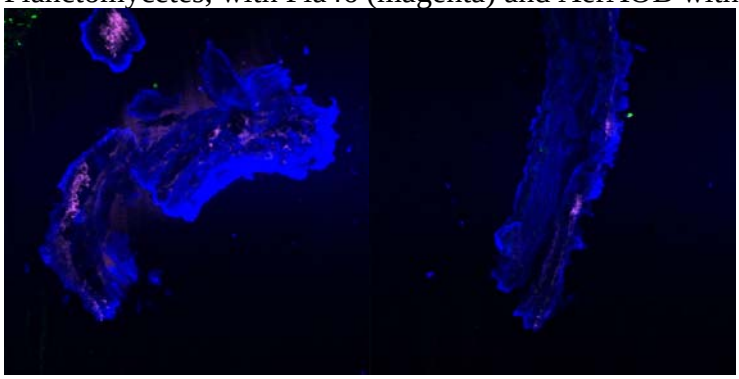

Port 1 Port 1

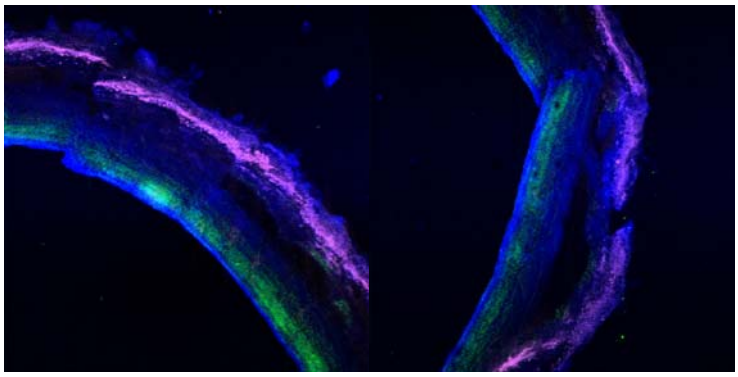

Port 2 Port 2

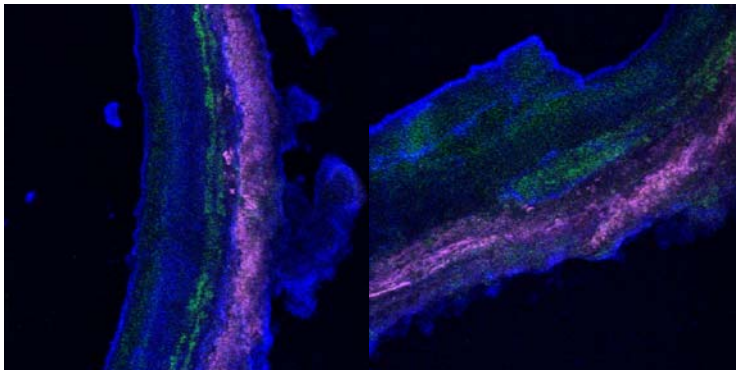

Port 3 Port 3

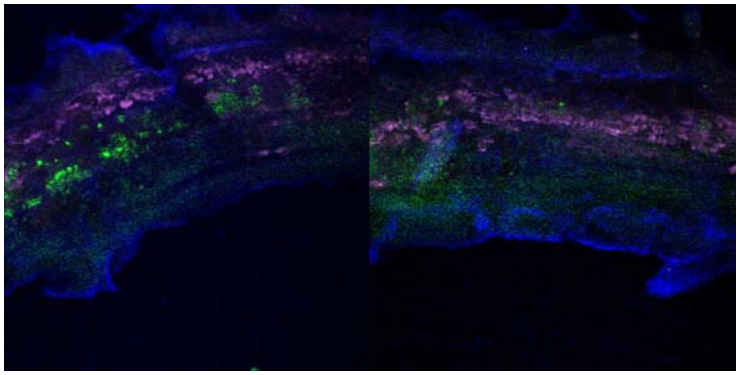

Port 4 Port 4

AerAOB with Nso190 (red) and *Nitrospira*-like NOB with Ntspa (green)

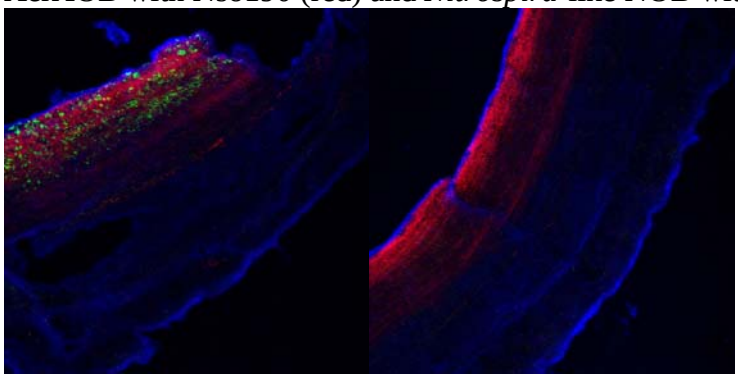

Port 1 Port 2

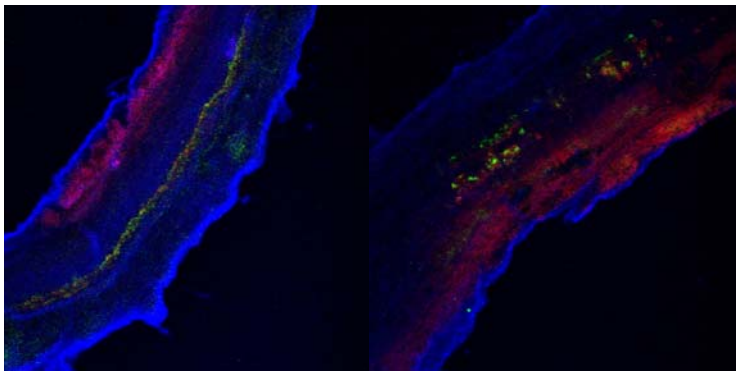

Port 3 Port 4

AerAOB with Nso190 (red) and *Nitrobacter*-like NOB with NIT3 (green)

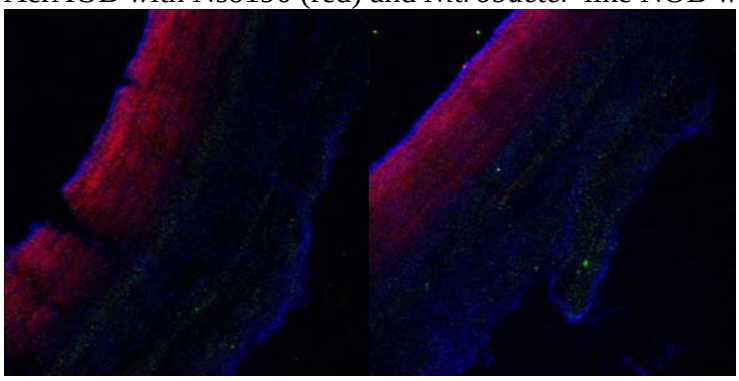

Port 1 Port 2

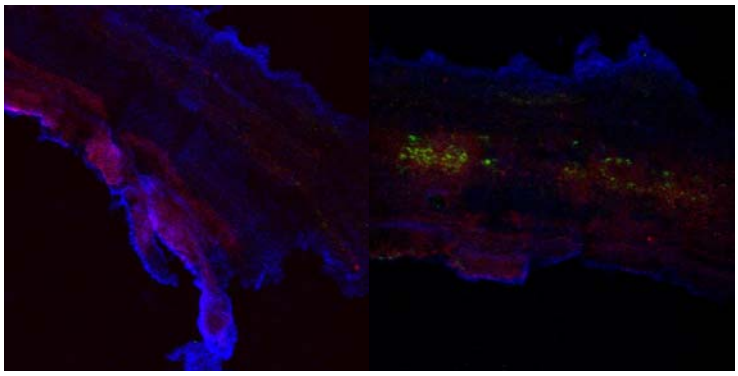

Port 3 Port 4

J.4. Controls

<u>Biofilm samples, no probe, with DAPI</u>

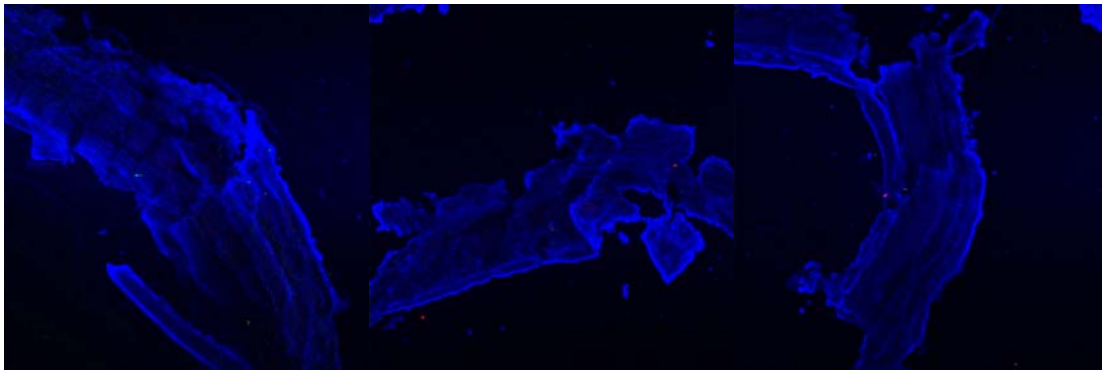

Port 1 Port 3 Port 4

<u>Biofilm samples, no probe, no DAPI</u>

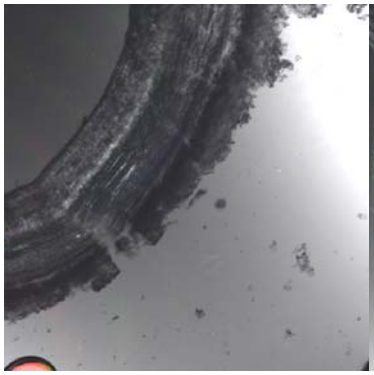
Port 1

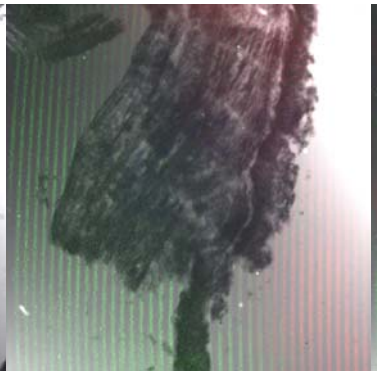
Port 2

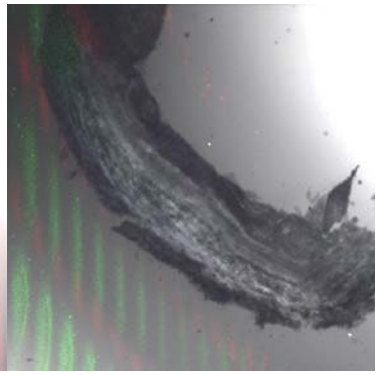
Port 4

AerAOB-positive controls, Nso190 (red/pink)

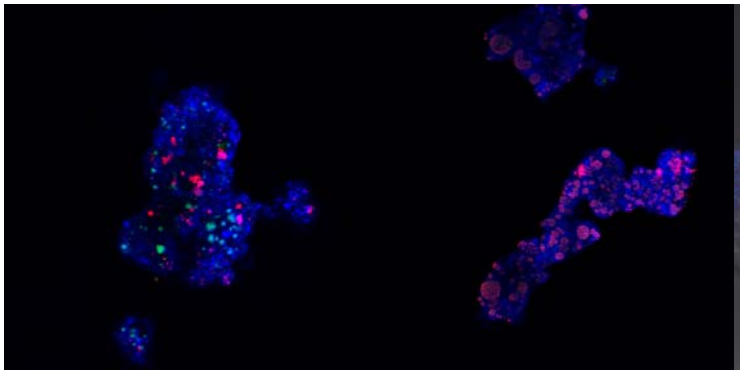
Activated sludge

Lab enrichment reactor

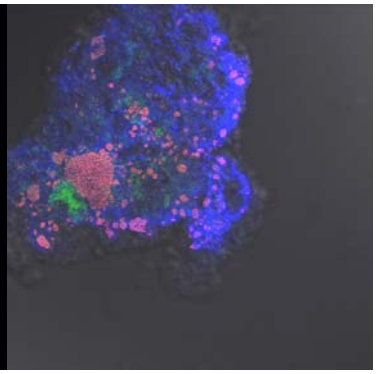
Lab enrichment reactor

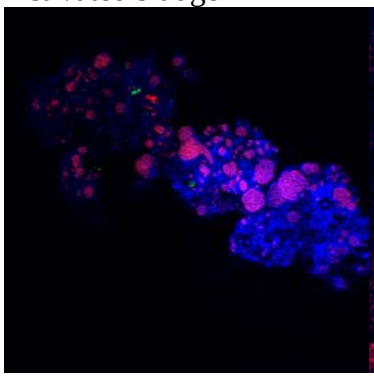
Lab enrichment reactor

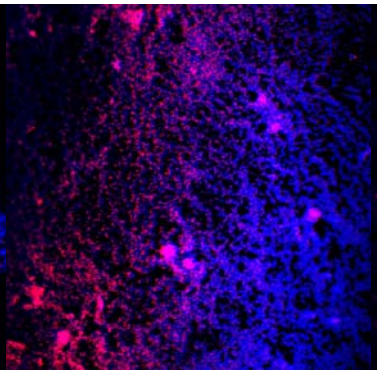
N. europaea

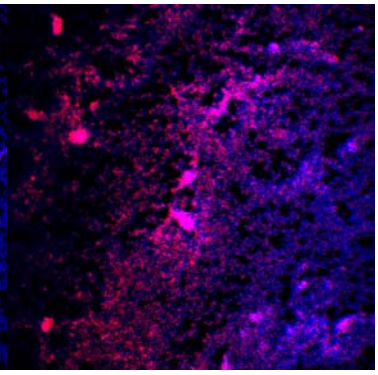
N. europaea

AerAOB-positive controls, Nso1225 (green)

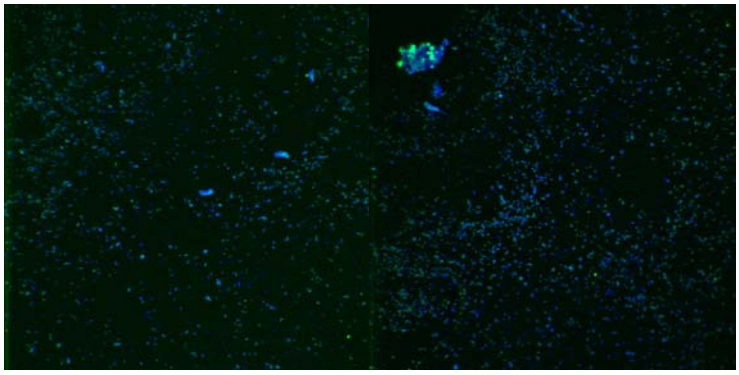

N. europaea *N. europaea*

AerAOB-negative controls

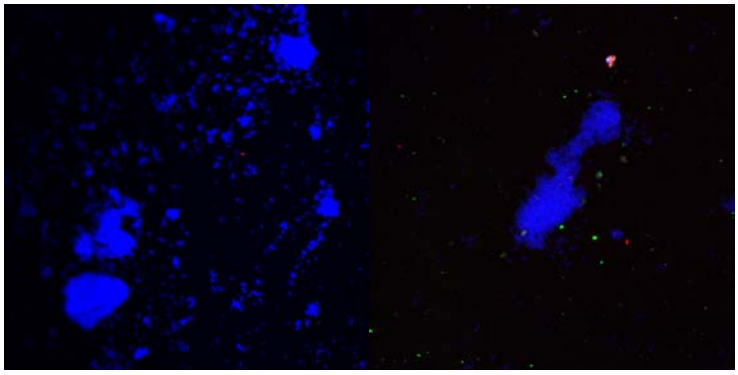

P. aeruginosa, Nso190 *P. aeruginosa*, Nso1225

NOB-positive controls, Ntspa662 (green)

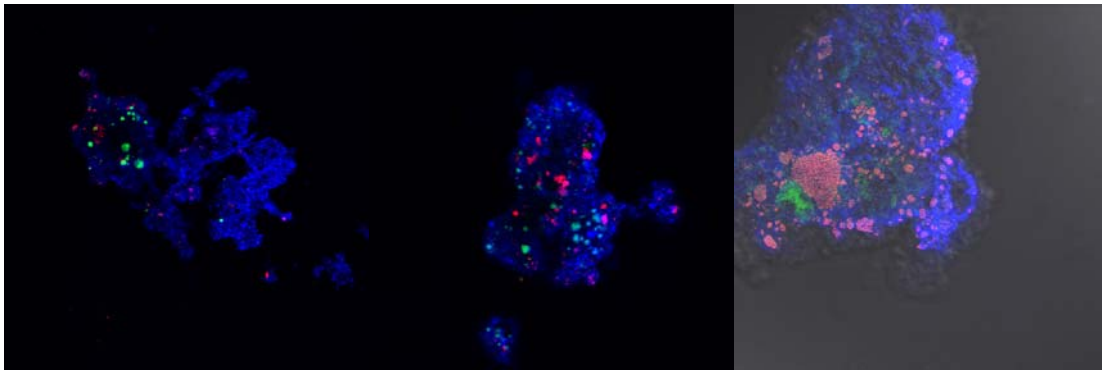

Nitrifying activated sludge Nitrifying activated sludge Lab enrichment reactor

NOB-positive controls, NIT3 (green)

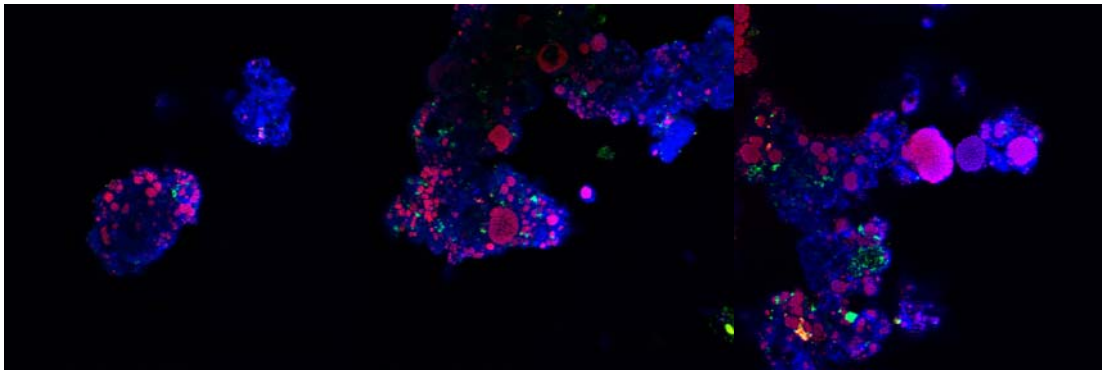

Lab enrichment reactor Lab enrichment reactor Lab enrichment reactor

NOB-negative controls, Ntspa (green)

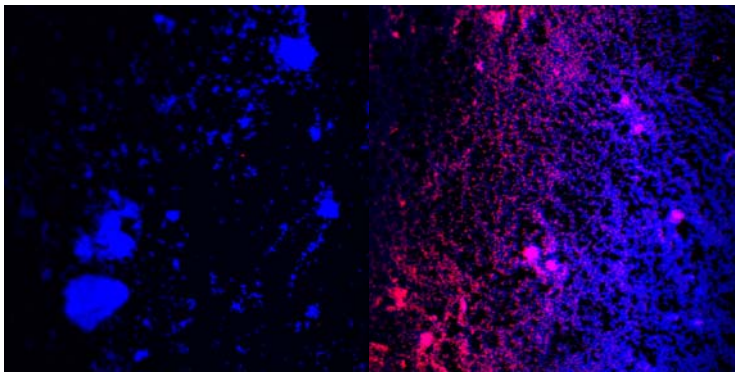

P. aeruginosa *N. europaea*

NOB-negative controls, NIT3 (green)

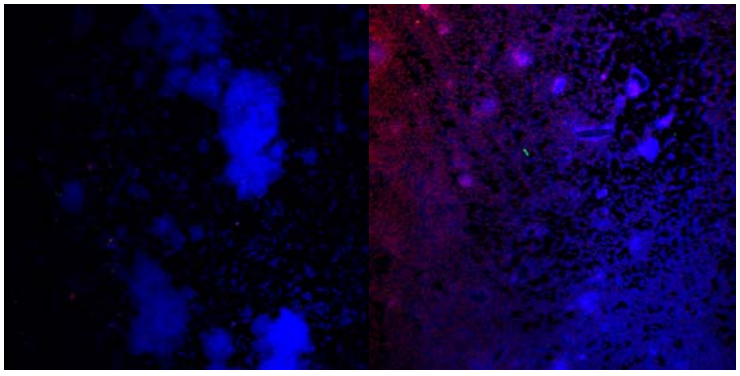

P. aeruginosa *N. europaea*

AnaerAOB-positive controls, Pla46 (magenta)

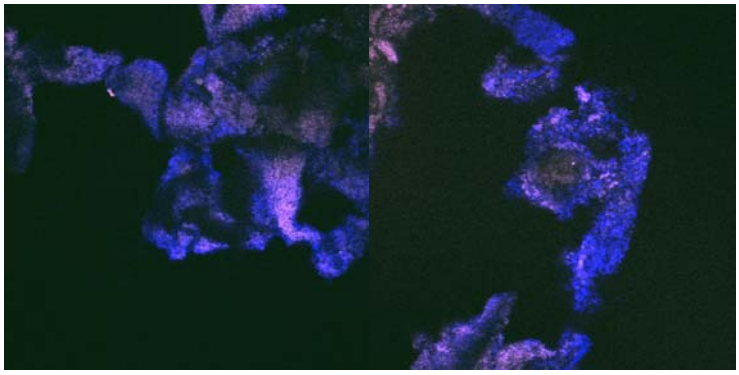

Both samples: deammonification biomass, Strass, Austria (Courtesy of B. Wett)

AnaerAOB-negative controls, Pla46 (magenta)

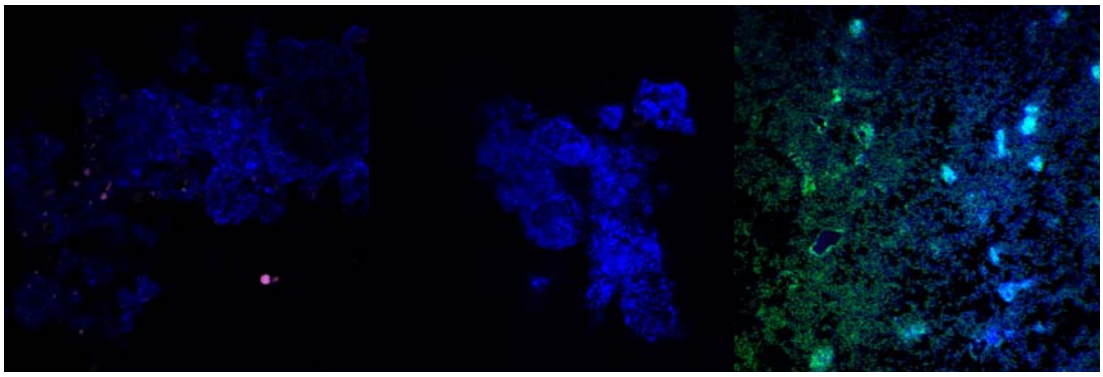

Aerobic activated sludge Lab enrichment reactor *N. europaea*

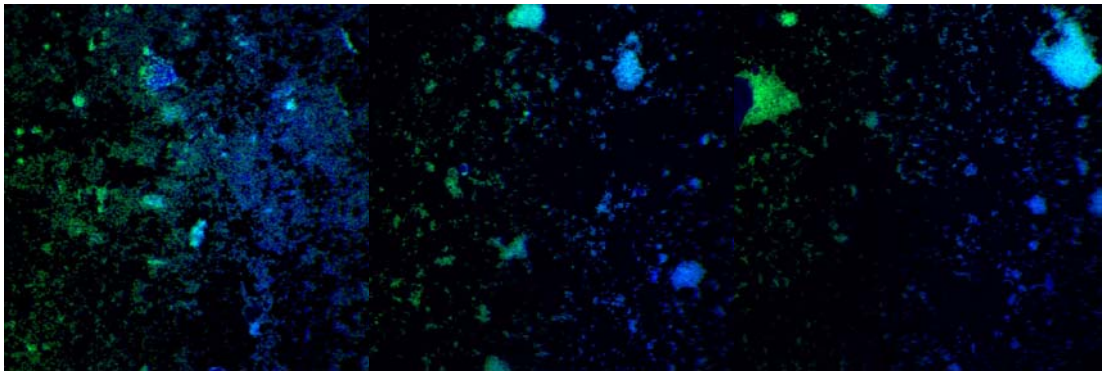

N. europaea *P. aeruginosa* *P. aeruginosa*

Data for this appendix can be found in the image file directories and in the spreadsheet files:
"Dissertation Appendix J Part a Day 192.xls"
"Dissertation Appendix J Part b Day 325.xls"
"Dissertation Appendix J Part c Day 538.xls"

APPENDIX K

PERTURBATION EXPERIMENTS

Appendix K. Perturbation Experiments

K.1 Oxic perturbation experiment on Day 127

The lumen pressure was increased from 5 psig to 9 psig for a 12-hour period. Gases and soluble nitrogen species were monitored for ~25 hours.

Table K.1. Lumen pressure during oxic perturbation test no. 1.

Time, hours	Pressure, psig
0.00	5.0
0.50	5.3
1.65	6.8
1.93	6.9
2.23	7.1
4.02	7.1
5.20	7.4
5.93	9.0
10.25	8.5
10.75	9.0
11.45	9.1
12.33	5.0
26.63	5.0

Table K.2. Soluble nitrogen species during oxic perturbation test no. 1.

Time, hours	NH_4^+ mg/l-N	NH_4^+ Std. Dev.	NO_2^-, mg/l-N	NO2-, ± range	NO_3^- mg/l-N	NO_3^- ± range
0.0	156	4.5	276	9.5	67	0.28
1.75	138	1.1	292	1.7	66	0.04
4.63	141	9.4	297	3.4	68	0.06
11.00	140	0.4	283	0	72	0.40
25.63	136	6.0	293	1.7	71	0.41

Table K.3. Gaseous species during oxic perturbation test no. 1.

Time, hours	N_2O ppm	N_2O range	N_2 %	N_2 95% C.I.	O_2 %	O_2 95% C.I.
0.0	3,339	1,459	82.6%	0.22%	12.0%	0.27%
1.75	3,758	1,113	85.4%	0.71%	9.8%	0.27%
4.63	2,465	864	84.3%	1.29%	10.2%	0.29%
11.00	2,432	838	86.6%	1.44%	9.0%	0.23%
25.63	2,310					

Power failures on GC led to problems in obtaining replicates for N_2O. As a result, 25 hour N_2O is a single data point (no replicates).

K.2 Oxic perturbation experiment on Day 162.

The lumen pressure was increased from 5 psig to 9 psig for a 12-hour period. Gases and soluble nitrogen species were monitored for ~7 days.

Table K.4. Lumen pressure during oxic perturbation test no. 2.

Time, hours	Time, days	Pressure, psig
0.00	0.00	5.5
0.15	0.01	5.8
0.23	0.01	6.0
0.50	0.02	6.6
0.93	0.04	6.9
1.02	0.04	7.5
1.10	0.05	8.0
1.22	0.05	8.3
1.33	0.06	8.5
1.65	0.07	9.0
1.73	0.07	9.1
2.18	0.09	9.1
2.40	0.10	10.2
2.62	0.11	10.4
5.50	0.23	10.0
11.50	0.48	10.0
13.60	0.57	4.0
25.00	1.04	4.0
25.55	1.06	4.2
26.47	1.10	5.9
26.68	1.11	4.2
26.87	1.12	4.9
27.23	1.13	5.0
30.00	1.25	5.0
46.50	1.94	5.0
71.38	2.97	5.0
171.00	7.13	5.5

Table K.5. Soluble nitrogen species during oxic perturbation test no. 2.

Time, days	NH_4^+ mg/l-N	NH_4^+ Std. Dev.	NO_2^-, mg/l-N	NO2-, ± range	NO_3^- mg/l-N	NO_3^- ± range
0	160	3.0	333	1.2	56	0.6
0.08	142	28.0	350	1.2	64	0.8
0.42	166	6.8	346	0.3	73	0.8
1.08	177	14.4	339	0.6	68	0.0
1.94	153	3.0	344	7.3	64	0.7
2.98	163	1.0	321	3.6	70	1.6
4.00	172	1.0	316	5.3	69	0.1
7.13	158	1.8	332	2.2		

Table K.6. Gaseous species during oxic perturbation test no. 2.

Time, days	N_2O ppm	N_2O ± range	N_2 %	N_2 95% C.I.	NO ppm	NO ± range	NO_x ppm	NO_2 ppm	NO_2 ± range
0	2,577	7.7	1.4%	0.12%	25.8	0.3	64.0	38.3	0.8
0.08	2,069	420	1.3%	0.05%	25.4	0.6	63.3	37.9	0.7
0.17	2,041	32.1	2.7%	0.07%	25.0	0.0	57.0	32.0	1.0
0.42	1,929	101	4.0%	0.04%	19.0	0.7	45.8	26.8	0.4
1.08	2,493	71.4	1.3%	0.05%	30.3	0.25	70.3	40.0	0.5
1.94	2,420	213	1.5%	0.07%	29.8	0.25	68.5	38.8	0.75
2.98	2,614	99	3.8%	0.07%	26.5	0.25	60.3	33.8	1.25
4.00	2,351	197	2.2%	0.08%	30.6	0.6	68.0	37.4	1.4
7.13	2,344	83	1.7%	0.10%	29.8	0.6	75.7	45.8	7.0

Oxygen was not quantified during the second oxic perturbation experiment, as the aeration gas had already been changed to argon/oxygen. Argon interferes with the oxygen quantification.

K.3 High pH perturbation experiment on Day 265

The pH was increased from 7 to 8 for a 12-hour period. Gases and soluble nitrogen species were monitored for 4 days

Table K.7. pH during high pH perturbation test no. 1.

Time, hours	Time, days	pH	Time, hours	Time, days	pH	Time, hours	Time, days	pH
0.0	0.000		20.5	0.854	7.29	41.0	1.708	7.20
0.5	0.021	7.07	21.0	0.875	7.28	41.5	1.729	7.19
1.0	0.042	7.53	21.5	0.896	7.26	42.0	1.750	7.17
1.5	0.063	7.99	22.0	0.917	7.26	42.5	1.771	7.16
2.0	0.083	7.86	22.5	0.938	7.24	43.0	1.792	7.15
2.5	0.104	7.75	23.0	0.958	7.23	43.5	1.813	7.14
3.0	0.125	8.04	23.5	0.979		44.0	1.833	7.13
3.5	0.146	7.95	24.0	1.000	7.21	44.5	1.854	7.12
4.0	0.167	7.88	24.5	1.021	7.21	45.0	1.875	7.11
4.5	0.188	7.81	25.0	1.042	7.20	45.5	1.896	7.11
5.0	0.208	7.75	25.5	1.063	7.18	46.0	1.917	7.10
5.5	0.229	8.01	26.0	1.083	7.17	46.5	1.938	7.09
6.0	0.250	7.94	26.5	1.104	7.16	47.0	1.958	7.08
6.5	0.271	7.88	27.0	1.125	7.15	47.5	1.979	7.08
7.0	0.292	7.81	27.5	1.146	7.14	48.0	2.000	7.07
7.5	0.313	7.75	28.0	1.167	7.13	48.5	2.021	7.06
8.0	0.333	7.93	28.5	1.188	7.13	49.0	2.042	7.06
8.5	0.354	7.88	29.0	1.208	7.11	49.5	2.063	7.05
9.0	0.375	7.84	29.5	1.229	7.11	50.0	2.083	7.05
9.5	0.396	7.78	30.0	1.250	7.10	50.5	2.104	7.04
10.0	0.417	7.94	30.5	1.271	7.09	51.0	2.125	7.04
10.5	0.438	7.89	31.0	1.292	7.08	51.5	2.146	7.03
11.0	0.458	7.84	31.5	1.313	7.07	52.0	2.167	7.03
11.5	0.479	7.79	32.0	1.333	7.07	52.5	2.188	7.02
12.0	0.500	7.75	32.5	1.354	7.07	53.0	2.208	7.01
12.5	0.521	7.70	33.0	1.375	7.06	53.5	2.229	7.01
13.0	0.542	7.66	33.5	1.396	7.05	54.0	2.250	7.01
13.5	0.563	7.63	34.0	1.417	7.05	54.5	2.271	7.00
14.0	0.583	7.59	34.5	1.438	7.04	55.0	2.292	6.99
14.5	0.604	7.56	35.0	1.458	7.03	55.5	2.313	6.99
15.0	0.625	7.52	35.5	1.479	7.03	56.0	2.333	6.99
15.5	0.646	7.49	36.0	1.500	7.02	56.5	2.354	6.98
16.0	0.667	7.48	36.5	1.521	7.02	57.0	2.375	6.98
16.5	0.688	7.44	37.0	1.542	7.01	57.5	2.396	6.98
17.0	0.708	7.42	37.5	1.563	7.00	58.0	2.417	7.21
17.5	0.729	7.40	38.0	1.583	7.00	58.5	2.438	7.19
18.0	0.750	7.37	38.5	1.604	6.99	59.0	2.458	7.17
18.5	0.771	7.37	39.0	1.625	6.99	59.5	2.479	7.17
19.0	0.792	7.33	39.5	1.646	6.99	60.0	2.500	7.16
19.5	0.813	7.32	40.0	1.667	6.98	60.5	2.521	7.15
20.0	0.833	7.31	40.5	1.688	6.98	61.0	2.542	7.14

Table K.7. pH during high pH perturbation test no. 1, continued.

Time, hours	Time, days	pH	Time, hours	Time, days	pH
61.5	2.563	7.13	82.0	3.417	7.14
62.0	2.583	7.13	82.5	3.438	7.13
62.5	2.604	7.12	83.0	3.458	7.12
63.0	2.625	7.11	83.5	3.479	7.12
63.5	2.646	7.11	84.0	3.500	7.11
64.0	2.667	7.10	84.5	3.521	7.11
64.5	2.688	7.09	85.0	3.542	7.10
65.0	2.708	7.09	85.5	3.563	7.09
65.5	2.729	7.08	86.0	3.583	7.09
66.0	2.750	7.08	86.5	3.604	7.09
66.5	2.771	7.08	87.0	3.625	7.37
67.0	2.792	7.08	87.5	3.646	7.34
67.5	2.813	7.07	88.0	3.667	7.31
68.0	2.833	7.07	88.5	3.688	7.30
68.5	2.854	7.07	89.0	3.708	7.29
69.0	2.875	7.05	89.5	3.729	7.27
69.5	2.896	7.05	90.0	3.750	7.25
70.0	2.917	7.04	90.5	3.771	7.24
70.5	2.938	7.05	91.0	3.792	7.23
71.0	2.958	7.05	91.5	3.813	7.22
71.5	2.979	7.04	92.0	3.833	7.21
72.0	3.000	7.03	92.5	3.854	7.20
72.5	3.021	7.03	93.0	3.875	7.19
73.0	3.042	7.02	93.5	3.896	7.19
73.5	3.063	7.02	94.0	3.917	7.17
74.0	3.083	7.02	94.5	3.938	7.17
74.5	3.104	7.01	95.0	3.958	7.15
75.0	3.125	7.00	95.5	3.979	7.15
75.5	3.146	7.00	96.0	4.000	7.15
76.0	3.167	7.00	96.5	4.021	7.13
76.5	3.188	6.99	97.0	4.042	7.13
77.0	3.208	6.99	97.5	4.063	7.12
77.5	3.229	6.98	98.0	4.083	7.26
78.0	3.250	6.98	98.5	4.104	7.26
78.5	3.271	6.98	99.0	4.125	7.24
79.0	3.292	7.22	99.5	4.146	7.23
79.5	3.313	7.19	100.0	4.167	7.23
80.0	3.333	7.18			
80.5	3.354	7.17			
81.0	3.375	7.16			
81.5	3.396	7.14			

Table K.8. Soluble nitrogen species during high pH perturbation test no. 1.

Time, days	NH_4^+ mg/l-N	NH_4^+ Std. Dev.	NO_2^-, mg/l-N	NO2-, 95% C.I.	NO_3^- mg/l-N	NO_3^- ± range
0.0	113	4.8	248	1.2	169	0.25
2.6	107	1.4	257	2.5	154	0.65
4.9	112	0.5	272	2.4	139	0.10
10.7	100	2.7	280	0.4	134	0.15
27.3	105	0.95	266	2.3	151	0.90
49.0	101	0.0	231	2.8	160	0.35
83.0	116	4.1	233	1.1	173	0.30

Table K.9. Gaseous species during high pH perturbation test no. 1.

Time, days	N_2O ppm	N_2O ± range	N_2 %	N_2 95% C.I.	NO ppm	NO ± range	NO_2 ppm	NO_2 ± range
0.0	791	10	3.1%	0.13%	23.1	+1.4/-0.68	10.46	0.26
2.7	1,069	1	3.9%	0.23%	22.5	+1.4/-1.6	7.06	+0.85/-0.17
5.0	934	27	0.0%	0.00%	19.6	0.26	6.04	+0.34/-0.42
10.8	1,251	25	4.0%	0.25%	25.9	0.13	6.50	0.13
27.4	1,109	+54/-50	2.9%	0.11%	21.9	0.26	7.40	0.26
49.0	1,003	+35/-32	12.5%	0.32%	18.7	0.13	7.01	0.13
83.0	1,190	+17/-9	0.9%	0.29%	22.2	0.26	7.91	0.26

K.4 High pH perturbation experiment on Day 300.

The pH was increased from ~7 to ~8 for a 12-hour period. Gases and soluble nitrogen species were monitored for ~4 days.

Table K.10. Soluble nitrogen species during high pH perturbation test no. 2.

Time, days	NH_4^+ mg/l-N	NH_4^+ Std. Dev.	NO_2^-, mg/l-N	NO2-, 95% C.I.	NO_3^- mg/l-N	NO_3^- ± range
0	22	0.48	8	0.03	108	0.01
3	24	1.17	7	0.19	113	0.17
5	19	0.59	8	0.12	114	0.25
10	24	2.39	9	0.19	106	0.44
23	26	0.2	7	0.05	107	0.03
49	38	0	8	0	106	2.96
72	24	0.76	5	0.06	112	0.09

Table K.11. Gaseous species during high pH perturbation test no. 2.

Time, hours	N_2O ppm	N_2O ± range	N_2 %	N_2 95% C.I.	NO ppm	NO ± range	NO_2 ppm	NO_2 ± range
0	BDL	N/A	3.04%	0.20%	5.1	0.025	1.475	0.025
3	BDL	N/A	2.58%	0.17%	5.0	+0.17/-0.33	1.175	+0.05/-0.025
5	BDL	N/A	4.93%	0.11%	5.3	+0.28/-0.42	1.158333	+0.042/-0.083
10	BDL	N/A	2.97%	0.50%	5.1	0.0875	1.675	0.025
23	BDL	N/A	2.93%	0.18%	6.3	0	1.45	0.05
47	BDL	N/A	2.99%	0.66%	6.4	0.025	1.525	0.025
71	BDL	N/A			6.4	0.05	1.5	0

BDL = Below detection limit of 100 ppm (N_2O).

Table K.12. pH during high pH perturbation test no. 2.

Time, hours	Time, days	pH	Time, hours	Time, days	pH	Time, hours	Time, days	pH
0.0	0	7.17	20.5	0.342	7.59	41.0	0.683	7.34
0.5	0.008	7.52	21.0	0.350	7.58	41.5	0.692	7.34
1.0	0.017	7.87	21.5	0.358	7.58	42.0	0.700	7.34
1.5	0.025	8.08	22.0	0.367	7.57	42.5	0.708	7.33
2.0	0.033	8.00	22.5	0.375	7.55	43.0	0.717	7.32
2.5	0.042	7.95	23.0	0.383	7.54	43.5	0.725	7.33
3.0	0.050	7.89	23.5	0.392	7.54	44.0	0.733	7.32
3.5	0.058	7.86	24.0	0.400	7.53	44.5	0.742	7.32
4.0	0.067	7.96	24.5	0.408	7.52	45.0	0.750	7.32
4.5	0.075	7.95	25.0	0.417	7.52	45.5	0.758	7.31
5.0	0.083	7.90	25.5	0.425	7.51	46.0	0.767	7.31
5.5	0.092	7.87	26.0	0.433	7.50	46.5	0.775	7.31
6.0	0.100	7.83	26.5	0.442	7.49	47.0	0.783	7.31
6.5	0.108	7.95	27.0	0.450	7.49	47.5	0.792	7.30
7.0	0.117	7.92	27.5	0.458	7.49	48.0	0.800	7.30
7.5	0.125	7.89	28.0	0.467	7.47	48.5	0.808	7.30
8.0	0.133	7.86	28.5	0.475	7.47	49.0	0.817	7.30
8.5	0.142	7.83	29.0	0.483	7.46	49.5	0.825	7.29
9.0	0.150	7.88	29.5	0.492	7.45	50.0	0.833	7.28
9.5	0.158	7.93	30.0	0.500	7.45	50.5	0.842	7.28
10.0	0.167	7.91	30.5	0.508	7.44	51.0	0.850	7.28
10.5	0.175	7.89	31.0	0.517	7.44	51.5	0.858	7.28
11.0	0.183	7.86	31.5	0.525	7.43	52.0	0.867	7.27
11.5	0.192	7.84	32.0	0.533	7.43	52.5	0.875	7.27
12.0	0.200	7.82	32.5	0.542	7.42	53.0	0.883	7.26
12.5	0.208	7.81	33.0	0.550	7.41	53.5	0.892	7.26
13.0	0.217	7.79	33.5	0.558	7.42	54.0	0.900	7.26
13.5	0.225	7.77	34.0	0.567	7.41			
14.0	0.233	7.75	34.5	0.575	7.40			
14.5	0.242	7.74	35.0	0.583	7.40			
15.0	0.250	7.72	35.5	0.592	7.39			
15.5	0.258	7.70	36.0	0.600	7.39			
16.0	0.267	7.70	36.5	0.608	7.39			
16.5	0.275	7.68	37.0	0.617	7.38			
17.0	0.283	7.67	37.5	0.625	7.37			
17.5	0.292	7.66	38.0	0.633	7.37			
18.0	0.300	7.65	38.5	0.642	7.37			
18.5	0.308	7.63	39.0	0.650	7.37			
19.0	0.317	7.62	39.5	0.658	7.36			
19.5	0.325	7.60	40.0	0.667	7.35			
20.0	0.333	7.60	40.5	0.675	7.35			

Data for this appendix can be found in the files:

“Dissertation Appendix K Part a High pH Perturbation 1.xls”
“Dissertation Appendix K Part b High pH Perturbation 2.xls”
“Dissertation Appendix K Part c Oxic Perturbation 1.xls”
“Dissertation Appendix K Part d Oxic Perturbation 2.xls”

APPENDIX L

ENGINEERING SIGNIFICANCE COST ANALYSIS

Appendix L. Engineering significance cost analysis

L.1 Assumptions

The following assumptions were employed in the cost analysis

Parameter	Value
General assumptions	
Scaled-up flow	1 MGD (3,780 m^3)
Influent NH_4^+-N concentration	620 mg/l-N[a]
Stoichiometric requirement of oxygen for conventional nitrification	4.57 g O_2/ g NH_4^+-N oxidized
Stoichiometric requirement of oxygen for autotrophic HFMBR metabolisms	3.0 g O_2/g NH_4^+-N oxidized[b]
Cost of electricity	\$0.05 / kW-h
COD required / Nitrate reduced	2.86 kg COD / kg NO_3^-N reduced
COD of methanol	1.5 kg COD / kg methanol
Density of methanol	791.3 kg/m^3
Cost of methanol	\$1.00 / gallon
HFMBR assumptions	
Temperature	30°C
Effluent NO_3^--N	110 mg/l-N[a]
Head loss across membrane module	1.5 psi (10.3 kPa)[c]
Oxygen transfer efficiency	25%, 50%, 75%, varied
Density of air at specified temperature	1.164 kg/m^3
Activated sludge assumptions	
Temperature	20°C
Effluent NO_3^--N	527 mg/l-N[d]
Head loss across piping	1 psi (6.9 kPa)[c]
Tank depth	5.5 m
Oxygen transfer efficiency	25%
Density of air at specified temperature	1.204 kg/m^3

[a] from last 250 days of operating data
[b] from reactor operation, $J_{O2}/J_{NH4+} = 3.0$
[c] assumed to be independent of oxygen transfer efficiency.
[d] assuming 85% of influent ammonia is recovered as effluent nitrate